



The Role of DDAH1 in Angiogenesis

By

Negara Tajbakhsh

*Thesis
Submitted to Flinders University
for the degree of*

Doctor of Philosophy

Department of Clinical Pharmacology
College of Medicine & Public Health
March 2022

TABLE OF CONTENTS

Contents

Table of contents	i
List of Figures	v
List of Tables	viii
List of Appendices	x
Summary	xii
Declaration.....	xiv
Acknowledgements.....	xv
List of abbreviations.....	xvii
Synopsis of Chapters.....	xxi
CHAPTER 1. Literature review	1
1.1 Overview of angiogenesis	1
1.1.1 Introduction	1
1.1.2 Blood vessel structure.....	1
1.1.3 Blood vessel generation.....	10
1.2 Regulation of angiogenesis	19
1.2.1 Introduction	19
1.2.2 Endogenous inhibitors of angiogenesis	21
1.2.3 Endogenous stimulators of angiogenesis	21
1.3 Inhibiting pathological angiogenesis.....	33
1.3.1 Introduction	33
1.3.2 Current clinical anti-angiogenic inhibitors, and their pros and cons.....	33
1.3.3 Limitations and disadvantages of current anti-angiogenic therapies	36
CHAPTER 2. Materials and Methods	48
2.1 Cell culture	48
2.2 Mycoplasma screening.....	50
2.3 Cell proliferation and cell death assays	51
2.3.1 Crystal violet assay.....	51

TABLE OF CONTENTS

2.3.2	Sulforhodamine B (SRB) assay	52
2.3.3	Real-time cell growth analysis	52
2.4	Agarose gel electrophoresis	53
2.5	Protein extraction, quantification, separation, and detection	53
2.5.1	Lysate preparation and protein extraction	53
2.5.2	Protein quantitation	54
2.5.3	Immunoblotting	55
2.6	Hypoxia induction	58
2.6.1	Human VEGF-A ELISA	59
2.7	<i>In vitro</i> Matrigel® tube formation assay	60
2.8	mRNA expression analysis.....	61
2.8.1	RNA extraction	61
2.8.2	RNA quantification.....	62
2.8.3	RNA purification.....	62
2.8.4	cDNA synthesis.....	62
2.8.5	Quantitative PCR (q-PCR).....	63
2.8.6	Primer design	63
2.9	Transient transfection	64
2.10	Cell transfection with small interfering RNAs (siRNAs).....	64
2.11	Mass Spectrometry	65
2.11.1	Cell culture	65
2.11.2	Sample preparation	65
2.12	Pathway Analyses.....	72
2.13	Statistical methods.....	76
2.14	Materials, reagents, and equipment.....	76
CHAPTER 3.	CHARACTERISATION OF NOVEL DDAH1 INHIBITORS	86
3.1	Introduction and aims	86
3.2	Results	87
3.2.1	Assessing the effects of DDAH1 inhibitors.....	87
3.2.2	The effect of DDAH1 inhibitors on angiogenesis.....	100

TABLE OF CONTENTS

3.2.3	Effect of DDAH1 inhibitors on eNOS protein expression.....	103
3.3	Discussion.....	105
3.3.1	Assessing the potential toxic or protective effect of DDAH1 Inhibitors.....	105
3.3.2	The effect of DDAH1 inhibitors on angiogenesis.....	110
3.3.3	The potential effect of DDAH1 inhibitors on eNOS protein expression: Was there a protein expression change involved in the DDAH1-dependent angiogenesis?.....	112
3.4	Conclusion.....	113
CHAPTER 4. DEVELOPING MODELS OF VEGF-A MODULATION AND THEIR EFFECT ON DDAH1 EXPRESSION.....		
4.1	Introduction.....	114
4.2	Results.....	115
4.2.1	Basal expression of DDAH1.....	115
4.2.2	Model 1: DDAH1 Expression changes during hypoxia-mediated VEGF-A upregulation.....	117
4.2.3	Model 2: DDAH1 expression changes during siRNA-mediated VEGF-A knockdown.....	120
4.2.4	Examining the crosstalk between DDAH1 and VEGF-A: VEGF-A expression changes during siRNA-mediated DDAH1 knockdown.....	122
4.3	Discussion.....	123
4.3.1	Basal Expression of DDAH.....	123
4.3.2	Model 1: DDAH1 expression changes during hypoxia-mediated VEGF-A upregulation.....	126
4.3.3	Model 2: DDAH1 expression changes during siRNA-mediated VEGF-A knockdown.....	129
4.3.4	Examining the crosstalk between DDAH1 and VEGF-A.....	129
4.4	Conclusion.....	131
CHAPTER 5. INVESTIGATING THE IMPACT OF THE DDAH1 INHIBITOR ZST316 ON INTRACELLULAR BIOCHEMICAL PATHWAYS USING MASS SPECTROMETRY ANALYSIS.....		
5.1	Introduction.....	132
5.1.1	Aims and hypotheses.....	134

TABLE OF CONTENTS

5.1.2	HEK-293: The cell line used for these drug discovery experiments	135
5.1.3	Mass Spectrometry	136
5.1.4	Pathway analysis	139
5.2	Methods	141
5.2.1	Experimental Workflow	141
5.2.2	Pathway Analysis Methods	144
5.3	Results	144
5.3.1	DIA analysis	144
5.3.2	Pathway Analysis	155
5.4	Discussion	162
5.4.1	Cell culture and sample preparation	162
5.4.2	DIA analysis	163
5.4.3	Pathway analysis	169
5.5	Conclusion	175
5.5.1	Overall interpretation of data and future perspective	175
5.5.2	Limitations of this work	177
CHAPTER 6.	General Conclusions and Future Directions	179
6.1	General conclusions	179
6.2	Future directions	185
References	187
Appendices	207

LIST OF FIGURES

Figure 1.1. Human circulatory system. Schematic overview of blood flow in the circulatory system via five types of blood vessels.	2
Figure 1.2. Capillary Structure. (a) precapillary sphincters surrounding microvessels, regulating capillary blood flow. (b) The three types of capillaries: continuous, fenestrated, and discontinuous.....	3
Figure 1.3. Structure of the major blood vessels walls in the human body: Arteries, capillaries, and veins.	4
Figure 1.4. The role of the endothelium in mediating a range of processes in the body.	6
Figure 1.5. NO synthase - an overview.	8
Figure 1.6. Structure of NOS domains.	9
Figure 1.7. Different physiological functions of NO [•] derived from eNOS in the body.	10
Figure 1.8. Schematic of vasculogenesis.....	11
Figure 1.9. Schematic of blood vessel generation in the body.....	12
Figure 1.10. Sprouting Angiogenesis. Migration of endothelial cells towards the angiogenic centre (VEGF-A).....	14
Figure 1.11. Schematic representation of pillar extension resulting in angle remodelling, vessel duplication, or pruning.....	16
Figure 1.12. Schematic illustration of a small capillary undergoing splitting angiogenesis. ...	17
Figure 1.13. Schematic illustration of the angiogenic balance. Angiogenic stimulators and inhibitors in the control of the angiogenic switch.....	20
Figure 1.14. HIF-1 α activity under hypoxia versus normoxia.	24
Figure 1.15. Oxidative stress (ROS generation) and angiogenesis.	27
Figure 1.16. Schematic diagram of angiogenesis signalling pathways regulated by oxidative stress.	31
Figure 1.17. Regulation of eNOS.....	40
Figure 1.18. Arginine methylation.	41
Figure 1.19. Methylarginine metabolism.....	42
Figure 1.20. Regulatory pathways of DDAH1-mediated angiogenesis.....	45

LIST OF FIGURES

Figure 1.21. Schematic illustration of ADMA/DDAH/NOS biochemical pathway and the role of DDAH1 inhibitor, ZST316, in angiogenesis inhibition.....	47
Figure 2.1. Western blot image showing the success of the digestion process.....	67
Figure 2.2. The screenshots illustrate steps to perform InnateDB pathway analysis, followed by over-representation analysis (ORA).....	76
Figure 3.1. Viability screening of PC-12 cells treated with ZST152, L-257, and MPP ⁺ toxin....	88
Figure 3.2. Viability of undifferentiated SH-SY5Y cells 48 hours post-treatment with DDAH1 inhibitors.....	89
Figure 3.3. Proliferation curve of undifferentiated SH-SY5Y cells treated with MPP ⁺ doses..	90
Figure 3.4. Dose-response viability curves of crystal violet assay for MPP ⁺ -treated undifferentiated SH-SY5Y cells.....	91
Figure 3.5. Viability of SH-SY5Y treated with DDAH1 inhibitors against MPP ⁺ -induced toxicity.....	92
Figure 3.6. Proliferation of SH-SY5Y cells treated with DDAH1 inhibitors and MPP ⁺	94
Figure 3.7. Viability of VeraVec cells treated with ZST316 in different conditions of media after 20 hours.....	95
Figure 3.8. Viability of VeraVec cells treated with ZST316 in different media conditions after 20 hours measured by crystal violet assay.	97
Figure 3.9. Real-time proliferation of VeraVec cells incubated with ZST316 compared to controls.	99
Figure 3.10. Inhibition of capillary-like structures in HUVEC cells treated with DDAH1 inhibitors using Matrigel.....	101
Figure 3.11. Inhibition of capillary-like structures in VeraVec cells treated with DDAH1 inhibitors using Matrigel.....	102
Figure 3.12. Western Blot showing basal protein expression in VeraVe endothelial cells. ...	103
Figure 3.13. Quantitative Western Blot showing eNOS protein expression in treated VeraVec cells with DDAH1 inhibitors.	104
Figure 4.1. Agarose gel (2%) electrophoresis of PCR amplified cDNA template from ARPE-19 cells.	116
Figure 4.2. Qualitative western blot analysis showing basal protein expression in ARPE-19 cells.	117

LIST OF FIGURES

Figure 4.3. Quantitative real-time PCR analysis of VEGF-A and DDAH1 mRNA levels in hypoxic vs. normoxic ARPE-19 cells.....	118
Figure 4.4. Quantitative real-time PCR analysis of mRNA levels in 18 h hypoxic vs normoxic ARPE-19 cells.....	118
Figure 4.5. The effect of 18 and 24 h hypoxia on VEGF-A in ARPE-19 cells.....	119
Figure 4.6. DDAH1 protein levels in hypoxic vs. normoxic ARPE-19 cell lysate.....	119
Figure 5.1. Chemical structure of the DDAH1 inhibitor, ZST316, relative to L-257 (the reference selective DDAH1 inhibitor).	133
Figure 5.2. Schematic overview of the data-dependent acquisition mass spectrometry (DDA-MS) and data-independent acquisition mass spectrometry (DIA-MS).....	138
Figure 5.3. Schematic outline of the MS workflow established for ZST316-treated or non-treated HEK-293T cells.....	143
Figure 5.4. Overview of the MS experimental design.	145
Figure 5.5. Stacked-bar graph showing the abundance of upregulated (red portion of bar) and downregulated (green portion of bar) proteins in HEK-293T cells treated with vehicle, 5, and 100 μ M ZST316.	146
Figure 5.6. Volcano plots for proteomic profiling of HEK-293T cells treated with vehicle, 5 and 100 μ M ZST316.	151
Figure 5.7. Venn diagrams represent comparisons made from two pairwise contrasts of HEK-293T cells treated with 5 and 100 μ M ZST316 versus control cells.	152
Figure 5.8. VEGF signalling pathway map adapted from KEGG (ID: has04379) with significantly enriched differentially expressed proteins.....	160

LIST OF TABLES

Table 1.1. Selected list of endogenous pro- and anti-angiogenic factors.	22
Table 1.2. Antiangiogenic therapies and clinical applications.	33
Table 2.1. Master Mix composition for mycoplasma contamination testing of cell lines.	51
Table 2.2. Composition of SDS-polyacrylamide gel.	56
Table 2.3. High-ph step-elution solution composition.	69
Table 2.4. HPLC chromatography gradient.	71
Table 2.5. List of chemicals and reagents.	77
Table 2.6. List of equipment and software.	80
Table 2.7. List of antibodies.	82
Table 2.8. Buffers and solutions.	83
Table 2.9. List of cells lines.	84
Table 2.10. Primers and oligonucleotides sequences for RT-PCR.	85
Table 5.1. Quantified proteins by Spectronaut in each sample set and the proportion of changes compared to the library.	148
Table 5.2. List of overlapping (A) 23 upregulated and (B) 16 downregulated protein descriptions (and their related genes if available) between 5 and 100 μ M ZST316-treated HEK-293T cells.	153
Table 5.3. The list of peptide sequence coverage for (A) DDAH1 and (B) DDAH2 proteins by MS.	154
Table 5.4. Enriched KEGG pathways over-represented with vehicle control HEK-293T cells, and the associated genes related to differentially expressed downregulated proteins.	156
Table 5.5. Enriched KEGG pathways over-represented with 5 μ M ZST316 treatments of HEK-293T cells and the associated genes related to differentially expressed (A. upregulated, B. downregulated) proteins.	156
Table 5.6. Enriched KEGG pathways over-represented with 100 μ M ZST316 treatments of HEK-293T cells and the associated genes related to differentially expressed (A. upregulated, B. downregulated) proteins.	157
Table 5.7. Identification of significantly (A) upregulated, or (B) downregulated proteins overlapped between 5 and 100 μ M ZS316 that were present in biological pathways. (The enriched pathways are marked with an asterisk sign).	158

LIST OF TABLES

Table 5.8. 30 KEGG signalling pathways classified as angiogenesis-related pathways. (hsa stands for homo sapiens).....	159
Table 5.9. Signalling pathways related to KEGG apoptosis pathway. (hsa stands for homo sapiens).	162

LIST OF APPENDICES

Appendix 1. Western blot images of related proteins to ADMA/DDAH/NOS pathway in VeraVec cell lysates.....	207
Appendix 2. Western blot images of eNOS protein expression in VeraVec cells treated with DDAH1 inhibitor, ZST316, versus non-treated cells.	208
Appendix 3. Agarose gel electrophoresis image of cDNA from related genes to ADMA/DDAH/NOS pathway in ARPE-19 cells.....	209
Appendix 4. Basal expression of DDAH2 and NOS proteins in ARPE-19 cells.....	210
Appendix 5. Differentially expressed proteins with the two biological replicates of vehicle control HEK-293T cells (experiment 1) (Log ₂ fold-change ≥ 0.6, Q-value < 0.05).....	211
Appendix 6. Differentially expressed proteins with 5 μM ZST316 treatment vs. vehicle control in HEK-293T cells (experiment 2) (Log ₂ fold-change ≥ 0.6, Q-value < 0.05).	211
Appendix 7. Differentially expressed proteins with 100 μM ZST316 treatment vs. vehicle control in HEK-293T cells (experiment 2) (Log ₂ fold-change ≥ 0.6, Q-value < 0.05).	211
Appendix 8. 23 upregulated proteins that overlapped between 5 and 100 μM ZST316 treatment in HEK-293T cells (Log ₂ fold-change ≥ 0.6, Q-value < 0.05).	211
Appendix 9. 16 downregulated proteins that overlapped between 5 and 100 μM ZST316-treated HEK-293T cells (Log ₂ fold-change ≥ 0.6, Q-value < 0.05).....	211
Appendix 10. Identification of significantly (A) upregulated, or (B) downregulated proteins in two biological replicates of vehicle-treated HEK-293T cells (experiment 1) that were present in biological pathways (enriched pathways are marked with an asterisk sign).	212
Appendix 11. Identification of significantly (A) upregulated, or (B) downregulated proteins associated with 5 μM ZS316-treated HEK-293T cells that were present in biological pathways (enriched pathways are marked with an asterisk sign).	213
Appendix 12. Identification of significantly (A) upregulated, or (B) downregulated proteins associated with 100 μM ZS316-treated HEK-293T cells that were present in biological pathways (enriched pathways are marked with an asterisk sign).	215
Appendix 13. Uniprot IDs of 23 upregulated proteins that overlapped between 5 and 100 μM ZST316 treatment in HEK-293T cells, conversion to Entrez genes using DAVID database tool.....	217

LIST OF APPENDICES

Appendix 14. Representative spectra of two peptides from (A) DDAH1 and (B) DDAH2.	219
Appendix 15. Exploris 480 DIA Method Summary.....	249

SUMMARY

Angiogenesis is the formation of new blood vessels from pre-existing ones. Although angiogenesis provides organs and tissues with oxygen and nutrients, excessive angiogenesis could potentially contribute to a variety of diseases including Alzheimer's, AIDS, cancer, ocular diseases, arthritis, and psoriasis.

The vascular endothelial growth factor-A (VEGF-A) in endothelial cells plays a crucial role in angiogenesis. VEGF-mediated angiogenesis requires nitric oxide (NO[•]), a key signalling molecule produced by the nitric oxide synthase (NOS) family of enzymes. However, overproduction of this molecule can lead to various disorders.

Dimethylarginine dimethylaminohydrolase-1 (DDAH1) is a key enzyme in the NO[•] regulation, metabolising asymmetric dimethylarginine (ADMA) and monomethyl arginine (L-NMMA). These methylarginines are endogenous inhibitors of NOS. The resulting decrease in NO[•] production leads to angiogenesis downregulation. Inhibition of DDAH1 reduces excessive angiogenesis via increasing ADMA and L-NMMA accumulation, representing a promising strategy in the treatment of NO[•] overproduction.

In this work, the anti-angiogenic effect of novel small molecule DDAH1 inhibitors was tested. The toxic effect of three of the most potent DDAH1 inhibitor molecules (ZST316, ZST152, and ZST086) were investigated using cell viability assays (Sulforhodamine B and crystal violet) and real-time analysis of cell proliferation (IncuCyte and xCELLigence). The results indicated no toxic effects in neuronal or endothelial cell models (PC-12, SH-SY5Y, and VeraVec cells).

Pharmacological DDAH1 inhibition significantly reduced endothelial cell tube formation *in vitro*. Furthermore, we investigated the potential positive correlation between DDAH1 and VEGF-A (as an essential mediator of angiogenesis), by testing the effect of VEGF-A up- (hypoxia) and down-regulation (siRNA) on DDAH1 expression. While hypoxia-mediated VEGF-A overexpression suppressed DDAH1 protein expression, siRNA-mediated knockdown of VEGF-A, led to DDAH1 protein rise. Mass spectrometry (MS) analysis, was planned to investigate the affected angiogenic signalling pathways by the inhibitors. However, due to limited endothelial cell availability, an alternative set of experiments was conducted in non-

SUMMARY

endothelial cells that contain proteins involved in angiogenesis, HEK-293T cells, aiming to investigate the potential off-target effects of the putative drug candidates in non-endothelial cells. ZST316 showed some off-target effects based on protein abundance measurements. However, the level of changes was only 1-2% of all analysed proteins. Importantly, while ZST316 treatment caused no change in DDAH1 expression, whereas DDAH2 protein was upregulated by two-folds, which might represent a compensatory effect of the isoforms on ADMA metabolism. Pathway analysis (InnateDB) was performed to identify the main biochemical pathways enriched by the differentially expressed proteins. Limited changes were observed in the signalling pathway profile of HEK-293T cells, which might be due to a DDAH2-mediated compensatory effect following DDAH1 inhibition. Overall, the minimal effect of ZST316 treatment on the biological pathways of HEK-293T cells, including apoptosis and angiogenesis, rules out the presence of tangible off-target effects at least in this cell line.

The mass spectrometry analysis requires further investigations on the effect of DDAH1 inhibitors on endothelial and non-endothelial cells, followed by *in vivo* studies to confirm the presence of tangible anti-angiogenic effects without overt systemic toxicity.

DECLARATION

I certify that this thesis does not incorporate without acknowledgement any material previously submitted for a degree or diploma in any university; and that to the best of my knowledge and belief it does not contain any material previously published or written by another person except where due reference is made in the text.

Negara Tajbakhsh

ACKNOWLEDGEMENTS

I would like to extend my appreciations to the many people who contributed generously to the work presented in this thesis.

My sincere appreciation goes to my main supervisor, Professor Arduino Mangoni, not only for his great deal of support, but also for giving me many wonderful opportunities from day one of joining his research laboratory as an employee throughout my whole PhD candidature to the very end. His support bundled with charm and kindness made this challenging journey interesting!

Profound gratitude goes to my lovely co-supervisor, Dr. Elke Sokoya, who has been a truly dedicated mentor. I am particularly indebted to Elke for her constant faith in me, and for her tremendous academic support. This journey would not have been possible without her kind help, support and guidance.

Similarly, I am also appreciative to Dr. Timothy Chataway who has the substance of a genius. I am grateful to him for sharing his mass spectrometry expertise so willingly and for his advice and helpful perspectives during the final production of this thesis, being so dedicated to his role as my secondary supervisor.

I wish to express my deepest gratitude to Professor Ross McKinnon whose kindness, thoughtfulness, and all the financial assistance he provided, were milestones in the completion of this project. He is a true gem.

I would also like to thank Dr. Ben Lewis who supervised me at the beginning of this project. His encouragement and good intentions had a key role on my choice of embarking on the PhD path. His trainings with regards to laboratory experiments are much appreciated.

My appreciations also go to Professor Claudine Bonder and Dr. Kate Parham (Centre for Cancer Biology, SA Pathology and University of South Australia) for contributing in tube formation experiments and providing me with all the knowledge and support in this field.

I am grateful to Professor Justine Smith, Dr. Binoy Appukuttan, and their laboratory staff for passing on their expert knowledge in the field of hypoxia and RPE cells.

ACKNOWLEDGEMENTS

My sincere thank you to Dr. Damian Hussey for his time, guidance, and feedback he provided with the pathway analysis.

I would also like to extend my appreciations to Ms Nusha Chegeni and Dr. Alex Colella for their contribution to the mass spectrometry field. I am thankful for their generosity with their time and expertise.

I am particularly grateful to my dear friend, Dr. Sara Tommasi, for her sisterly love, help, and support in every way she could. I would also like to thank my departmental colleagues, especially Dr. Julie-Ann Hulin and Dr. Dhilushi Wijayakumara, for the support they provided over my PhD.

I am so grateful to the most important people of my life: my mum and my dad, and also my sister, Samira, who have been there for me with their love and support during the ups and downs of this journey.

I am also thankful to all my dear friends who have given me encouragement and support, particularly Ayla Orang and Keyvan Pourhassan. The world needs more friends like them.

This work is dedicated to the memory of my dear Grandma whom I lost during the course of this research.

This research was supported by an Australian Government Research Training Scheme Scholarship.

LIST OF ABBREVIATIONS

ADMA	Asymmetric dimethylarginine
AGC	Automatic gain control
Akt	Protein kinase B (PKB) also known as Akt Ak strain transforming
AMD	Age-related macular degeneration
AMPK	Adenosine monophosphate (AMP)-dependent kinase
Ang-2	Angiotensin-2
ArgMe	Arginine methylation
ATCC	American Type Culture Collection
ATM	Ataxia-telangiectasia mutated
ATP	Adenosine 5'-triphosphate
BSA	Bovine serum albumin
BH ₄	Tetrahydrobiopterin
Ca ²⁺	Calcium
CAM	Cell adhesion molecules
CaM	Calmodulin
CAP	Carboxyalkyl pyrrole
CAR-T	Chimeric antigen receptor T
CAT	Cationic amino acid transporter
Cav-1	Caveolin-1
cDNA	Complementary deoxyribonucleic acid
CEP	Carboxyethylpyrrole
cGK	Protein kinase G
cGMP	Cyclic guanosine monophosphate
CSF	Colony-stimulating factors
DDAH	Dimethylarginine dimethylaminohydrolase
DHA	Docosahexaenoic acid
DLL4	Delta-like ligand 4
DMEM	Dulbecco's Modified Eagles Medium
DMSO	Dimethyl sulfoxide

LIST OF ABBREVIATIONS

DNA	Deoxyribonucleic acid
dNTP	Deoxynucleotide triphosphate
DTT	Dithiothreitol
ECL	Enhanced chemiluminescence
EDHF	Endothelium-derived hyperpolarizing factor
EDRF	Endothelium-derived relaxing factor
EDTA	Ethylenediaminetetraacetic acid
eNOS	Endothelial nitric oxide synthase
ER	Endoplasmic reticulum
ERK	Extracellular signal-regulated kinase
ERR- α	Estrogen-related receptor- α
FAD	Flavin adenine dinucleotide
FBS	Fetal bovine serum
FDA	U.S. Food and Drug Administration
FGF	Fibroblast growth factors
FLT3	FMS-like receptor tyrosine kinase-3
FMN	Flavin mononucleotide
Foxo	Forkhead box O
GAPDH	Glyceraldehyde-3- phosphate dehydrogenase
GMP	Guanosine monophosphate
GTP	Guanosine 5'-Triphosphate
HIF-1 α	Hypoxia-inducible factor-1
Hsp90	Heat shock protein 90
HUVEC	Human umbilical vein endothelial cell
ICAM-1	Intercellular Adhesion Molecule-1
IFN- α	Interferon- α
IgG	Immunoglobulin G
IL	Interleukin
iNOS	Inducible nitric oxide synthase
kb	Kilobase
kDa	KiloDaltons

LIST OF ABBREVIATIONS

L-Arg	L-arginine
L-Cit	L-citrulline
L-NAME	N ^G -nitro-L-arginine methyl ester
LPS	Lipopolysaccharide
mAbs	Monoclonal antibodies
MALP	Macrophage-activating lipopeptide
MAPK	Mitogen-activated protein kinase
MEM	Minimum Essential Medium
miRNA	MicroRNA
MMA	Monomethylarginine
MMP	Matrix metalloproteinase
MS	Mass Spectrometry
mTOR	Mammalian target of rapamycin
NADPH	Nicotinamide-adenine-dinucleotide phosphate
NFκB	Redox-sensitive nuclear factor -kappaB
nNOS	Neuronal nitric oxide synthase
NO [·]	Nitric oxide
NOS	Nitric oxide synthase
NOX	NADPH oxidase
nt	Nucleotide
OD	Optical density
OxLDL	Oxidation of low-density lipoproteins
PAGE	Polyacrylamide gel electrophoresis
PBS	Phosphate buffered saline
PCR	Polymerase chain reaction
PDGF	Platelet-derived growth factor
PEX	Peroxis
PI3K	Phosphatidylinositol 3-kinase
PKC	Protein kinase C
PLCγ	Phospholipase C gamma
PPIA	Peptidylprolyl isomerase A

LIST OF ABBREVIATIONS

PRMT	Protein arginine methyl transferase
PTM	Post translational modification
PUFA	Polyunsaturated fatty acid
rAAV	Recombinant adeno-associated virus
RIPA	Radioimmunoprecipitation assay
RNA	Ribonucleic acid
ROS	Reactive oxygen species
RT-qPCR	Reverse transcription quantitative polymerase chain reaction
SDMA	Symmetric dimethylarginine
SDS	Sodium dodecyl sulphate
siRNA	Small interfering RNA
SIRT1	Sirtuin1
SNO	S-nitrosothiol
TAE	Tris-acetate EDTA electrophoresis buffer
TBS	Tris-buffered saline
TIMP	Tissue inhibitors of metalloproteinase
TLR	Toll like receptor
TNF	Tumour necrosis factor
Tris	Tris[hydroxymethyl]aminomethane
TSP-1	Thrombospondin-1
uHPLC	Ultra high performance liquid chromatography
VCAM-1	Vascular cell adhesion molecule-1
VEGF-A	Vascular endothelial growth factor-A
VEGFR	Vascular endothelial growth factor receptor

SYNOPSIS OF CHAPTERS

In Chapter one, I looked into the literature and reviewed what is known about angiogenesis and the mechanisms involved in the regulation of this process. Then, I described the pathological conditions associated with angiogenesis and the current clinical approaches, their advantages, and their limitations. Finally, I explained how DDAH1 inhibition could play a role as a potential strategy to inhibit excessive angiogenesis, introducing our novel and potent small molecule DDAH1 inhibitor compounds.

In Chapter two, I discussed the methods used in detail. These include information on the cell models and the culture techniques used for each experiment, cell proliferation and cell death assays using colorimetric (Crystal Violet and Sulforhodamine B) or real-time cell analysis systems (x-CELLigence and IncuCyte), protein extraction and analysis by immunoblotting, creating hypoxic conditions for cell culture, ELISA, Matrigel® Tube formation assay, RNA extraction and quantitative PCR, transfection with siRNA, and finally, Mass Spectrometry analysis followed by pathway analysis.

The initial step for any drug discovery process is characterisation. In Chapter three, I investigated and described the potential toxic or protective effect of the novel DDAH1 inhibitors on endothelial and non-endothelial cells using different methodologies. Moreover, I investigated their biological influence on angiogenesis *in vitro*, using Matrigel® tube formation assay, and further tested whether they affect eNOS protein expression.

In Chapter four, I tested the effect of VEGF-A modulation on DDAH1 expression by developing two models of VEGF-A modulation. To develop the first model, I attempted to increase VEGF-A expression by establishing an *in-vitro* model of hypoxia in cell culture. I used an opposite strategy to create the second model, by knocking down VEGF-A gene using siRNA technique. Next, I examined the cross-talk between DDAH1 and VEGF-A using the siRNA-induced silencing of DDAH1 gene and measuring VEGF-A expression changes.

In Chapter five, I investigated the intracellular biochemical pathways underneath the anti-angiogenic effects of DDAH1 inhibitors. As the VeraVec endothelial cells that I used before were unavailable, I used an established cell line for drug development studies, HEK-293T, as non-

SYNOPSIS OF CHAPTERS

endothelial cells expressing DDAH1. For this purpose Mass Spectrometry analysis was used following KEGG pathway analysis using InnateDB.

CHAPTER 1. LITERATURE REVIEW

1.1 Overview of angiogenesis

1.1.1 Introduction

The circulatory system (cardiovascular system) transports oxygen, nutrients, and immune defense agents throughout the organism, clearing waste products and maintaining cellular homeostasis (Jarvis, 2018).

The formation of the human circulatory system occurs relatively early during embryonic development through a complex process called vasculogenesis (Risau, 1997). From here, vessels can split (a process known as intussusception) and then sprout (a process known as angiogenesis). The ability to grow new blood vessels is preserved in adulthood although, particularly when uncontrolled, this can also be associated with pathological processes such as tumour development and diabetic retinopathy. However, the mechanisms underlying angiogenesis are not fully understood.

1.1.2 Blood vessel structure

Blood vessels are classified into five main types: arteries (elastic and muscular), small arteries and arterioles (resistance vessels), capillaries, venules, and veins, varying in their structure depending on their function (Patton and Thibodeau, 2018) (**Fig. 1.1**). For instance, elastic arteries have a considerable amount of elastic fibres that assist with stretching during systole and recoil during diastole. By contrast, muscular arteries are rich in smooth muscle cells which, through their contraction-relaxation function, control the blood flow to organs according to their metabolic need.

CHAPTER 1

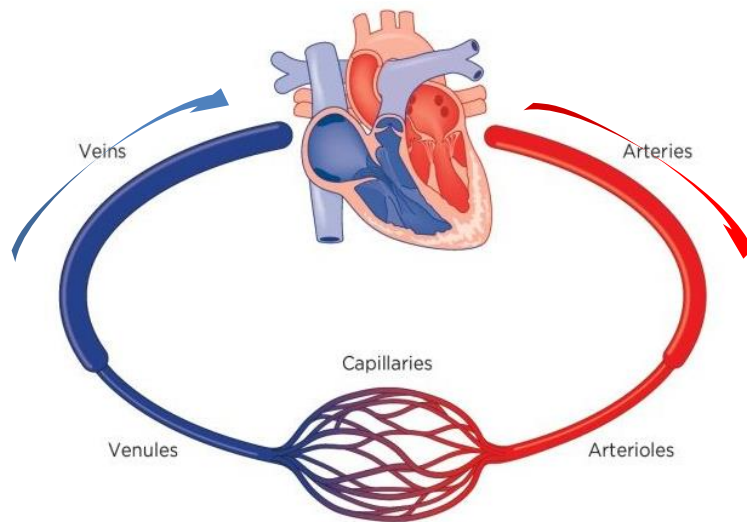


Figure 1.1. Human circulatory system. Schematic overview of blood flow in the circulatory system via five types of blood vessels.

Capillaries are sites of exchange with a thin wall made of a single layer of endothelial cells surrounded by a basement membrane (a unique extracellular matrix embedded with pericytes required for vessel remodelling) (Stratman and Davis, 2012) (**Fig. 1.2, b**). Circular smooth muscle cells that surround these microvessels, called precapillary sphincters, regulate capillary blood flow (**Fig. 1.2, a**). There are three types of capillaries: continuous, fenestrated, or sinusoid (discontinuous) (**Fig. 1.2, b**). Continuous capillaries, the most common type, are constituted by a continuous layer of endothelial cells connected by tight junctions (transmembrane proteins connecting adjacent endothelial cells and working as a selective barrier to fluid) (Anderson and Van Itallie, 2009). Fenestrated capillaries are found in tissues where extensive molecular exchange with the blood is required, such as the small intestine (the main site of nutrient absorption), endocrine glands and the kidney (which filter the blood). These capillaries have pores (fenestrations) in their endothelial cell layer as well as tight junctions, enabling the passage of large molecules. Discontinuous capillaries, the least common type, have incomplete basement membranes and extensive intracellular gaps that allow the transfer of plasma proteins or even blood cells to pass through.

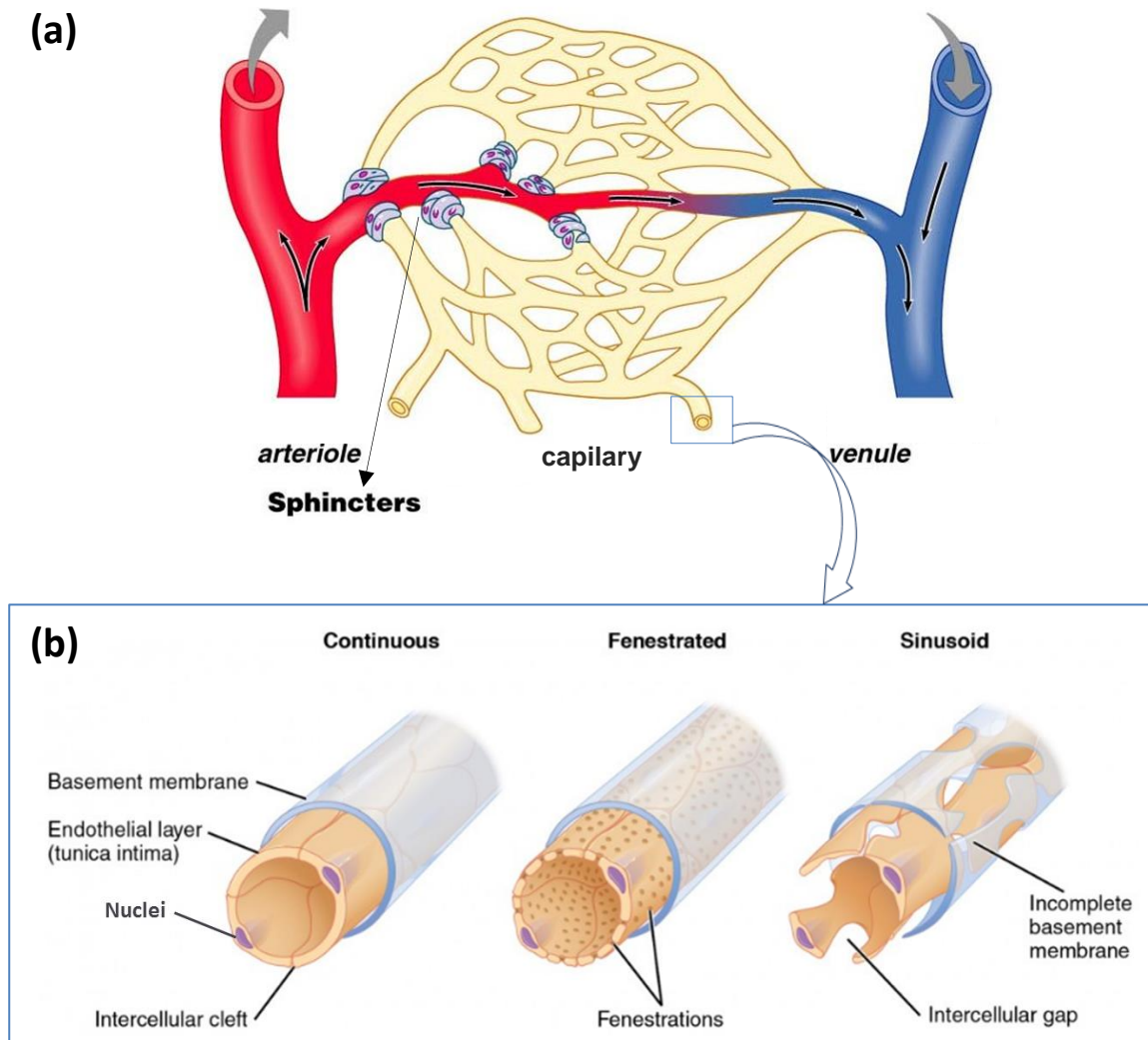


Figure 1.2. Capillary Structure. (a) precapillary sphincters surrounding microvessels, regulating capillary blood flow. (b) The three types of capillaries: continuous, fenestrated, and discontinuous.

Adapted from VanPutte *et al.*, 2021 (VanPutte *et al.*, 2021) and Allen *et al.*, 2004 (Allen, 2004), , reproduced with permission.

Following the capillary exchange, deoxygenated blood from tissues moves into venules and progressively larger veins towards the heart. The porous and thin-wall structure of venules not only allows fluid exchange but also transfer of white blood cells into the interstitium. The compliant nature of vein walls ensures the maintenance of relatively low intraluminal pressures despite large blood volumes (**Fig. 1.3**).

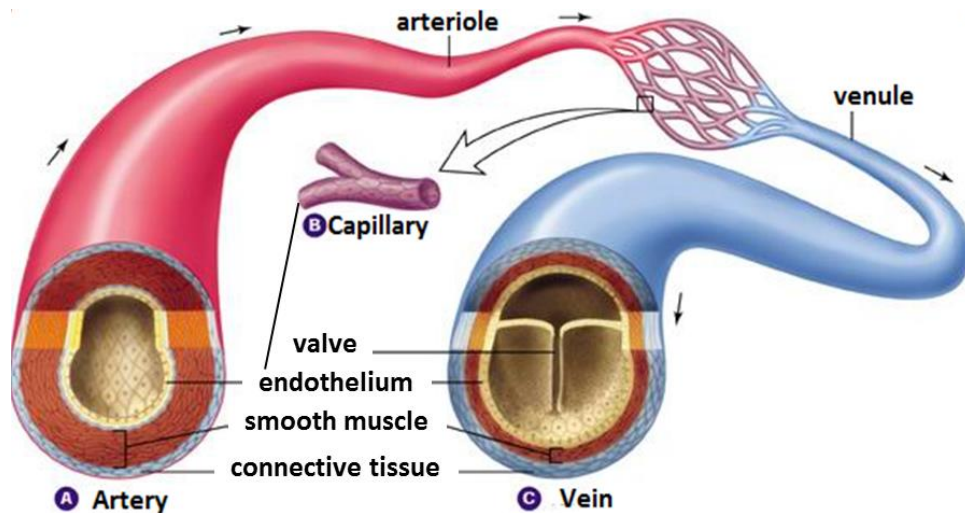


Figure 1.3. Structure of the major blood vessels walls in the human body: Arteries, capillaries, and veins.

(A) Elastic and muscular arteries are comprised of three main layers, carrying oxygen-rich blood away from the heart, (B) Capillaries are tiny vessels with only one cell thick (endothelium), bringing oxygen and nutrients to the cells. (C) Veins are comprised of three main layers, carrying wastes and oxygen-poor blood back to the heart with the help of valves and their elastic walls.

1.1.2.1 Endothelium at the molecular level

A single layer of endothelial cells, known as the endothelium, lines the inner surface of blood vessels. The endothelium not only represents a physical barrier between the blood and the tissues, but also play a vital role in controlling vascular tone, inflammation, coagulation, and angiogenesis (Félétou, 2011, Jag et al., 1980) (**Fig. 1.4**).

Vascular tone: The endothelium produces several vasodilators and vasoconstrictors. Nitric oxide (NO[•]), endothelium-derived hyperpolarizing factor (EDHF), and prostacyclin are endothelial-derived vasodilators. Endothelin-1 and thromboxane-A2 are endothelial-derived vasoconstrictors (Galley and Webster, 2004).

Inflammatory response: In response to an acute infection, the endothelium plays an integral role in transporting leukocytes from the blood into the underlying tissue. A family of cell adhesion molecules (CAM family such as ICAM-1 (Intercellular Adhesion Molecule-1) and VCAM-1 (vascular cell adhesion molecule-1)) favours the binding of leukocytes to endothelial cells and the subsequent migration of leukocytes into the local site of inflammation (Cibor et al., 2016, Galley and Webster, 2004). Activated endothelial cells also produce a variety of other cytokines and chemokines such as colony-stimulating factors (CSFs), interleukins (ILs), tumour necrosis factor

CHAPTER 1

(TNF) receptors (p55 and p75), growth factors, and interferons which promote the recruitment of leukocytes (Cibor et al., 2016).

Coagulation: Endothelial cells inhibit coagulation with the aid of anti-coagulant factors bound to their surface (Watson, 2009). Thrombin, synthesised in the liver and secreted into the plasma in its inactive form (prothrombin), has a key role in the coagulation process. At the site of vascular injury, blood factors escape from damaged endothelial cells and bind to the components of the surrounding tissue (collagen and von Willebrand factor), becoming activated. Activated platelets aggregate and become adhesive to the endothelium. More importantly, prothrombin is transformed into thrombin which converts soluble fibrinogen into insoluble fibrin, which, in combination with platelets forms a blood clot (Marti et al., 2012). Platelet activation is prevented by endothelium-derived NO[•], through the increase in cyclic guanosine monophosphate (cGMP) levels within platelets. This causes a decrease in intracellular Ca²⁺ and the consequent inhibition of coagulation pathways (Radomski and Salas, 1995).

Tight junctions: Adjacent endothelial cells are connected by protein complexes called tight junctions. These dynamic protein structures act as a selective barrier by regulating the passage of water, ions, and various macro-molecules, maintaining cell polarity (Anderson and Van Itallie, 2009). Tight junctions play an important role, particularly at the blood-brain-barrier interface, by restricting the passive passage of ions, blood products and pathogens into the brain (Wolburg et al., 2009, Choi and Kim, 2008).

Angiogenesis: The Vascular Endothelial Growth Factor-A (VEGF-A) is the most potent initiation factor of vasculogenesis and angiogenesis. VEGF-A is expressed at low levels in many cell types including tumour cells (Boocock et al., 1995, Itakura et al., 2000), macrophages (Sunderkötter et al., 1994), and platelets (Verheul et al., 1997). Endothelial cells express a family of receptors to VEGFs on their surface called VEGFRs. These receptors are high-affinity tyrosine kinases with VEGFR-2 being the predominant receptor in angiogenic signalling (Carmeliet and Jain, 2011).

In situations where vessel formation is required (e.g., embryonic tissues, placenta, corpus luteum, injury, inflammation sites, or tumours) cells are exposed to hypoxia, and VEGF is expressed at high levels (Carmeliet, 2005). Each VEGF binds to a VEGFR located on the surface of endothelial cells and activates it by dimerisation and phosphorylation.

CHAPTER 1

Depending on the severity of hypoxia and the concentrations of VEGF-A, one of two modes of angiogenesis, sprouting or splitting (intussusceptive), becomes dominant. Accordingly, VEGFR-1 or -2 is initially activated to splitting or sprouting angiogenesis, respectively (Zhan et al., 2018). Under severe hypoxic conditions, VEGF-A binds with VEGFR-2 and initiates tyrosine kinase phosphorylation, activating downstream signalling enzymes such as protein kinase B (PKB) (also known as Akt), extracellular signal-regulated kinase (ERK), and endothelial nitric oxide synthase (eNOS). This further activates several intracellular signalling pathways including the Ras/Raf/MAPK/ERK and the PI3K/Akt, finally promoting sprouting angiogenesis (Shibuya, 2011). This process also involves an increased secretion of matrix metalloproteinases (MMPs) responsible for extracellular matrix protein degradation. The latter increases microvascular permeability, endothelial cell proliferation and migration towards the direction of VEGF signals (Esser et al., 1998, Lohela et al., 2009). The extension and migration of endothelial cell from the pre-existing capillary form a multi-cellular sprout. This sprout grows until it meets the neighbouring capillary and ultimately forms a new endothelial cell (sprouting angiogenesis). On the other hand, with moderate hypoxia, VEGFA-VEGFR-1 binding occurs, leading to extension of the endothelial cells into the capillary lumen until the initial capillary splits into two (splitting angiogenesis) (Carmeliet and Jain, 2011).

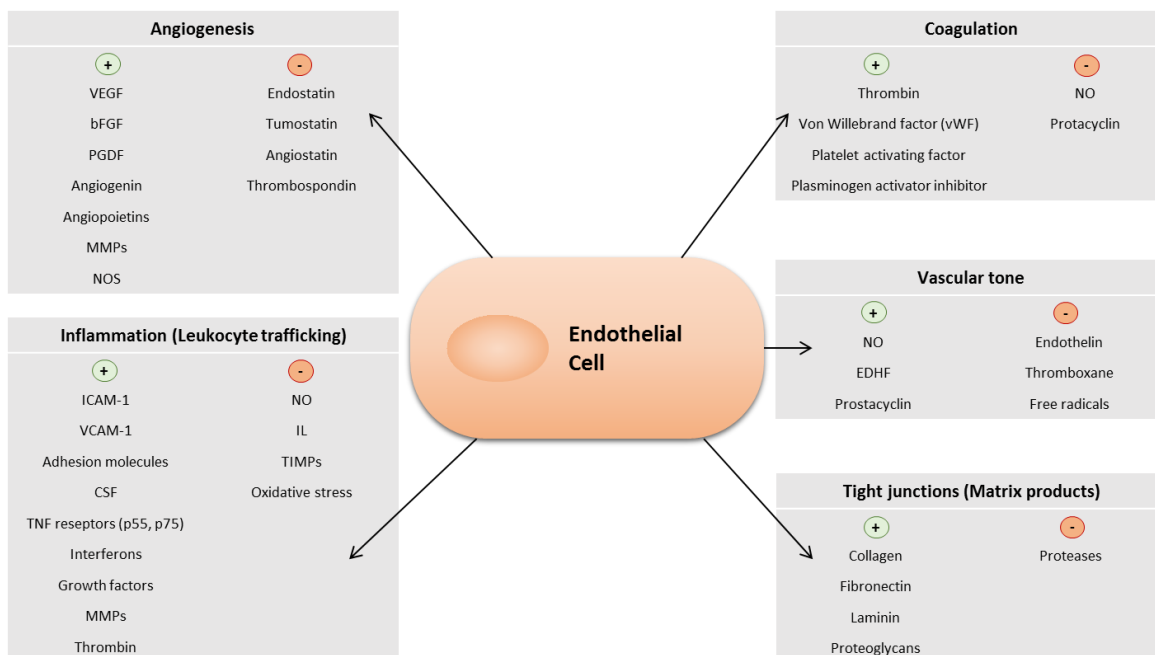


Figure 1.4. The role of the endothelium in mediating a range of processes in the body.

Adapted from Jourde-Chiche *et al.* (Jourde-Chiche et al., 2019), reproduced with permission.

1.1.2.2 Endothelium-derived NO Production and Function

Endothelial cells can be directly triggered by substances released as a result of local metabolic needs or stress. In response to these factors, endothelial cells release a variety of vasoactive mediators. Among these, NO[·] maintains basal vascular tone and is a key determinant of vascular homeostasis. Reduced NO[·] bioavailability is related to the progression of vascular diseases where several factors can be involved. These include decreased substrate bioavailability, decreased eNOS expression or activity, decreased cofactor availability, or oxidative stress and generation of ROS (Levine et al., 2012, Paolucci et al., 2001).

NO[·] is a highly reactive radical gas with a half-life of a few seconds (Furchgott, 1984, Furchgott, 1999). This free radical has pivotal roles in the vascular system as a signalling molecule, including blood flow regulation and immune defense (Tousoulis et al., 2012). NO[·] was discovered by Furchgott and Zawadzki in 1980. They first reported the endothelium-dependent relaxation of rabbit aorta from a free unstable gas, the so-called endothelium-derived relaxing factor (EDRF) (Furchgott and Zawadzki, 1980). This soluble gas is continuously synthesised in endothelial cells by a group of calcium-calmodulin-dependent enzymes, nitric oxide synthases (NOSs) (Knowles and Moncada, 1994).

Three different isoforms of NOS have been identified in mammals: neuronal (nNOS, NOS I), inducible (iNOS, NOS II), and endothelial (eNOS, NOS III), based on the tissues they were originally isolated from (Förstermann et al., 1998). They are a family of oxidoreductase enzymes that produce NO[·] through the conversion of the amino acid L-arginine (L-Arg) to L-citrulline (L-Cit). This reaction occurs in two steps. During the first step, L-Arg gets reduced using co-enzyme nicotinamide-adenine-dinucleotide phosphate (NADPH) and an oxygen molecule to generate N^G-hydroxy-L-Arginine, the intermediate step of the reaction. Afterwards, the second reduced NADP binds to NOS to reduce oxygen and form L-Cit and water (Kone et al., 2003, Knowles and Moncada, 1994). Importantly, the NO[·] generated in this reaction is a free radical, an extremely reactive chemical species (**Fig. 1.5, A**).

CHAPTER 1

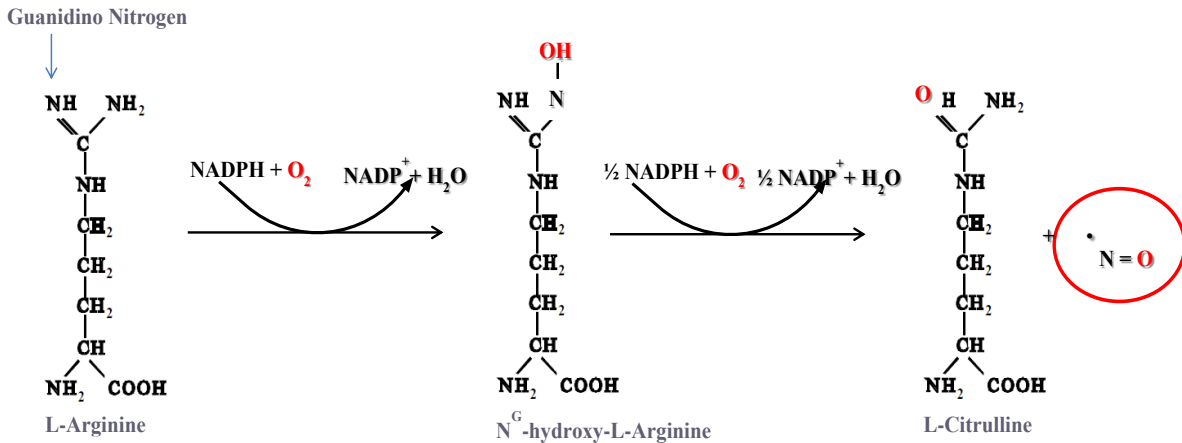
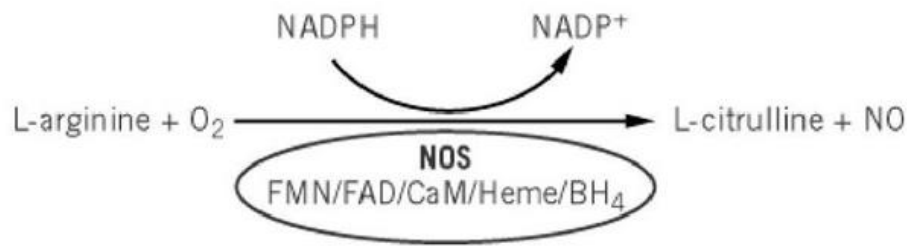


Figure 1.5. NO synthase - an overview.

(A) Summary of NO[•] production by NOS enzyme and co-factors. (B) NO production two-step reaction.

The reduction-oxidation reactions of NOS can independently occur in the two domains of the enzyme, reductase and oxygenase (**Fig. 1.6**). However, NO[•]-synthesis is dependent upon the formation of a NOS dimer, where the reductase domain of one NOS monomer couples with the oxygenase domain of another NOS partner (Kone et al., 2003, Andrew and Mayer, 1999). This reaction requires the cofactors reduced NADPH, flavin adenine dinucleotide (FAD), flavin mononucleotide (FMN), heme (Fe²⁺), tetrahydrobiopterin (BH₄), and zinc (**Fig. 1.6**) (Kone et al., 2003, Förstermann and Sessa, 2012). Heme and zinc ions from each monomer play a central role in the formation of the homodimer (coupled NOS) whereas BH₄ stabilises the structure (Li et al., 1999). Uncoupling of NOS (caused by BH₄ and/or arginine deficiency) results in impaired NO[•] production.

CHAPTER 1

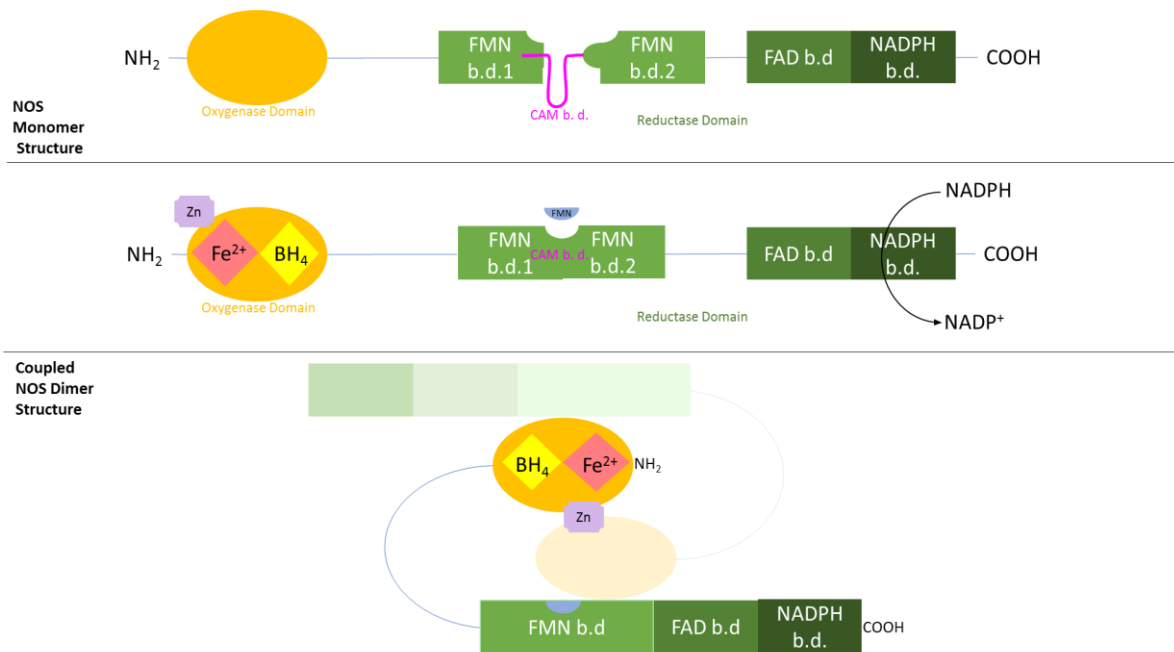


Figure 1.6. Structure of NOS domains.

At the top, the monomer structure of NOS enzyme is shown that consists of two domains: reductase domain (orange) and oxygenase domain (green). The middle image illustrates the reduction-oxygenation reaction and the required cofactors, reduced NADPH, flavin adenine dinucleotide (FAD), flavin mononucleotide (FMN), heme (Fe^{2+}), tetrahydrobiopterin (BH_4), and zinc ion (Zn^{2+}). The bottom image demonstrates a functional NOS dimer; Two NOS monomers have dimerized.

Under physiological conditions, NO^{\cdot} is mainly produced by eNOS in the vessel wall (Nathan and Xie, 1994), although this isoform has also been detected in cardiac myocytes, platelets, certain brain neurons, placenta, and kidney tubular epithelial cells (Förstermann and Sessa, 2012).

NO^{\cdot} is a potent and multi-functional signalling molecule, and a key determinant of endothelial function, metabolic and vascular health (Levine et al., 2012). In addition, it can affect the nervous and immune systems. Protective effects of NO^{\cdot} occur at pico- to nano-molar concentrations. This low, but tightly regulated concentration of NO^{\cdot} has a critical role in regulating cardiovascular homeostasis. However, at higher concentrations, NO^{\cdot} and its derivatives become cytotoxic.

Endothelial-derived NO^{\cdot} has several physiological functions and has been identified as the most important endothelium-derived relaxing factor. This endogenous vasodilator continuously modulates vessel diameter and maintains homeostasis. When eNOS is stimulated by increased shear stress in blood vessels, NO^{\cdot} diffuses to the nearby smooth muscle cells, stimulating soluble guanylyl cyclase to produce cGMP. This leads to dephosphorylation of myosin, hyperpolarisation and vasorelaxation (**Fig. 1.7**) (Knowles and Moncada, 1994).

CHAPTER 1

Endothelium-derived NO[•] also contributes to coagulation. As a platelet adhesion and aggregation inhibitor, NO[•] keeps the vascular smooth muscle surface non-adhesive and non-thrombogenic for circulating blood cells.

In addition, NO[•] controls vascular integrity and the maintenance of physiological blood flow and pressure.

Importantly, endothelium-derived NO[•] is also a mediator of angiogenesis. Angiogenic factors such as VEGF upregulate NOS expression and NO[•] release in endothelial cells (Servos et al., 1999). By contrast, reduced NO[•] synthesis attenuates angiogenesis. The main roles of NO are shown in

Figure 1.7.

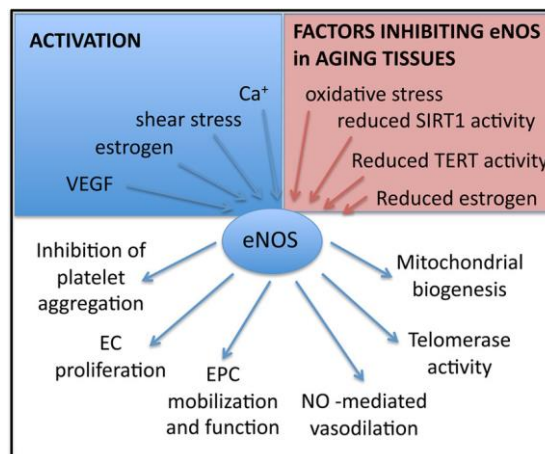


Figure 1.7. Different physiological functions of NO[•] derived from eNOS in the body.

Adapted from Favero *et al.*, 2014 (Favero et al., 2014), reproduced with permission.

1.1.3 Blood vessel generation

Two main processes are involved in the formation of a blood vessel network, vasculogenesis and angiogenesis. Vasculogenesis occurs during embryonic development where blood vessels are created *de novo* from mesodermal cells. By contrast, angiogenesis is the formation of new capillaries from pre-existing ones (Risau, 1997).

The process of vasculogenesis initiates from the development of mesoderm-derived precursor for endothelial cells (hemangioblasts) into new blood vessels (Risau and Lemmon, 1988, Flamme et al., 1997). In the developing embryo, since oxygen consumption is greater than the delivered oxygen, the tissue becomes hypoxic. This stimulates hemangioblasts to secrete signalling molecules such as VEGF-A which promote their migration to form clusters called blood islands.

CHAPTER 1

Within the blood island, the peripheral cells form angioblasts which then mature into endothelial cells. On the other hand, the central cells form hemocytoblasts (also known as hematopoietic stem cells), differentiating into blood cells (**Fig. 1.8 and 1.9**) (Risau, 1991).

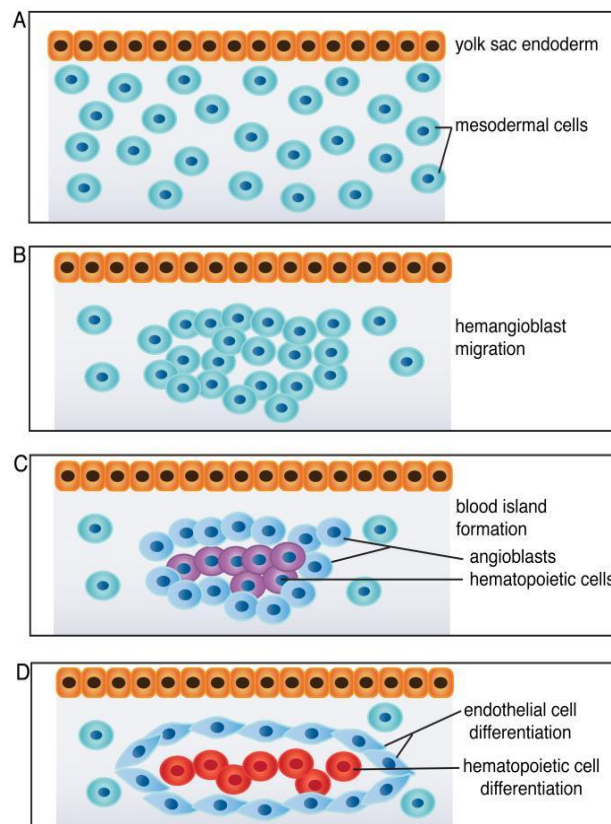


Figure 1.8. Schematic of vasculogenesis.

(A) Endodermal cells (orange) induce mesodermal cells (aqua), initiating vasculogenesis, (B) Hemangioblasts migration and association, (C) Central formation of hematopoietic cells (purple) surrounded by angioblasts (blue), (D) Angioblasts differentiate into endothelial cells (blue) and hematopoietic cells (red). Adapted from Patel-Hett *et al.*, 2011 (Patel-Hett and D'Amore, 2011), reproduced with permission.

Once this primary capillary plexus is formed, it serves as a template for angiogenesis. This physiological angiogenesis not only plays a pivotal role during embryonic development and tissue remodeling (Carmeliet and Jain, 2011), but also in adults during wound healing, the reproductive cycle, bone repair, exercise, and in the adipose tissue (Lemoine *et al.*, 2013, Carmeliet, 2005, Carmeliet and Jain, 2011, Risau, 1997). In these circumstances, angiogenesis is tightly regulated by the balance between pro- and anti-angiogenic molecules. However, any loss in this balance leads to pathological angiogenesis, contributing to various diseases including diabetic retinopathy, rheumatoid arthritis, atherosclerosis, endometriosis, psoriasis, Alzheimer's disease, and several tumour types (Carmeliet, 2003, Carmeliet and Jain, 2011).

CHAPTER 1

The process of angiogenesis takes place through two events known as sprouting and splitting (intussusceptive) angiogenesis as described in detail below.

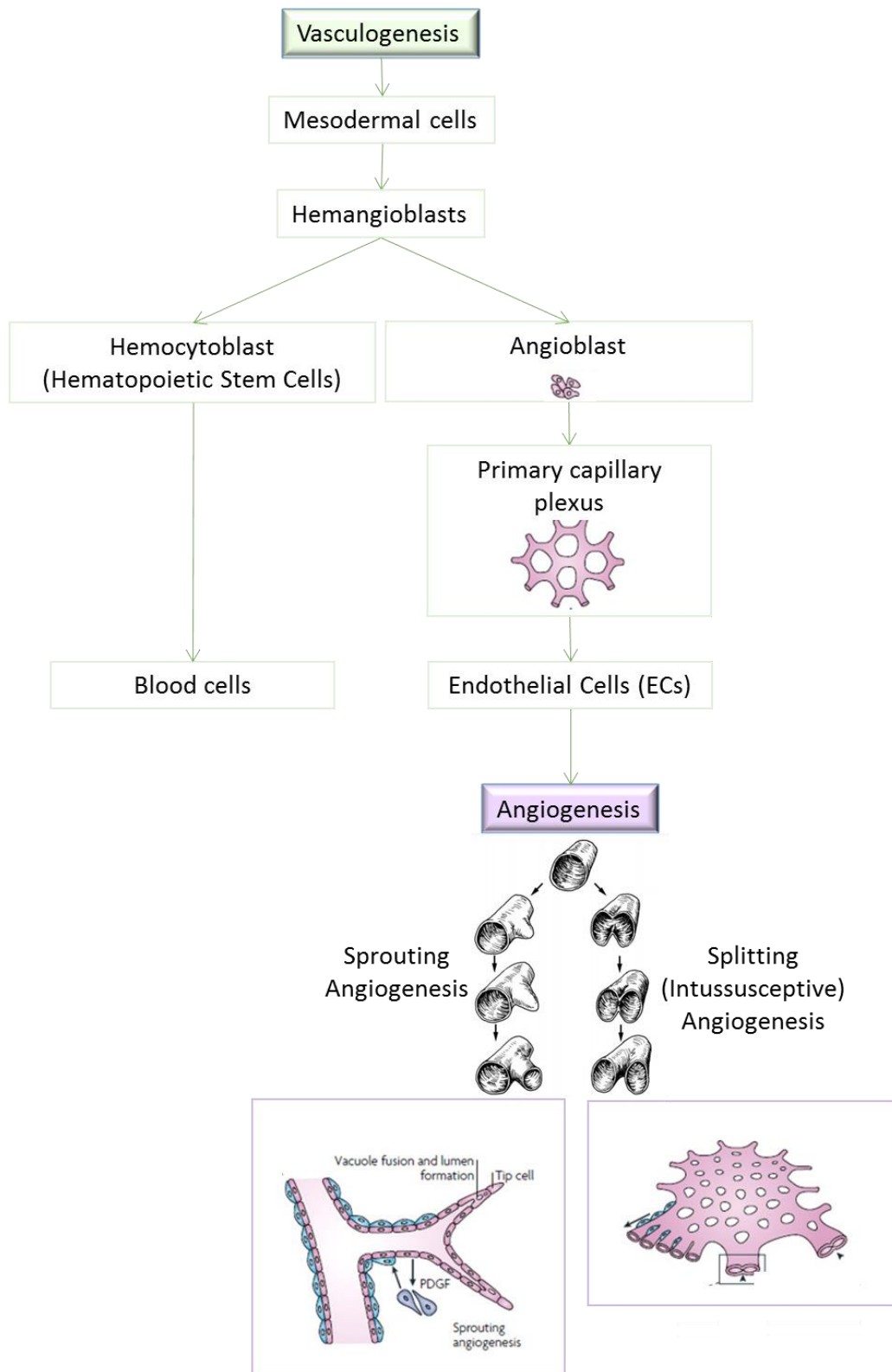


Figure 1.9. Schematic of blood vessel generation in the body.

Vasculogenesis (during embryonic life), and angiogenesis (during adulthood). Adapted from Prior *et al.*, 2004 (Prior *et al.*, 2004) and Kolte *et al.*, 2016 (Kolte *et al.*, 2016), reproduced with permission.

1.1.3.1 Sprouting Angiogenesis

Sprouting angiogenesis is the process of budding new capillaries from “parental” capillaries, producing sprouts. This process occurs through several steps. Initially, a stimulus such as hypoxia or inflammation induces endothelial cells to release angiogenic factors including VEGFs, fibroblast growth factors (FGFs), platelet-derived growth factor (PDGF), angiotensin-2 (Ang-2), or chemokines. VEGF-A is the most potent factor involved in sprout generation. During the first step of sprouting called “tip-cell selection”, a single endothelial cell closest to the source of VEGF-A is most likely to become the tip cell, guiding the sprout towards the VEGF-A stimulus (**Fig. 1.10, a**). Tip cells have high amounts of VEGF-A receptors (VEGFRs) on their surface with an enhanced affinity for VEGF-A (**Fig. 1.10, b**). This allows tip cells to detect differences in VEGF-A concentrations. There are three VEGFRs (VEGFR-1, 2, and 3), among which VEGFR-2 has a high expression level in endothelial cells, with greater tyrosine-kinase activity; hence, it is the major receptor in angiogenic signalling (Shibuya, 2013). In response to the high secretion of VEGF-A, VEGFR-2 on a tip cell is activated and starts the migration towards the direction of VEGF-A (**Fig. 1.10, b**). The migration process involves producing fine long structures called filopodia (Isogai et al., 2003, Bentley et al., 2009). These filopodia secrete various proteolytic enzymes including MMPs, plasminogen activators, gelatinase, and collagenases, resulting in the degradation of the basement membrane and the extracellular matrix and the detachment of pericytes. Subsequently, the filopodia, covered in VEGFR-2, migrate towards the direction of VEGF-A, and proliferate to produce new endothelial cells called stalk cells (**Fig. 1.10, c**) (Gerhardt et al., 2003). Moreover, in response to VEGFR-2 activation, tip cells express high levels of delta-like ligand 4 (DLL4), preventing neighbouring endothelial cells from becoming tip cells. This process is known as Notch receptor activation on neighbouring endothelial cells. DLL4-expressing tip cells bind to Notch receptors on adjacent stalk cells. The consequent downregulation of VEGFR-2 expression desensitises these cells VEGF-A, preventing their migration. Thereby, Notch signalling suppresses the formation of the tip cell phenotype, inhibiting excessive branching and sprouting angiogenesis (Lobov et al., 2007, Hellström et al., 2007, Suchting et al., 2007) (**Fig. 1.10, d**).

The second step is the “sprout extension” where the stalk continues to proliferate and becomes elongated to form a tube as it navigates closer to the angiogenic centre until VEGFR-2 binds to VEGF-A (**Fig. 1.10, e, and f**). In the final step called “lumen formation”, the two sprouts fuse (**Fig. 1.10, f**), and the luminal space of the sprout connects with the parent vessel. During this step, the recruitment of pericytes and fibroblasts stabilise the endothelial cells by forming the basement

CHAPTER 1

membrane; a step known as pericyte stabilisation (Carmeliet, 2000) (**Fig. 1.10, g**). Blood can now circulate through the newly generated capillary to oxygenate the hypoxic tissue. Once this process is complete, the tissue will stop producing VEGF-A and the homeostatic regulation of angiogenesis will be maintained (Tung et al., 2012, Wacker and Gerhardt, 2011, Eilken and Adams, 2010).

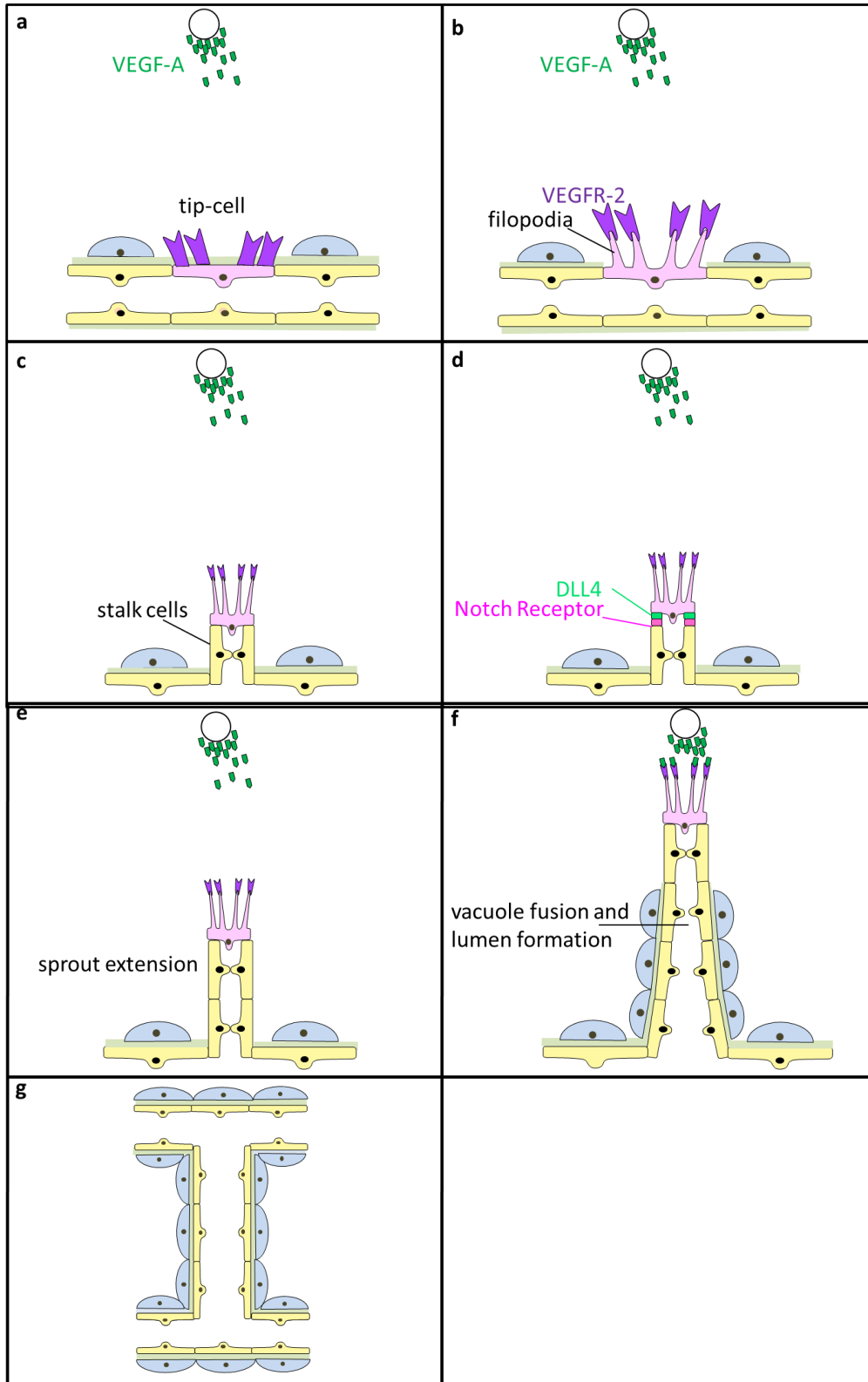


Figure 1.10. Sprouting Angiogenesis. Migration of endothelial cells towards the angiogenic centre (VEGF-A).

CHAPTER 1

(a) Endothelial cells of a capillary, (b) Generation of filopodia, (c) Beginning of Endothelial cells' migration towards VEGF-A due to the VEGFR-2 receptors, (d) degradation of the vascular basement membrane and activation of dormant Endothelial cells,(e) Sprouting and proliferation of Endothelial cells, (f) Protruding and elongation of endothelial cells towards VEGF source, (g) Beginning of lumen formation within the lar tubes, and coverage of vascular tubes with mature vascular basement membrane in association with vascular sprouts, thereby creating a vacuole with supporting pericytes.

1.1.3.2 Splitting Angiogenesis

Splitting or intussusceptive angiogenesis is the process where the capillary wall extends into the lumen and splits a single vessel into two. This less studied process involves a restructuring of existing vascular cells. Rather than new vessel formation, splitting angiogenesis is also responsible for vascular remodeling, which involves branching or pruning of excessive or large microvessels (**Fig. 1. 11**) (De Spiegelaere et al., 2012).

In response to several factors, including oxygen concentration, VEGF concentration, and blood flow, tissue pillars confronting high blood flow, can undergo serial divisions, rapidly splitting the vessels and expanding the microvascular network (Mentzer and Konerding, 2014). In the narrow sense, only these columns that are involved in capillary doubling are considered as an angiogenic mechanism. These pillars are hallmarks of splitting angiogenesis that have been identified in the developing chick chorioallantoic membrane (*ex vivo* models of angiogenesis) (Hlushchuk et al., 2011), chemically-induced murine colitis (Konerding et al., 2010), several tumours (Ribatti and Djonov, 2012), and in skeletal muscle (Hudlicka and Brown, 2009, Egginton et al., 2001).

CHAPTER 1

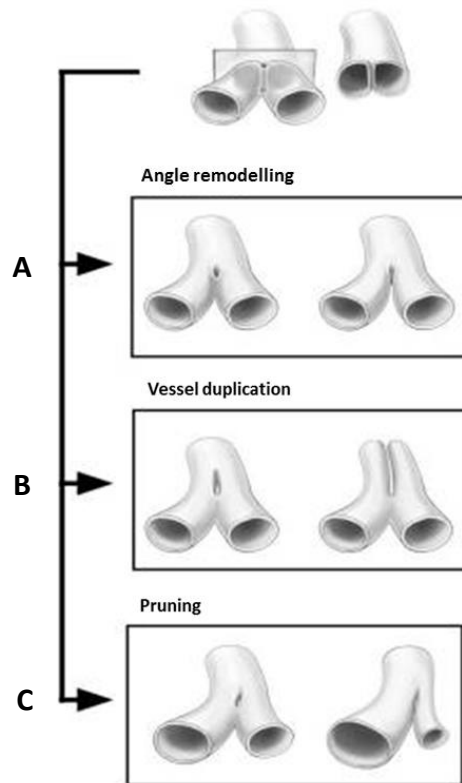


Figure 1.11. Schematic representation of pillar extension resulting in angle remodelling, vessel duplication, or pruning.

(A) The development of the pillar toward the vessel angle results in remodelling of the vessel branching. (B) Extension of the pillar down the axis of the vessel results in vessel duplication. (C) Asymmetric growth of the pillar results in pruning of energetically inefficient vessel. Adapted from Mentzer *et al.*, 2014 (Mentzer and Konerding, 2014), reproduced with permission.

Similar to sprouting angiogenesis, splitting angiogenesis is regulated by inflammatory cytokines and growth factors. VEGF-A and its interaction with VEGFR-2 are the main factors in splitting angiogenesis (De Spiegelaere *et al.*, 2012, Carmeliet, 2005, Carmeliet and Jain, 2011, Wilting *et al.*, 1996, Hellstrom *et al.*, 1999, Crivellato *et al.*, 2004), even though a recent study also suggests a role for VEGFR-1 (Zhan *et al.*, 2018). In contrast to sprouting angiogenesis, shear stress can stimulate splitting angiogenesis (Gianni-Barrera *et al.*, 2011). The consequent eNOS-NO activation leads to vasodilation (D'Amico *et al.*, 2020). This in turn increases the blood flow (shear stress) which is sensed by endothelial cells, promoting splitting angiogenesis (De Spiegelaere *et al.*, 2012, Djonov *et al.*, 2002, Mentzer and Konerding, 2014, D'Amico *et al.*, 2020). Even though numerous growth factors and receptors are involved in splitting angiogenesis, the exact molecular mechanisms remain elusive, in contrast to the well-established sprouting angiogenesis.

CHAPTER 1

The steps involved in splitting angiogenesis are as follows. First, the two opposing capillary walls come into contact to form an inter-endothelial column (Fig. 1.12, a-c). Once the intercellular pillars junctions rearrange and the vessel walls become permeable (Fig. 1.12, d), the pericytes push themselves in between the column, where they produce collagen to form part of the new extracellular matrix (Fig. 1.12, d). Finally, the junctions fuse to the neighbouring ones until the primary capillary is split into two newly formed capillaries, each completely coated by basement membrane and pericytes (Fig. 1.12, e) (De Spiegelaere et al., 2012, Makanya et al., 2009, Gianni-Barrera et al., 2014).

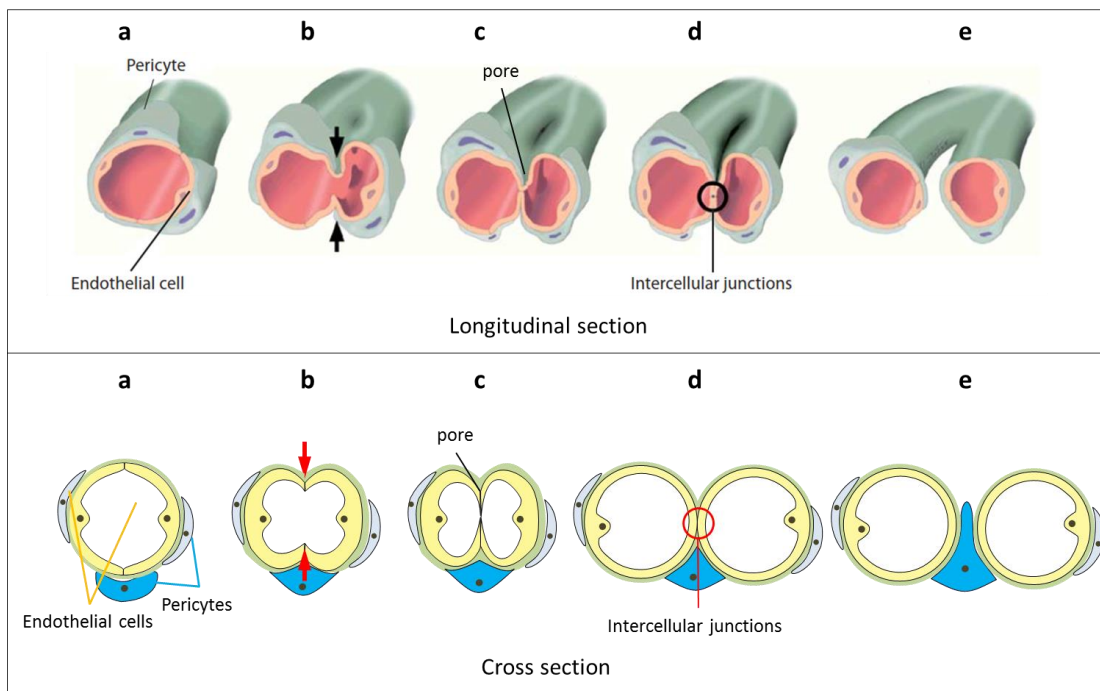


Figure 1.12. Schematic illustration of a small capillary undergoing splitting angiogenesis.

Sprouting angiogenesis initiates by activation of a small capillary surrounded by pericytes (a). The opposite walls of two capillaries start to migrate to each other (b) and an inter-endothelial column is formed (c). The intercellular junctions of the opposing endothelial cells are rearranged (d). Subsequently, further growth of the junctions leads to the spitting of the primary blood vessel into two newly formed vessels (e). Adapted from De Spiegelaere *et al.*, 2012 (De Spiegelaere et al., 2012).

Notch signalling is also thought to be activated in splitting angiogenesis (Gianni-Barrera et al., 2011). Since during splitting angiogenesis, vessels growth is limited to circumferential enlargement, the phenotype is expected to be limited to stalk cells only (no tip cells and thus no sprouting). Therefore, it is hypothesised that alternative Notch activation could determine which angiogenesis mode is activated (Gianni-Barrera et al., 2011). Further research is required for a thorough understanding of the Notch signalling role in this context.

CHAPTER 1

Taken together, various studies have demonstrated the complementary role of sprouting and splitting angiogenesis processes, which may draw the common pattern of angiogenic response to a hypoxic or an ischemic situation. In this pattern, *in vivo* sprouting angiogenesis is initiated within a VEGF-A gradient field (Uccelli et al., 2019), when endothelial cells detect hypoxia in the surrounding tissue that demands new blood vessel formation to meet their metabolic demand. This process is followed by splitting angiogenesis in order to develop the newly generated capillaries (Makanya et al., 2007, Djonov et al., 2001, Schlatter et al., 1997, Gianni-Barrera et al., 2011). However, there are situations where only splitting angiogenesis takes place. This has been observed in skeletal muscle contraction during exercise (Gianni-Barrera et al., 2013, Hudlicka and Brown, 2009, Egginton et al., 1998, Ogawa, 1977). Notably, increased blood flow forces can trigger splitting angiogenesis while sprouting starts in vessels with interstitial flow and the absence of shear stress, and is triggered by overexpression of VEGF-A (Campinho et al., 2020, Mentzer and Konerding, 2014, Zhan et al., 2018, Gerhardt et al., 2003, Gianni-Barrera et al., 2011, Ruhrberg et al., 2002). Nevertheless, uncertainty remains with respect to distinct initiating events underlying the sprouting or splitting angiogenesis. Furthermore, the majority of studies on angiogenesis have been performed on sprouting angiogenesis. Therefore, in this study, the term angiogenesis is referred to sprouting angiogenesis as the fundamental and general mechanism of vessel formation.

1.2 Regulation of angiogenesis

1.2.1 Introduction

Several factors can turn angiogenesis on (angiogenic stimulators) or off (angiogenic inhibitors) (Jain, 2003, Carmeliet and Jain, 2011). These angiogenic regulators, originally called “angiogenic factors” by Dr. Judah Folkman 50 years ago, include growth factors, cytokines and chemokines, angiogenic enzymes, and endothelial-specific receptors.

Under basal conditions, the balance of production of angiogenic stimulators and inhibitors remains in equilibrium. In this situation, the angiogenic switch is off (**Fig. 1.13, A**). However, in response to an increase in local metabolic demand, the angiogenic switch is on as the activity of angiogenic stimulators outweighs angiogenic inhibitors (**Fig. 1.13, B**) (Liekens et al., 2001). This can occur during both physiological and pathological conditions. During physiological angiogenesis, the increased activity of angiogenic stimulators is tightly controlled, leading to the division and extension of a quiescent monolayer of endothelial cells, only to an extent that the growing tissue requires (Papetti and Herman, 2002). Notably, this regulated process has two hallmarks. Firstly, it is brief and short-lived, and secondly, the newly generated capillaries will either regress (such as in wound healing), or progress to become established microvessels (such as in embryonic development).

However, during pathological angiogenesis, in response to chronic metabolic demand, there is a sustained increase in angiogenic stimulator activity which leads to uncontrolled, excessive, and rapid endothelial cell proliferation that may persist for months or years (Maloy and Hughes, 2013). These fast-growing microvessels have thinner walls, disturbed basement membrane, with sparse or no pericytes (Maloy and Hughes, 2013, Carmeliet, 2005). This occurs, for instance, in solid tumours, proliferative retinopathies (such as age-related macular degeneration, or diabetic retinopathy), rheumatoid arthritis, obesity, and atherosclerosis (Gariano and Gardner, 2005, Pepper, 1997).

Alternatively, overproduction of angiogenic inhibitors and reduced angiogenic signalling, or reduced VEGF levels, can lead to insufficient angiogenesis and capillary regression (**Fig. 1.13, C**) (Bisht et al., 2010). This condition is characteristic of conditions such as coronary heart disease, postpartum cardiomyopathy, peripheral vascular disease, delayed ulcers or wound healing, pulmonary fibrosis, hypertension, osteoporosis, respiratory distress, pre-eclampsia, endometriosis, ovarian hyperstimulation syndrome, stroke, age-related diseases such as

CHAPTER 1

nephropathy or bone loss, and neurodegenerative diseases (Bisht et al., 2010, Greenberg and Jin, 2005, Carmeliet, 2003, Carmeliet, 2005). Pathologies characterised by suppressed angiogenesis are not the focus of this thesis and therefore are not discussed further.

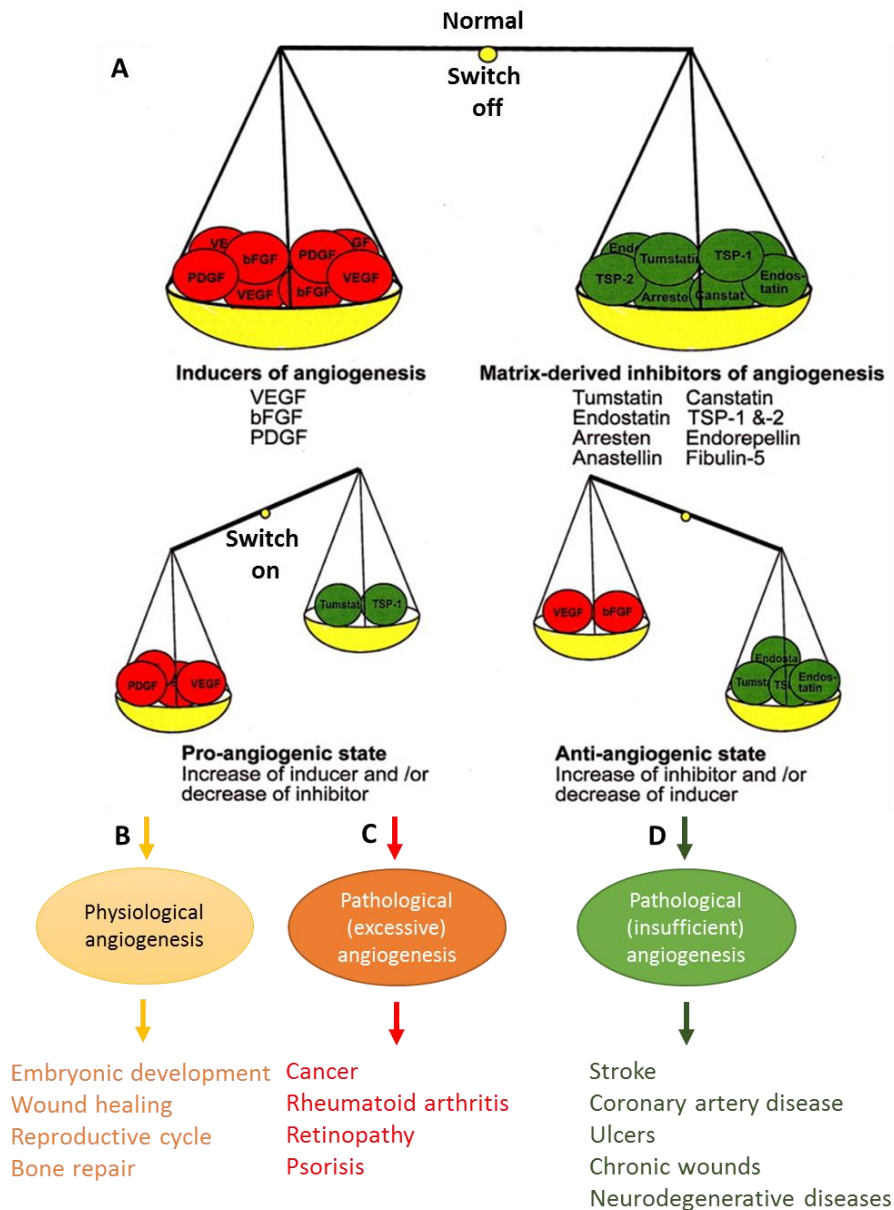


Figure 1.13. Schematic illustration of the angiogenic balance. Angiogenic stimulators and inhibitors in the control of the angiogenic switch.

(A) Under normal condition, angiogenic switch is off and pro- and anti-angiogenic factors are in balance. Angiogenesis occurs when the total activity of pro-angiogenic factors exceeds that of the anti-angiogenic factors. Therefore, the balance is switched to favour angiogenesis. Adapted from D'Andrea *et al.* (D'Andrea et al., 2010). The lower portion describes two types of angiogenesis i.e., physiological (B), and pathological (C), and a hypothetical model proposed for targeting tumour angiogenesis and escaping physiological angiogenesis through decoding the angiogenic switch (D). Adapted from Sund *et al.*, 2005 (Sund et al., 2005), reproduced with permission.

1.2.2 Endogenous inhibitors of angiogenesis

Many endogenous inhibitors of angiogenesis are products of enzymatic digestion of extracellular matrix, known as endogenous matrix-derived angiogenic inhibitors. The latter include endostatin and tumostatin (fragments of collagen), thrombospondins, fibulin, and fibronectin (**see Table 1.1**).

Another class of inhibitors includes growth factors and cytokines such as interferons (typically released during virus infection), interleukins, pigment epithelium-derived factor (PEDF), angiostatin, and platelet factor-4 (fragments of coagulation factors). There are other unclassified factors including Tissue inhibitors of metalloproteinases (TIMPs) (controlling the activity of enzymes responsible for the degradation of the extracellular matrix), methoxyestradiol, peroxins, troponin, and vasostatin.

More recently, a new class of molecules has been identified in the category of microRNAs (miRNAs) (Kumar et al., 2012, Suárez and Sessa, 2009). These short non-coding RNAs (about 22 nucleotides) can degrade mRNA transcripts, thus, preventing their translation, with consequent inhibition of gene expression (Cannell et al., 2008). Anti-angiogenic miRNAs, such as miR-126 and miR-221/222, are highly expressed in endothelial cells and downregulate multiple pro-angiogenic factors, decreasing endothelial cell migration, proliferation, and formation of new capillaries (Leone et al., 2019). However, miRNAs can also act as pro-angiogenic factors (Leone et al., 2019, Wang et al., 2018).

Moreover, some analogues of L-arginine, ADMA (asymmetric dimethylarginine), L-NAME (N^G-nitro-L-arginine methyl ester), and L-NMMA (N^G-monomethyl-L-arginine), are endogenous NOS inhibitors (Vallance and Leiper, 2004) that have been shown to inhibit angiogenesis *in vitro*, either by directly decreasing NO[•] biosynthesis or by affecting other pro- or anti-angiogenic factors (Wojciak-Stothard et al., 2007, Vanella et al., 2011, Wang et al., 2016).

1.2.3 Endogenous stimulators of angiogenesis

Endogenous stimulators of angiogenesis include a diverse range of proteins, growth factors (such as VEGF and PDGF, TNF, angiogenin, angiopoietin, MMPs, and NOSs (**see Tale1.1**) (Folkman, 1995, Pugh and Ratcliffe, 2003). Furthermore, angiogenic stimulants can increase the expression of several miRNAs; miR-21, miR-155, MiR-566, miR-210 are well-known angiogenic promoter miRNAs, activating pro-angiogenic signalling pathways, thus expressing pro-angiogenic proteins that ultimately increase proliferation, invasion, migration, and tube formation (Leone et al., 2019, Wang et al., 2018).

CHAPTER 1

Table 1.1. Selected list of endogenous pro- and anti-angiogenic factors.

Endogenous Pro-Angiogenic Factors	Endogenous Anti-Angiogenic Factors
Angiogenin transforming growth factor	Angiostatin
Angiopoietin	Anti-thrombin
Angiotropin	Arresten
Fibroblast growth factor (FGF)	Canstatin
Hepatocyte growth factor	Collagen
Tubulin proteins	Endostatin
Matrix metalloproteinase (MMPs)	Fibronectin fragment
Cyclooxygenase 2(COX-2)	Fibulin
Platelet-derived growth factor (PDGF)	Interferons
Tumour necrosis factor (TNF)	Interleukins
Proliferin	L-Arginine analogues (ADMA, L-NMMA, L-NAME)
Vascular endothelial growth factor (VEGF)	Pigment epithelium derived factor (PEDF)
Placental growth factor	Platelet factor-4
Interlukin 8 (IL-8)	Prolactin fragments
Hypoxia-inducible factor (HIF)	PEX
P53	Tissue inhibitors of matrix metalloproteinases (TIMPs)
	Thrombospondin-1 and 2
	Troponin I
	Vasostatin

1.2.3.1 Hypoxia-induced angiogenesis

The ultimate purpose of angiogenesis is to deliver oxygen to oxygen-demanding tissues. In other words, oxygenation determines microvascular growth or regression. This is due to the limited intracellular storage of oxygen compared to other metabolic substances such as glucose, amino acids, or fatty acids. Oxygen requirement is even more compelling for tumour cells. When primary tumours start to grow larger than 1mm³ in diameter, they develop hypoxic areas; hence, there is an urgent need for oxygen supply. As a result, their survival, growth, and ultimately metastasis are dependent upon angiogenesis (Carmeliet, 2000). Therefore, it is not surprising that oxygen is the master regulator of physiological and pathological angiogenesis (Adair and Montani, 2010).

In adults, physiological or pathological angiogenesis is mediated by multiple genetic and environmental factors, but mainly initiated by tissue hypoxia. This is a condition where oxygen levels in organs, tissues, or cells drop to 0.5 - 3%, relative to the physiological concentration of O₂ (Carreau et al., 2011). This could be the result of reduced oxygen supply (due to insufficient blood vessels or red blood cells carrying O₂), or an imbalance between oxygen supply and consumption (due to a sudden cell growth rate such as in solid tumours (Muz et al., 2015)).

Hypoxia stimulates angiogenesis via VEGF upregulation, primarily through hypoxia-inducible factor-1 (HIF-1). HIF-1 protein is a key regulator of oxygen homeostasis within cells. As a transcription factor, it regulates the expression of several genes involved in maintaining homeostasis according to changes to oxygen concentrations (Ziello et al., 2007). HIF-1, as a

CHAPTER 1

hallmark of hypoxia, is a heterodimer made of two different protein subunits: HIF-1 α and HIF-1 β , where the complete dimer complex within the nucleus is required for its stabilisation and activity (Wang and Semenza, 1995).

Under normal oxygen conditions (normoxia), oxygen-dependent hydroxylation of HIF-1 α allows binding of a tumour suppressor protein called Von Hippel–Lindau protein (pVHL), leading to HIF-1 α ubiquitination and degradation. Therefore, instead of the complete heterodimer formation, only HIF-1 β is present in the nucleus, resulting in HIF-1 instability and degradation (**Fig. 1.14, a**). In addition to the pVHL negative regulation, HIF-1 is also post-translationally modulated by the C-terminal transactivation domain (C-TAD). C-TAD hydroxylates HIF-1 under normoxia which blocks the interaction between the two domains of HIF-1, causing gene inactivation (Dann et al., 2002) (**Fig. 1.14, b**). In contrast, when cells become hypoxic, HIF-1 α escapes the above degradation and binds to HIF-1 β to form the active HIF-1 complex. In the nucleus, the HIF-1 complex hits the transcription factor, acting as a gene expression enhancer or repressor (**Fig. 1.14, c**).

In the endothelium, HIF-1 α is the master transcriptional regulator of various genes involved in different steps of angiogenesis and oxygen transport (Semenza, 2000). Most importantly, HIF-1 α expression directly upregulates the expression of the most potent angiogenic promoter, VEGF-A, and its receptor, VEGFR-2. This activates the HIF-1 α /VEGF pathway which is essential for endothelial cell survival, growth, migration, and tube formation (Krock et al., 2011). Other important examples of pro-angiogenic genes regulated by HIF-1 α include NOS (regulating vascular tone), FGF, and genes involved in matrix metabolism such as MMPs (Pugh and Ratcliffe, 2003). Accordingly, hypoxia and HIF-1 α activation induce the production of these angiogenic factors which ultimately increase angiogenesis.

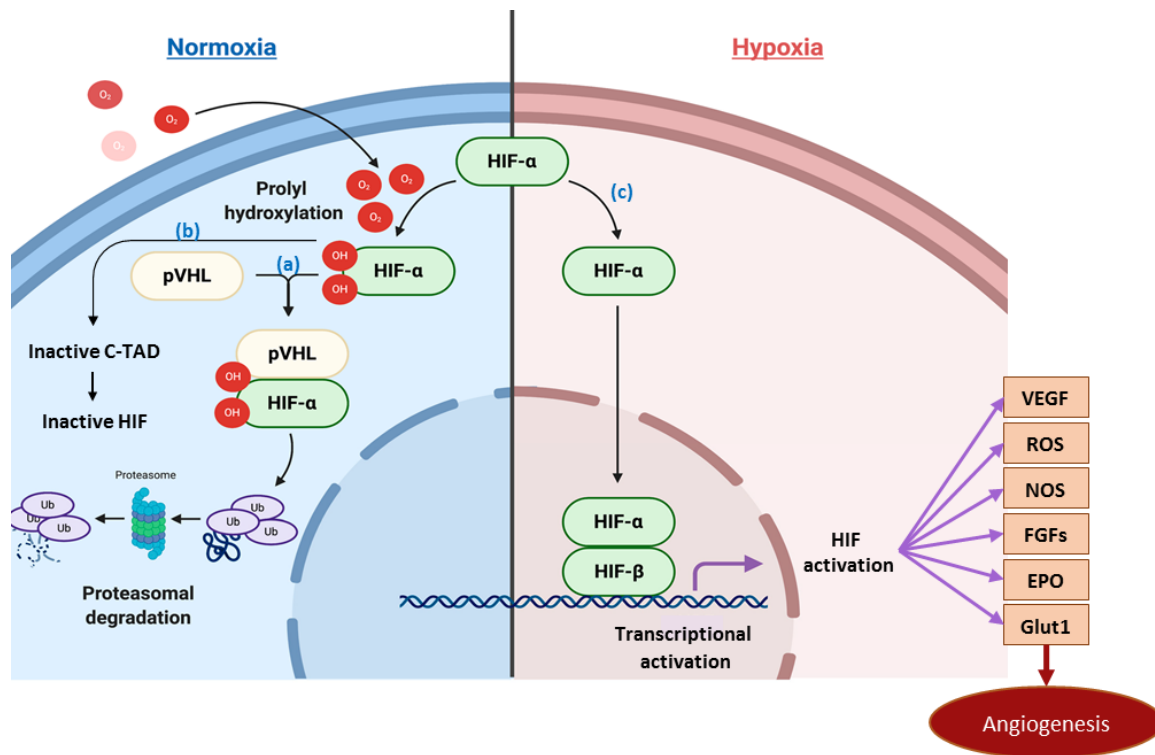


Figure 1.14. HIF-1 α activity under hypoxia versus normoxia.

Left: Under normoxia, HIF-1 α is inactivated via (a) Proteasomal degradation or (b) specific C-TAD inhibition. Right: Under hypoxia, HIF-1 α is dimerised and activated, thereby activating hypoxia-induced genes (c). Adapted from Vito *et al.*, 2020 (Vito *et al.*, 2020), reproduced with permission.

NO is also involved in angiogenesis. However, previous research has shown contradictory results as to whether hypoxia upregulates (Strijdom *et al.*, 2006, Justice *et al.*, 2000, Chen and Meyrick, 2004), or downregulates NO production (Takemoto *et al.*, 2002, McQuillan *et al.*, 1994). In some studies, hypoxia activated eNOS and increased NO production in endothelial cells in a time-dependent manner via heat shock protein 90 (Hsp90) and PI3K/Akt pathways (Chen and Meyrick, 2004). However, other studies reported eNOS inhibition in hypoxic endothelial cells via transcriptional and post-transcriptional mechanisms (McQuillan *et al.*, 1994), and Rho protein kinase (Takemoto *et al.*, 2002).

Another important mechanism regulated by VEGF under hypoxia is adenosine. Under hypoxia, the major source of adenosine is by dephosphorylation of adenosine monophosphate (AMP). Adenosine activates a family of adenosine receptors (A_1 , A_{2A} , A_{2B} , and A_3), enhancing eNOS activation, NO formation, and finally VEGF upregulation, leading to adenosine-induced angiogenesis (Escudero *et al.*, 2014, Adair, 2004). Nevertheless, the pro-angiogenic role of

CHAPTER 1

adenosine can also occur independently of VEGF-A. However, the exact mechanisms involved are not established yet (Adair, 2004).

Furthermore, AMP-dependent kinase (AMPK) is a stress-activated protein kinase that is activated by an increase in AMP/ATP ratio. Activated AMPK by hypoxia or other cellular stresses (e.g. oxidative stress) upregulates VEGF and stimulates angiogenesis. This process has been observed in ischemic conditions (Ouchi et al., 2005, Fraisl et al., 2009). Nevertheless, both pro- and anti-angiogenic effects have been observed for AMPK (Li et al., 2019). On the one hand, AMPK activation regulates stress responses to facilitate autophagy, leading to stabilisation of HIF-1 α , thereby VEGF overexpression and angiogenesis upregulation. On the other hand, AMPK can inhibit angiogenesis induced through signalling pathways such as PI3K/Akt/mTOR (Li et al., 2019).

In addition to regulating well-known pro-angiogenic molecules, hypoxia and HIF stimulate several miRNAs, which themselves are chief mediators of several genes. Hypoxia-driven HIF-1 α targets miRNAs with pro-angiogenic effects, e.g. miR-210, promoting endothelial cell migration and proliferation (Krock et al., 2011). On the other hand, some other miRNAs have shown anti-angiogenic effects *in vitro* by downregulating VEGF, including miR-125a, miR-15b, miR-16, miR-20a, and miR-20b. Hypoxia has been shown to suppress these miRNAs, thereby enhancing angiogenesis (Hua et al., 2006).

Several studies have demonstrated hypoxia-induced angiogenesis via generation of reactive oxygen species (ROS) in both physiological and pathological conditions (Hielscher and Gerecht, 2015, Devasagayam et al., 2004, Dworakowski et al., 2006).

ROS are key signalling molecules in the progression of inflammation. These molecules are natural by-products of oxygen metabolism (such as superoxide anion (O₂⁻), hydroxyl (OH⁻), and other oxidants) *in vivo* (Hayyan et al., 2016). Furthermore, due to the unpaired electrons in these free radicals, they are highly reactive and act as a double-edged sword in vascular biology. If these pro-oxidants are produced in high amounts, they are cytotoxic and mutagenic, causing oxidative stress which can damage DNA, RNA, or proteins (Reuter et al., 2010). In contrast, low levels of ROS regulate the activity of various intracellular signalling molecules and transcription factors, including pro-angiogenic, initiating endothelial cell migration and proliferation (**Fig. 1.16**) (Griendling, 2004, Zhao et al., 2009, Li and Shah, 2004). All vascular cell types, including the endothelium, can produce ROS. Increasing evidence suggests that the mechanism of oxidative

CHAPTER 1

stress-induced angiogenesis (also known as ROS-mediated angiogenesis) is highly regulated by HIF/VEGF/VEGFR expression and signalling (Xia et al., 2007).

A range of mechanisms may lead to hypoxia-induced ROS generation and angiogenesis, including HIF-1 α stabilisation (Hypoxia/ROS/HIF-1 α pathway) (Hielscher and Gerecht, 2015). Apart from the primary oxygen-binding mechanism of HIF-1 α activation, hypoxia can increase ROS via electron transfer in mitochondria (**Fig. 1.15, left**) (Guzy and Schumacker, 2006, Hamanaka and Chandel, 2009). Mitochondrial-derived ROS can activate pro-angiogenic factors (including VEGF) or other VEGF-independent intracellular pathways leading to tumour growth and angiogenesis (**Fig. 1.15**) (Hielscher and Gerecht, 2015). As an example, mitochondrial ROS has been shown to stimulate the expression of a transcription factor, NF- κ B (redox-sensitive nuclear factor -kappaB), involved in cell proliferation, angiogenesis, and tumour metastasis (Lluis et al., 2007). However, it is not yet clear whether this mechanism is VEGF-dependent or -independent (Hielscher and Gerecht, 2015). Moreover, miRNAs (miR-210) have also shown to be regulated by the hypoxia/ROS/HIF-1 α pathway (Favaro et al., 2010, Tong and Rouault, 2000).

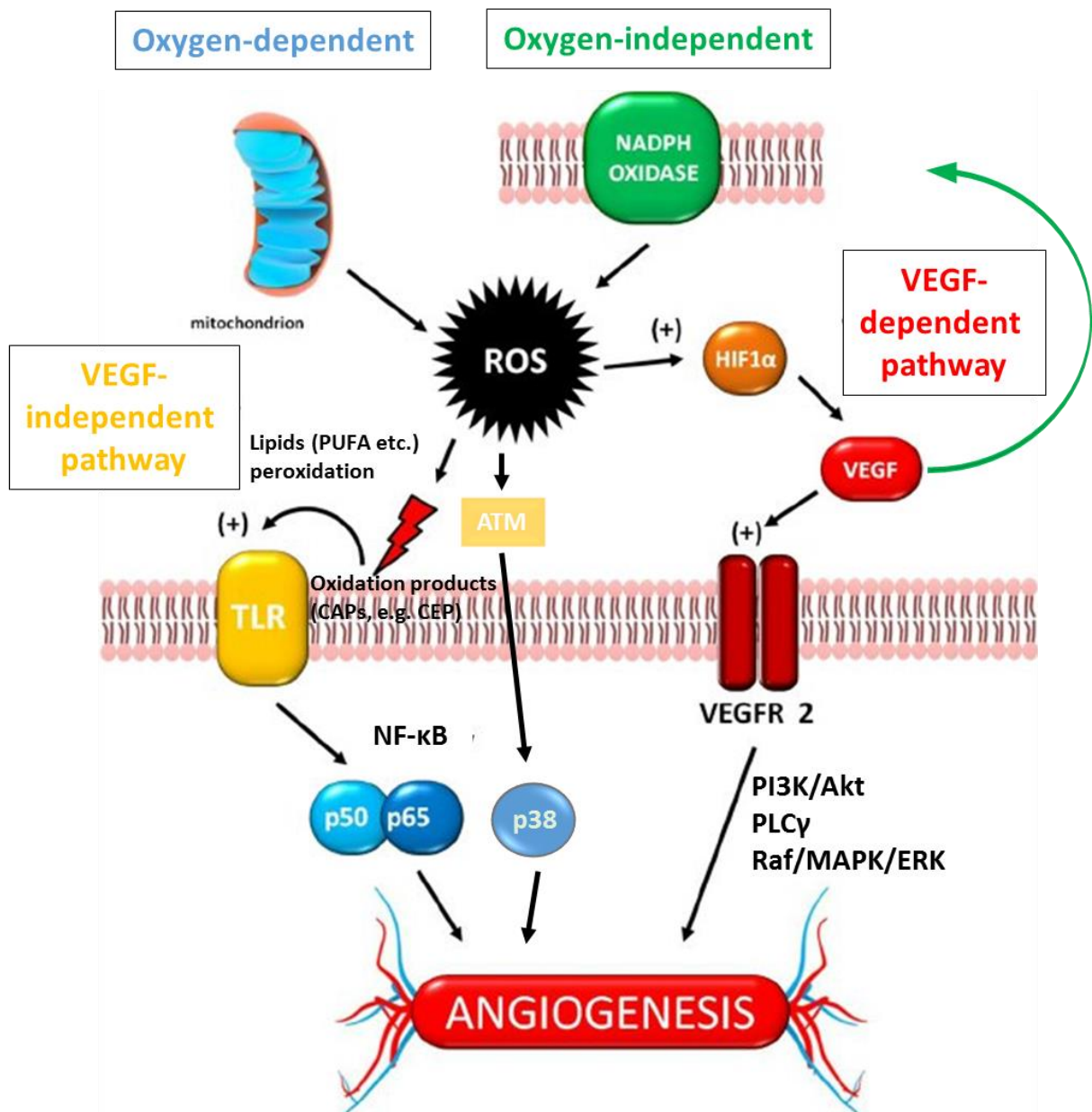


Figure 1.15. Oxidative stress (ROS generation) and angiogenesis.

ROS, generated through two main sources, mitochondria and NADPH oxidase, triggers angiogenesis via two main mechanisms: VEGF-dependent pathway via HIF- VEGF/VEGFR-2 signalling, or VEGF-independent pathway involving lipid oxidation products, Toll Like Receptor (TLR) and NF-κB pathway, and Ataxia-telangiectasia mutated (ATM). Adapted from Sanhueza *et al.*, 2015 (Sanhueza et al., 2015), and Xian *et al.*, 2019 (Xian et al., 2019), reproduced with permission.

1.2.3.2 Hypoxia-independent angiogenesis

Despite the critical role of hypoxia in angiogenesis as the principal regulatory factor for HIF-1α activation, several hypoxia-independent processes also impact on HIF-1α protein levels, stability and function, and consequently VEGF signalling.

1.2.3.2.1 HIF/VEGF-dependent pathways

Under normoxic conditions, multiple growth factors, cytokines, and chemokines can upregulate angiogenesis via overexpression of the HIF-1 α /VEGF/VEGFR-2 pathway (Masoud and Li, 2015, Xian et al., 2019).

VEGF is essential for physiological and pathological angiogenesis and is influenced by ROS (Ushio-Fukai and Alexander, 2004). ROS-driven VEGF/VEGFR-2 activation is one of the main mechanisms involved in many vascular-related pathologies, such as vascular injuries (Kim and Byzova, 2014). Apart from the mitochondrial generation of ROS during hypoxia, many studies have shown that under normoxia, NADPH oxidases (NOX) and eNOS uncoupling are the major sources of vascular ROS, generating superoxide oxide (O₂⁻) instead of peroxide or NO, respectively (Ushio-Fukai and Alexander, 2004). Moreover, NOX-derived ROS upregulates the expression of VEGF and FGF, adhesion molecules, cytokines, and MMPs via activation of the MAPK and/or NF- κ B pathway, leading to the degradation of the basement membrane, and consequently promoting endothelial cell migration and angiogenesis (Zhao et al., 2009). On the other hand, VEGF itself can also act upstream to ROS and further stimulate angiogenesis via activation of NADPH oxidase in endothelial cells (**Fig. 1.15**) (Ushio-Fukai and Alexander, 2004). Therefore, ROS interaction with VEGF, whether upstream or downstream, regulates angiogenesis.

Endothelial-derived-NO, as a type of ROS, is a major contributor to angiogenesis, specifically endothelial-derived NO. VEGF enhances the synthesis of endothelial-derived NO via activating the Ca²⁺-calmodulin/Akt pathway, the protein kinase C (PKC) pathway, and the PI3K-Akt pathway, leading to endothelial cell proliferation, migration, and angiogenesis (**Fig. 1.16**) (Dulak et al., 2000, Xian et al., 2019, Murohara et al., 1999, Ziche et al., 1997b). Reciprocally, NO also modulates VEGF, even though contradictory reports exist in the literature regarding the positive or negative regulation of VEGF by NO; while several studies found upregulation of VEGF by NO through different pathways, including HIF-1 α activation, (60, 62, 91, 92) (Dulak et al., 2000), other reports showed downregulation of VEGF and HIF-1 α by NO, under the influence of a potent NO donor (sodium nitroprusside (SNP)) (Tsurumi et al., 1997, Ghiso et al., 1999). These conflicting data are believed to be associated with different NO concentrations (Kimura and Esumi, 2003). Low levels of NO, mainly generated by eNOS, stimulate VEGF expression via the HIF-1 pathway. However, high amounts of NO, produced by iNOS in macrophages and tumour cells, inhibit VEGF (Kimura and Esumi, 2003). Nevertheless, the negative feedback of iNOS-derived NO on VEGF expression is likely overcome by the significant hypoxia-mediated HIF-1 activity in tumours (Kimura and Esumi,

2003). Interestingly, some studies have also demonstrated a direct pro-angiogenic effect of NO, in absence of VEGF or other growth factors (Babaei and Stewart, 2002).

Furthermore, ROS accumulation facilitates the oxidation of low-density lipoproteins (OxLDL) in the vascular wall. OxLDL strongly stimulates HIF-1 α and VEGF, and consequently angiogenesis (**Fig. 1.16**) (Xian et al., 2019). OxLDL is known to be an early event in atherosclerosis (Leiva et al., 2015). ROS-activated VEGF/VEGFR-2 via HIF-1 α upregulation (and regardless of oxygen levels), allows activation of multiple intracellular signalling pathways via phosphorylation and activation of downstream kinases (Sang et al., 2003, Minet et al., 2000). These signalling pathways include phospholipase C gamma (PLC γ) and PI3K/Akt/mTOR, which further stimulates the Ras/Raf/MEK/ERK (also known as MAPK) pathway. These signalling pathways are involved in cell survival, apoptosis, proliferation, migration, inflammation, and angiogenesis (Agani and Jiang, 2013, Xian et al., 2019) (**Fig. 1.16**).

Other metabolic regulators also play a critical role in regulating angiogenesis in a VEGF-dependent manner, regardless of oxygen levels (Fraisl et al., 2009). Examples include PGC-1 α , a regulator of mitochondrial biogenesis in cells, that induces HIF-1 α and VEGF-A expression via interaction with estrogen-related receptor- α (ERR- α), thereby stimulating angiogenesis (Fraisl et al., 2009). In addition, adipokines, such as leptin and adiponectin, also affect angiogenesis. While leptin stimulates angiogenesis via inducing VEGF and FGF2, adiponectin can act both as an angiogenic stimulator or inhibitor, by increasing eNOS activity involving VEGF-A, or inducing endothelial cell apoptosis respectively (Fraisl et al., 2009, Ouchi et al., 2004). Peroxisome proliferator-activated receptors (PPARs) also modulate angiogenesis. Of the three isoforms of PPARs, the PPAR α isoform inhibits angiogenesis by direct or indirect downregulation of VEGF or VEGFR-2, but also by increasing thrombospondin-1 (TSP-1) and other angiogenic inhibitors. Similarly, PPAR γ (a regulator of adipose development and insulin sensitivity) inhibits angiogenesis but the mechanism is not clear (Fraisl et al., 2009). On the contrary, the PPAR β isoform, a lipid oxidation regulator, stimulates capillary maturation and proliferation via increasing VEGF (Fraisl et al., 2009).

Another example of HIF-regulation of angiogenesis, independent of oxygen levels, is via heat shock protein 90 (Hsp90). Hsp90 is a chaperon protein that stabilises proteins against heat shock and helps in protein folding, maturation, and degradation (Hoter et al., 2018). The mechanism of action in angiogenesis involves the binding to HIF-1 α and consequent dimerisation with HIF-1 β , leading to HIF-1 stability (Isaacs et al., 2002).

CHAPTER 1

Interleukins (ILs) cause NF- κ B activation. As such, IL-6, a proinflammatory cytokine, increases VEGF, promoting angiogenesis in gastric carcinoma (Huang et al., 2004).

Forkhead box O transcription factors (Foxo), a family of proteins that play an important role in cell-cycle arrest, DNA repair, and apoptosis, have shown a conflicting role in angiogenesis. Foxo1 and Foxo3 are activated during fasting, increasing the expression of genes involved in lipid-oxidation (Fraisl et al., 2009). While Foxo1 downregulation disrupts angiogenesis during development, Foxo3 suppression in adults has been shown to increase endothelial cell migration and tube formation *in vitro* and *in vivo* (Potente et al., 2005). Overall, however, Foxo members have been shown to inhibit angiogenesis *in vivo* (Fraisl et al., 2009).

Mechanical forces such as shear stress can also stimulate angiogenesis. Mechanosensitive cation channels, such as calcium-potassium (KCa) channels, are sensitive to shear fluctuations. Shear stress activates these channels and triggers eNOS, and thus NO production, which has critical functions in angiogenesis (Sewduth and Santoro, 2016).

1.2.3.2.2 HIF/VEGF-independent pathways

While VEGF is typically activated during both physiological and pathological angiogenesis, the latter appears to be closely associated with inflammatory processes and subsequent ROS generation and oxidative stress (Kim et al., 2013).

Recent studies have identified ROS as a chief mediator of several HIF/VEGF-independent pathways to stimulate angiogenesis, particularly the carboxyethylpyrrole (CEP) and the ataxia-telangiectasia mutated (ATM) pathways (Kim et al., 2013, Kim and Byzova, 2014, Xian et al., 2019).

Another angiogenesis mechanism that is ROS-mediated and VEGF-independent is the oxidation of lipids such as polyunsaturated fatty acids (PUFAs), present within membrane phospholipids (Gueraud et al., 2010, Negre-Salvayre et al., 2010). An important PUFA phospholipid is docosahexaenoic acid (DHA), a highly abundant fatty acid in many human tissues, especially the retina and the brain. PUFA is oxidised by ROS at the sites of injury or inflammation with the consequent generation of CEP (the main family member of carboxyalkyl pyrrole (CAP) proteins) (Kim et al., 2013). CEPs are important biomarkers for oxidative stress-induced angiogenesis in wound-healing and also in several pathologies such as age-related macular degeneration (AMD) or tumours (Kim and Byzova, 2014). CEPs activate Toll-like receptors (TLRs), a family of protein receptors expressed in the innate immune system (on leukocytes membrane) but also in non-

immune cells (such as fibroblasts, epithelial and endothelial cells) (**Fig. 1.15 and 1.16**) (Kim and Byzova, 2014). Studies have shown a significant association between the TLR pathway and oxidative driven-driven angiogenesis, where NF- κ B plays a critical role. Well-known pro-angiogenic ligands of TLRs on endothelial cells, including CEP, lipopolysaccharide (LPS), and macrophage-activating lipopeptide-2 (MALP2), stimulate angiogenesis through different VEGF-independent pathways as shown in **Fig. 1.16**. (Kim et al., 2013, Xian et al., 2019).

ROS also stimulate the production of the protein kinase ATM to regulate angiogenesis (Xian et al., 2019). This serine-threonine kinase is involved in DNA damage repair and cell cycle regulation. Unlike the CEP-TLR pathway, the role of the ATM pathway is limited to pathological angiogenesis and only affects endothelial cells via the p38 pathway (**Fig. 1.15 and 1.16**) (Xian et al., 2019).

Another oxidative stress-driven factor, PDGF (known to be essential for wound healing), is activated by H_2O_2 and upregulates angiogenesis in a VEGF-independent manner. The mechanism of action of PDFG is via the PI3K/Akt and MAPK pathways, also used by VEGF-dependent factors (**Fig. 1.15**) (Xian et al., 2019).

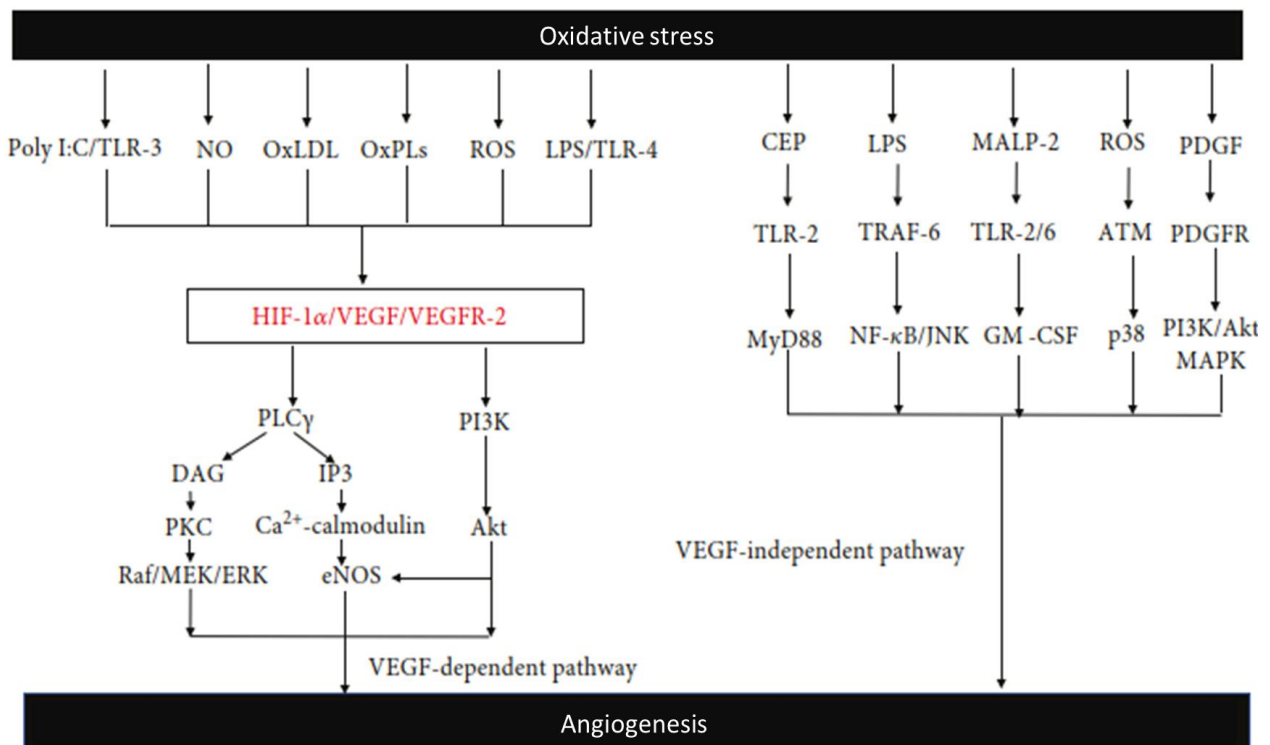


Figure 1.16. Schematic diagram of angiogenesis signalling pathways regulated by oxidative stress.

In response to oxidative stress, two main signalling pathways are described: VEGF-dependent, and VEGF-independent signalling pathway. (Left) In the VEGF-dependent pathway, oxidative stress causes Poly I:C, ROS, NO, OxLDL, OxPLs, and LPS to stimulate HIF-1 α /VEGF/VEGFR-2 pathway and induce angiogenesis. (Right) In the VEGF-independent pathway, oxidative stress induces other mediators including CEP, LPS, MALP-2, ROS, and PDGF. Once coupled to their

CHAPTER 1

receptors, or activate their downstream mediator targets, they promote angiogenesis, Adapted from Xian *et al.*, 2019 (Xian et al., 2019), reproduced with permission.

Studies have shown a positive feedback loop between angiogenesis and oxidative stress. Newly generated blood vessels enhance the recruitment of inflammatory cells that generate pro-angiogenic factors. This leads to further angiogenesis stimulation, which again triggers inflammation and oxidative stress until it becomes a chronic process (Kim et al., 2013).

1.3 Inhibiting pathological angiogenesis

1.3.1 Introduction

Angiogenesis has become an attractive goal for drug therapy given its significant contribution to the development of pathologies such as proliferative diabetic retinopathy, AMD (Paulus and Sodhi, 2016), obesity (Lemoine et al., 2013), psoriasis (Xian et al., 2019), atherosclerosis (Kimura et al., 2007, Jain et al., 2007) and several solid tumours (Rajabi and Mousa, 2017, Keefe et al., 2011, Jászai and Schmidt, 2019).

The idea of inhibiting angiogenesis as a therapeutic target was initially suggested by Dr. Judah Folkman in cancer (Folkman, 1971). His laboratory then introduced the first anti-angiogenic agent, interferon- α (IFN- α) in 1980 (Folkman, 2007), based on the assumption that angiogenesis inhibition can exert anti-cancer effects by preventing the access of cancer cells to oxygen and nutrients. In addition, blocking angiogenesis could effectively prevent tumour cell metastasis (Shih and Lindley, 2006).

1.3.2 Current clinical anti-angiogenic inhibitors, and their pros and cons

Anti-angiogenesis agents are categorised into seven major groups:

1. Monoclonal antibodies (mAbs) (more importantly anti-VEGFs)
2. Micro RNAs (miRNAs) / small interfering RNAs (siRNAs)
3. Aptamers
4. Gene therapy
5. Small molecules
6. Angiostatin / Endostatin
7. Chimeric antigen receptor T cells (CAR-T) therapy

The clinical application of these therapies is described in **Table 1.2** and the following sections.

Table 1.2. Antiangiogenic therapies and clinical applications.

Reproduced from Fallah *et al.*, 2019 (Fallah et al., 2019). Copyright © 2019, Elsevier Masson SAS. All rights reserved.

Anti-angiogenic therapies	Clinical names and applications
Monoclonal antibodies (mAbs)	Bevacizumab (Avastin®) an anti-VEGF-A ₁₆₅ mAb (Ferrara and Adamis, 2016) for solid tumours (Shih and Lindley, 2006), diabetic retinopathy (Avery et al., 2006), Cetuximab for tumours (Zhang et al., 2007), Ranibizumab (an anti-VEGF antigen binding fragment) for AMD (Ferrara et al., 2006) and diabetic retinopathy (in combination with a small molecule) (Fallah et al., 2019), Aflibercept for AMD (Balaratnasingam et al., 2015)

CHAPTER 1

Micro RNAs (miRNAs) / Small interfering RNAs (siRNAs)	miR126 (Zhou et al., 2016), miR143 and miR145 for cancer and neovascular eye diseases (Rupaimoole and Slack, 2017, Kim and D'Amore, 2012) VEGF siRNA–PEG/PEI PEC micelles (Kim et al., 2006)
Aptamers	Pegaptanib sodium (an anti-VEGF aptamer) for retinal vascular disorders (Ng et al., 2006)
Gene therapy	VEGF scFv Adenovirus, VEGFR2 AAV and VEGF AAV (Guijarro-Munoz et al., 2013), AAVrh.10 bevacizumab
Small molecules	Sorafenib, Sunitinib, Everolimus and Temsirolimus (mTOR inhibitors) (Ferrara and Adamis, 2016), Regorafenib (Grothey et al., 2013)
Angiostatin and endostatin	Recombinant Human Endostatin Adenovirus (RetinoStat) for macular degeneration (Campochiaro et al., 2017), Lentiviral Vector Gene Transfer of Endostatin/Angiostatin for head and neck cancer (Ye et al., 2014)
Chimeric antigen receptor T cell (CAR-T)	CAR-modified T lymphocytes with human VEGFR-1 specificity (V-1 CAR) for tumours (Wang et al., 2013)

1.3.2.1 Monoclonal antibodies (mAbs)

mAbs have been developed to target VEGFs, VEGFRs, and signalling molecules of VEGFs. Clinical studies have shown that the intraocular injection of anti-VEGF mAbs reverts angiogenesis and significantly improves the vision of patients with AMD, diabetic retinopathy, and retinopathy of prematurity (Paulus and Sodhi, 2016, Al-Latayfeh et al., 2012, Jager et al., 2008, Avery et al., 2006).

Bevacizumab (also known by its brand name, Avastin®), the first anti-VEGF mAb used as an anti-angiogenic agent, targets the VEGF-A isoform 165, the major ligand of VEGFR-2 (Ferrara et al., 2004). This drug has been used in colorectal cancer (Zinser-Sierra et al., 2011) and, in combination with chemotherapy, in breast cancer (Ferrara and Adamis, 2016, Ferrara et al., 2004). Other commonly used anti-angiogenic mAbs include cetuximab, a direct inhibitor of the EGFR-dependent pathway (EGFR/Ras/Raf/MAPK/ERK) which results in VEGF inhibition (Folkman, 2007, Weiner et al., 2010, Pozzi et al., 2016), ramucirumab, a recombinant human IgG1 mAb against VEGFR-2, ranibizumab (Lucentis), which binds to VEGF-A and inhibits its binding to VEGFRs (Tolentino, 2011), and aflibercept (Eylea) and zivafibercept (Zaltrap), synthetic soluble proteins that act as VEGFRs traps, preventing VEGF function (Balaratnasingam et al., 2015). They have been used in eye diseases (such as AMD and diabetic macular degeneration) (Balaratnasingam et al., 2015), and colorectal cancer (Stanel et al., 2017). However, similar to any mAb, they also have the potential

to cause inappropriate immune responses that could result in treatment withdrawal (Fu and Xiang, 2020).

1.3.2.2 MicroRNAs (miRNAs) / small interfering RNAs (siRNAs)

MicroRNAs are important angiogenic regulators *in vitro*. miR-126 has been shown to have dual functions in pathological angiogenesis; while increased miR-126 stimulates angiogenesis, its silencing exerted anti-angiogenic effects in a mouse model of AMD (Zhou et al., 2016). In addition, its anti-VEGF effect on epithelial cells also confirmed the cell type- and disease-specific function of miR-126 in angiogenesis (Zhou et al., 2016, Laham-Karam et al., 2015). The miR-143/145 cluster has also been shown to bind to several mRNAs that encode angiogenic proteins such as VEGF, EGFR, and ERK in colon and pancreatic tumours, inducing mRNA translational repression or degradation (Rupaimoole and Slack, 2017). Other RNA interference-based therapies involving siRNAs to silence mRNA of pro-angiogenic factors have shown great potential for combating excessive angiogenesis in prostate cancer (Laham-Karam et al., 2015, Kim et al., 2006).

1.3.2.3 Aptamers

Aptamers are single-stranded DNA (ssDNA) or RNA (ssRNA) oligonucleotides (20-80 nt) that, similar to mAb, can bind with high affinity to a specific ligand (Fu and Xiang, 2020). However, aptamers have significant advantages over mAb. Most importantly, they are non-immunogenic, even at high doses (Fu and Xiang, 2020). This has been confirmed in cancer (Ireson and Kelland, 2006) and AMD (Group, 2002). Other advantages of aptamers include their high carrying capacity (allowing for a broader range of target delivery into cells (Keefe et al., 2010)), high penetration rate due to their small size (about 20 kDa), short production time with fewer costs, less batch-to-batch variations, and long shelf-life (Fu and Xiang, 2020). By contrast, their short half-life is disadvantageous in the clinical setting (Fu and Xiang, 2020).

1.3.2.4 Gene therapy

Angiogenic gene therapy involves the design of a vector (DNA or RNA) encoding for angiogenic stimulators (such as VEGF and FGF). An example is recombinant adeno-associated virus (rAAV) vectors, used *in vitro* as anti-VEGF therapy, encoding soluble VEGFR-1. In these studies, the growth rate and activity of FMS-like receptor tyrosine kinase-3 (FLT3) (involved in tumour progression and angiogenesis) in human umbilical vein endothelial cells (HUVECs) were significantly inhibited (Mahendra et al., 2005). Advantages of gene therapy compared to protein-based treatments include less immunogenicity and more efficient tumour cell penetration (Zhang et al., 2007, Sanz

et al., 2004). However, a significant challenge is keeping the transgene in the target cell long enough to deliver its therapeutic effect (Fallah et al., 2019).

1.3.2.5 Small molecule inhibitors

Small molecule angiogenic inhibitors can target a variety of processes involved in angiogenesis. These include the FDA-approved drugs sorafenib (Nexavar®), sunitinib, pazopanib, and axitinib. These multi-kinase inhibitors have shown high target affinity and reduced off-target effects versus mAbs. In addition, regorafenib, which interferes with different kinases involved in angiogenesis (e.g. VEGFRs, Tie-2), is the first and only treatment that has demonstrated a significant improvement in oxidative stress in hepatocellular carcinoma patients (Bruix et al., 2017). Small anti-angiogenic molecules are being used in metastatic breast cancer, pancreatic neuroendocrine cancer, gastrointestinal stromal cancer, renal cell cancer, hepatocellular and colorectal cancers (Fallah et al., 2019, Zirlik and Duyster, 2018). Moreover, angiogenesis and VEGF signalling, as one of the important features in skin diseases such as psoriasis, has also been targeted by anti-VEGF agents (in particular sorafenib, bevacizumab, and sunitinib) in these patients (Xian et al., 2019).

1.3.2.6 Angiostatin / endostatin

Angiostatin and endostatin are endogenous angiogenic inhibitors. Previous studies have shown that gene transfer of endostatin/angiostatin suppresses angiogenesis (by inhibiting VEGF/VEGFR binding) in *ex vivo* corneal angiogenesis (Murthy et al., 2003), *in vivo* macular degeneration (Campochiaro et al., 2017), solid tumours such as ovarian cancer (Yokoyama et al., 2000), and leukemia (Scappaticci et al., 2001).

1.3.2.7 Chimeric antigen receptor T cells (CAR-T) therapy

CAR-T cell therapy is a novel and FDA-approved immunotherapeutic method of cancer treatment. The anti-angiogenic engineered T cells are designed to recognise and kill tumour cells through the high affinity of their receptors for angiogenic factors (e.g. VEGFR-2) (Holzer et al., 2013).

1.3.3 Limitations and disadvantages of current anti-angiogenic therapies

Despite the therapeutic benefits of anti-angiogenic therapies, a significant hurdle is represented by their off-target effects. Targeting the VEGF signalling pathway in normal tissues will cause endothelial dysfunction and interfere with other homeostatic mechanisms, with consequent toxicity (Chen and Cleck, 2009, Rapisarda and Merilli, 2012). This includes hypertension (Chen and Cleck, 2009, Belcik et al., 2012), thrombosis, abnormal fetal development, reproduction, kidney function, and wound healing (Rajabi and Mousa, 2017, Cook and Figg, 2010).

Furthermore, currently available antiangiogenic therapies have the potential to trigger drug resistance, resulting from further hypoxia and oxidative stress due to accumulation of CEPs, followed by subsequent vessel formation in a VEGF-independent manner (Kim et al., 2013).

Other important challenges with current anti-angiogenic therapies include their inability to distinguish between physiological and pathological angiogenesis (Fallah et al., 2019) and the high cost of specific treatments, i.e., gene and cell therapy (Ferrara and Adamis, 2016). For these reasons, there is an intense focus on better understanding the molecular mechanisms regulating angiogenesis in order to develop more safe and effective treatments. Therefore, the focus of this project was to identify new druggable targets that overcome the limitations of existing anti-angiogenic therapies.

1.3.3.1 NOS inhibition, as a potential strategy to inhibit excessive angiogenesis

NOS enzymes produce NO by using L-arginine (L-Arg) and NADPH as substrates. Studies have shown that NOS inhibition using the NOS antagonist N^w-nitro-L-arginine methyl ester (L-NAME) suppresses angiogenesis *in vitro* and *in vivo* (Babaei et al., 1998, Ziche et al., 1994). However, the contribution of NOS isoforms in this process is different. In particular, eNOS and iNOS have shown to be induced by VEGF in endothelial cells *in vitro* (Fukumura et al., 2001, Hood et al., 1998, Kroll and Waltenberger, 1998, Papapetropoulos et al., 1997).

1.3.3.1.1 Contribution of NOS enzymes in NO production

Collagen gel implantation studies in eNOS knock-out mice demonstrated significantly lower angiogenesis compared to wild-type mice (Fukumura et al., 2001). While eNOS has been reported to be the major NOS isoform mediating angiogenesis, the additive and/or complementary role of iNOS cannot be ignored. According to prior studies, selective inhibition or gene deletion of iNOS slowed but not suppressed angiogenesis. In contrast, eNOS gene deletion significantly attenuated VEGF-induced angiogenesis (Fukumura et al., 2001). iNOS is regulated by various inflammatory cytokines, lipopolysaccharides and other stimuli, generating high amounts of NO which is cytotoxic (Duda et al., 2004, Rao et al., 2010). However, the activity of this enzyme is calcium-independent (Murphy, 1999). At normal intracellular Ca²⁺ levels, iNOS-derived NO is dependent on enzyme, substrate, or co-factor presence. However, even at lower expression levels, iNOS can still have a considerable impact on angiogenesis. During normal conditions, Ca²⁺-dependent eNOS and nNOS enzymes in their inactive state produce minimum amounts of NO (Murphy, 1999). However, during hypoxia VEGF activates eNOS in endothelial cells via elevating Ca²⁺ levels (Arnould et al.,

1992, Murphy, 1999), or in a Ca^{2+} -independent fashion via recruitment of Hsp90, and NOS phosphorylation by PI3K/Akt pathway (Duda et al., 2004). Similarly, nNOS can also become activated during neurotoxicity, producing excessive amounts of NO (Murphy, 1999).

1.3.3.1.2 NO signalling: Protective/cytotoxic activity of NO

NO is involved in a variety of physiological and pathological processes *in vivo*. This signalling molecule exerts its effect via three mechanisms. The first involves the activation of guanylate cyclase by binding to its heme group, producing soluble cGMP from GTP, which further activates protein kinase G (cGK) (Münzel et al., 2003). The second involves the S-nitrosylation of a wide range of proteins with the formation of S-nitrosothiol (SNO) groups (Lima et al., 2010). Finally, NO reacts with the superoxide anion (O_2^-) to generate peroxynitrite, a strong oxidant that activates several cell pathways including PI3K/Akt and MAPKs (Liaudet et al., 2009).

NO has a range of protective effects on the endothelium, the arterial wall, and the nervous and immune systems which occur at pico- to nanomolar concentrations (Valko et al., 2007). However, higher concentrations of NO and its derivatives (such as peroxynitrite), whether from iNOS upregulation or exposure of eNOS to chronically elevated calcium, can cause oxidative stress, apoptosis, and mitochondrial dysfunction (Levine et al., 2012, Zenebe et al., 2007). Excessive NO production is known to be involved in pathological conditions associated with angiogenesis including neurodegenerative disorders, rheumatoid arthritis, septic shock, and several tumours (Pacher et al., 2007). Therefore, NOS inhibition appears to be a promising target to inhibit angiogenesis in these conditions. Since eNOS, among the NOS isoforms, has a critical role in regulating angiogenesis, understanding its regulatory mechanisms may provide additional and novel therapeutic approaches to treat angiogenic-dependent pathologies.

1.3.3.1.3 Regulation of eNOS

NOS enzymes regulate NO synthesis at the level of expression, via transcriptional and post-transcriptional modifications (PTMs), or depending on their availability and activity (Förstermann and Sessa, 2012). Various mechanisms modulate eNOS availability and activity by either affecting eNOS mRNA stability or eNOS protein interaction with binding partners (Heiss and M Dirsch, 2014). PTMs are among the most common protein modifications that regulate eNOS function in response to physiological and pathological stimuli and include acylation, acetylation, glutathionylation, glycosylation, methylation, nitrosylation and phosphorylation (Heiss and M Dirsch, 2014). Among these, phosphorylation is the most studied PTM known to influence eNOS

activity. However, other PTMs such as methylation of arginine residues have emerged as important modulators of eNOS function (Leiper and Nandi, 2011). Protein arginine methylation is known to be an important PTM involved in DNA transcriptional regulation, cellular signalling, and protein function (Bedford and Richard, 2005, Tang et al., 2000, Zakrzewicz and Eickelberg, 2009). Upon cellular proteolysis, methylated proteins release free monomethylarginine (MMA), symmetric dimethylarginine (SDMA), or asymmetric dimethylarginine (ADMA) (**Fig. 1.20**). Methylarginines regulate NOS protein functions and thereby angiogenesis, as discussed below.

1.3.3.1.3.1 Regulation of eNOS by phosphorylation (calcium-dependent or independent)

In the plasma membrane of endothelial cells, the majority of eNOS is located within the caveolae, and in association with caveolin-1 (Cav-1) protein, in an inactive state (**Fig.1.17, a**). eNOS is particularly sensitive to intracellular calcium concentrations ($[Ca^{2+}]_i$). Several stimuli, such as growth factors (e.g. VEGF), acetylcholine and bradykinin, can increase $[Ca^{2+}]_i$ in endothelial cells which, in turn, binds to calmodulin (CaM) (calcium-modulated protein) and causes the dissociation of eNOS from Cav-1 (**Fig.1.17, b**). Subsequently, Hsp90 protein, induced by VEGF and shear stress, binds to eNOS and further facilitates its detachment from the caveolin clamp (Hoter et al., 2018, Amour et al., 2009) (**Fig.1.17, c**). Caveolin-free eNOS undergoes phosphorylation at serine residue-1177 via the PI3K/Akt or AMPK pathways (**Fig. 1.17, red arrows**) and deacetylation by sirtuin-1 (SIRT-1) (**Fig. 1.17, purple arrows**) (Triggle et al., 2012). The phosphorylated or deacetylated eNOS is active, catalysing L-Arg to L-Cit (**Fig. 1.17, green arrows**) (McCabe et al., 2000, Fulton et al., 1999, Duda et al., 2004). eNOS can also be activated in a calcium-independent manner through the activation of PI3K/Akt and protein kinase A (PKA) and consequent phosphorylation of eNOS at Ser-1177 (Fleming and Busse, 2003). However, calcium-independent eNOS activation results in relatively low NO synthesis (Fleming et al., 2001). Of note, phosphorylation of other eNOS sites (including Ser-116 and Thr-495) inhibits eNOS activity (Triggle et al., 2012).

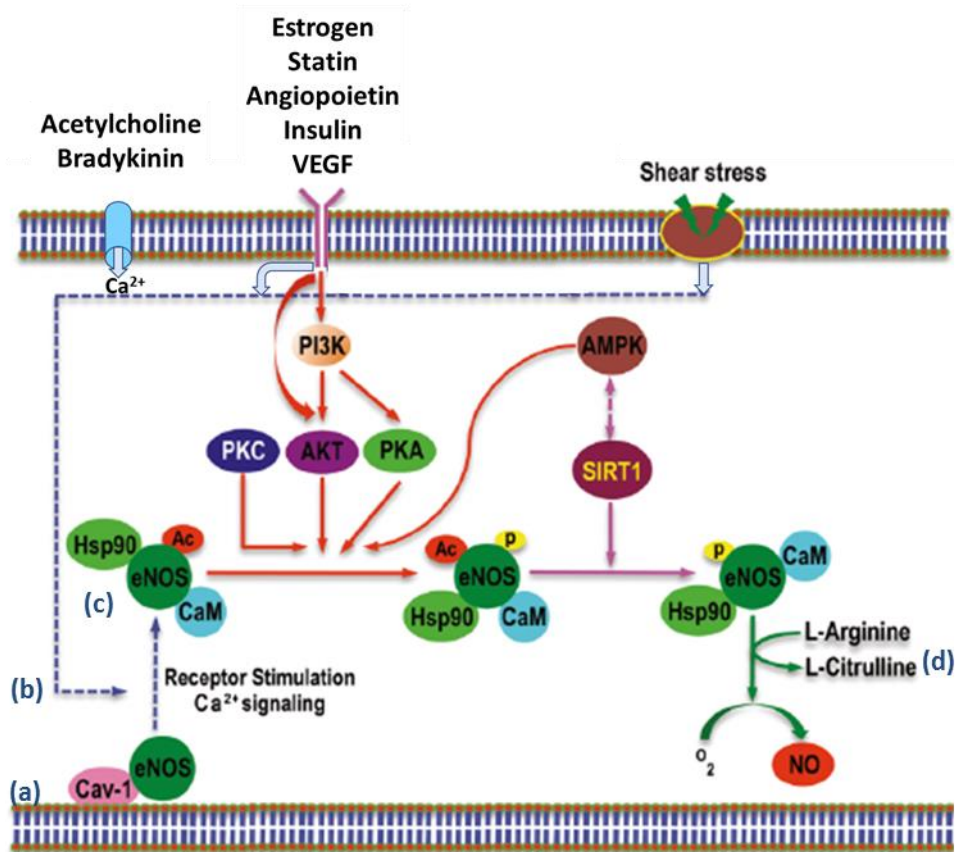


Figure 1.17. Regulation of eNOS.

In the plasma membrane, eNOS is mainly associated with Cav-1, inhibiting calmodulin binding and activation of eNOS (a). An increase in free $[Ca^{2+}]_i$, as well as receptor-mediated agonist stimulation, results in eNOS dissociation from caveolae and binding of the calcium–calmodulin (CaM) complex (b). Recruitment of Hsp90 to the complex further results in a stronger binding of Ca^{2+} /CaM and release of caveolin inhibitory clamp (c). Based on the physiological stimuli, eNOS travels between cytosol and Golgi. Cav-1-free eNOS can get activated via phosphorylation (by protein kinases: PKA, PKB (or Akt), PKC, or AMPK) (red arrows) or deacetylation (by SIRT-1) (purple arrows). Finally, active eNOS catalyses the conversion of oxygen molecule to NO via converting L-arginine (substrate) to L-citrulline (d) (green line). Adapted from Triggler *et al.*, 2012 (Triggler *et al.*, 2012), reproduced with permission.

1.3.3.1.3.2 Regulation of eNOS by methylated arginines

Arginine methylation (ArgMe) is a common PTM, regulating NOS function. Incorporated L-Arg in proteins is methylated by protein arginine methyl transferases (PRMTs) types I and II. While both subtypes can monomethylate arginine to create L-NMMA, transfer of the additional methyl group is specific, where only PRMT I catalyses ADMA, and PRMT II creates SDMA (**Fig. 1.18**) (Yang and Bedford, 2013, Cooke, 2004). PRMT type I is the predominant PRMT in mammalian cells, modifying around 90% of methylated arginines (Tang *et al.*, 2000). The transfer of two methyl groups to the arginine side chain by PRMTs is considered to be stable (Vallance and Leiper, 2004).

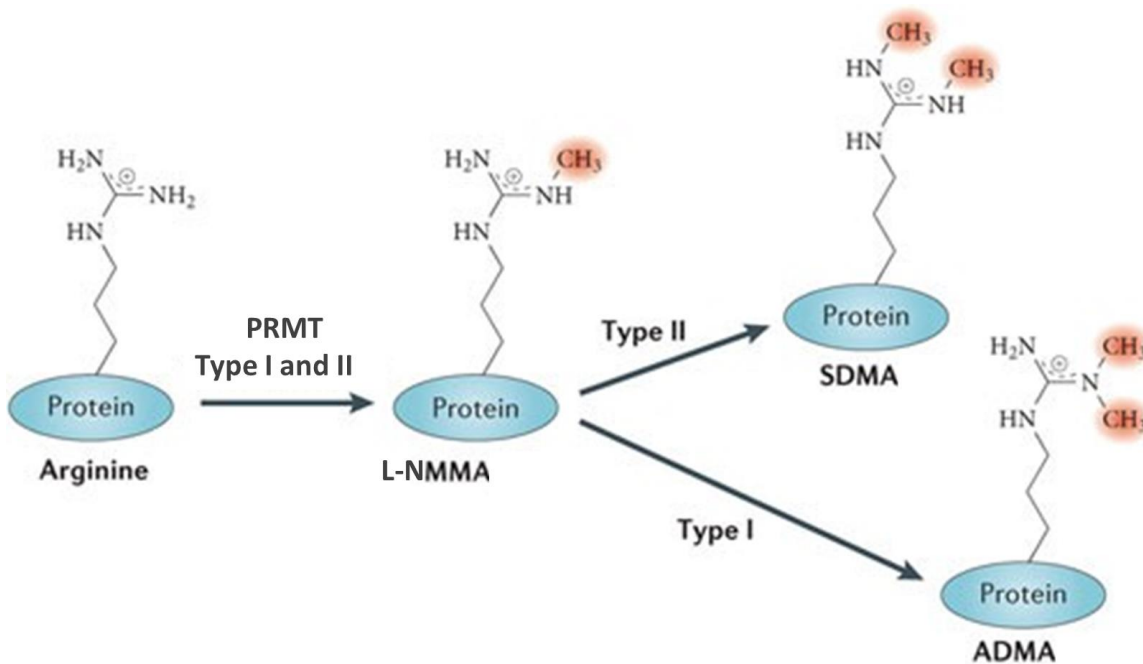


Figure 1.18. Arginine methylation.

Types I, II and III protein arginine methyltransferases (PRMTs) generate monomethylarginine (L-NMMA) by transfer of one methyl group to the guanidino amino group of arginine. The subsequent transfer of a second methyl group to the same nitrogen by type I PRMTs, results in generation of an asymmetric dimethylarginine (ADMA). Type II PRMTs transfer the additional methyl group to the opposite terminal nitrogen, producing symmetric dimethylarginine (SDMA). Adapted from Yang *et al.*, 2013 (Yang and Bedford, 2013), reproduced with permission.

Upon proteolysis of proteins, methylated arginines are released in the cytosol (Vallance and Leiper, 2004). As methylated arginines are almost identical to L-Arg, they can compete for the active site of all NOS enzymes (Vallance and Leiper, 2004). Interestingly, the inhibition only occurs with asymmetrically methylated arginines (e.g. L-NMMA and ADMA), whereas SDMA does not directly inhibit NOS (Vallance and Leiper, 2004). However, SDMA can compete with arginine for its membrane transporter CAT (cationic amino acid transporter), thereby affecting arginine availability within the cell.

Although both L-NMMA and ADMA have almost equal potency for NOS inhibition, the latter is the predominant methylarginine with plasma levels of 10-fold greater than those of L-NMMA. Therefore, the overall impact of ADMA on NO regulation is greater than that of L-NMMA (Leone *et al.*, 1992). Accumulation of ADMA in cytosol and plasma provides a marker of risk for many cardiovascular disorders with demonstrated impairment in NOS and NO synthesis, including hypertension, diabetes, insulin resistance, hypercholesterolemia and hypertriglyceridemia (Cooke, 2004, Zhang *et al.*, 2011).

1.3.3.1.3.3 Regulation of eNOS by DDAH (central role of DDAH in ADMA clearance)

In vivo, ADMA and L-NMMA are eliminated through renal excretion (Teerlink, 2005). However, approximately 70% of elimination (Achan et al., 2003) occurs by catabolism of ADMA and L-NMMA to L-citrulline and mono- or diamines through the enzyme dimethylarginine dimethylaminohydrolase (DDAH) (Fig 1.19) (Vallance and Leiper, 2004, Sibal et al., 2010). Therefore, DDAH influences NO synthesis via regulating ADMA levels.

Increasing DDAH expression or activity could be used to treat diseases with increased ADMA and reduced NO signalling, such as insulin resistance, kidney disease and coronary artery disease (Zoccali, 2006, Schnabel et al., 2005). However, inhibition of DDAH can also represent a novel therapeutic strategy in disorders with excessive NO production, including septic shock, certain cancers, and arthritis (Thiemermann, 1994, Thomsen and Miles, 1998, Dulak and Józkwicz, 2003).

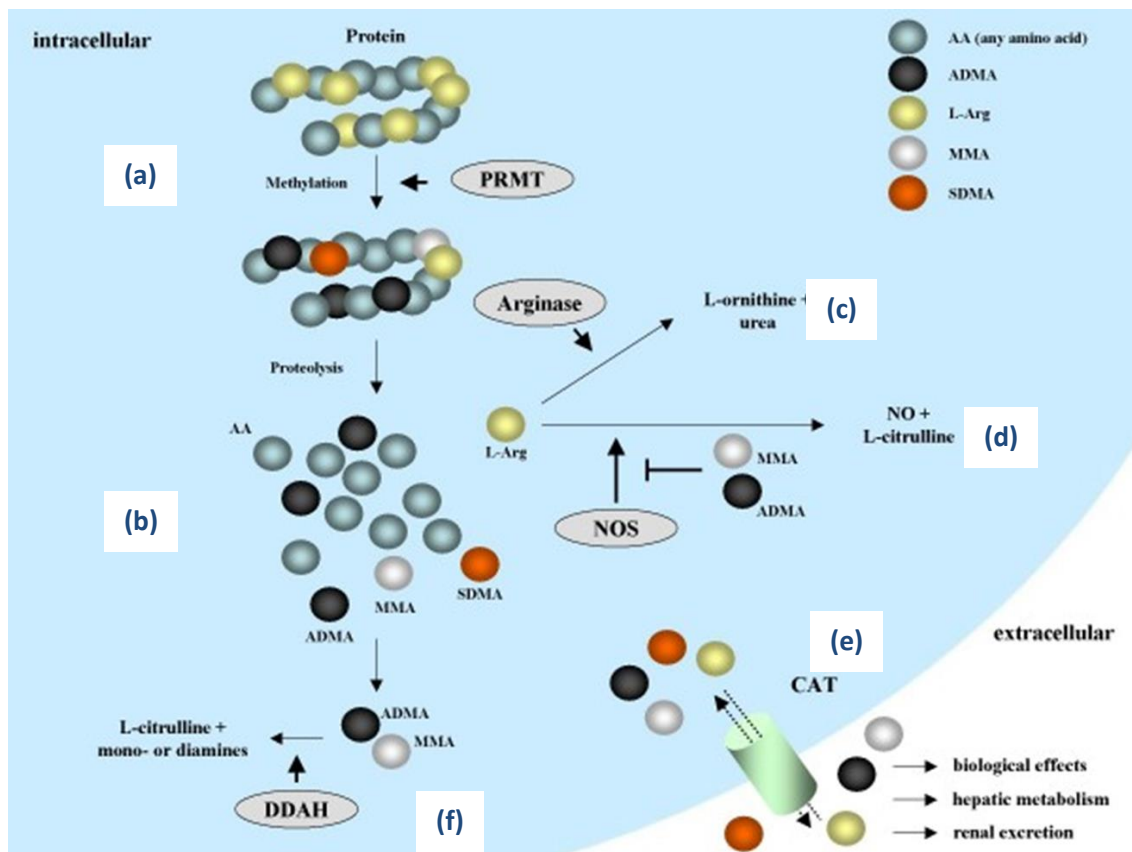


Figure 1.19. Methylarginine metabolism.

The methylation of amino acid L-Arg is performed by enzyme PRMT (a). Proteolysis of arginine-methylated proteins results in free MMA, ADMA or SDMA, depending upon the number and position of the incorporated methyl groups (b). Free L-Arg can either get metabolised by arginase enzymes to generate L-ornithine and urea (c), or by NOS enzymes to NO and L-citrulline (d). Cells can also release methylarginines to the extracellular space through CAT transporters (e) to exert specific biological effects, or to get eliminated via hepatic metabolism or renal excretion. DDAH enzymes can use MMA and ADMA, but not SDMA, as substrates to generate L-citrulline and mono- or diamines (f). In particular, both DDAH substrates, MMA and ADMA, act as potent endogenous inhibitors of NOS enzymes. Adapted from Zakrzewicz and Eickelberg, 2009 (Zakrzewicz and Eickelberg, 2009), reproduced with permission.

CHAPTER 1

The DDAH family includes the isoforms DDAH1 and DDAH2 (Vallance and Leiper, 2004). These isoforms have highly conserved amino acid sequences in humans (62%) and across species (human, mouse, rat, and bovine gene) (DDAH1: 92%, DDAH2: 95%) (Tran et al., 2003, Leiper et al., 1999, Hulin et al., 2020). DDAH1 is mainly expressed in tissues with nNOS expression, including the brain (Greco et al., 2015) and sensory neurons (D'Mello et al., 2015), while DDAH2 is highly expressed in eNOS-expressing tissues (e.g. blood vessels and endothelium) with key role in embryonic development (Palm et al., 2007), the retina and choroid (Lange et al., 2016), pancreas (Hasegawa et al., 2013), and infected tissues (Amrouni et al., 2011). Interestingly, DDAH2 has been identified to regulate both eNOS and iNOS in endothelial cell cytosol and smooth muscle cells, respectively (Ueda et al., 2003, Cillero-Pastor et al., 2012). Regardless of their location, both isoforms are reported to be bound with a Zn^{2+} ion, and are localised in the cytosol (Knipp et al., 2001). Nevertheless, due to their hydrophobic secondary structure, they are found in lipid membranes (e.g. mitochondrial membrane) (Cillero-Pastor et al., 2012).

There is increasing evidence that ADMA and L-NMMA are not substrates for DDAH2, and the impact of DDAH2 on the concentrations of these methylarginines may be through an indirect mechanism (Lambden et al., 2015, Lange et al., 2016). Based on current evidence, DDAH1 has more contribution in overall metabolism and clearance of ADMA and L-NMMA, and consequently NO homeostasis and angiogenesis (Leiper et al., 1999, Wilcken et al., 2007, Hu et al., 2011a, Zhang et al., 2011). Therefore, understanding the mechanism of angiogenic regulation by DDAH1 is of high importance.

1.3.3.1.4 Regulation mechanisms of DDAH1-mediated angiogenesis

Several studies have demonstrated the involvement of DDAH1 in both physiological and pathophysiological angiogenesis (Hulin et al., 2020). The possible mechanisms involved are described in **Figure 1.20** and include the Akt pathway (phosphorylation of endothelial Akt (p-Akt^{Ser473})), indicated by prior immunoblot and tube formation studies (Zhang et al., 2011). DDAH1 activates Ras signalling, which is known to phosphorylate and activate Akt via the PI3K pathway, and consequently phosphorylates eNOS (p-eNOS^{Ser1177}). This mechanism can be either ADMA-dependent (**Fig. 1.20, a**) or independent (**Fig. 1.20, b**), and via NO-cGMP pathway (Zhang et al., 2011).

The well-studied regulatory role of DDAH on angiogenesis is via mediating the ADMA pathway and its consequent impact on eNOS regulation and NO availability. The DDAH/ADMA/NOS pathway

CHAPTER 1

plays a major role in angiogenesis both *in vitro* and *in vivo* (Jacobi et al., 2005, Achan et al., 2005). Heterozygous deletion of DDAH1, siRNA silencing, or pharmacological inhibition led to increased levels of ADMA in plasma, tissue, or culture medium, and reduced NO production, without affecting eNOS protein expression. This resulted in tube formation inhibition and endothelial dysfunction (Leiper et al., 2007, MacAllister et al., 1996, Zhang et al., 2011). Interestingly, DDAH1 reduction or heterozygous knockout with consequent ADMA accumulation inhibited VEGF-induced endothelial cell migration and tube formation *in vitro* and *in vivo*, while it did not affect endothelial cells under basal conditions (with no VEGF induction) (Fiedler et al., 2009).

The role of DDAH1 on angiogenesis has also been confirmed by DDAH1 overexpression studies, where reduced tissue ADMA raised NO synthesis and enhanced angiogenic responses *in vitro* (Kostourou et al., 2002, Smith et al., 2003), stimulated sprouting from aortic rings (Wojciak-Stothard et al., 2007, Konishi et al., 2007), and also induced angiogenesis in tumours and other ischemic vascular diseases (Kostourou et al., 2002, Jacobi et al., 2005).

Another mechanism by which the DDAH/ADMA/NO pathway regulates angiogenesis is via the Rho GTPase. The Rho family of GTPase (part of the Ras superfamily) are key regulators of actin polymerisation and cytoskeletal rearrangement, controlling actin-based endothelial cell motility and angiogenesis (Fiedler and Wojciak-Stothard, 2009, Wojciak-Stothard et al., 2007). Heterozygous knockout of DDAH, or treating endothelial cells with ADMA, dephosphorylates and thus activates RhoA (Fiedler and Wojciak-Stothard, 2009). This enhances stress fibres (contractile actin bundles found in non-muscle cells), inhibiting endothelial cell motility, migration, and proliferation *in vitro* (**Fig 1.20, c**) (Wojciak-Stothard et al., 2007). This mechanism can be reversed by protein kinase G (PKG) via phosphorylating RhoA at serine residue 188, thereby downregulating its activity, leading to angiogenesis upregulation (Fiedler, 2008).

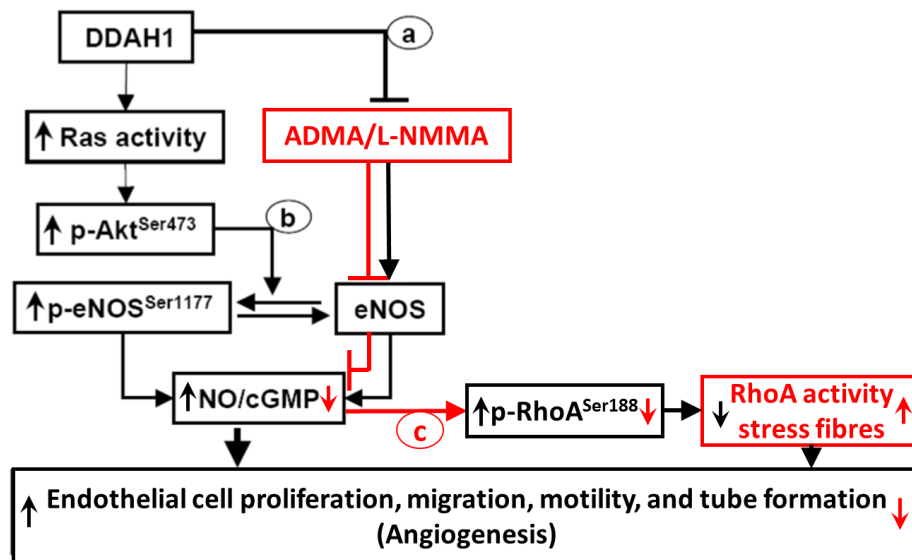


Figure 1.20. Regulatory pathways of DDAH1-mediated angiogenesis.

(a) DDAH1 overexpression, increased tube formation via accumulation of ADMA and inhibition of eNOS (b) DDAH1 overexpression increased angiogenesis through phosphorylation of Akt (Ser473) and eNOS (Ser1177), an independent pathway from ADMA and NO-cGMP. (c) DDAH1 inhibition or ADMA increase, results in elimination of NO, leading to RhoA de-phosphorylation and therefore activation of stress fibres and ultimately inhibition of angiogenesis. Adapted from Zhang *et al.*, 2011 (Zhang *et al.*, 2011) and Fiedler *et al.*, 2008 (Fiedler, 2008), reproduced with permission.

The effect of DDAH on angiogenesis is believed to be VEGF-dependent (Fiedler *et al.*, 2009). Previous studies have shown that DDAH1 overexpression eliminated the inhibitory effect of ADMA and restored normal angiogenesis via NO production, but only in the presence of VEGF (Fiedler *et al.*, 2009). Therefore DDAH/ADMA-mediated angiogenesis is dependent on VEGF/VEGFR-2 activation (Cooke, 2003, Murohara and Asahara, 2002, Olsson *et al.*, 2006). On the other hand, other studies have demonstrated that VEGF is mediated by DDAH; DDAH upregulation enhanced VEGF expression in glioma cells (Kostourou *et al.*, 2002), and human and mice endothelial cells (Smith *et al.*, 2003), stimulating angiogenesis. These findings suggest a potential therapeutic benefit for DDAH1 inhibition, suppressing VEGF pathway in disorders associated with excessive angiogenesis.

1.3.3.1.5 Endogenous regulation of DDAH1

DDAH activity is endogenously modulated via several mechanisms including PTM. An important PTM mechanism regulating enzymatic activity is S-nitrosylation of a cysteine residue, known to be associated with increased iNOS (Palm *et al.*, 2007). High NO, generated from iNOS, can bind to DDAH cysteine, inhibiting this enzyme (Palm *et al.*, 2007). S-nitrosylated DDAH causes ADMA and L-NMMA accumulation, resulting in NOS inhibition (Leiper *et al.*, 2002). Moreover, many factors

associated with oxidative stress, such as shear stress, TNF- α , or OxLDL, can inhibit DDAH expression and activity (Osanai et al., 2003), leading to ADMA elevation. Accumulation of ADMA in endothelial cells may inhibit NOS and NO production, leading to endothelial dysfunction (Dayal and Lentz, 2005). By contrast, there are other oxidative stress-related agents that cause DDAH elevation, including estrogen (Holden et al., 2003) and interleukin-1 β (IL-1 β) (Ueda et al., 2003).

1.3.3.2 DDAH inhibition, as a potential strategy to inhibit excessive angiogenesis

DDAH1 overexpression and subsequent NO overproduction have been associated with multiple pathologies including tumour growth and angiogenesis (Fiedler and Wojciak-Stothard, 2009). This suggests a potential therapeutic role for DDAH inhibition in this pathway against pathologies linked with excessive angiogenesis.

Early therapeutic strategies directly targeting NOS or scavenging NO by using L-NMMA have been unsuccessful during clinical studies (Kinasewitz et al., 2008, López et al., 2004). This was due to the severe adverse effects from excessive vasoconstriction, myocardial depression, immune suppression, and mortality (Wang et al., 2014). Alternatively, pharmacological inhibition of DDAH, by limiting overproduction of NO in an indirect fashion without disrupting the homeostatic functions of this key messenger molecule, may deliver a promising strategy to overcome these disorders. Several DDAH inhibitor compounds have been synthesised and used *in vitro* by research groups (Linsky and Fast, 2011). Many of these inhibitors have presented relatively good selectivity and inhibitory potential, either against bacterial DDAH (*Pa*DDAH), such as SR445 and pentafluorophenyl (PFP) sulphonates (Kotthaus et al., 2008, Vallance et al., 2005), or human DDAH, most importantly L-VINO and L-257 (Kotthaus et al., 2008, Leiper and Nandi, 2011). However, a selective human DDAH inhibitor has yet to make it to clinical trials.

Our research group has designed and synthesised 12 novel recombinant human arginine analogue DDAH1 small molecule inhibitors, originated from the initial L-257 scaffold, due to its relatively high potency and lack of inhibitory potential towards NOSs and arginases (Tommasi et al., 2015). Among these novel compounds, ZST316 (compound 10a), and ZST152 (compound 14b), exhibited a greater inhibitory potential than the reference DDAH1 inhibitor, L-257, with a K_i of 1 and 7 μ M respectively, and ZST086 (compound 14a) had the third level of potency and comparable to L-257. Thus, they were selected for future *in vitro* experiments to detect their anti-angiogenic potential.

DDAH1 inhibition by ZST316 and ZST152 was demonstrated both in isolation (Tommasi et al., 2015), and in a cellular model of triple-negative breast cancer (MDA-MB-231 cells) (Hulin et al.,

CHAPTER 1

2019). Upon incubation of MDA-MB-231 cells with different concentrations of ZST316 and ZST152, a marked decrease in the intracellular levels of the DDAH1 product, L-citrulline, and a simultaneous increase in the enzyme substrate ADMA were demonstrated (Hulin et al., 2019). *In vitro* tube formation assay using these compounds resulted in significant inhibition of cell migration and vasculogenic mimicry in these cells in a dose dependent manner (Hulin et al., 2019). Notably, no effect was observed on cell proliferation. This demonstrates the biological effect of our DDAH1 inhibitors on inhibiting vascularisation *in vitro* (Fig. 1.21, B).

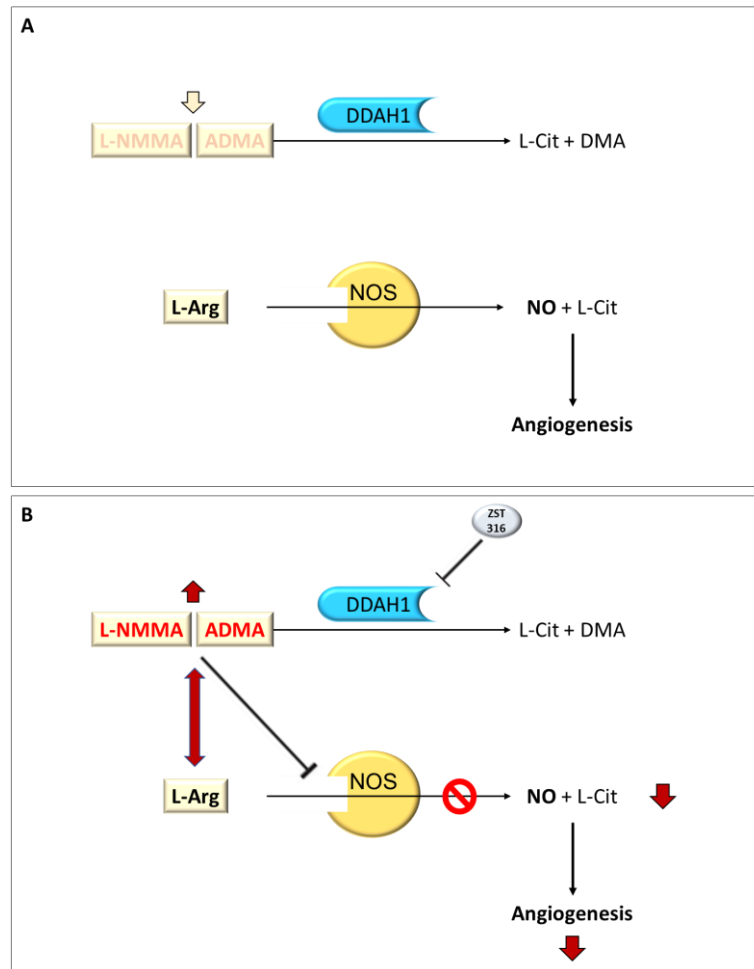


Figure 1.21. Schematic illustration of ADMA/DDAH/NOS biochemical pathway and the role of DDAH1 inhibitor, ZST316, in angiogenesis inhibition.

DDAH enzyme metabolises and degrades the majority of ADMA and L-NMMA to form dimethylamine (DMA) and L-citrulline (L-Cit). (A) DDAH overexpression leads to degradation of ADMA and L-NMMA, and thus, insufficient concentrations of these methylarginines. NOS enzyme is activated, producing increased amounts of nitric oxide (NO[•]), thereby promoting angiogenesis. (B) DDAH inhibitor, ZST316, binds to the active site of DDAH enzyme, inhibiting its activity, leading to accumulation of ADMA and L-NMMA substrates. These arginine analogues compete with L-arginine (L-Arg) for the active site of NOS enzyme. Upon occupation of NOS binding sites by ADMA or L-NMMA, the enzyme becomes dysfunctional, leading to a reduction in NO[•] synthesis and thus, inhibition of angiogenesis.

CHAPTER 2. MATERIALS AND METHODS

2.1 Cell culture

A number of cell lines and a primary cell with different characteristics were used for this study.

The HEK-293T cell line (CRL-3216) (ATCC, Manassas, Virginia, USA), human embryonic kidney 293 cells, also known more informally as HEK cells, is derived from human embryonic kidney cells grown in tissue culture taken from an aborted female fetus. HEK-293 cells were purchased from American Type Culture Collection (ATCC, Manassas, Virginia, USA) and transfected by a temperature-sensitive allele of the SV40 large T antigen (Dr. Ben Lewis, Flinders University, SA, Australia). They were maintained in Dulbecco's Modified Eagle's Medium, DMEM, (Gibco, Life Technologies (ThermoFisher Scientific), Grand Island, NY, USA) supplemented 10% (v/v) Fetal Bovine Serum (FBS) (Bovogen Biologicals, VIC, Australia) with 1% (v/v) MEM non-essential amino acids (Gibco, Life Technologies, Grand Island, NY, USA) and buffered with sodium bicarbonate (3.7 g/L of media).

The PC-12 Adh (CRL-1721.1) (ATCC, Manassas, Virginia, USA), an adherent version of the PC-12 cell line, is derived from a pheochromocytoma of the rat adrenal medulla, with an embryonic origin from the neural crest that has a mixture of neuroblastic cells and eosinophilic cells. F-12K Medium (Corning Life Sciences, NY, USA) formulation adjusted as per ATCC recommendation was used as the base medium for this cell line. To make the complete growth medium, 2.5% FBS and 15% horse serum (Gibco, Life Technologies, Grand Island, NY, USA) were added to the base medium.

The SH-SY5Y (CRL-2266) (ATCC, Manassas, Virginia, USA) is a human-derived cell line, originally subcloned from cell line SK-N-SH, isolated from a bone marrow biopsy of a four-year-old female with neuroblastoma. The medium for this cell line consisted of a mixture of 1:1 DMEM: F-12 medium, ATCC formulated, completed with 10% FBS.

The human umbilical vein endothelial cells (HUVECs) (Dr. Claudine Bonder, Adelaide University, Australia), derived from the endothelium of veins from the umbilical cord, is used to study the endothelial cell function and the pathology (e.g. angiogenesis). Complete HUVEC media contained 1% HEPES buffer (Invitrogen (ThermoFisher): #15630-080) at final concentration of 10mM, 1% Glutamax 100X-solution (ThermoFisher: #35050061), 1% Antibiotic-Antimycotic 100X-solution (Invitrogen (ThermoFisher): #15240-062), 0.2% Normocin (InvivoGen catalog # antnr-1) and 20%

CHAPTER 2

FBS in Medium 199 with Earle's Balanced Salt Solution (EBSS), with L-Glutamine (HyClone #SH30253.01,), 50 µg/ml of endothelial cell growth supplement (ECGS) (Biomedical Technologies: #BT-203) and heparin (Sigma: #H3149-100KU) added fresh to culture at the time of experiment.

The VeraVec™ HUVEC (hVera101) (Angiocrine Bioscience, generous donation of Dr. Claudine Bonder, Uni SA, Australia), were originally isolated from the umbilical cord vein – HUVECs. Utilizing a single protein from Adenovirus (serotype 5), E4ORF1, these adherent cells are adapted to culture for multiple passages, but not immortalised. In this study, the first and “classic” human VeraVec endothelial cells, hvera101, were used. The resistant characteristics of these cells allow for long-term culture in typical serum-containing media, without negative effects of serum over prolonged passaging; they remain stable and viable in the absence of complex media additives. Complete medium complex suitable for these cells was the same as HUVEC cells.

The ARPE-19 human retinal pigment epithelial cell line (CRL-2302) (ATCC, Manassas, Virginia, USA) were cultured in DMEM/F12 1:1 supplemented with 10% FBS, and 1% L-alanyl-L-glutamine (GlutaMAX; Invitrogen, Carlsbad, CA) (GPS), and used through ≥ 30 passages. Media were changed twice a week.

All cell lines were generally plated and maintained in T75 or T175 tissue culture flasks (Nunc, Roskilde, Denmark) uncoated or pre-coated with one µg/mL human Fibronectin (Roche Life Sciences, Basel, Switzerland, catalogue number 10 838 039 001) in case of HUVEC and VeraVec cells. All cells were cultured in humidified 37°C cell culture incubator with 5% CO₂ and re-fed with fresh media every two days.

Upon confluency (when cells reach 90-95% confluence), cells were sub-cultured (passaged). The medium was aspirated and discarded, and the cells were rinsed with 1x phosphate-buffered saline (PBS) to remove traces of FBS which naturally contains trypsin inhibitor. PBS was aspirated and a minimal amount of 0.5% trypsin-EDTA (10x) (0.05%) (Gibco, Life Technologies, Grand Island, NY) was added to adherent cells. Flasks were incubated at 37°C for approximately one minute. After a few firm gentle taps on flask sides and checking under a microscope (OLYMPUS, NSW, Australia) for cell detachment, cell suspensions were collected and diluted into pre-warmed complete media which inactivates trypsin enzymatic activity. HEK-293T, PC-12, and SH-SY5Y cell mixtures were transferred directly to fresh new flasks at a split ratio of 1:4 to 1:8 for cell lines and incubated at 37°C incubator. For HUVEC and VeraVec subculturing, cell suspensions were transferred into sterile tubes for centrifugation at 1500 rpm for five minutes at room temperature. The

CHAPTER 2

supernatant was aspirated, and the pellet resuspended in 3x volume fresh HUVEC media to make a 1:3 cell suspension seeded on Three Fibronectin-coated 75 cm flasks. Heparin and endothelial growth supplement (**Table 2.5**) were added to the medium (ten μL per one mL HUVEC media) prior to incubation at 37°C incubator.

Cells were allowed to passage at least twice after thawing to recover from freeze-thawing stresses and re-establish their normal cell cycle. After at least two passages, they were ready to be utilised for experiments.

The remaining cells were optionally stored by adding approximately 1×10^6 cells in 90% FBS and 10% Dimethyl sulfoxide, DMSO (Sigma-Aldrich, St Louis, MO, USA) in Nunc™ Cryogenic tubes (ThermoFisher Scientific, Waltham, MA, USA). The cells were frozen gradually by placing them in -80°C freezer for a short term prior to transferring and storing long-term in liquid nitrogen.

High-passaged cell lines (above passage 20) were discarded. VeraVec cells were only freeze-thawed once and used at passages 7-12 for experiments and any left-over cells were discarded.

2.2 Mycoplasma screening

Cells were tested to be mycoplasma-free once purchased. To prepare samples for mycoplasma testing, cells grown in media without antibiotics for at least one week in T-75 flask were trypsinised, neutralised to deactivate trypsin, and 300 μL aliquots of suspended cells were transferred to a sterile 1.5 ml Eppendorf tube topped with one mL PBS to dilute the growth medium. The tube was centrifuged at 12,000 rpm for three minutes at room temperature and the supernatant medium was aspirated out as much as possible. Using sterile pipette tips at all times, 90 μL 0.05 M NaOH was added to the pellet and pipetted up and down to resuspend evenly. To lyse the cells and extract the DNA, the suspension was heated at 98°C for ten minutes and let to cool followed by the addition of ten μL one M Tris, pH 7.4 (Astral Scientific, Taren Point, NSW, Australia). To amplify the extracted DNA with mycoplasma, genus-specific primer sets and mycoplasma-specific positive control primer set as internal controls were used. The Master Mix composition for PCR is listed in **Table 2.1**.

CHAPTER 2

Table 2.1. Master Mix composition for mycoplasma contamination testing of cell lines.

Reagent	Volume to Add Per Reaction
NEB 10X Thermopol Buffer	2.5 μ L (Containing final MgCl ₂ concentration of 2 mM)
4X 10 mM dNTP	0.5 μ L
Primer mix (5 mM each primer)	2 μ L
NEB Taq Polymerase (5 units/ μ L)	0.15 μ L
H ₂ O	17.85 μ L
Total	23 μ L

2% agarose gel was made by dissolving 1.5 g Agarose (AppliChem, Darmstadt, Germany) in 75 mL 1x Tris-acetate EDTA electrophoresis (TAE) buffer (**Table 2.8**) and 7.5 μ L Gel Red (Biotium, California, USA) added to detect the bands. The samples were diluted in dye containing glycerol and loaded on to the gel along with the 1000 bp (1kb) standard DNA ladders (Promega, Madison, WI, USA) used as size markers. Electrophoresis was performed at 80-120 volts for approximately one hour in a Bio-Rad Mini-Sub Gel GT electrophoresis system. The gel was imaged on ChemiDoc™ Imaging Systems (BioRad, California, USA).

2.3 Cell proliferation and cell death assays

2.3.1 Crystal violet assay

Crystal violet is a simple assay to obtain quantitative information about the relative density of the adherent cells to the culture plate via DNA staining. The 10x Crystal violet solution was prepared by dissolving two g/L Crystal violet (Sigma-Aldrich, Missouri, USA) in 10% buffered-formalin (Orion Labs, California, USA). The Crystal violet was further diluted in buffered formalin. To perform the assay, culture media on cells seeded and grown in 96-well plates (Nunc, Roskilde, Denmark) was carefully aspirated out of the wells and the plate was washed twice with 200 μ L 1x PBS. 1x Crystal violet solution was added to each well (50 μ L per well), and the plate was incubated at room temperature for ten minutes. Afterwards, the plate was immersed in a large beaker three times to remove the unbound crystal violet stain and then drained upside down on a paper towel overnight or until completely dry. The stained DNA in each well was solubilised by adding 50 μ L of 33% v/v acetic acid to each well and the plate was agitated on an orbital shaker for ten minutes at room temperature until a uniform colour was achieved. To quantify the total DNA content of the cells the absorbance at 570 nm was measured using a VERSAmax Absorbance Microplate Reader (Molecular Devices, San Jose, CA, USA).

2.3.2 Sulforhodamine B (SRB) assay

Another colorimetric in vitro assay for cytotoxicity screening is based on staining cellular proteins with Sulforhodamine B (SRB, Acid Red 52; Sigma-Aldrich, St Louis, MO, USA), and measuring the total biomass. The seeded cells on a 96 well plate were removed out of the incubator into laminar flow hood and 50 μ L cold SRB fixative solution (50% w/v Trichloroacetic Acid (TCA)) was layered on top of the 200 μ L media in each well (4:1 ratio of fixative solution to media). The plate was then incubated for one hour at 4°C and then rinsed with water several times to remove TCA solution, serum proteins. The plates were air dried overnight or until completely dry. The next day, 0.4% SRB solution was added to each well at a volume enough to cover the wells surface area (50 μ L per well), and allowed to stain with the dye for 30 minutes at room temperature. The unincorporated dye is then gently removed by aspiration and wells were quickly rinsed with wash solution (1% acetic acid). The washing step is repeated until the excess dye is removed. After the plates were completely air-dried, the incorporated dye is liberated from the cells and solubilised in 200 μ L SRB solubilisation solution (ten mM Tris base solution). The plate is gently agitated on orbital shaker for five minutes at room temperature to enhance the mixing of the dye. The VERSAmax Absorbance Microplate Reader (Molecular Devices, San Jose, CA, USA) was used to measure absorbance at a wavelength of 490 nm. Background absorbance at 690 nm was subtracted from the measurement at 490 nm. An increase or decrease in the number of cells (total biomass) results in a change in the amount of incorporated dye to the cultured cells, which indicates the degree of cytotoxicity.

2.3.3 Real-time cell growth analysis

Cell proliferation was measured using the IncuCyte™ Live-cell Analysis System (Essen BioScience, Michigan, USA). The system acquires, analyses, and quantifies images from living cells overtime via performing live content imaging. Seeding cell densities for different experiments were dependent upon the cell type and incubation period. The proliferation of the cells was tracked by IncuCyte every two hours and the data were presented as the percentage of the cell confluency over time.

Proliferation validation experiments were performed using the xCELLigence RCTA platform (ACEA Biosciences, California, USA). VeraVec endothelial cells were seeded in fibronectin-coated E-plates (ACEA Biosciences, California, USA), and cell proliferation was assayed as measures of cell index inferred by changes in electrical conductivity of cell media. Prior to readings, the cell indices were adjusted to zero by adding 50 μ L of media with 10% FBS.

2.4 Agarose gel electrophoresis

To analyse the purity of DNA fragments and plasmids from culture preparations or PCR amplification, agarose gel electrophoresis was used. Agarose gel (2%) was made by adding 1.5 g Agarose (AppliChem, Darmstadt, Germany) to 75 mL 1x TAE buffer (**Table 2.8**) and 7.5 μ L Gel Red (Biotium, California, USA). Two μ L of DNA sample was added to 23 μ L of the prepared Master Mix (**Table 2.1**) and the PCR program was set as described in **section 2.2**. Five μ L PCR products were diluted in dye containing glycerol and loaded on to the gel along with the 1kb DNA ladders (Promega, Madison, WI, USA) used as size markers. Electrophoresis was performed at 80-120 volts for approximately one hour in a Bio-Rad Mini-Sub Gel GT electrophoresis system. The gel was imaged on ChemiDoc™ Imaging Systems (BioRad, California, USA).

2.5 Protein extraction, quantification, separation, and detection

2.5.1 Lysate preparation and protein extraction

One cOmplete™ mini protease inhibitor cocktail tablet and one PhosSTOP™ phosphatase inhibitor cocktail tablet (Roche Applied Science, Mannheim, Germany) was dissolved freshly, in ten mL according lysis Radioimmunoprecipitation assay (RIPA) buffer (**Table 2.8**).

After media removal, cells were rinsed twice with pre-chilled 1x PBS pH7.4 (or TBS for Phosphorylation study) and flasks were put on ice while cells were scraped and collected in eight mL pre-chilled TBS and transferred to a ten mL tube. The cell suspension was centrifuged at 1500 rpm for five minutes at 4 °C. The supernatant was aspirated, and the previous washing step was repeated two additional times. After the last wash, seven mL of the supernatant was removed, and the cell pellet was resuspended gently and transferred to pre-chilled two mL Maxymum Recovery tubes (Axygen). A final spin at 2000 rpm, for five minutes at 4°C was performed. The wet pellet was weighed and dissolved in ice-cold lysis buffer (aiming to achieve final protein concentration of one mg/mL).

The homogenisation of extracts of broken cells was performed with an ultrasonic processor (Vibra-Cell™ Ultrasonic Liquid Processor, Sonics & Materials, Inc, Connecticut, USA) for ten minutes adjusted pulse: one second on / 59 seconds off for up to ten minutes, or until the pellet is dissolved completely. Samples were then passed through separate 27-gauge (G) BD PrecisionGlide™ needles (Becton Dickinson Medical Pte Limited, Singapore) to ensure the

complete lysis of the cells. The lysed cells were then centrifuged at 14,000 g for five minutes at 4°C and protein concentration was measured.

2.5.2 Protein quantitation

Total protein concentrations in the extracted samples were determined using either a colorimetric Bradford assay, or a fluorescence-based EZQ™ Protein Quantitation assay (Thermo Scientific Revco, Waltham, MA, USA).

2.5.2.1 Bradford assay

This is a colorimetric protein assay based on an absorbance shift of the Bradford reagent, which is an acidified solution of Coomassie brilliant blue G-250 and thus, it is primarily protonated and red. Four serial dilutions between 0-1 mg/mL were performed from the protein standard, bovine serum albumin (BSA) (New England Biolabs, Beverly, MA, USA) with dH₂O.

Two µL of each sample lysate was diluted in 18 µL dH₂O (1:10 dilution of lysate) and ten µL of each diluted sample or standard were added to cuvettes in duplicate. One ml of 1x Bradford dye (Sigma, St Louis, MO, USA) was added to each cuvette containing sample or standards, vortexed well and incubated at room temperature for maximum 30 minutes. Absorbance at 595 nm was obtained using a Varian CARY 300 BIO UV-Visible Spectrophotometer (New Life Scientific, Cridersville, OH, USA). Protein concentration was estimated by comparison to a BSA standard curve of known concentrations (0, 0.1, 0.2, 0.4, 0.6, and 1.0 mg/mL).

2.5.2.2 EZQ assay

Six serial dilutions of 0.02-2 mg/mL from the two mg/mL Ovalbumin stock (BioRad, California, USA) were prepared and used as the standard protein to generate the standard curve for protein quantification.

One µL of standards and protein samples were spotted on EZQ assay paper in triplicates and allowed to completely dry on the paper on low heat using Easy Breeze™ Gel Dryer (Hoefer Inc, Massachusetts, USA). To fix proteins on paper, 40 mL 100% methanol was poured into the tray and incubated on a rotator (50 rpm) for five minutes. Subsequently, the assay paper was dried on low heat by the dryer and 35 mL of EZQ Protein Quantitation Reagent was added and rotated during 30 minutes incubation at room temperature to stain the proteins with proprietary fluorescent dye. The paper was then rinsed three times for two min in 40 mL EZQ destain containing 10% methanol and 7% acetic acid in dH₂O. For fluorescence-detection from the protein spots,

CHAPTER 2

ChemiDoc™ Touch Imaging Systems (BioRad, California, USA) was used and the data were analysed using ImageLab™ Software (BioRad, California, USA). A standard curve was created by plotting the corrected fluorescence values of the standards versus the corresponding protein mass and the protein concentration of the samples was extrapolated based on the standard protein curve.

2.5.3 Immunoblotting

2.5.3.1 SDS-PAGE (*polyacrylamide gel electrophoresis*) gels

For SDS-PAGE protein separation, either the ten well 4-20% Stain-Free™ Mini-PROTEAN precast gels (BioRad, California, USA), or freshly prepared 10% SDS-PAGE gels (**see table 2.2**) were used.

To prepare the 10% SDS-PAGE gels, first, 10% separating gel mix was poured into 1.5 mm thick gel assembly and was left to set for 30 minutes. Second, the stacking gel solution was made, and three mL was added on top of the separation gel mix within the cascades. Combs were inserted and incubated at room temperature for 30 minutes before removing the comb and loading the protein samples.

CHAPTER 2

Table 2.2. Composition of SDS-polyacrylamide gel.

10% SDS-polyacrylamide Separating gel (for 2 x 1.75 cm gels)	
Buffer	Volume
Distilled water	9.62 mL
1.5 M Tris-HCl, pH 8.8	5 mL
10% (w/v) SDS	200 μ L
40% Acrylamide-Bis Solution (BioRad, California, USA)	5 mL
10% (w/v) APS (Sigma-Aldrich, St Louis, MO, USA)	100 μ L
TEMED (Tetramethylethylenediamine) (BioRad, California, USA)	80 μ L
4% SDS-polyacrylamide Separating gel (for 2 x 1.75 cm gels)	
Buffer	Volume
Distilled water	6.34 mL
0.5 M Tris-HCl, pH 6.8	2.5 mL
10% (w/v) SDS	100 μ L
40% Acrylamide-Bis Solution (BioRad, California, USA)	1 mL
10% (w/v) APS (Sigma-Aldrich, St Louis, MO, USA)	50 μ L
TEMED (BioRad, California, USA)	24 μ L

2.5.3.2 Protein separation by gel electrophoresis

The appropriate volume of cell lysate was mixed with five μ L of 4x SDS sample buffer (loading dye) (**Table 2.8**) in the total volume of 20 μ L in order to achieve the desired μ g of protein. Samples were denatured (the unfolding of secondary/tertiary structures in proteins) by boiling at 95°C on a heat block for five minutes.

The vertical electrophoresis cell was set up with the SDS-PAGE gel and filled with 1x SDS running buffer (**Table 2.8**). Samples, as well as a reference molecular weight marker Precision Plus Protein™ Dual Color Standards (BioRad), were loaded onto the gel wells and separated on SDS-PAGE electrophoresed at 170 volts using Mini-Protean II Cell equipment (Bio-Rad, California, USA) for approximately one hour until the loading dye reached the base of the gel.

The gel was carefully removed from the apparatus and if the stain-free precast gel was used, the gel was imaged using ChemiDoc™ Touch Imaging System (BioRad, California, USA) and stain-free gel protocol in order to confirm that the proteins had been successfully separated on the gel.

2.5.3.3 Electrophoretic transfer

After completion of electrophoresis, the proteins on the gel were transferred onto either Nitrocellulose membranes (BioRad, California, USA) (used for low molecular weight proteins, e.g. DDAH and VEGF), or 0.45 μ M low-fluorescent Polyvinylidene difluoride (LF-PVDF) membranes (BioRad, California, USA) (used for high-molecular-weight proteins, e.g. NOSs).

Nitrocellulose membranes were soaked in transfer buffer for ten minutes. The LF-PVDF membranes were pre-incubated in methanol for one minute in order for the membrane pores to open up. They were then rinsed in distilled water and incubated for at least ten minutes in transfer buffer. The gels were also incubated in the transfer buffer for at least ten minutes. The gel and a membrane were sandwiched between the two filter papers and two sponges pre-soaked for 20 minutes in cold transfer buffer and transferred by wet transfer system. Low molecular weight proteins were transferred at 90 volts for two hours at 4°C using a Mini Trans-Blot Cell apparatus (BioRad, California, USA). High molecular weight proteins were transferred at 300 volts at a constant current of 240 mA for 1.5 hours.

To confirm the complete transfer of proteins from the gel, the 10% gels were incubated overnight in Coomassie blue (**Table 2.5**), and the precast stain-free gels were imaged using the ChemiDoc™ Touch Imaging System (BioRad, California, USA). The membranes used for the stain-free mini protein gels were imaged to determine the total protein transferred to the membrane.

2.5.3.4 Immunoblotting for detection of target proteins

Following the transfer, membranes were blocked to prevent the non-specific binding of the antibodies to the membrane. Nitrocellulose membranes were blocked overnight in 3% (w/v) skim milk powder in PBS-T (**Table 2.8**) at 4°C under agitation and a further one hour at room temperature the next morning. LF-PVDF membranes were blocked for one hour at room temperature in 5% soy milk in TBS-T, shaking on an orbit shaker.

After blocking, membranes were incubated with agitation with the desired primary antibody for either two hours at room temperature or overnight at 4°C, depending on the antibodies used (**Table 2.7**). Primary antibody dilutions were made based on the manufacturer's datasheet. Membranes were washed four times, each time for ten minutes in 1X TBS-T, prior to incubation with appropriate horseradish peroxidase (HRP)- conjugated secondary antibody (**Table 2.7**) at the recommended dilution based on antibody datasheet. Membranes were incubated under

agitation for one hour at room temperature. After four more washes with 1X TBS-T, the membranes were imaged.

2.5.3.5 Chemiluminescence imaging

Proteins were detected using the Pierce™ Enhanced chemiluminescence (ECL) substrate. Membranes were placed protein-side down on freshly mixed ECL substrate (one part ECL substrate, one part enhancer) and incubated for five minutes in the dark. Protein bands were visualised using ChemiDoc™ Touch Imaging Systems (BioRad, California, USA).

The protein band intensities were normalised to total protein using Image Lab™ Software (BioRad, California, USA) for precast gels. For 10% SDS-PAGE gels, the relative blots were imaged using the Image Lab™ Software (BioRad, California, USA) before reblotting with the reference protein (β -actin) used as endogenous controls.

For accurate quantitation of proteins loaded on each lane, total protein densitometry was performed on the chemiluminescent image of the blots by comparing the intensity of frames created around each protein lane, to the global background intensity using ChemDoc™ software (BioRad, California, USA).

2.6 Hypoxia induction

Gas mixtures containing 1% oxygen (O_2), with 5% CO_2 in nitrogen (N_2) were purchased from BOC Gas (Australia) and used to correspond to hypoxic oxygen levels, for immortalized human retinal pigment epithelial (RPE) cells (ARPE-19). Confluent cells were cultured in T75 flasks (Nunc, Roskilde, Denmark) for western blot experiments, or 6-well plates (Nunc, Roskilde, Denmark) for PCR assays, under conditions of normoxia ($O_2 = 21\%$), or hypoxia ($O_2 = 1\%$ gas mixtures) achieved in a commercially available air-tight Modulator Incubator Chamber (Billups-Rothenberg, Del Mar, CA) flushed with hypoxic gas at flow rate ten L/min for 3x ten minutes (at times zero, five hours after the start, and three hours before the finish) with > 60 flushes, according to manufacturer's protocol, to ensure adequate exposure. The chamber was sealed and returned to the 37 °C incubator for 1, 4, 8, 18, or 24 hours according to the experiment. Hypoxic ARPE-19 was removed from the chamber in the fume hood. Resealed gas confirmed a good seal for hypoxic exposure. The medium was removed and the adherent cells were washed 1x with warm PBS (methods adapted from Stempel *et al.* (Stempel et al., 2012)).

CHAPTER 2

For western blot experiments, 200 μ L of lysis buffer (with PMSF and protease inhibitors) was added to T75 flasks. Cells were scraped in the flask and the liquid was used to wash all the cellular lysate to the corner of the flask. The lysate was removed from the flask to a 1.7 mL tube and stored on ice. The whole process took four minutes (two minutes until the addition of lysis buffer). Normoxic cells were removed from the incubator and medium was removed and cells were washed with PBS. Cells were scraped and lysed similar to the previous procedure and used as a control.

For RNA analysis experiments with PCR, cells were cultured in plates. Upon removal of the media, the wells were quickly washed with warm PBS, and TRIzol[®] Reagent (Life Technologies, California, USA) was immediately added to each well. RNA was extracted from cells according to **methods section 2.7**.

2.6.1 Human VEGF-A ELISA

To measure VEGF-A protein levels in the normoxic vs. hypoxic media of ARPE-19 cells, Human VEGF-A ELISA Kit (Product #: 0028, Elisakit, Caribbean Park, VIC, Australia), was used. This ELISA kit recognises natural and recombinant human VEGF-A, with no significant cross-reaction with human VEGF-A. The kit contained an eight-well strip-well plate pre-coated with human VEGF-A capture antibody.

The wash buffer and standard reagents were prepared by diluting the 20X wash buffer, or the lyophilised standard, respectively, according to the manufacturer's protocol for cell culture samples. The anti-human VEGF-A biotin-labelled detection antibody solution and streptavidin-HRP conjugate solution were prepared from the stocks immediately prior to use. To perform the standard curve, standard solutions were prepared by seven serial dilutions starting at 2000 pg/mL and diluted 1:2 down to 31.25 pg/mL, using a multichannel pipette.

The standards (in duplicate), samples (media from normoxia- or hypoxia-treated ARPE-19 cells), and zero standard controls (media) (in triplicate) were added to the plate. The plate was then sealed with the adhesive cover provided and incubated for two hours at room temperature. Afterwards, each well of the plate was aspirated and washed 4x with 250 μ L wash buffer, using a multichannel pipette. To remove residual wash buffer, the plate was inverted and tapped on paper towels between each wash. 100 μ L of biotin labelled detection antibody was added to each well, and the plate was sealed with the adhesive cover provided and incubated for 1.5 hours at room temperature. After this period, the aspiration/wash step was repeated. Next, 100 μ L of the

CHAPTER 2

freshly diluted streptavidin-HRP conjugate was added to each well and the plate was sealed and incubated for 45 minutes at room temperature. Each well was aspirated and washed thoroughly 5x with 250 μ L wash buffer as explained before to reduce unwanted background. 100 μ L of TMB (3,3',5,5'-Tetramethylbenzidine) substrate was added to each well and incubated in dark for approximately 15 minutes at room temperature. The development process (blue colour generation) was checked every 5 minutes to prevent overdevelopment of the plate. After this period, the reaction was stopped by adding 50 μ L of stop solution to each well (the wells were turned from blue to yellow in colour). The optical density (OD) of the plate was determined using a microplate reader set at 450 nm, and for wavelength correction (background) it was set at 570 nm, using a VERSAmax absorbance microplate reader (Molecular Devices, San Jose, CA, USA).

The standard curve was created by plotting the mean OD of each standard on the y-axis versus the standard concentration on the x-axis. A best-fit curve was plotted through the standard points and overlaid a linear trend-line. When fitting a trend-line, if the r-squared value of regression (R^2) was not 0.99 or higher, the linear portion of the graph was found by removing the higher standard points from the analysis. The resultant equation displayed on the graph was used to calculate the unknown sample concentrations by solving for x. The concentration read from the standard curve was multiplied by the dilution factor for the diluted samples.

2.7 *In vitro* Matrigel[®] tube formation assay

The angiogenic potential of endothelial cells was determined using an established Matrigel[®] - based tube formation assay (DeCicco-Skinner et al., 2014, Shao and Guo, 2004).

Growth factor-reduced Matrigel[®] (Corning Life Sciences, NY, USA) was aliquoted into the wells of a 15 well μ -plate Angiogenesis culture plate (Ibidi, Verona, WI, USA) and incubated at 37 C for 30^oC minutes to set.

Matrigel (Corning) aliquots were thawed overnight on ice and on the day of the experiment, ten μ L/well was carefully pipetted into each well of an ibidi μ -plate. The Matrigel layer was allowed to be set by incubating the plate at 37^oC for minimum 30 minutes.

Preincubated endothelial cells for 18 hours with the compounds were resuspended in the medium without growth factors and heparin and cell numbers were determined using Trypan Blue and a hemocytometer. A cell suspension at a density of 7×10^3 cells from each category was transferred to separate new tubes and media was replaced by complete media with the relevant

CHAPTER 2

concentration of the compounds, calculated to the final volume of 50 μL /well. Cell suspensions were then reseeded in Matrigel-coated wells in quintuplicate and incubated for another five hours to form the vascular phenotype. Capillary-like structure formation was assessed after five hours: Wells were imaged with inverted phase-contrast microscopy (EVOS[®] FL Auto Cell Imaging System) (Thermo Scientific Revco, Waltham, MA, USA). Tubes, loops, and branches formed on Matrigel were counted per well, using Image J (National Institute of Health, USA), and compared to their vehicle control. Elongated multi-cellular tubule-like structures were defined as tubes, and circular holes separated by tube-like structures were defined as loops. Data were expressed as a mean number of capillary-like structures.

The initial assay on HUVEC cells was done by Dr. Kate Parham at Adelaide University, SA.

2.8 mRNA expression analysis

2.8.1 RNA extraction

Cells were grown in a 12-well plate (Nunc, Roskilde, Denmark) and total RNA was extracted using TRIzol[®] Reagent (Life Technologies, California, USA) according to the manufacturer's instructions.

Cell media was removed and 500 μL TRIzol was added to each well in the culture dish. Cells were lysed by pipetting up and down several times and then transferred to a 1.5 ml microfuge tube kept on ice. Homogenised samples were incubated for three minutes at room temperature to permit complete dissociation of the nucleoprotein complex. 100 μL chloroform (Chem-supply, Gillman, SA, Australia) was added and TRIzol/chloroform mix was vortexed vigorously for 15 seconds, incubated at room temperature for three minutes, and then centrifuged at 12,000 \times g for 15 min at 4°C. This process separates the sample into three distinct phases: 1. Organic red lower phase containing phenol red-chloroform mix, 2. White organic interphase containing protein and DNA, 3. The clear upper aqueous phase contains RNA. The third layer was carefully removed, avoiding any withdrawal of the interphase or organic phase, and was transferred into a new microfuge tube on ice. To precipitate the RNA, 250 μL of 100% isopropanol (Chem-supply, Gillman, SA, Australia) was added to tubes and inverted to mix, then incubated ten minutes at room temperature, followed by centrifugation at 12,000 \times g for ten minutes at 4°C. This supernatant was discarded, leaving the RNA pellet at the bottom of the tube. The pellet was washed by adding 1 ml of chilled 70% ethanol (Chem-supply, Gillman, SA, Australia) and flicked to dissolve the RNA pellet. The sample was vortexed and centrifuged at 10,000 \times g for five minutes at 4°C. The ethanol wash was then aspirated, and the remaining RNA pellet was air-dried on ice for approximately 30 minutes. The

CHAPTER 2

RNA pellet was then resuspended in 20 μL of Nuclease-free water (Promega Corporation, Madison, Wisconsin, USA), flicked, and heated to 62°C for ten minutes, then stored at -20°C until they were ready for quantitation.

2.8.2 RNA quantification

RNA quality and concentration were measured using a measured by spectrophotometry using a GeneQuant II RNA/DNA calculator (Pharmacia Biotech (GE Healthcare), Buckinghamshire, England).

Two μL of each RNA sample was first diluted in 98 μL of sterile mass spec grade water (1:50 dilution of RNA). The machine was calibrated and blanked with 100 μL of the same water. Optical absorbance was measured at 260 nm. Absorbance readings were given as one unit = 40 ng/ μL single strand RNA. Therefore, the concentration of RNA was calculated at:

Absorbance (OD₂₆₀) x 40 x 50 (dilution factor)

The quality of the RNA samples (RNA to protein ratios) was determined by having an OD₂₆₀/280 value between 1.6 to 2.0, respectively. Samples that were not within that range were discarded. RNA samples were stored at -20°C.

2.8.3 RNA purification

The RNA samples were treated with DNase to ensure that there was no genomic DNA in the samples. One μg of RNA was diluted with nuclease-free water to the total volume of 12 μL and treated with DNase I enzyme (InvivoGen, San Diego, CA, USA). To every μg of RNA, three μL of Master Mix (one μL DNase I, 1.5 μL of 10x DNase buffer, and 0.5 μL RNase inhibitor (InvivoGen, San Diego, CA, USA)) was added and made up to the total volume of 15 μL with nuclease-free water and incubated at room temperature for 15 minutes. Subsequently, 1.5 μL of EDTA (final concentration of 2.5 mM) was added in order to inactivate the DNase by incubation at 65°C for ten minutes. Samples were then stored on ice for a minimum of five minutes.

2.8.4 cDNA synthesis

First strand complementary DNA (cDNA) was synthesised using Random Hexamer Primers. The eight μL was added to eight μL of Master Mix (one μL (50 ng/ μL) of Random Hexamer primers (Invitrogen, Life Technologies, California, USA), one μL of ten mM deoxynucleotide triphosphate

CHAPTER 2

(dNTP) Mix (Bioline, NSW, Australia) and six μL nuclease-free water). The mixture was incubated at 65°C for five minutes followed by two minutes incubation on ice.

Four μL of Master Mix containing two μL 10x m-muLV Reverse Transcription (RT) buffer (Lucigen, Astral Scientific, NSW, Australia), one μL m-muLV Reverse Transcriptase enzyme (Lucigen, Astral Scientific, NSW, Australia) and one μL RNase inhibitor (InvivoGen, San Diego, CA, USA) added to make a 20 μL total volume. Reverse transcription occurred during one hour incubation at 42°C to generate cDNA strands, followed by heating at 90°C for ten minutes for the reaction to stop. The resulting cDNA was then diluted 1:5 using Nuclease-free water (20 μg cDNA solution in 80 μL water). Synthesised cDNA was stored at -20°C .

2.8.5 Quantitative PCR (q-PCR)

Two μL of diluted cDNA was added to 16 μL of Master Mix containing two μL of five μM gene-specific forward primer, two μL of five μM gene-specific reverse primer (**Table 2.3**) (at a final concentration of 625 nM each), eight μL of 2x GoTaq[®] qPCR Master Mix (Promega Corporation, Madison, Wisconsin, USA) and four μL nuclease-free water.

Reverse-transcription quantitative Polymerase Chain Reaction (RT-qPCR) was carried out using a Corbett Rotor-Gene 3000 (Corbett Research, Mortlake, NSW, Australia) according to the manufacturer's instructions. The cycle conditions were a 95°C hold for 15 minutes, followed by 40 cycles of 90°C for 15 seconds, 62°C for 15 seconds, and 72°C for 20 seconds. All reactions were performed in duplicate and negative control (water) was included in each PCR run. At the end of the experiments, the Cycle Threshold (CT) values were exported as an excel data file. The expression levels of targeted genes were presented relative to that of the housekeeping genes using the $\Delta\Delta\text{CT}$ method (Livak and Schmittgen, 2001). β -actin was used as the internal control to normalise gene expression in real time PCR.

2.8.6 Primer design

To quantify the RNA expression levels for extracted RNAs, forward and reverse primers were designed, aiming for the PCR product size of less than 150 base pairs (bp) for efficient amplification in real-time PCR. The annealing temperature (T_m) was set to a minimum of 57°C and a maximum of 63°C with a maximum difference of 3°C in the T_m of the forward and reverse primer pairs. The 3' end of the primer contained a C or G residue and to ensure a stable primer-template binding, the GC content was set around 40-60%. To increase primer sensitivity to a specific splice variant, they were designed to span the splice sites at an exon-intron junction on

target mRNA (Ye et al., 2012). Thereupon one half hybridises to the 3' end of one exon and the other half to the 5' end of the adjacent exon. Forward and reverse primer sequences used in this thesis are listed in **Table 2.10**. Primers were synthesised by Sigma-Aldrich (Sigma-Aldrich, St Louis, MO, USA).

2.9 Transient transfection

All transfections were performed using Lipofectamine™ 2000 Transfection Reagent (Invitrogen, Life Technologies, California, USA) according to the manufacturer's protocol. For HEK-293T transfections, cells were seeded in complete DMEM media supplemented with 10% FBS into six-well plates at approximately 5×10^5 cells per well the day before transfection and grown overnight. nNOS, iNOS, and eNOS/pIRES plasmids, were utilised for these experiments. For each transfection, 500 μL of serum-free medium, two μg of each plasmid, and four μL of lipofectamine were used. Lipofectamine was first incubated with 250 μL serum-free medium for five minutes at room temperature, and plasmids were diluted in a separate tube containing 250 μL serum-free media. Both tubes were combined, mixed gently, and incubated for 20 minutes at room temperature before adding to cells. The plate was gently mixed by rocking and then placed back into the incubator. Six hours post transfection, cell media was replaced with fresh complete media to minimize cellular toxicity effects of lipofectamine according to the manufacturer's instruction. Cells were harvested 48 hours post transfection and then lysed and stored at -20°C .

2.10 Cell transfection with small interfering RNAs (siRNAs)

Cells were transfected with siRNAs using the Lipofectamine™ 2000 Transfection Reagent (Invitrogen, Life Technologies, California, USA). Cells were seeded at the density of 1.2×10^5 cells per well of a six-well plate and transfected the following day. Thirty micromolar stocks of targeted siRNA (DDAH1 or VEGF-A siRNA) and non-targeting siRNA (negative control) were diluted to a final concentration of two nM. For each siRNA well, 250 μL of serum-free medium, two μL siRNA, and eight μL of lipofectamine were prepared in duplicate according to the manufacturer's instructions. The complexes were incubated for 20 minutes at room temperature before adding to the cells. Six hours post-transfection, cell medium was replaced with fresh complete medium to minimize cellular toxicity effects of lipofectamine according to the manufacturer's instruction. Cells were harvested 72 hours after and transfection efficiency was determined using Real-Time PCR (mRNA expression) and ELISA or Western Blotting (protein expression). ELISA readouts were normalised to the corresponding cell counts obtained from the crystal violet assay.

CHAPTER 2

Control siRNA and DDAH1-targeting siRNA (Santa Cruz Biotechnology), and control siRNA and VEGF-A-targeting siRNA (Sigma-Aldrich, St Louis, MO, USA) were transfected at 30 nM.

2.11 Mass Spectrometry

2.11.1 Cell culture

HEK-293T cells were seeded into 12x T175 flasks at 8×10^4 cells/cm² and incubated overnight to allow attachment. The next day, they were treated in three sets of quadruplicates with zero (vehicle: water), five or 100 μ M ZST316. After 24 hours treatment, cells were $\geq 95\%$ confluence.

The supernatant media was aspirated out and cells in each flask were rinsed twice with 20 mL warmed TBS. Flasks were then placed on ice and mechanical detachment of cells was performed by gently scraping the cells in ten mL ice cold TBS by rubber scraper. Detached cells were transferred into 50 mL Eppendorf Low Protein Binding Conical Tubes. The washing and scraping steps were repeated two more times for each flask to the total of 30 mL cell suspension per flask in each tube. Tubes were kept on ice (each quadruplicate set at a time) until they were centrifuged at 1500 rpm for six minutes at 4°C. Supernatant TBS from each tube was aspirated out and wet cell pellets in each tube were weighed before the appropriate volume of ice cold 20 mM Tris base lysis buffer (containing fresh protease and phosphatase inhibitor cocktail tablets) was added to each. The amount of lysis buffer added to each wet pellet was estimated assuming that 5% of the wet weight of the pellet is the extractable protein content (mg), aiming to get two mg/ml final concentration. Quickly after adding the lysis buffer to the cell pellets and gently pipetting up and down, tubes were snap frozen in liquid nitrogen (two minutes per tube) and stored at -80°C.

2.11.2 Sample preparation

2.11.2.1 Protein extraction

Sample lysates were homogenised using a seven mL Dounce tissue grinder (Wheaton, Mainz, Germany). Then, the homogenates were transferred into ten mL ultracentrifuge tubes suitable for a Beckman 50Ti rotor (Beckman Coulter Life Sciences). Samples were then ultracentrifuged using a Beckman XPN-80 ultracentrifuge (Beckman Coulter Life Sciences) at 50,000 rpm (112,000 g) for 30 minutes at 4°C. The extracted proteins from lysates were quantified by EZQ protein assay (BioRad, California, USA) to estimate protein concentration in each sample.

2.11.2.2 Reduction and alkylation

Two mg of each cell protein extract was transferred to Maxymum Recovery tubes (Axygen). Dithiothreitol (DTT) was added to a final concentration of ten mM and samples were incubated at 56°C for one hour. Subsequently, chloroacetamide was added to a final concentration of 20 mM and a final volume of 2550 microliters. Samples were incubated at room temperature for one hour while being protected from light.

2.11.2.3 In-solution trypsin digestion of proteins

Samples were subjected to trypsin digestion in the presence of one mM Calcium Chloride and 100mM Ammonium Bicarbonate. Trypsin enzyme (Pierce Biotechnology, MA, USA) was added to a final protease: protein ratio of 1:50 (w/w) in a 40 ml final volume. Samples were incubated at 37°C overnight.

2.11.2.4 Quenching of trypsin activity

The trypsin digestion process was stopped via acidification (pH <4), by adding trifluoroacetic acid (TFA) to a final concentration of 0.1%.

2.11.2.5 Freeze-drying samples

The digested samples (40 mL /digest) were placed at -80°C for 20 minutes and then transferred to liquid nitrogen before being freeze-dried in a Christ freeze drier (Alpha 2-4 LDplus, Osterode am Harz, Germany).

2.11.2.6 1D SDS PAGE using BioRad precast gels

Digests originally had 40 mL volume before freeze-drying, and a Tris molarity of 20 mM. Freeze-dried digests were resuspended in a volume of dH₂O to achieve a final 50 mM Tris concentration.

One-dimensional gel electrophoresis (1D SDS PAGE) was performed to confirm that the digest process was successful using an 18 well 4-20% MIDI-PROTEIN®TGX™Precast Protein Gel (BioRad, California, USA).

Prior to preparing the samples for 1D gel electrophoresis, samples were diluted 1:5 to avoid pipetting errors. An undigested HEK-293T cell lysate was used as control for the digest and only this control sample was reduced by DTT and heated at 95°C. 10 µg of the already reduced, alkylated and digested samples were loaded onto the gel in a 20 µL final volume. Electrophoresis was carried out at 300 volts for 23 minutes, using Trans-Blot® Turbo™ Transfer System (Bio-Rad, Hercules, CA, USA). Once complete, the gel was imaged using the Bio-Rad Gel-Doc EZ Imager, with

five minutes Activation/Optimal Auto Exposure (10.3 seconds). Complete digestion of the proteins into peptides was achieved in all samples (**Fig. 2.1**).

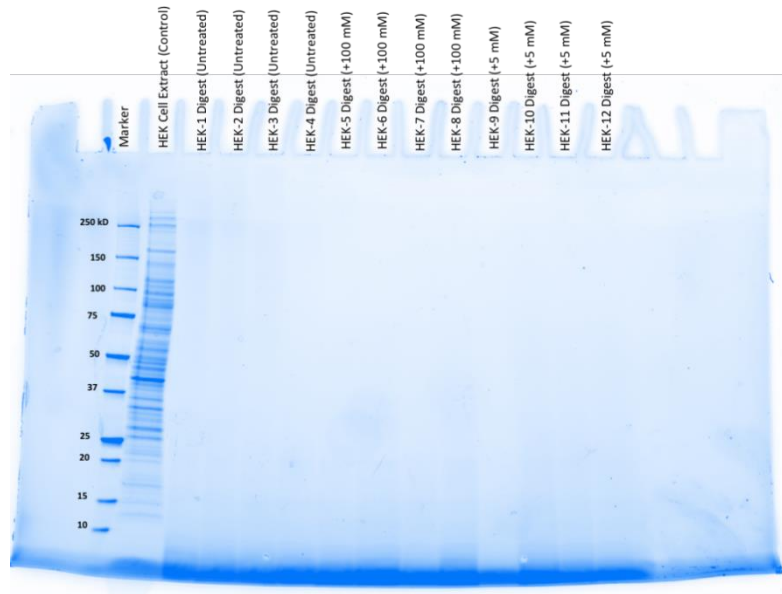


Figure 2.1. Western blot image showing the success of the digestion process.

2.11.2.6.1 Spectral library

Prior to performing DIA analysis, a spectral library is required. The more comprehensive the library is, the greater the number of proteins that can be quantified. Consequently, two spectral library generation methods were performed and then combined. The first method utilised high pH reversed-phase fractionation to generate eight fractions which were then analysed by DDA analysis using a Thermo Fusion Lumos mass spectrometer (ThermoFisher Scientific). Fractionation decreases the complexity of proteins in each sample thereby increasing the ability of the instrument to detect low abundance proteins and therefore increasing the size of the library.

2.11.2.7 High pH reversed-phase fractionation of proteolytic digests

A number of methods can be used to perform the fractionation such as cation exchange chromatography. However, most of these methods suffer from significant run to run variation. Consequently, high pH reversed phase fractionation is widely performed due to its run-to-run reproducibility. The fractionation is performed at the peptide level and results in hundreds of thousands of peptides in the sample to be spread over eight fractions which increases the opportunity of the mass spectrometer to identify each peptide. Reversed phase chemistry utilising C18 beads is employed with an alkaline pH used instead of the usual acidic pH. This is because the high-performance liquid chromatography (HPLC) column that is placed at the inlet of the mass

CHAPTER 2

spectrometer separates the peptides uses C18 beads at an acidic pH. However, the peptide fractionation needs to be orthogonal to the separation prior to mass spectrometry to maximise the separation of peptides entering the instrument. Therefore, high pH is employed as peptides separate differently on C18 columns at alkaline pH compared to acidic pH because the peptides are more negatively charged. The alkaline pH C18 fractionation is followed by low pH C18 separation prior to entry into the mass spectrometer and provides two levels of separation which allows the mass spectrometer to identify more peptides.

For this step, Pierce™ High pH Reversed-Phase Peptide Fractionation Kit (ThermoFisher Scientific) was used. Initially, five µg of each sample (100µL) was pooled into a maximum recovery tube (total Protein: 60 µg, total volume: 1200 µL). The pooled sample was dried down in a Christ RVC 2-25 CD plus vacuum concentrator (Christ, Osterode am Harz, Germany) for 4.5 hours.

Fractionation solutions were prepared in 2.0 mL tubes, according to Tables below (**Table 2.3**).

CHAPTER 2

Table 2.3. High-ph step-elution solution composition.

Fraction #	Acetonitrile %	Acetonitrile (μL)	Triethylamine (0.1%) (μL)	Total (μL)	Volume per Sample (μL)
1	5	17	317	333	300
2	7.5	25	308	333	300
3	10	33	300	333	300
4	12.5	42	292	333	300
5	15	50	283	333	300
6	17.5	58	275	333	300
7	20	67	267	333	300
8	50	167	167	333	300

2.11.2.7.1 Conditioning of the spin columns

The protective white tip from the bottom of the column containing C18 beads was removed and discarded. The column was placed into a 2.0 mL Maxymum Recovery tubes (Axygen). Centrifugation at 5000 g for two minutes was performed to remove the storage solution and pack the resin material. Then flow-through was discarded. The column was washed twice with 300 μL of 100% acetonitrile (ACN) via centrifugation at 5000 g for two minutes. ACN was discarded and wash steps were repeated using 0.1% TFA solution.

The spin column was then placed into a new 2.0 mL Maxymum recovery sample tube and 300 μL of the sample solution was loaded onto the column. The top cap was replaced, and centrifugation was performed at 3000 x g for two minutes. Eluate was retained as “flow-through” fraction.

The column was placed into a new 2.0 mL sample tube and washed using 300 μL of ultra-pure water. Centrifuged was performed at 3000 x g for two minutes. The wash flow-through was discarded. The column was then placed into a new 2.0 mL maxymum recovery tube and 300μL of the first fractionation solution (5% ACN in 0.1% TFA) was loaded and centrifuged at 3000 x g for two minutes to collect the first fraction. This step was repeated for the remaining fractionation solutions resulting in a total of eight fractions. The liquid content of each fraction was evaporated to dryness using a Christ vacuum concentrator. Each dried fraction was re-suspended in six μl of 0.1% formic acid, sonicated for one minute and transferred to mass spectrometry vials before LC-MS analysis.

2.11.2.7.2 Thermo Fusion Lumos mass DDA spectrometry library data acquisition

Each of the eight fractions were analysed on a Thermo Fusion Lumos mass spectrometer fitted with a FAIMS Pro ion mobility interface (ThermoFisher Scientific) and coupled to a Thermo Dionex nano uHPLC (Dionex, Sunnyvale, California, USA). The FAIMS Pro ion mobility interface provides an additional element of separation by employing a stream of nitrogen gas which impedes the flow of peptides into the instrument. This impedance is overcome by negative compensation voltages to increase the attraction of the positively charged ions. The result is that uncharged ions (neutrals) are mostly eliminated as they are unable to navigate around the compensation voltage electrode, and that additional separation of peptides occurs through the differential CCS (collisional cross section) of each peptide. For example, two peptides may have the same m/z , but if one of the two ions is doubly charged and the other is triply charged, the actual mass of the triply charged ion will be 50% larger and will possess a larger CCS and will travel more slowly through the nitrogen gas “headwind” and therefore will enter the instrument later than the doubly charge ion.

The instrument was operated in positive ion mode utilising 60,000 MS1 resolution, 30,000 MS2 resolution, charge states of +2 to +6 were selected with an automatic gain control (AGC) target of 40,000 and an intensity threshold of 50,000. Twenty MS2 scans were performed following each MS1 scan. Maximum injection time was set to auto. Internal mass calibration using EASY-IC™ (ThermoFisher) was enabled. The FAIMS Pro was operated with compensation voltages of -50 volts and -70 volts. Expected peak width was 30 seconds and dynamic exclusion was set to 15 seconds after a single hit with high and low mass tolerances of ten ppm. For the complete list of settings, **see Appendix 15**. Approximately one μg of each sample was loaded onto a Thermo Acclaim PepMap 100 trap column (75 μm x two cm, three μm C18 beads with 100Å pore size) and then eluted onto an inhouse pulled-tip nano HPLC column created from 75 μm inner diameter fused silica capillary packed with 1.9 μm ReproSil-Pur C18 beads (Dr. Maisch, Ammerbuch, Germany) to a length of 25cm. The column was heated to 60°C using a Sonation PRSO-V2 column heater (Sonation lab solutions, Biberach, Germany). The spray tip was pulled using a Sutter p-2000 laser tip puller (Sutter Instrument Company, California, USA). The flow rate for loading samples onto the trap was three μL per minute and the flow rate for the gradient pump was 300 nL per minute. The column and trap were equilibrated in Solvent A (0.1% formic acid in water) and eluted with solvent B (0.1% formic acid in 80% ACN) using a 2-30% linear gradient over 107 minutes (**Table 2.4**). Total run time was 140 minutes.

Table 2.4. HPLC chromatography gradient.

Time	Solvent B
0 min	2%
8 min	2%
115 min	30%
120 min	60%
125 min	100%
129 min	100%
130 min	2%
140 n	2%

2.11.2.7.3 Thermo Exploris 480 mass spectrometry GPF library generation

To enhance the DDA spectral library, HEK-293T tryptic digests were also analysed on a Thermo Exploris 480 coupled to a Thermo Dionex Ultimate 3000 nano uHPLC which was fitted with the same specification C18 trap, custom lab manufactured spray tip column heated to 60°C and 300 nL flow rate as described for the Fusion Lumos. Gas phase fractionation was employed in conjunction with DIA for this analysis. MS1 Gas phase fractionation (GPF) separates peptides in the gas phase i.e., once peptides have entered the instrument in the gas phase. It is implemented by analysing multiple injections of the same sample with only 100 m/z mass range analysed in each injection. For example, the first injection analyses the 398-504 m/z mass range, and the second injection analyses the 498-604 m/z mass range. In total, seven injections covering the 398-1104 m/z are performed. A lower limit of 398 m/z is used because peptides below that m/z are too small (less than six amino acids) to generate useful data, and tryptic digests produce very few peptides of greater than 1100 m/z. The MS1 m/z windows had an overlap of two m/z to ensure no peptides are missed. Subsequently, each 104 m/z MS1 window was subjected to MS2 DIA utilising four m/z windows. It might sound counterintuitive to use GPF with narrow range DIA to generate a DIA library. However, the software package Spectronaut can do this because of the low complexity of the MS2 data due to the fractionation and the narrow four m/z windows.

The HPLC chromatography was the same as described for the Fusion Lumos. For each injection, MS1 resolution was 60,000, normalised AGC target = 300% and max injection time 100 ms. MS2 four m/z windows were employed at resolution of 30,000, normalised AGC = 100% with 28 % collision energy with first mass at 110 m/z and data was centroided. For a complete list of instrument settings, **see Appendix 16.**

CHAPTER 2

Consequently, both DDA and GPF narrow window DIA methods were used and combined to maximise the library coverage.

The eight DDA data files and the eight DIA data files were used to generate an HEK-293T spectral library using Spectronaut software v 15.0.2.210615.50606 (Biognosys, Schlieren, Switzerland). Spectronaut uses the Pulsar search engine and a human Uniprot database 10-2019 (186,679 entries) and identified 70,439 peptides and 6,203 protein groups in the library.

The Exploris 480 was also used to generate the label free quantification data using DIA on the 12 test samples (4 x control, 4 x 5 μ M and 4 x 100 μ M) using the same HPLC system setup. However, the instrument settings were as follows.

The Exploris 480 was operated in DIA mode. MS1 resolution was 60,000, MS2 resolution was 15,000 and ten m/z MS2 DIA windows were set from 375-980 m/z with one m/z overlap. Internal calibration was set to “off”, normalised AGC target was set to 100% for MS1 and 200% for MS2. Complete instrument settings are listed in **Appendix 17**.

2.11.2.7.4 Spectronaut label free quantification

The control, five μ M and 100 μ M data files were analysed by Spectronaut software using the in house generated HEK-293T spectral library and default analysis settings which identifies proteins that are differentially expressed by a \log_2 Fold-change ≥ 0.6 and Q-value ≤ 0.05 which equates to greater than 50% or less than 50%.

2.12 Pathway Analyses

For pathway analysis, the InnateDB software (version 5.4) was used (publicly available at <http://www.innatedb.com>). Uniprot IDs from the list of differentially expressed proteins in each set (vehicle or ZST316-treated samples) were uploaded and used for pathway analysis. The steps of analysis are as follows:

On the first page of InnateDB software, “Pathway Analysis” was selected by clicking on the “Analysis” button (**Fig. 2.2, A**). “Web Form” (**Fig. 2.2, B**) was selected, and Uniprot IDs from the list of differentially expressed proteins for each treatment group (**Appendices 6 to 10**) were uploaded (**Fig. 2.2, C**). To specify the columns, “Column1” was selected and defined as “Cross-Reference ID”, and then “Uniprot” was specified as the cross-reference database by clicking on the OK button (**Fig. 2.2, D**), and the specified list is generated (**Fig. 2.2, E**). By clicking the “Next”

CHAPTER 2

button, the list of associated pathways with the uploaded protein IDs appeared which was downloaded (MS Excel) and saved to an excel sheet (**Fig. 2.2, F**). Next, to perform the over-representation analysis, the red “Pathway ORA” button at the top of the page was clicked. This step was performed by a “hypergeometric” test algorithm and corrected for multiple comparisons using the “Benjamini Hochberg” method as recommended by the software (**Fig. 2.2, F and G**). The generated table was downloaded and saved to an excel sheet (**Fig. 2.2, H**). Of note, the statistical analysis on ORA has also been conducted by Bonferroni as the correction method which generates the same results. Pathways with false discovery rate (FDR)-adjusted p-value (Q-value) <0.05 were considered significantly enriched.

A

B

If you use InnateDB for your research, please cite the following publication:
Breuer et al. InnateDB: systems biology of innate immunity and beyond - recent updates and continuing curation. *Nucl. Acids Res.* (2013) 41 (Q1).

InnateDB is being developed jointly by the [Brinkman Laboratory](#) (Simon Fraser University, British Columbia, Canada), the [Hancock Laboratory](#) (University of British Columbia, Vancouver, British Columbia) and the [Lynn EMBL Australia Group](#) (South Australian Health & Medical Research Institute and Flinders University, Adelaide, Australia).

Funding is currently provided by Allergan and EMBL, Australia. Previous funding has been provided by Genome Canada, the Foundation for the National Institutes of Health through the Grand Challenges in Global Health initiative and by Teagasc. InnateDB curated interactions are licensed under the [Design Science License](#). All other data is licensed under the terms of the originating database. Contact: innatedb-mail@sfu.ca

CHAPTER 2

C

Pathway Analysis - Upload D

InnateDB Pathway Analysis enables users to determine InnateDB incorporates pathway annotation (all pathways comprehensive sources of pathways available).

To do a Pathway Analysis, first upload a tab-delimited expression data fold-changes and p-values) from up to 10000 genes (human, mouse or cow only) and any associated quantitative data (e.g. gene IDs) are accepted.

Once you have a list of pathways associated with your gene list, you can view the pathways and their associated genes (e.g. in a given gene/protein list). InnateDB also provides pathway annotations (e.g. KEGG, INOH, BioCarta and PID and is thus one of the most comprehensive sources of pathways available).

Enter your dataset here:

A8K2P3

Cancel Upload

If you use InnateDB for your research, please cite the following publication:
 Breuer et al. *InnateDB: systems biology of innate immunity and beyond - recent updates and continuing curation*. *Nucl. Acids Res.* (2013) 41 (D1).

InnateDB is being developed jointly by the [Binkman Laboratory](#) (Simon Fraser University, British Columbia, Canada), the [Hancock Laboratory](#) (University of British Columbia, Vancouver, British Columbia) and the [Lynn EMBL Australia Group](#) (South Australian Health & Medical Research Institute and Flinders University, Adelaide, Australia).

Funding is currently provided by Allergan and EMBL Australia. Previous funding has been provided by Genome Canada, the Foundation for the National Institutes of Health through the Grand Challenges in Global Health initiative and by Teagasc. InnateDB curated interactions are licensed under the [Design Science License](#). All other data is licensed under the terms of the originating database. Contact: innatedb-mal@sfu.ca

D

Please note that when using InnateDB identifiers, only gene IDs are valid, not interaction IDs!

If you have included gene expression data - identify which columns contain the gene expression values and their associated p-values.

You may also identify the column containing the probe IDs if you have included them in your file.

Check this checkbox if you have uploaded a list of bovine gene identifiers and want to include results predicted by orthology to human genes.

This column is:

Cross-reference ID

Please specify the cross-reference database: UniProt

Close OK

Column 1
B4DY21
Q9H1Z4
A6NKZ2
B3KXY4
H3BM91
Q9NR48
ADA024RDT6
ADA024R366
ADA0C4DGH6
B4E070

Showing 1 to 10 of 72 entries

« Previous Next »

E

Pathway Analysis - Specify which data is in each column

Click on the column headers to specify which column in your data file contains the identifiers/accession numbers for each gene (human, mouse or cow only) and which database they come from. This is called the "Cross-reference ID".

Please note that when using InnateDB identifiers, only gene IDs are valid, not interaction IDs!

If you have included gene expression data - identify which columns contain the gene expression values and their associated p-values.

You may also identify the column containing the probe IDs if you have included them in your file.

Check this checkbox if you have uploaded a list of bovine gene identifiers and want to include results predicted by orthology to human genes.

Cross-reference ID

B4DY21
Q9H1Z4
A6NKZ2
B3KXY4
H3BM91
Q9NR48
ADA024RDT6
ADA024R366
ADA0C4DGH6
B4E070

Showing 1 to 10 of 72 entries

« Previous Next »

If you use InnateDB for your research, please cite the following publication:
 Breuer et al. *InnateDB: systems biology of innate immunity and beyond - recent updates and continuing curation*. *Nucl. Acids Res.* (2013) 41 (D1).

InnateDB is being developed jointly by the [Binkman Laboratory](#) (Simon Fraser University, British Columbia, Canada), the [Hancock Laboratory](#) (University of British Columbia, Vancouver, British Columbia) and the [Lynn EMBL Australia Group](#) (South Australian Health & Medical Research Institute and Flinders University, Adelaide, Australia).

Funding is currently provided by Allergan and EMBL Australia. Previous funding has been provided by Genome Canada, the Foundation for the National Institutes of Health through the Grand Challenges in Global Health initiative and by Teagasc. InnateDB curated interactions are licensed under the [Design Science License](#). All other data is licensed under the terms of the originating database. Contact: innatedb-mal@sfu.ca

CHAPTER 2

F

Result: 41 distinct pathway(s) found

25 records per page

Query Xref	Organism	Query Name	Source	Pathway
A6NHL2	Homo sapiens	TUBAL3	KEGG	Coli infection
A6NHL2	Homo sapiens	TUBAL3	KEGG	Gap junction
A6NHL2	Homo sapiens	TUBAL3	KEGG	Phagosome
O95059	Homo sapiens	RPP14	KEGG	RNA transport
P00491	Homo sapiens	PNP	KEGG	Purine metabolism
P00491	Homo sapiens	PNP	INOH	Nicotinate Nicotinamide metabolism
P00491	Homo sapiens	PNP	KEGG	Pyrimidine metabolism
P00491	Homo sapiens	PNP	INOH	Purine nucleotides nucleosides metabolism
P00491	Homo sapiens	PNP	REACTOME	Purine salvage
P00491	Homo sapiens	PNP	REACTOME	Purine metabolism
P00491	Homo sapiens	PNP	KEGG	Nicotinate and nicotinamide metabolism
P00491	Homo sapiens	PNP	REACTOME	Purine catabolism
P00491	Homo sapiens	PNP	REACTOME	Metabolism
P00491	Homo sapiens	PNP	REACTOME	Metabolism of nucleotides
P61026	Homo sapiens	RAB10	REACTOME	Translocation of GLUT4 to the plasma membrane
P61026	Homo sapiens	RAB10	REACTOME	Membrane Trafficking
Q15599	Homo sapiens	SLC9A3R2	PID_NCI	LPA receptor mediated events
Q15599	Homo sapiens	SLC9A3R2	KEGG	Aldosterone-regulated sodium reabsorption
Q2M1P5	Homo sapiens	KIF7	REACTOME	Signaling by Hedgehog
Q2M1P5	Homo sapiens	KIF7	REACTOME	Hedgehog 'off' state
Q2M1P5	Homo sapiens	KIF7	REACTOME	Signal Transduction
Q2M1P5	Homo sapiens	KIF7	NETPATH	Hedgehog
Q8IWW7	Homo sapiens	UBR1	REACTOME	Adaptive Immune System
Q8IWW7	Homo sapiens	UBR1	REACTOME	Antigen processing: Ubiquitination & Proteasome degradation
Q8IWW7	Homo sapiens	UBR1	REACTOME	Immune System

Showing 1 to 25 of 46 entries

← Previous 1 2 Next →

G

Result: 41 distinct pathway(s) found

25 records per page

Pathway Over-Representation Analysis

Warning: NO gene expression data uploaded.
The analysis will identify over-represented pathways without considering gene expression values.

Analysis Algorithm and P-Value Correction Method Selection
Please choose between the following algorithms and correction methods:

Choose algorithm: Hypergeometric (recommended)

Choose Correction Method: Benjamini Hochberg (recommended)

Cancel Do analysis

Query Xref	Organism	Query Name	Source	Pathway
A6NHL2	Homo sapiens	TUBAL3	KEGG	Coli infection
A6NHL2	Homo sapiens	TUBAL3	KEGG	Gap junction
A6NHL2	Homo sapiens	TUBAL3	KEGG	Phagosome
O95059	Homo sapiens	RPP14	KEGG	RNA transport
P00491	Homo sapiens	PNP	KEGG	Purine metabolism
P00491	Homo sapiens	PNP	INOH	Nicotinate and nicotinamide metabolism
P00491	Homo sapiens	PNP	KEGG	Pyrimidine metabolism
P00491	Homo sapiens	PNP	INOH	Purine nucleotides nucleosides metabolism
P00491	Homo sapiens	PNP	REACTOME	Purine salvage
P00491	Homo sapiens	PNP	REACTOME	Purine metabolism
P00491	Homo sapiens	PNP	KEGG	Nicotinate and nicotinamide metabolism
P00491	Homo sapiens	PNP	REACTOME	Purine catabolism
P00491	Homo sapiens	PNP	REACTOME	Metabolism
P00491	Homo sapiens	PNP	REACTOME	Metabolism of nucleotides
P61026	Homo sapiens	RAB10	REACTOME	Translocation of GLUT4 to the plasma membrane

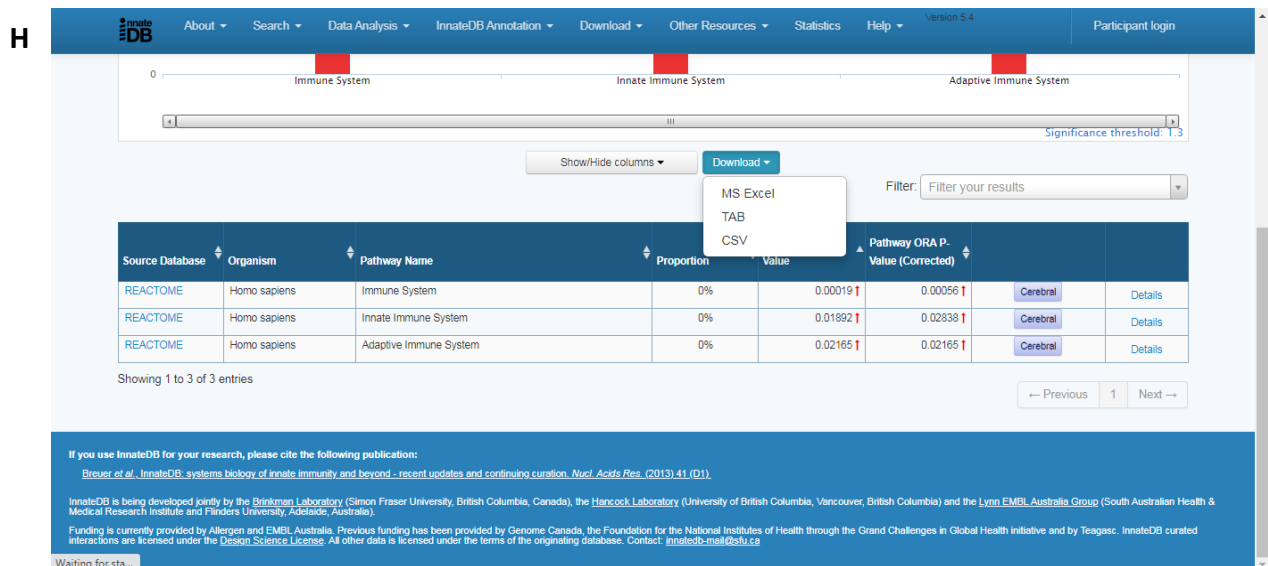


Figure 2.2. The screenshots illustrate steps to perform InnateDB pathway analysis, followed by over-representation analysis (ORA).

2.13 Statistical methods

For statistical analyses of multiple comparisons, one-way Analysis of Variance (ANOVA) was performed in SPSS, followed by Bonferroni post hoc tests. Statistical analyses of tube formation assay were performed using GraphPad Prism 6 software (GraphPad Inc., La Jolla, CA, USA), with a two-tailed independent t-test. Two-group comparisons were performed by using parametric unpaired Student's t-test. P-value ≤ 0.05 was considered statistically significant. Results are presented as mean \pm standard error (SEM).

2.14 Materials, reagents, and equipment

L257, a reference DDAH1 inhibitor (Rossiter et al., 2005), and the novel DDAH1 inhibitor compounds, ZST316, ZST152, and ZST086, synthesised in The Department of Clinical Pharmacology, Flinders University (Tommasi, 2015), were used in the experiments.

L-257, the NOS inhibitors, SDMA (symmetric dimethylarginine, N^G , N^G -Dimethyl-L-arginine), and L-NMMA (N^G -Monomethyl-L-arginine), and DDAH1 inhibitors were dissolved in sterile mass spec grade water to make the desired concentrations. Stock solutions were aliquoted and stored frozen at -20°C .

CHAPTER 2

Table 2.5. List of chemicals and reagents.

Chemicals or Reagents	Supplier
27-gauge (G) BD PrecisionGlide™ needle	Becton Dickinson Medical Pte Limited, Singapore
2-β-mercaptoethanol	Sigma-Aldrich, St Louise, MO, USA
40% Acrylamide-Bis solution	BioRad Laboratories, CA, USA
4–20% Mini or MIDI-PROTEAN® TGX™ Precast Protein Gel	Bio-Rad, Hercules, CA, USA
Acetic acid	Ajax Finechem, Seven Hills, NSW, Australia
Acetonitrile (ACN)	Thermofisher Scientific, Waltham, MA, USA
Agarose	AppliChem, Darmstadt, Germany
Ammonium Bicarbonate	Sigma-Aldrich, St Louise, MO, USA
Ammonium per sulphate (APS)	Sigma-Aldrich, St Louise, MO, USA
Antibiotic-Antimycotic 100X-solution	Thermofisher Scientific, Waltham, MA, USA
Bovine serum albumin (BSA) solution	New England Biolabs, Beverly, MA, USA
Bradford reagent	Sigma-Aldrich, St Louis, MO, USA
Bromophenol blue	Sigma-Aldrich, St Louise, MO, USA
Buffered-formalin	Orion Labs, California, USA
Calcium Chloride	BDH chemicals (analaR), Australia
Chloroacetamide	Sigma-Aldrich, St Louise, MO, USA
cOmplete™ protease inhibitor cocktail	Roche Diagnostics, Mannheim, Germany
Coomassie Blue R250	BioRad Laboratories, CA, USA
Crystal violet	Sigma-Aldrich, St Louise, MO, USA
DDAH1 inhibitors ZST086, ZST152, ZST316	Department of Clinical Pharmacology, Flinders University, SA, Australia
Dimethylsulphoxide (DMSO)	Merck KGaA, Darmstadt, Germany
Dithiothreitol (DTT)	Fisher Bioreagents, (ThermoFisher), Pittsburgh, Pennsylvania, USA
DNA ladder (1kb)	Promega, Madison, WI, USA
DNase I enzyme	InvivoGen, San Diego, CA 92121 USA
dNTP Mix (cat# BIO-39029)	Bioline, NSW, Australia
Dulbecco's modified eagle medium (DMEM)	Gibco, Life Technologies, Grand Island, NY, USA
ELISA Kit (Human VEGF-A, product #: 0028)	Elisakit, Caribbean Park, VIC, Australia
Endothelial cell growth supplement (ECGS)	Sigma-Aldrich, St Louis, MO, USA
Enhanced chemiluminescence (ECL) substrate, 32106	Pierce™ Enhanced chemiluminescence (ECL)
F-12K Medium	Corning Life Sciences, NY, USA
Fetal bovine serum (FBS)	Bovogen Biologicals, VIC, Australia
GlutaMAX™ Supplement	Thermofisher Scientific, Waltham, MA, USA

CHAPTER 2

Chemicals or Reagents	Supplier
Glycerol	BDH Laboratory supplied, Poole, UK
Glycine	Sigma-Aldrich, St Louise, MO, USA
GoTaq® qPCR Master Mix (cat# A6002)	Promega Corporation, Madison, Wisconsin, USA
Heparin	Sigma-Aldrich, St Louis, MO, USA
HEPES buffer 1M	ThermoFisher Scientific, Waltham, MA, USA
Horse Serum, heat inactivated, New Zealand origin	Gibco, Life Technologies, Grand Island, NY, USA
Human Fibronectin	Roche Life Sciences, Basel, Switzerland
HyClone Medium 199 (with Earle's Balanced Salt Solution (EBSS), with L-Glutamine)	Cytiva, Marlborough, Massachusetts, USA
Hydrochloric acid (HCl)	Merck, Kilsyth, VIC, Australia
In Vitro Toxicology Assay Kit, Sulforhodamine B based, Cat # TOC6	Sigma-Aldrich, St Louis, MO, USA.
Isopropanol	Ajax-Finechem, Seven Hills, NSW, Australia
L-257 (reference DDAH inhibitor)	Donated by Dr. James Leiper, University of Glasgow, Scotland
L-alanyl-L-glutamine (Glutamax)	Invitrogen, Carlsbad, CA
Lipofectamine™ 2000	Invitrogen, Grand Island, NY, USA
Matrigel®	Corning Life Sciences, NY, USA
MEM non-essential amino acids	Gibco, Life Technologies, Grand Island, NY, USA
Methanol	RCI Labscan, Bangkok, Thailand
MPP+ Iodide	Sigma-Aldrich, St Louis, MO, USA
N, N, N', N'-tetramethylethylenediamine (TEMED)	Promega, USA
NG,NG'-Dimethyl-L-arginine di(p-hydroxyazobenzene-p'-sulfonate) salt (SDMA)	Sigma-Aldrich, St Louise, MO, USA
NG,NG-Dimethylarginine dihydrochlorid (ADMA)	Sigma-Aldrich, St Louise, MO, USA
NG-Methyl-L-arginine acetate salt (L-NMMA)	Sigma-Aldrich, St Louise, MO, USA
Normocin	InvivoGen, San Diego, CA 92121 USA
Nuclease-free water	Promega Corporation, Madison, Wisconsin, USA
Nunc™ Biobanking and Cell Culture Cryogenic Tubes	ThermoFisher Scientific, Waltham, MA, USA
Nunc™ Cell Culture Treated EasyFlasks T75, or T175,	Nunc, Roskilde, Denmark
Nunc™ Cell-Culture Treated Multidishes (6-, 12-, or 96-well plates)	Nunc, Roskilde, Denmark
NxGen® M-MuLV Reverse Transcriptase (cat# 30222-1)	Lucigen, Astral Scientific Pty. Ltd., NSW, Australia
NxGen® RNase Inhibitor (cat# 30281-1)	Lucigen, Astral Scientific Pty. Ltd., NSW, Australia
Ovalbumin stock	BioRad, California, USA
PhosStop™ Easy Pack phosphatase inhibitor cocktail	Roche Diagnostics, Mannheim, Germany

CHAPTER 2

Chemicals or Reagents	Supplier
Pierce™ High pH Reversed-Phase Peptide Fractionation Kit	ThermoFisher Scientific, Waltham, MA, USA
Pierce™ Trypsin enzyme Protease, MS grade	Pierce Biotechnology, MA, USA
Protein ladder (Dual Color protein Western Standards (Cat# 161-0377))	BioRad Laboratories, California, USA
RNase inhibitor	InvivoGen, San Diego, CA 92121 USA
Skim milk powder	Fonterra Brands, NZ
Sodium bicarbonate (NaHCO ₃)	Chem Supply, Gillman, SA, Australia
Sodium chloride	Chem Supply, Gillman, SA, Australia
Sodium dodecyl sulphate (SDS)	BDH Laboratory supplied, Poole, UK
β-Mercaptoethanol	Sigma-Aldrich, St Louis, MO, USA
Trifluoroacetic acid (TFA)	Sigma-Aldrich, St Louis, MO, USA
Trizma-base	Astral Scientific, Taren Point, NSW, Australia
TRIzol® Reagent	Life Technologies, California, USA
Trypan Blue	Sigma-Aldrich, St Louis, MO, USA
Trypsin-EDTA 0.5% (10x)	Gibco, Life Technologies, Grand Island, NY
Tween-20	Sigma-Aldrich, St Louis, MO, USA

CHAPTER 2

Table 2.6. List of equipment and software.

Equipment or Software	Supplier
Air-tight Modulator Incubator Chamber	Billups-Rothenberg, Del Mar, CA
Axygen 1.5 mL Maxymum Recovery microcentrifuge tube	Corning. Axygen Scientific Inc, union city, CA, USA
Beckman 50Ti rotor	Beckman Coulter Life Sciences
Beckman XPN-80 ultracentrifuge	Beckman Coulter Life Sciences
Beckman XPN-80 ultracentrifuge	Beckman Coulter Life Sciences
Bio-Rad Gel-Doc EZ Imager	Bio-Rad, Hercules, CA, USA
Bio-Rad Mini-Sub GT electrophoresis system	Bio-Rad, Hercules, CA, USA
ChemiDoc™ Touch Imaging System	Bio-Rad, Hercules, CA, USA
Christ Freeze Dryer - Alpha 2-4 LDplus	John Morris Scientific Pty Ltd, Osterode am Harz, Germany
Christ RVC 2-25 CD plus vacuum concentrator	Christ, Osterode am Harz, Germany
Corbett Rotor-Gene 3000	Corbett Research, Mortlake, NSW, Australia
Dry block heater	Ratek laboratory equipment, Boronia, VIC, Australia
Easy Breeze™ Gel Dryer	Hoefler Inc, Massachusetts, USA
EASY-IC™	Thermo Scientific Revco, Waltham, MA, USA
E-plates	ACEA Biosciences, California, USA
EVOS® FL Auto Cell Imaging System	Thermo Scientific Revco, Waltham, MA, USA
EZQ™ Protein Quantitation assay	Thermo Scientific Revco, Waltham, MA, USA
FAIMS Pro ion mobility interface	ThermoFisher Scientific, Thebarton, SA, Australia
Gel tank blotting system	Bio-Rad, Hercules, CA, USA
GeneQuant II RNA/DNA calculator	Pharmacia Biotech (GE Healthcare), Buckinghamshire, England
GraphPad Prism 6 software	GraphPad Inc., La Jolla, CA, USA
Hy-Lite Ultra Plane Haemocytometer	Hausser Scientific, USA
ImageJ software	National Institute of Health, USA
Imagelab™ software	Bio-Rad, Hercules, CA, USA
IncuCyte™ Live Cell Image Analysis System	Essen Bioscience, Michigan, USA
InnateDB software (version 5.4)	http://www.innatedb.com
Inverted microscope (CK2)	OLYMPUS, NSW, Australia
LF-PVDF membrane	
Medium Orbital Shaker – Analogue – EOM5	Ratek, Boronia, VIC, Australia
Nitrocellulose membrane	Bio-Rad, Hercules, CA, USA
Nunc™ EasYFlask™ Cell Culture Flasks (T75 and T175)	Thermofisher Scientific, Waltham, MA, USA
Personal Vortex Mixer – VM1 (IC-VM1)	Ratek laboratory equipment, Boronia, VIC, Australia
Plastic 2mL Micro centrifuge Tube Low Binding	Corning. Axygen Scientific Inc, union city, CA, USA

CHAPTER 2

Equipment or Software	Supplier
DNase/RNase Free	
Power-Pac Basic	Bio-Rad, Hercules, CA, USA
Pulled-tip nano HPLC column	Made inhouse, Proteomics, facility, Flinders University, SA, Australia
Refrigerated Centrifuge MIKRO 200R (Hettich)	LabGear, South Melbourne, VIC, Australia
ReproSil-Pur C18 beads (1.9 µm)	Dr. Maisch, Ammerbuch, Germany
RotorGene 3000 instrument	Corbett Research, Mortlake, NSW, Australia
Sonation PRSO-V2 column heater	Sonation lab solutions, Biberach, Germany
Spectronaut software v 15.0.2.210615.50606	Biognosys, Schlieren, Switzerland
Spectrophotometer GeneQuant II	Pharmacia Biotech (GE Healthcare), Buckinghamshire, England.
Sutter p-2000 laser tip puller	Sutter Instrument Company, California, USA
Tempette Junior TE-85 water bath	Techne, Staffordshire, UK
Thermo Dionex Ultimate 3000 nano uHPLC	Dionex, Sunnyvale, California, USA
Thermo Exploris 480	ThermoFisher Scientific, Thebarton, SA, Australia
Thermo Fusion Lumos mass spectrometer	ThermoFisher Scientific, Thebarton, SA, Australia
Trans-Blot®Turbo™Transfer System	Bio-Rad, Hercules, CA, USA
Ultra-low temperature freezer (-80°C)	Thermo Scientific Revco, Waltham, MA, USA
Varian CARY 300 BIO UV-Visible Spectrophotometer	New Life Scientific, Cridersville, OH, USA
VCX 130 (Vibra-Cell™ Ultrasonic Liquid Processor	Sonics & Materials, Connecticut, USA
VERSAmax Absorbance Microplate Reader.	Molecular Devices, San Jose, CA, USA
Weigh scales	Shimadzu, Kyoto, Japan
WHEATON® Dounce Tissue Grinder, 7 mL	Wheaton, Mainz, Germany
xCELLigence RCTA platform	ACEA Biosciences, California, USA
µSlide angiogenesis slides	Ibidi, Verona, WI, USA

CHAPTER 2

Table 2.7. List of antibodies.

Antibody	Dilution	Catalogue number and supplier
Primary Antibodies		
DDAH1 (Goat anti-DDAH1 IgG)	1:1000	Ab 2231 (Goat pAb), Abcam, Cambridge, UK
DDAH2 (Goat anti-DDAH2 IgG)	1:1000	Ab1383 (Goat pAb), Abcam, Cambridge, UK
NOS 1 (nNOS)	1:1000	Ab76067 (Rabbit mAb), Abcam, Cambridge, UK
NOS 2 (iNOS)	1:200	H-174 sc-8310 (Rabbit pAb), Santa Cruz, CA, USA
NOS 3 (eNOS)	1:1000 1:1000	1) 49G3 (Rabbit mAb), Cell Signalling 2) 610296 (Purified Mouse Ab), BD Biosciences, USA
VEGF-A (Mouse anti human VEGF)	1:1000	V2110-12 (mAb), US Biological, MA, USA
β -actin (Rabbit anti-actin)	1:1000	BA3R (Mouse mAb), Sigma, St Louise, MO, USA
Phospho-eNOS (Ser1177)	1:1000	9571 (Rabbit), Cell Signalling Technology, MA, USA
Secondary Antibodies		
Donkey anti-Rabbit HRP	1:3000	J1-711-035-152, Jackson ImmunoResearch Laboratories, Inc, Pennsylvania, USA
Donkey anti-Mouse HRP	1:3000	J1-711-035-150, Jackson ImmunoResearch Laboratories, Inc, Pennsylvania, USA

CHAPTER 2

The composition of general buffers used throughout this thesis is listed in **Table 2.8**. Sterilisation was achieved either by autoclaving (121°C) or ultra-filtration (0.2-0.45 µM).

Table 2.8. Buffers and solutions.

Buffer	Formula
Coomassie blue staining solution	0.1% (w/v) Coomassie brilliant blue G-250 in 50% (v/v) methanol: H ₂ O, with 10% (v/v) acetic acid solution.
PBST (1x)	1x PBS, 0.1% Tween-20 Add 1 mL 10x Tween-20 to each L of 1x PBS
Phosphatase inhibitor solution	One PhosSTOP Phosphatase inhibitor cocktail tablet, 10 mL water
Phosphate Buffer Saline (PBS) (1x) (pH7.4)	137mM NaCl, 2.7 mM KCl, 10mM Na ₂ HPO ₄ , and 2mM KH ₂ PO ₄
RIPA Buffer	10 mM Tris-HCl pH 7.4, 150 mM NaCl, 1mM EDTA, 0.5% Triton X-100, 1% deoxycholate, 0.1% SDS, 1 mM DDT. For 50 mM: 0.5 mL 1 M Tris/HCl, 6.25 mL 1.2 M NaCl, 1 mL 50 mM EGTA, 0.5 mL Triton X-100, 5 mL 10% deoxycolate, 0.5 mL 10% SDS, 50 µL 1M DTT, water to 50 mL.
SDS Running Buffer (10x)	125 mM Tris Base, 1 M Glycine, 0.5% SDS. For 500 mL: 7.57 g Tris/HCl, 37.5 g Glycine, 25 mL of 10% SDS, water to 500 mL.
SDS Sample Buffer (4x loading dye)	For 10 mL: 2.5 mL 1 M Tris pH 6.8, 4 mL Glycerol, 0.8 g SDS (sodium dodecyl sulphate), 0.8 mL 2-β-mercaptoethanol, 40 mg Bromophenol blue, 100 µL 10% APS, 12 µL TEMED (N,N,N',N'-Tetramethylethylenediamine), Milli-Q® water to 10 mL.
Sulforhodamine B (SRB) Solution	0.4% SRB in 1% acetic acid
TAE buffer (1x)	40 mM Tris (pH 8), 20 mM acetic acid, 1 mM EDTA
TBS (10x)	0.2 M Tris Base, 1.37 M NaCl. For 500 mL: 12.1 g Tris Base, 40 g NaCl, water to 500 mL. pH adjusted to 7.6, using concentrated HCl.
TBST (1x)	1x TBS, 0.05% Tween-20 Add 0.5 mL 10x Tween-20 to each L of 1x TBS
Trichloroacetic acid (TCA) 50% (w/v) Solution	15 g solid TCA, 22 mL dH ₂ O
Western Transfer Buffer	For 1 L: 200 mL of 5x BioRad Transfer buffer, 600 mL 100% ethanol, water to 1 L

CHAPTER 2

Table 2.9. List of cells lines.

Cell line	Supplier	Catalogue number
PC-12	ATCC®, Manassas, VA, USA	CRL-1721.1
SH-SY5Y	ATCC®, Manassas, VA, USA	CRL-2266
ARPE-19	ATCC®, Manassas, VA, USA. (Donated by Professor Justine Smith, Flinders University, SA, Australia)	CRL-2302
Primary HUVEC	Established in the laboratory of Dr. Claudine Bonder, University of Adelaide, SA, Australia	N/A
VeraVec™ HUVEC	Angiocrine Bioscience, NY, USA (Donated by Dr. Claudine Bonder, University of Adelaide, SA, Australia).	hVera101
HEK-293	ATCC®, Manassas, VA, USA	CRL-3216

CHAPTER 2

Table 2.10. Primers and oligonucleotides sequences for RT-PCR.

Primers	Sequence (Forward (F) and Reverse (R)) / Catalogue number	Supplier
CAT-2 (SLC7A2 solute carrier family 7 (cationic amino acid transporter, y+ system), member 2 NM_001008539.3)	F: 5'-GAGAGCTGTGGGCCTTCAT-3' R: 5'-CAGGCTCTTGCAACACTTGA-3'	Universal Probe Library, probe: Sigma-Aldrich, St Louise, MO, USA
DDAH1 (Transcript variant 1) NM_012137.3	F: 5'-CTCCGGACTGCGTCTTC-3' R: 5'-TGCTTCTTTCATCATGTCAACC-3'	Universal Probe Library, probe: Sigma-Aldrich, St Louise, MO, USA
DDAH1 (Transcript variant 2) NM_001134445.1	F: 5'-CTCAAGTCTGCCAAAGAC-3' R: 5'-CCTTTCCATACAGATGAAACCA-3'	Universal Probe Library, probe: Sigma-Aldrich, St Louise, MO, USA
DDAH2	F: 5'-GACACGGCCCTAATCACG-3' R: 5'-AAGAGAACGTCAGTGCCATC-3'	Sigma-Aldrich, St Louise, MO, USA
eNOS (Transcript variant 1: longest isoform) NM_000603.4)	F: 5'-CATCAACCAGTACTACAGCTCCA-3' R: 5'-CCTAAGCTGGTAGGTGCCTGT-3'	Universal Probe Library, probe: Sigma-Aldrich, St Louise, MO, USA
iNOS (NM_000625.4)	F: 5'-AGGATCCAGTGGTCCAACC-3' R: 5'-ATGGCCGACCTGATGTTG-3'	Universal Probe Library, probe: Sigma-Aldrich, St Louise, MO, USA
nNOS (Predominant transcript (Isoform 1) NM_000620.4)	F: 5'-AAGGCAGAGATGAAAGATATGGG-3' R: 5'-CCATAGGTCATTGAAGACTCGG-3'	Sigma-Aldrich, St Louise, MO, USA
VEGF-A (NM_001025366.2)	F: 5'-GTGCATTGGAGCCTTGCTTG-3' R: 5'-ACTCGATCTCATCAGGGTACTC-3'	Sigma-Aldrich, St Louise, MO, USA
β-actin	F: 5'-CTGGCGGCACCACCATGTACCCT-3' R: 5'-GGAGGGGCCGACTCGTCATACT-3'	Sigma-Aldrich, St Louise, MO, USA
18S	F: 5'-CGATGCTCTTAGCTGAGTGT-3' R: 5'-GGTCCAAGAATTCACCTCT-3'	Sigma-Aldrich, St Louise, MO, USA
DDAH1 siRNA	sc-105276	Santa Cruz Biotechnology
Control siRNA-A for DDAH1	sc-37007	Santa Cruz Biotechnology
VEGF-A siRNA	SASI_Hs01 00201117	Sigma-Aldrich, St Louise, MO, USA
Control siRNA for VEGF-A	SIC001	Sigma-Aldrich, St Louise, MO, USA
Mycoplasma Genus PCR primers	Genus 1: GGGAGCAAACAGGATTAGATACCCT Genus 2: TGCACCATCTGTCACTCTGTTAACCTG	Sigma-Aldrich, St Louise, MO, USA

CHAPTER 3. CHARACTERISATION OF NOVEL DDAH1 INHIBITORS

3.1 Introduction and aims

Several small molecule anti-angiogenic agents have been developed and widely used against pathologies and implications associated with excessive angiogenesis including cancer, arthritis, and psoriasis. Nevertheless, rather than targeting angiogenic pathways, these agents may also interact with un-intended biological targets, inducing multiple signalling pathways, most importantly those associated with cytotoxicity, leading to adverse effects. Therefore, early identification of any potential cellular toxicity is one of the most important steps in developing a new drug, including the novel DDAH1 inhibitors.

Furthermore, majority of the current anti-angiogenic drugs have focused on the VEGF pathway as the most dominant target for blocking angiogenesis. However, several adverse side-effects have been reported after systemic and local administration of anti-VEGF therapies, including haemorrhage and thrombosis, hypertension, impaired wound healing, and cardiac impairment (Nuzzi and Tridico, 2015, Kamba and McDonald, 2007).

NOS inhibition has previously shown to suppress angiogenesis *in vitro* and *in vivo* (Babaei et al., 1998, Ziche et al., 1994). Therefore, direct or indirect inhibition of NOS by novel DDAH1 inhibitors can be a potential strategy to inhibit excessive angiogenesis without having the severe side-effects of blocking VEGF.

To date, the adverse cellular effects of a wide range of doses of our novel DDAH1 inhibitors in different cell lines including endothelial and non-endothelial cells have not been tested. We therefore investigated such effects in terms of potential synergism with common neurotoxic insults in neuronal cell models (PC-12 and SH-SY5Y cell lines), assessing cell viability by end point colorimetric assays (Sulforhodamine B (SRB) and crystal violet assay) and proliferation by real-time quantitative analysis (Incucyte and xCELLigence). We then assessed the effects of DDAH1 inhibition on the ability of endothelial cells to form capillary-like structures by means of Matrigel tube formation assay to determine their capacity to modulate angiogenesis *in-vitro*.

3.2 Results

3.2.1 Assessing the effects of DDAH1 inhibitors

3.2.1.1 Neuronal cells

A dose response experiment was performed using ZST152, one of our most potent DDAH1 inhibitors (based on their inhibitory constant, K_i), in cultured neuronal cell lines. Four-day treatment of undifferentiated PC-12 cells with 500 μ M of the neurotoxin 1-methyl-4-phenylpyridinium (MPP^+) (used as positive control) resulted in 66% cell death. By contrast, MPP^+ concentrations between 1 μ M and 100 μ M did not affect cell viability when compared to non-treated control cells (**Fig. 3.1, A**) (**For the choice of MPP^+ doses, refer to discussion section, page 106**). The SRB assay showed that treatment of PC-12 cells with ZST152 concentrations up to 100 μ M had no tangible effect on cell viability over a period of four days compared to the vehicle control cells. However, ZST152 500 μ M caused cell death as reflected by a 72% reduction in absorbance (**Fig. 3.1, B**). By contrast, another DDAH1 inhibitor used as a reference, L-257, did not cause PC-12 cell death at concentrations up to 500 μ M (**Refer to discussion section 3.3.1.1, page 107**), when compared to vehicle control cells ($P \leq 0.05$) (**Fig. 3.1, C**).

CHAPTER 3

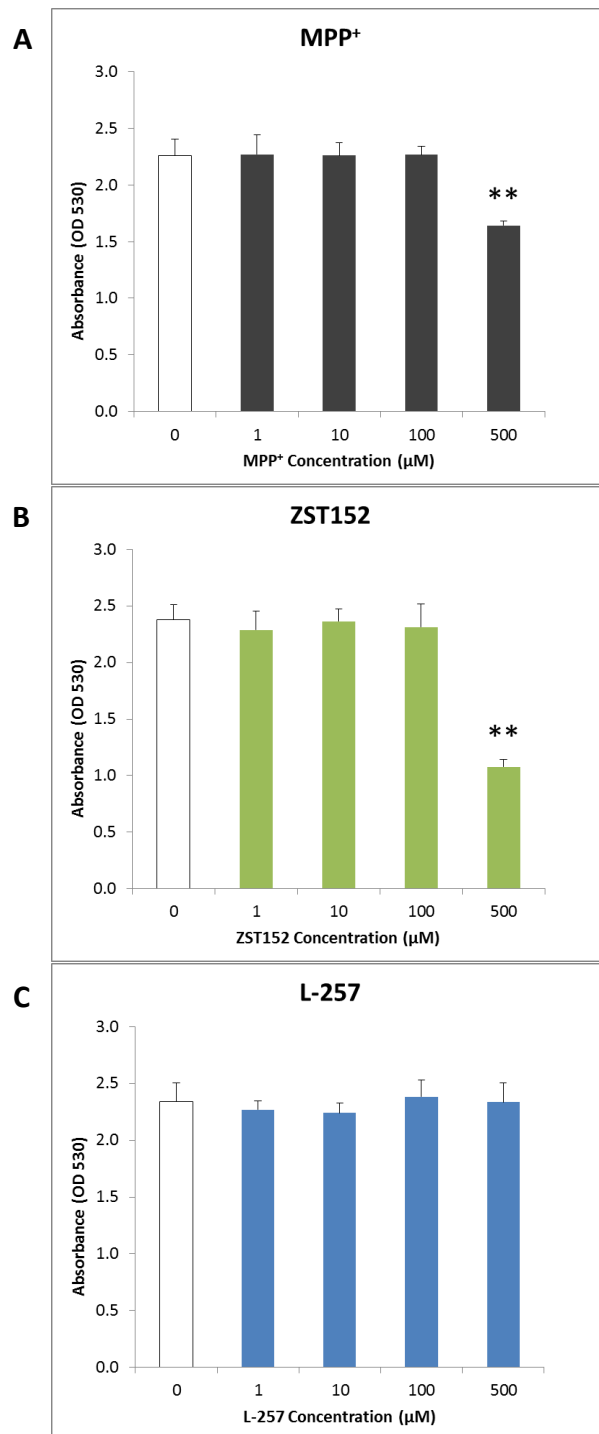


Figure 3.1. Viability screening of PC-12 cells treated with ZST152, L-257, and MPP⁺ toxin.

SRB absorbance measurements in undifferentiated PC-12 cells treated for four days with concentrations of 0, 1, 100, or 500 μM of neurotoxin MPP⁺ (A), ZST152 (B), and L-257 (C). The level of absorbance was measured at 530 nm, indicating the cell mass. One way ANOVA was used to compare treated cells with control (0 μM compound), followed by Bonferroni post-hoc test. Results are expressed as mean ± SEM of 4 technical replicates (**P ≤ 0.01).

To further investigate cell viability, we tested three of our most potent DDAH1 inhibitors, ZST316, ZST152 and ZST086, in decreasing potency order, in undifferentiated SH-SY5Y cells (human neuroblastoma epithelial cell line).

CHAPTER 3

None of the compounds had any significant effect on SH-SY5Y cells using concentrations between 5 and 125 μM for 48 hours. Quantitative results of crystal violet staining of treated SHSY5Y cells are shown in **Figure 3.2**.

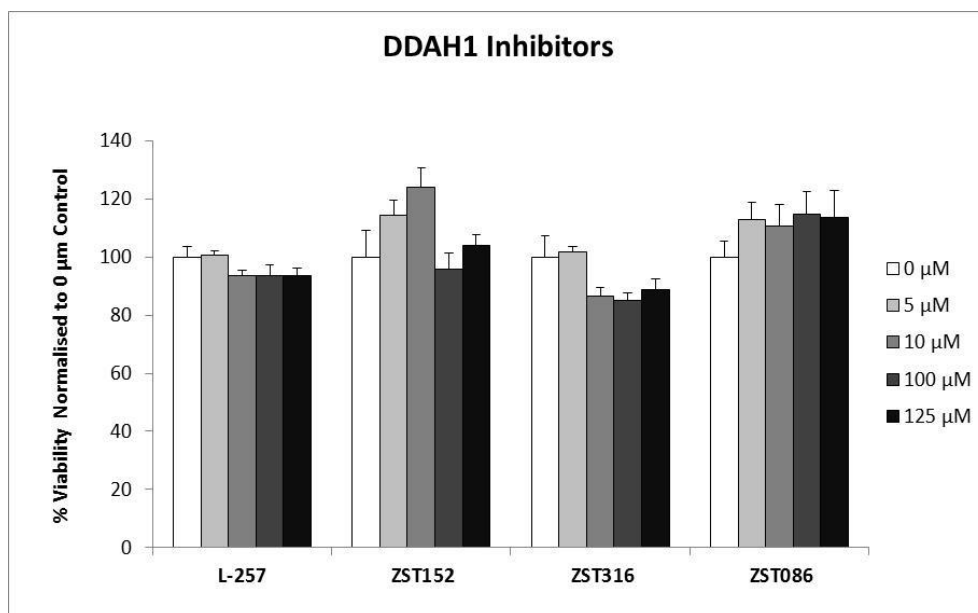


Figure 3.2. Viability of undifferentiated SH-SY5Y cells 48 hours post-treatment with DDAH1 inhibitors.

Quantitative results of crystal violet staining of undifferentiated SH-SY5Y cells showing the effect of different concentrations of ZST316, ZST152, ZST086, and L-257 on cell proliferation.

Cells were incubated (48 h/37 $^{\circ}\text{C}$) with different concentrations of inhibitor (0, 5, 10, 100, and 125 μM). Absorbance data are compared to untreated control and results are expressed as mean \pm SEM of 4 technical replicates. One way ANOVA was used to compare the treated groups with control (0 μM compound), followed by Bonferroni post hoc test.

The compounds were then tested in neuronal cells exposed to MPP^+ to investigate whether they would augment MPP^+ -mediated toxicity.

Initially, we investigated the toxic dose of MPP^+ . The effect of MPP^+ on undifferentiated SH-SY5Y cell proliferation was confirmed over a period of 24 and 48 hours after treatment, and the values of the absorbance obtained from the IncuCyte system were normalized (0–100% range). The cytotoxic dose of MPP^+ over the 24 hours incubation period was ≥ 2 mM, with a reduction of 35.2% in cell proliferation. However, a quarter of this dose (500 μM MPP^+) was sufficient to reduce cell proliferation by 47.7% when cells were incubated for 48 hours. Doses higher than 500 μM MPP^+ led to higher toxicity (**Fig. 3.3**).

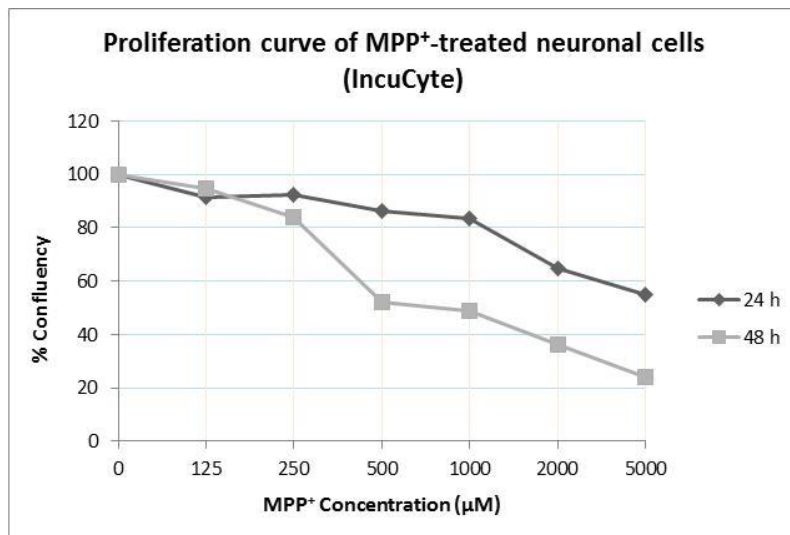


Figure 3.3. Proliferation curve of undifferentiated SH-SY5Y cells treated with MPP⁺ doses.

Percent confluency measurements for undifferentiated SH-SY5Y cells treated with MPP⁺ with doses between 125 and 5000 µM compared to control medium using the IncuCyte Live Cell Analysis System. MPP⁺ treatment was performed for 24 hours (Dark grey line), and 48 hours (light grey line) (n=1).

A crystal violet assay was then used to evaluate the toxic dose of MPP⁺ on undifferentiated SH-SY5Y cells. Significant neurotoxicity was observed with MPP⁺ ($\geq 2\text{mM}$) after both 24 hours (**Fig. 3.4, A**), and 48 hours (**Fig. 3.4, B**) incubation.

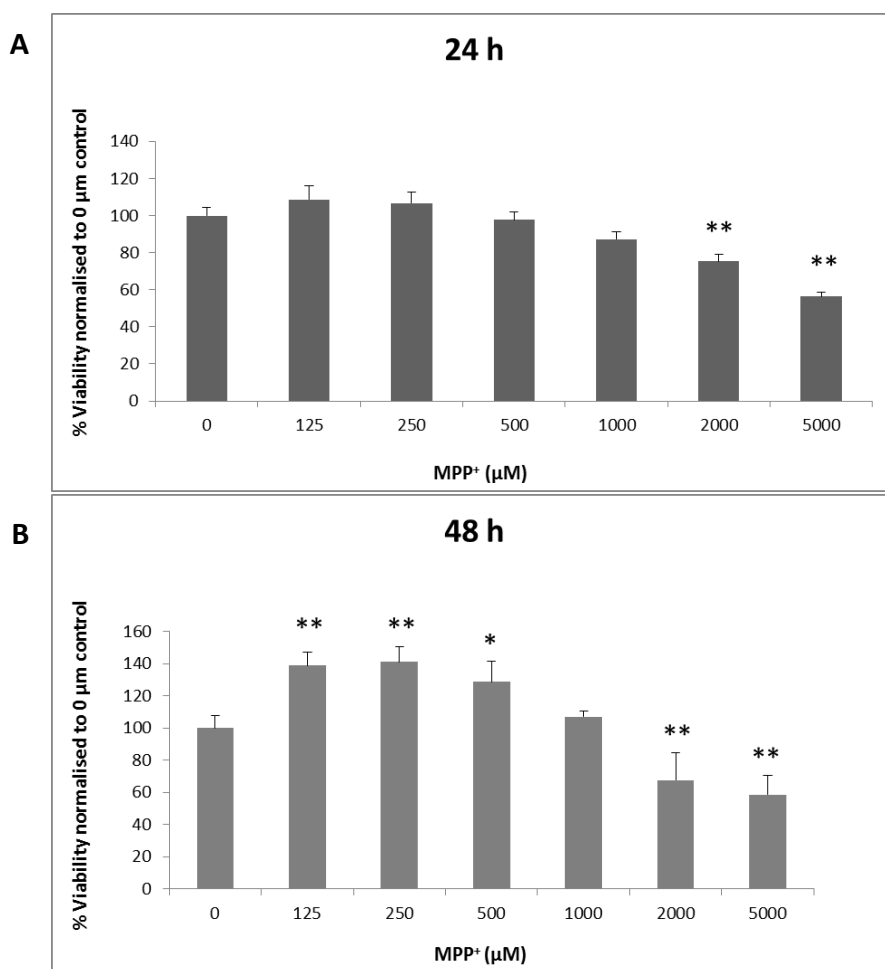


Figure 3.4. Dose-response viability curves of crystal violet assay for MPP⁺-treated undifferentiated SH-SY5Y cells.

Crystal violet absorbance measurements in undifferentiated SH-SY5Y cells treated with MPP⁺ (125-5000 µM) after (A) 24 hours, or (B) 48 hours incubation, compared with cells in control media. Results are expressed as mean ± SEM of 3 biological replicates for 24 h, or 4 technical replicates for 48 h experiments. One way ANOVA was used to compare the treated groups with **control (0 µM compound)**, followed by **Bonferroni post hoc test** (*P ≤ 0.05, **P ≤ 0.01).

We then studied the combined effect of DDAH1 inhibitors and 2 mM MPP⁺ using crystal violet assay. 24-hour incubation of undifferentiated SHSY5Y cells with MPP⁺ confirmed cytotoxicity at 2 mM compared to control cells (**Fig. 3.5**). When cells were preincubated with ZST316, ZST152, ZST086, and L-257 (5, 25 and 100 µM) a paradoxical protective effect against MPP⁺-induced toxicity was observed for all concentrations (**Fig. 3.5**). As these experiments were conducted twice, each with four technical replicates, statistical analysis was not performed (Refer to **discussion section 3.3.1.1, page 107** for more information on concentration selection).

CHAPTER 3

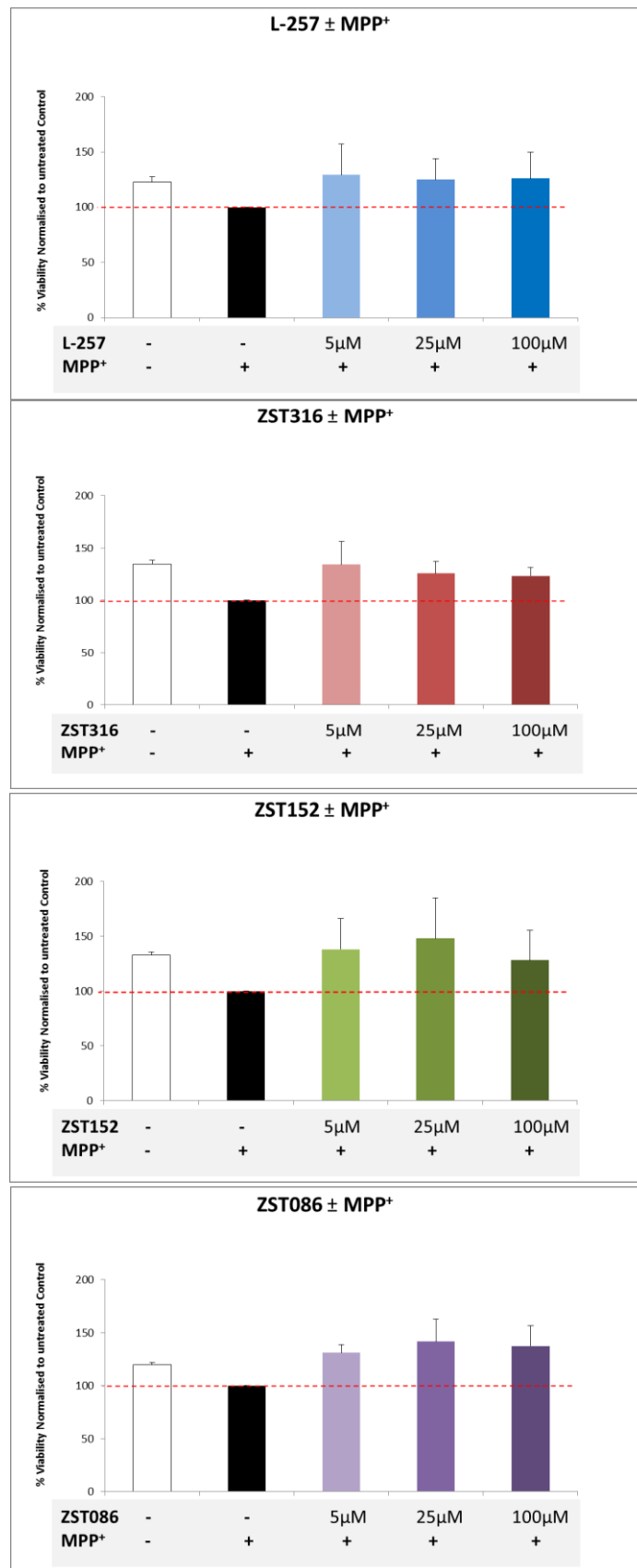


Figure 3.5. Viability of SH-SY5Y treated with DDAH1 inhibitors against MPP⁺-induced toxicity.

Crystal violet assay was performed to measure the viability of undifferentiated SH-SY5Y cells 24 h post-treatment with ZST316, ZST152, and ZST086, and L-257 vs MPP⁺ (n=2, each with 4 technical replicates).

CHAPTER 3

The attenuation of MPP⁺-induced toxicity by our DDAH1 inhibitors was re-evaluated and confirmed using the real-time imaging and analysis platform, IncuCyte Live Cell Analysis system (**Fig. 3.6**).

CHAPTER 3

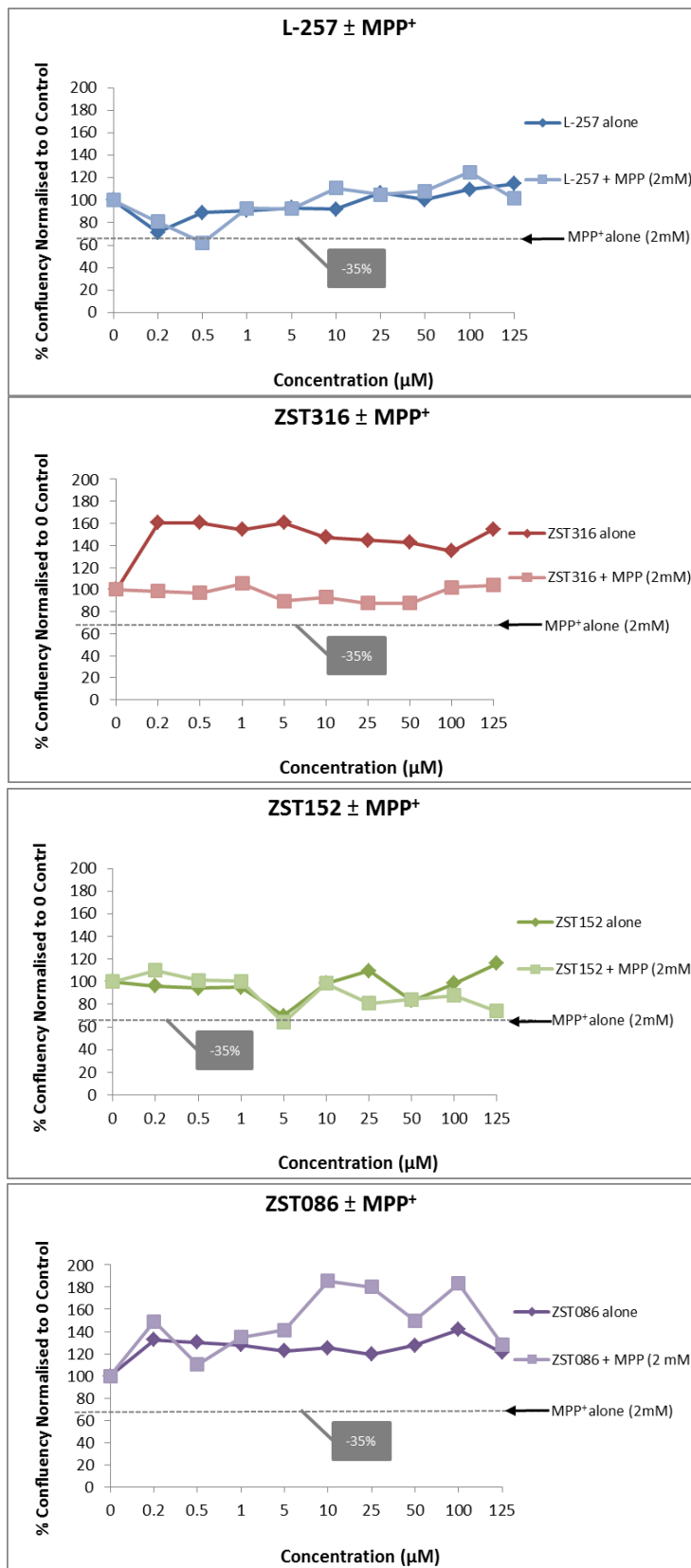


Figure 3.6. Proliferation of SH-SY5Y cells treated with DDAH1 inhibitors and MPP⁺.

Undifferentiated SH-SY5Y cells preincubated for 24 hours with DDAH1 inhibitors were incubated for a further 24 h with MPP⁺ (2 mM). The IncuCyte live-cell imaging system was used to measure the proliferation of SH-SY5Y cells (n=1).

3.2.1.2 Endothelial cells

3.2.1.2.1 The effect of DDAH1 inhibitor ZST316 on VeraVec cells (SRB assay)

VeraVec™ cells, engineered human endothelial primary cells isolated from umbilical cord vein-HUVEC, adapted to culture multiple passages, were treated with 5 and 100 μM ZST316 in media containing EGF and heparin, but with various FBS concentrations: recommended amount for VeraVec culture (20% FBS) or under serum starvation (1% FBS). After 20 hours incubation, the SRB assay was performed, and the optical density was measured. No significant difference was found in treated VeraVec groups compared with the vehicle control. This result was consistent in either media condition, 1% or 20% FBS (**Fig. 3.7**).

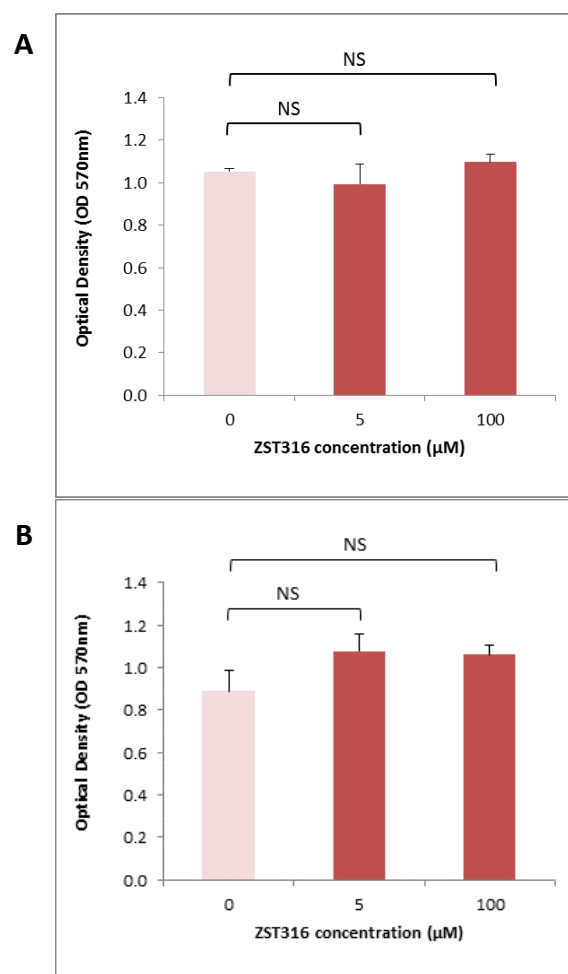


Figure 3.7. Viability of VeraVec cells treated with ZST316 in different conditions of media after 20 hours.

The SRB assay measured the toxicity of 5 and 100 μM ZST316 on VeraVec cells incubated for 20 h with (A) serum-supplemented (20% FBS) medium or (B) serum starvation (1% FBS). One way ANOVA was used to compare groups with control (0 μM ZST316), followed by Bonferroni post hoc test. Results are expressed as mean \pm SEM of 3 technical replicates.

CHAPTER 3

3.2.1.2.2 The effect of DDAH1 inhibitor ZST316 on VeraVec cells viability (Crystal violet assay)

A crystal violet assay was performed to further investigate whether our DDAH1 inhibitors are toxic to VeraVec cells, and to confirm that the potential effects are not influenced by the inclusion of serum (For rationalisation, refer to **discussion section 3.3.1.2, page 109**).

VeraVec cells were incubated with 5 and 100 μM ZST316 overnight (20 hours), at different culture conditions: 1 and 20% fetal bovine serum (FBS), with or without endothelial growth factor (EGF) supplements and heparin. No significant change in VeraVec cell viability or proliferation was observed with different concentrations of serum, growth factors or supplements (**Fig. 3.8.**).

CHAPTER 3

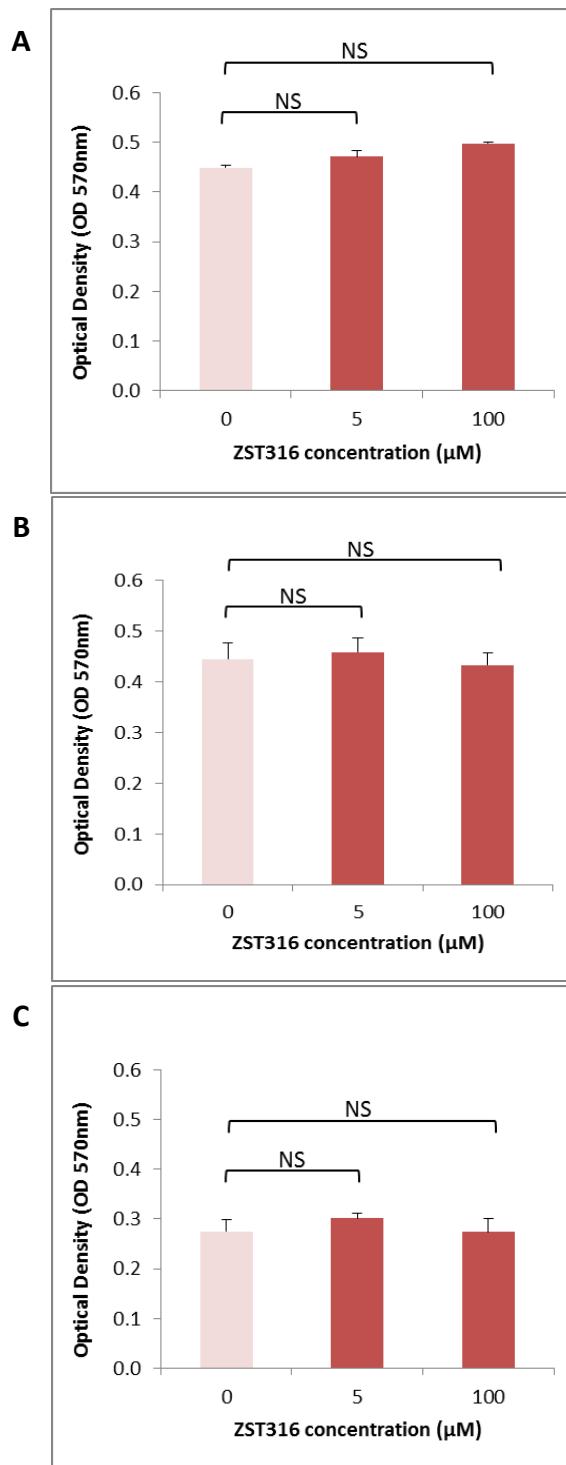


Figure 3.8. Viability of VeraVec cells treated with ZST316 in different media conditions after 20 hours measured by crystal violet assay.

The effect of different conditions of media, (A) Complete media with 20% FBS, endothelial growth factor (EGF) and heparin, (B) 20% FBS without EGF and heparin, and (C) under serum and growth factor starvation (1% FBS, no EGF or heparin), was examined in cells treated with 5 and 100 μM ZST316 for 20 hours using crystal violet staining by absorbance measured at 570 nm. Cell viability is compared to vehicle control. One way ANOVA was used to compare groups with control (0 μM ZST316), followed by Bonferroni post hoc test. Results are expressed as mean ± SEM of 4 technical replicates.

3.2.1.2.3 Real-time viability and proliferation validation of DDAH1 inhibitors on VeraVec cells (xCELLigence)

In further experiments, real-time cell analysis with xCELLigence was used to assess the proliferation of cells treated with 100 μ M ZST316, 1 mM L-NMMA (as positive control for DDAH1 inhibition), and 10 μ M SDMA (as negative control for DDAH1 inhibition), compared to control cells.

72-hour incubation with ZST316 did not affect the proliferation rate of VeraVec cells compared to untreated or vehicle control cells, similar to the negative control SDMA. Interestingly, selective inhibition of NOS by L-NMMA significantly increased cell growth, indicated by a 19% increase in cell index (**Fig. 3.9**). These experiments were performed with three technical replicates.

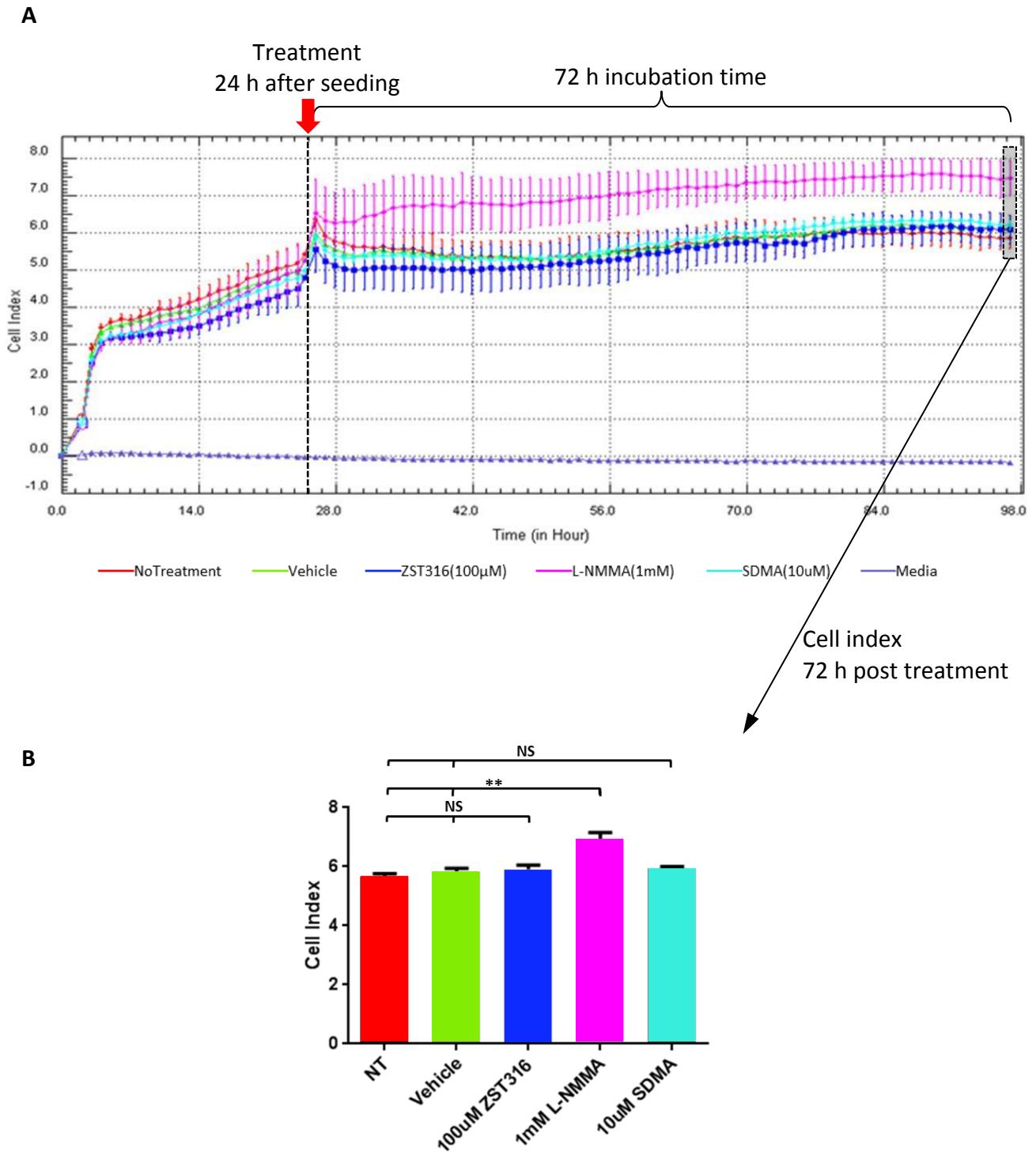


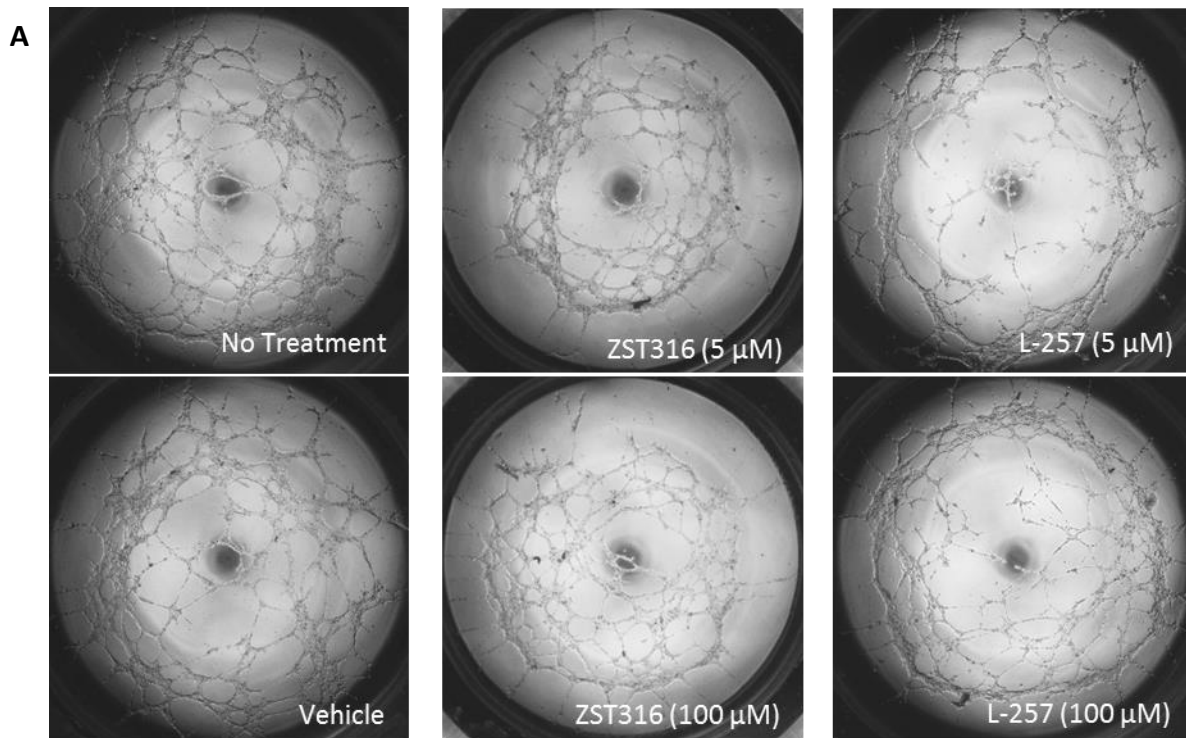
Figure 3.9. Real-time proliferation of VeraVec cells incubated with ZST316 compared to controls.

Cells were seeded onto fibronectin-coated E-plates and treated with compounds or vehicle (A) Dynamic real-time xCELLigence screen of proliferation of treated VeraVec cells over 72 hours post treatment. VeraVec cells were treated 24 hours after seeding with control medium (NT), vehicle control, 100 μ M ZST316, 1 mM L-NMMA (positive control for DDAH1 inhibition), and 10 μ M SDMA (negative control for DDAH1 inhibition) and cell growth were monitored real time for 72 hours. (B) Data show the mean \pm SD of three culture replicates (n=3). One way ANOVA was used to compare treated cells with no treatment and vehicle control, followed by Bonferroni post hoc test (NS $P > 0.05$, ** $P \leq 0.01$).

3.2.2 The effect of DDAH1 inhibitors on angiogenesis

Following the toxicity screening, the potential anti-angiogenic effect of our DDAH1 inhibitors were examined in HUVEC and VeraVec cells using a Matrigel-based tube formation assay.

Control HUVEC cells (untreated and vehicle control) formed an extensive network of tube-like structures, branches and loops within 5 hr of seeding on Matrigel (**Fig. 3.10, A**). However, when pre-treated with 5 μ M DDAH1 inhibitors, ZST316 and L-257, a significant reduction was observed in the number of tubes (**Fig. 3.10, B**), loops (**Fig. 3.10, C**), and branches (**Fig. 3.10, D**) compared to their vehicle control. Impairment in the formation of capillary-like structures was not observed for treated HUVECs with 100 μ M of either ZST316 or L-257 (**Fig. 3.10, B, C and D**).



CHAPTER 3

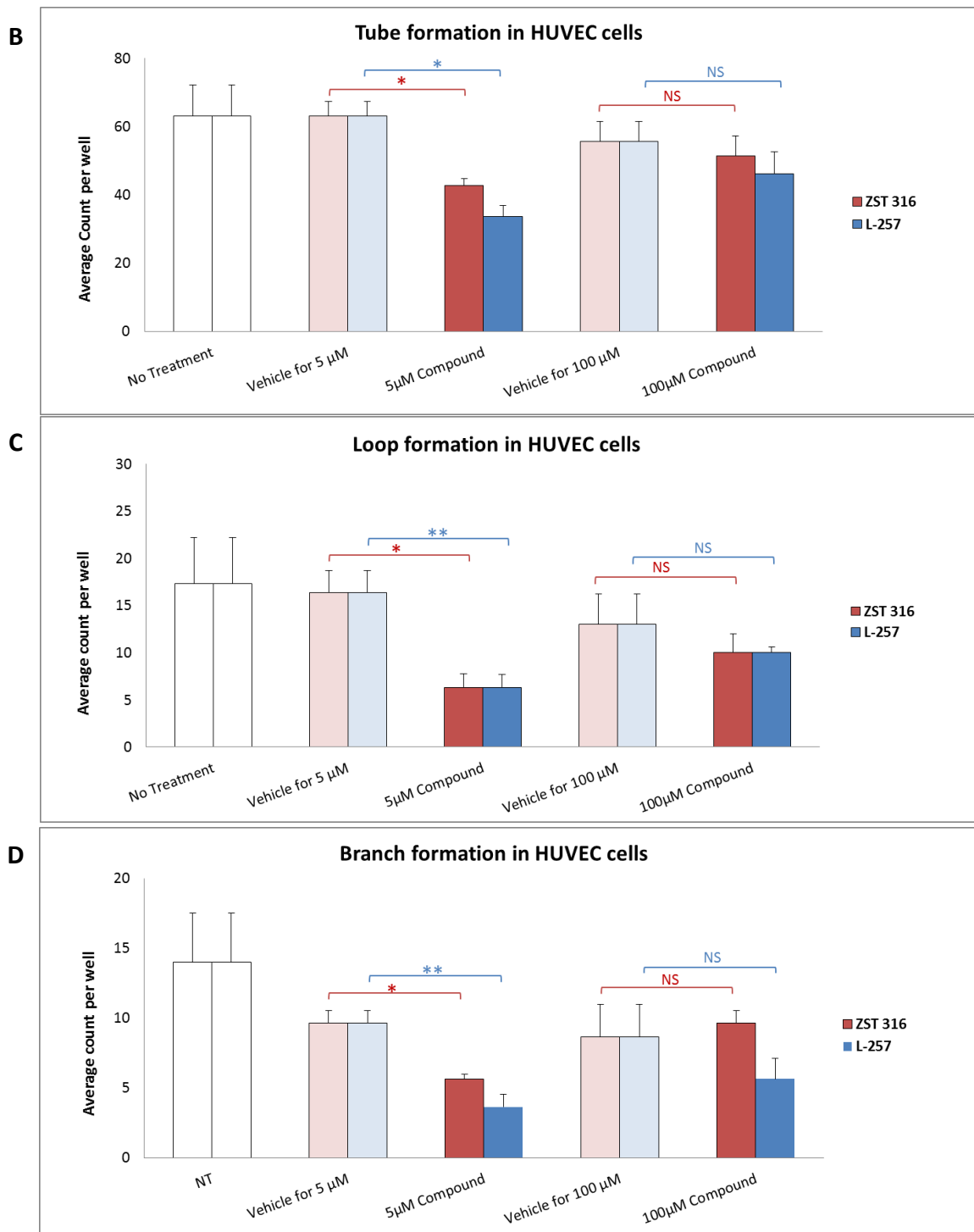


Figure 3.10. Inhibition of capillary-like structures in HUVEC cells treated with DDAH1 inhibitors using Matrigel.

HUVEC cells were pre-treated for 18 h with DDAH1 inhibitors, ZST316, and L-257 (as an indicator), or vehicle or no treated controls and seeded on Matrigel and treated for a further 5 h and imaged. Effect of DDAH1 inhibition on HUVEC cells were compared to their relative vehicle control. (A) Representative phase contrast images are shown. Total number of tubes (B), loops (C) or branches (D) formed were counted by Image J software. Data expressed relative to their vehicle control. Data shown are mean of three technical replicates. * $P \leq 0.05$ and ** $P \leq 0.01$, vs. vehicle, according to Student's t-test. Data are presented as mean \pm SEM.

CHAPTER 3

In further experiments, human VeraVec endothelial cells were preincubated for 18 hours with two concentrations of ZST316, 5 and 100 μM , and Matrigel tube formation assay was performed over 5 hours. The formed tubes and loops were imaged and counted by Image J software. Both doses of ZST316 significantly reduced the formation of tubes and loops in VeraVec cells, in contrast with HUVEC cells (**Fig. 3.11, B**). Even though there was a greater effect on loop formation with 100 μM , both doses significantly reduced the number of loops (**Fig. 3.11, C**).

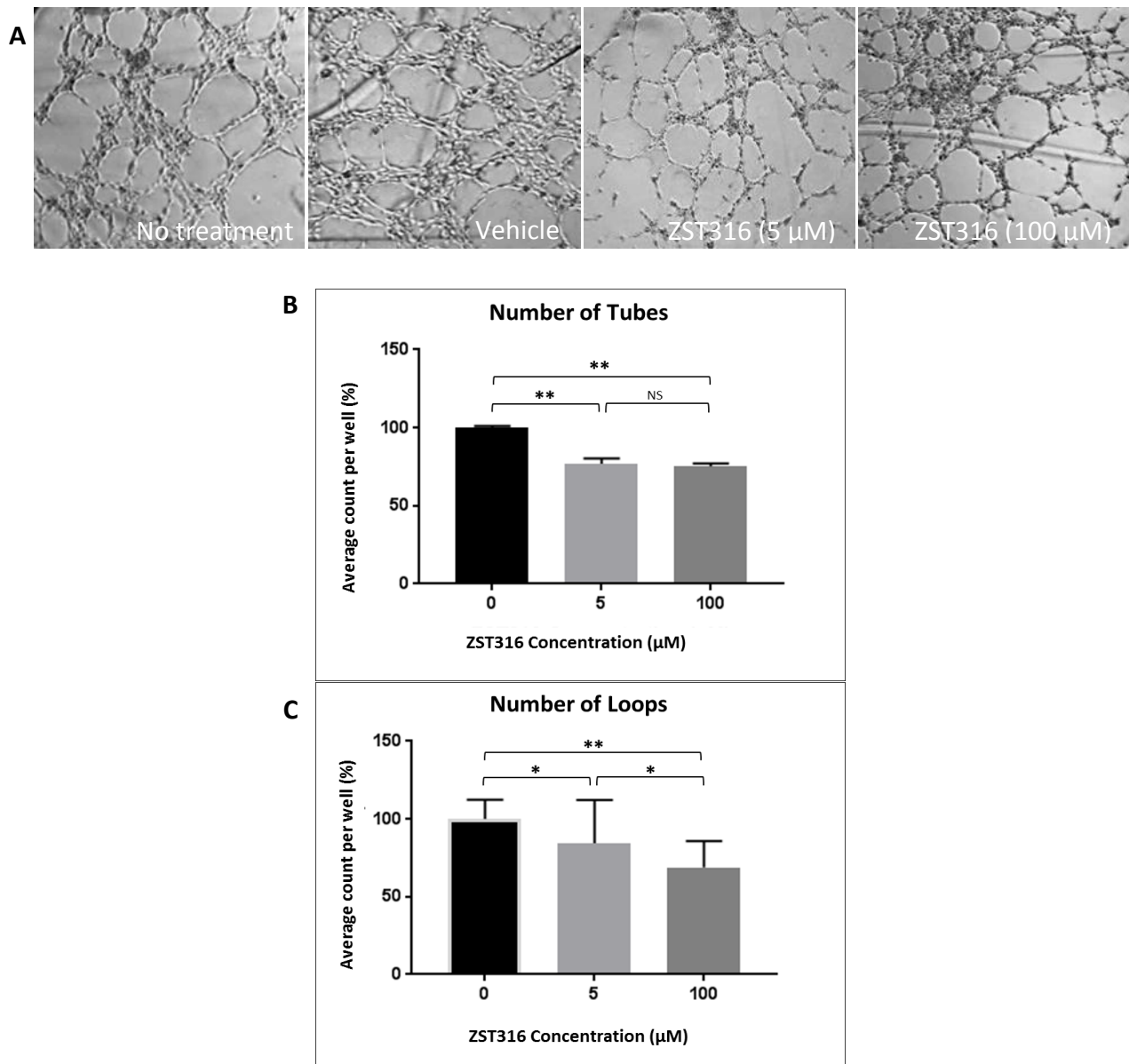


Figure 3.11. Inhibition of capillary-like structures in VeraVec cells treated with DDAH1 inhibitors using Matrigel.

VeraVecs were pre-treated for 18 h with 5 and 100 μM of ZST 316, vehicle or no treatment controls, followed by Matrigel tube formation assay. The number of (B) tubes, and (C) loops formed per well were quantified by ImageJ 5 hours after seeding on Matrigel. (A) Representative phase contrast images of treated VeraVec cells. Data were obtained from five independent biological experiments ($n=5$). One-way ANOVA was used to compare the groups, followed by Bonferroni post hoc test. Data values are expressed as mean \pm SEM and the statistical significance is indicated with asterisks (* $P \leq 0.05$ and ** $P \leq 0.01$).

3.2.3 Effect of DDAH1 inhibitors on eNOS protein expression

To determine whether the tube formation reduction observed was related to the DDAH/ADMA/NOS pathway, the expression levels of DDAH1, DDAH2, eNOS, nNOS and iNOS proteins were investigated in VeraVecs.

3.2.3.1 Basal protein expression with DDAH1 inhibitors

Qualitative western blot analysis resulted in a faint band for DDAH1 with a few non-specific bindings (**Fig. 3.12, A**), and confirmed the endogenous expression of eNOS proteins in VeraVec cells (**Fig. 3.12, B**).

By contrast there was no protein expression for nNOS, iNOS, or VEGF. The DDAH2 protein band was markedly faint, with several non-specific bindings for VeraVec lysate, and could not be considered as a positive result. Western blot image for these experiments can be found in **Appendix 1**.

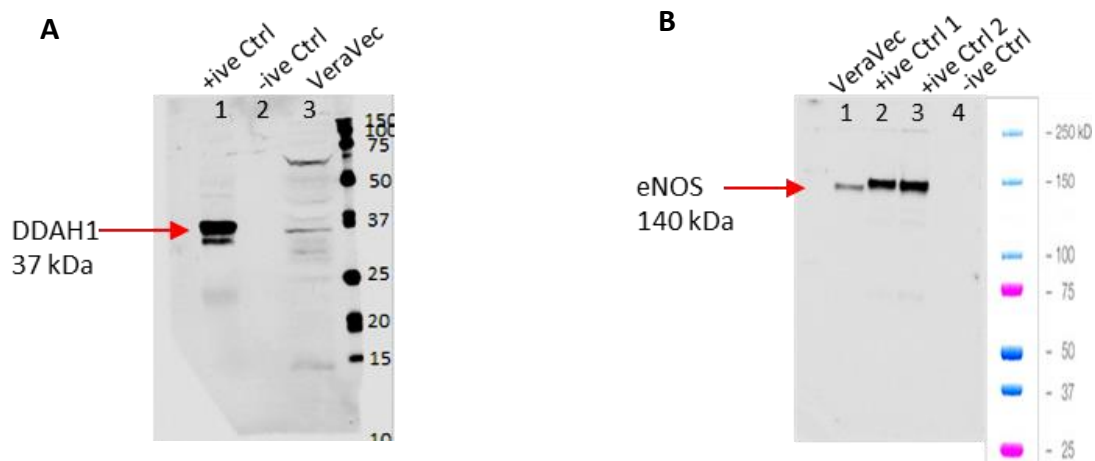


Figure 3.12. Western Blot showing basal protein expression in VeraVec endothelial cells.

Endogenous expression of proteins (A) DDAH1 (n=1), and (B) eNOS (n=2) were tested in VeraVec cells by immunoblot analysis. (A) DDAH1 blot: lane 1: Stably transfected DDAH1-HEK-293T cell lysate used as positive control, Lane 2: Intact HEK293T cell lysate used as negative control, and Lane 3: VeraVec lysate, blotted with DDAH1 antibody (Abcam). (B) eNOS blot: lane 1: VeraVec lysate, Lane 2: Transiently transfected eNOS-HEK293T cell lysate used as positive control 1, Lane 3: Stably transfected eNOS-HEK293T cell lysate used as positive control 2, and Lane 4: Intact HEK-293T cell lysate used as negative control, blotted with eNOS antibody (BD Biosciences antibody).

3.2.3.2 The effect of DDAH1 inhibitors on eNOS protein expression

To investigate whether the DDAH1 inhibitor ZST316 exerts any effect on eNOS protein expression, western blot analysis was performed on VeraVec cell lysates, using three different batches of cells. Quantification of eNOS protein bands on the blot, normalised to total protein, revealed that 18-hour incubation with 5 μ M of ZST316 induced a non-significant downregulation in eNOS protein by 37 ± 10 % versus vehicle control. 100 μ M of the compound also did not have a significant effect on eNOS protein expression (**Fig. 3.13**), similar to the positive (L-NMMA), and the negative (SDMA) controls.

For complete western images refer to **Appendix 2**.

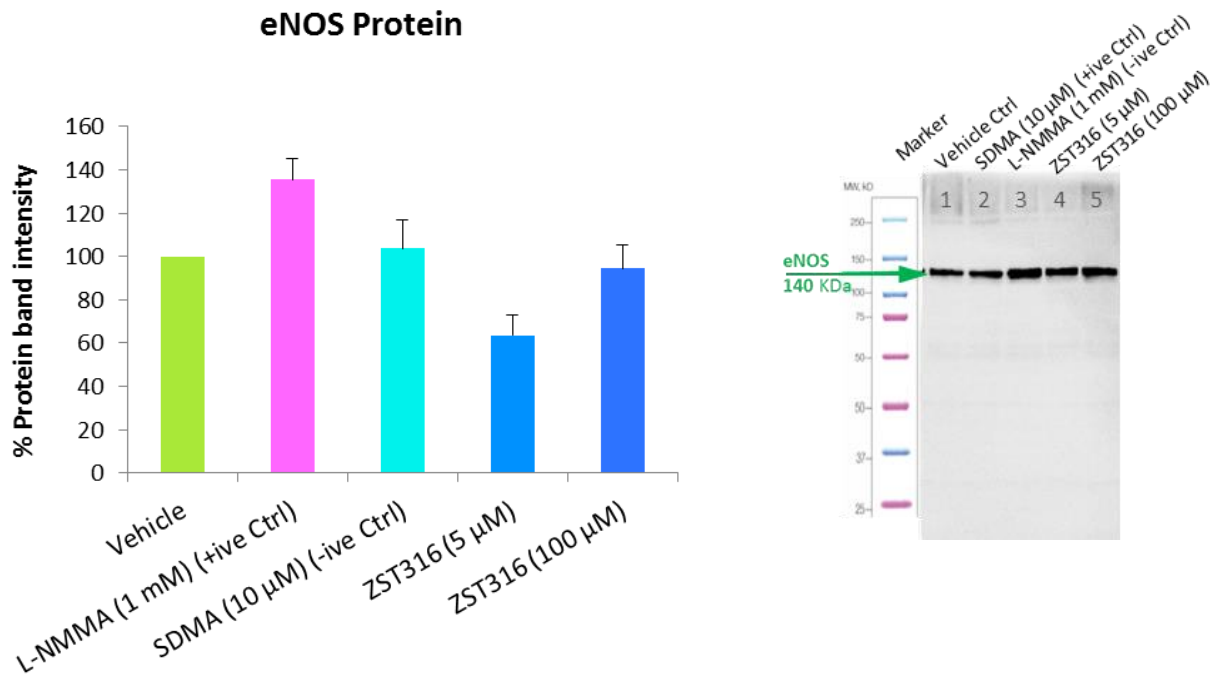


Figure 3.13. Quantitative Western Blot showing eNOS protein expression in treated VeraVec cells with DDAH1 inhibitors.

VeraVec cells were treated with concentrations of 5 and 100 μ M ZST316 (n=6), 1 mM L-NMMA (as positive control for NOS activity inhibition) and 10 μ M SDMA (as negative control for NOS activity inhibition) (n=3), for 18 h. Total protein was used for loading control. The expression of eNOS protein was quantified as a %change of vehicle to total protein by immunoblotting. One-way ANOVA was used to compare the groups, followed by Bonferroni post hoc test. Mean \pm SEM of six independent experiments is shown.

3.3 Discussion

3.3.1 Assessing the potential toxic or protective effect of DDAH1 Inhibitors

The biological characteristics of our novel DDAH1 inhibitors were examined to investigate their therapeutic potential as angiogenesis inhibitors. One of the most critical factors in early stages of drug discovery and development programs is safety (Horvath, 1980), assessed in a series of *in vitro* cytotoxicity tests. These screening tests should be performed by suitable methods on a variety of cell line models, to cover any potential toxicity. To avoid false conclusions, limitations and reliabilities of the assays should be considered (Bácskay et al., 2018). Also, well-characterised cell lines were chosen in order to examine any potential effects from these compounds, as the lack of toxicity in endothelial cells does not necessarily rule out a potential toxic effect in non-endothelial cells. This will ensure reliable information about the dosage and cell-drug incubation time that may influence future experiments and potential applications of the compounds.

3.3.1.1 Toxicity effect of DDAH1 inhibitors on neuronal cells compared to neurotoxin MPP⁺

To investigate the potential cytotoxicity of our novel DDAH1 inhibitors, a SRB cytotoxicity assay was initially used in two different neuronal cell lines, PC-12 and SH-SY5Y. This assay relies on the ability of the SRB dye to bind and stain the cellular proteins (amino-acids) under acidic pH (Vichai and Kirtikara, 2006), thereby determining cell density based on the measurement of total protein mass.

For the initial experiment, the toxicity effect of one of our DDAH1 inhibitors was assessed in undifferentiated PC-12 cell lines. This tumour-derived cell line, initially isolated from a pheochromocytoma of the rat adrenal medulla (Greene and Tischler, 1976), is used as a dopaminergic cell model of Parkinson's disease (Soldner et al., 1999, Bao et al., 2019). PC-12 cells have been reported to be susceptible towards the toxic effects of MPP⁺ due to their binding sites for the toxin (Marongiu et al., 1988). Therefore, this cell line was used to determine whether our compounds exert additional negative effects to those exerted by MPP⁺.

A classic neurotoxin, MPP⁺ is the active metabolite of 1-methyl-4-phenyl-1,2,3,6-tetrahydropyridine (MPTP) (Singer et al., 1988, Aimé et al., 2018). MPP⁺ is a substrate for dopamine transporter (DAT) expressed in PC-12 and SH-SY5Y cells. MPP⁺ accumulates into mitochondria, inhibiting ATP production, which induces the formation of reactive free radicals, and cell death (Kopin, 1987, Jeong et al., 2015).

CHAPTER 3

MPP⁺ neurotoxin was used as a positive control for cell death in our experiments. PC-12 cells were exposed to 500 μ M MPP⁺ as this concentration has previously been shown to cause 50% cell death over 24 (Lee et al., 2005), or 72 hours (Marongiu et al., 1988). Four-day incubation with 500 μ M of MPP⁺ resulted in nearly 70% cell death in undifferentiated PC-12 cells based on the reduction in total protein mass (an indication of cell death) using the SRB toxicity assay. However, lower concentrations did not have any tangible toxic effect (**Fig. 3.1, A**). These results are in line with previous studies showing that the concentration of MPP⁺ necessary to reduce the number of undifferentiated PC-12 cells by 50% (IC₅₀) was 500 μ M and 100 μ M was considered sub-lethal (Lee et al., 2005, Marongiu et al., 1988). Although these studies were conducted over different time periods (24 hours (Lee et al., 2005) and 72 hours (Marongiu et al., 1988)), it has recently been reported that MPP⁺-induced toxicity increased in a dose and time-dependent manner (Bao et al., 2019). This difference can be explained by the difference in the passage number of the utilised cells. According to a recent study on PC-12 susceptibility to various stress conditions, higher-passage PC-12 cells were more resistant than cells with lower passage numbers (Kinarivala et al., 2017). The PC-12 cells used in our studies, at passage < 20, fall into the category of higher passage number and perhaps more resistant according to these studies.

L-257 was used as a reference, not only because it is the mostly studied and widely used selective DDAH1 inhibitor (Leiper et al., 2007, Nandi et al., 2012, Kotthaus et al., 2012, Rossiter et al., 2005), but also because it has been used as the template for the synthesis of our novel DDAH1 inhibitors (Tommasi et al., 2015).

ZST152 concentrations of up to 100 μ M did not have any cytotoxic effect (**Fig. 3.1, B**), similar to L-257 control (**Fig. 3.1, C**), even though significant cytotoxicity was observed with four-day treatment with 500 μ M of ZST152 (**Fig. 3.1, B**). However, this dose is supra-physiological considering the 95% DDAH1 inhibition at 1 mM, IC₅₀ = 18 μ M, and K_i = 7 μ M (Tommasi et al., 2015). Furthermore, toxicity of compounds was tested on PC-12 cells utilising SRB assay over a four day period. Even though this assay is a fast, sensitive and reproducible method to measure drug-induced cytotoxicity, obtaining a linear relationship between seeding density and optical density is challenging for higher cell densities (Papadimitriou et al., 2019). As PC-12 cells grew to almost confluent over the four days incubation time, we used crystal violet assay over a shorter period of time, 48 hours.

CHAPTER 3

In the next series of experiments, our three most potent DDAH inhibitors, ZST316, ZST152 and ZST086 were tested on human neuroblastoma SH-SY5Y cells, another tumour-derived cell model of neuronal disease, originally derived from a metastatic bone tumour biopsy. Undifferentiated SH-SY5Y cells were used to assess cytotoxicity of compounds at different concentrations (1- 125 μM) and viability was assessed over 48 hours. These concentration ranges were chosen to cover concentrations that are equal to, or greater than the K_i (constant of inhibition) of the compounds, and also to account for potentially low cellular uptake. Application of supraphysiological concentration of compounds for *in vitro* studies has been recommended in previous studies (Kittel and Maas, 2014). None of these concentrations showed any cytotoxic effects on undifferentiated SH-SY5Y cells over 48 hours compared to the control (**Fig. 3.2**). L-257 concentrations between 50 and 100 μM have been previously used in cell culture experiments and have been effective to inhibit DDAH1 and increased ADMA by 60% in human dermal microvascular endothelial cells, while cells remained viable (Ghebremariam et al., 2014). Based on our results, showing the lack of cytotoxicity of DDAH inhibitors, up to 100 μM of these compounds (a supraphysiological concentration) was planned to be used in future experiments.

Previous evidence has shown that pharmacological and genetic reduction of DDAH1 activity elicits protective effects against lipopolysaccharide-induced endotoxic shock (Nandi et al., 2012). Further experiments were conducted to investigate while DDAH inhibitors showed no cytotoxicity per se, whether they would be toxic in combination with a toxin.

Initially, the toxic dose of MPP^+ (as the positive control for cytotoxicity) on undifferentiated SH-SY5Y neuroblastoma cells was determined by live-cell imaging IncuCyte and crystal violet assay. IncuCyte proliferation assay showed that application of 2 mM of the toxin reduced cell proliferation by about 35% in 24 hours. Doubling the incubation time led to significant cell death only with 500 μM of the toxin (**Fig. 3.3**). However, the crystal violet assay revealed a significant lack in cell viability in the presence of ≥ 2 mM toxin after 24 or 48 hours incubation (**Fig. 3.4**).

Previous studies on undifferentiated SH-SY5Y cells have demonstrated that 500 μM of MPP^+ is enough to reduce viability (IC_{50}) by 50% in 24 hours (Arshad et al., 2014, Khwanraj et al., 2015). Incubation periods > 24 hours revealed a significant cell death in the presence of ≥ 250 μM MPP^+ toxin (Khwanraj et al., 2015). Notably, these researchers used the MTT assay for their detection method. However, according to recent studies comparing the reliability of crystal violet and MTT assays, while the crystal violet assay is metabolism-independent, the MTT assay is affected by

oxidative stress (Śliwka et al., 2016). This is the mechanism of action involved in MPP⁺-mediated neurotoxic effect (Anantharam et al., 2007). Therefore, testing the MPP⁺ effect on cells using the MTT assay is unreliable as it can provide false-positive results (Śliwka et al., 2016). Based on this information and considering the mechanism of action of MPP⁺, using the MTT assay was not recommended. Besides, our previous IncuCyte experiment supports the toxic dose of 2 mM MPP⁺ in our SH-SY5Y cells over 24 hours.

The 2 mM MPP⁺ dose was used as positive control for cytotoxicity. Then, the potential effect of DDAH inhibitors when combined with MPP⁺ was examined in human SH-SY5Y cells. The DDAH1 inhibitors, ZST316, ZST152, ZST086, and L-257, were tested to investigate whether they could augment MPP⁺-mediated cytotoxicity. However, unexpectedly, DDAH inhibition prevented or minimized MPP⁺-mediated toxicity as the combined treatment resulted in more viable cells than MPP⁺ alone, suggesting a possible neuroprotective effect of the inhibitors (**Fig. 3.5**). The IncuCyte experiment was performed once (**Fig. 3.6**) due to the limited access to the instrument and high costs. Nevertheless, the key finding based on the overall trend of treated cell proliferation rate confirmed the previous results.

It has been previously demonstrated that MPP⁺ initiates oxidative stress, which induces apoptotic cell death in a neuronal cell model of Parkinson's disease (Anantharam et al., 2007). The primary source of ROS and oxidative damage is plasma membrane NADPH oxidase (Anantharam et al., 2007). Furthermore, NADPH oxidase causes NOS uncoupling and thus, reduces NO synthesis (Czesnikiewicz-Guzik et al., 2008). Interestingly, a NOS inhibitor, L-NAME, has been shown to have a similar effect to NADPH oxidase inhibition, i.e., suppress ROS production (Czesnikiewicz-Guzik et al., 2008). Therefore, on possible mechanism accounting for the reduced MPP⁺-induced toxicity by DDAH inhibitors involves NOS inhibition and/or targeting NADPH oxidase. Pending confirmatory studies, pharmacological DDAH1 inhibition might significantly influence oxidative stress, with potential therapeutic applications in Parkinson's disease as well as other chronic diseases associated with oxidative stress such as cancer, atherosclerosis, and rheumatoid arthritis.

3.3.1.2 The effect of DDAH1 inhibitors on endothelial cells

After confirming the lack of cytotoxicity of DDAH inhibitors on neuronal cells, we investigated their potential anti-angiogenic activity in human VeraVec endothelial cells (hVera101, Angiocrine Bioscience) using our most potent DDAH inhibitor, ZST316.

CHAPTER 3

Initially, we confirmed that the proliferation and viability of VeraVec cells were independent of the media content (i.e., amount of FBS, EGF, and heparin in the media). Since the culture medium for human endothelial cells was supplemented with high amounts of serum, growth factors, and heparin to stimulate cell growth, testing needs to be done to firstly rule out the potential influence of these factors on our endpoints. Secondly, since the tube formation assays are performed with serum-free medium (Francescone III et al., 2011), it was important to confirm whether VeraVec cells remain viable to serum- and growth factor- reduced media, in the presence or absence of DDAH inhibitors. According to the manufacturer, the engineered hVera101 are adapted to various media formulations, including serum-free conditions, and are not susceptible to reduced growth factor or serum content in media).

Incubation with 5 and 100 μM of ZST316 exerted no cytotoxic effect to VeraVec cells in different culture conditions using SRB and crystal violet methods (**Fig. 3.7 and 3.8**). However, these methods are based on binding of the dye to cellular proteins (SRB) both protein and DNA (crystal violet) of both live and dead cells, as long as the cells are adherent to the plate (Aslantürk, 2018). Also, actively proliferating cells may detach from plates and wash off. Therefore, they do not provide information on what caused the reduction in the biomass, i.e., whether it was cell death or reduced proliferation, and are unable to measure the proliferation rate (Feoktistova et al., 2011). Therefore, assays that allow real-time measurement of cell proliferation with maximum incubation time provide valuable and complementary information on the cytotoxic effect of compounds. Therefore, a subsequent set of experiments was designed to investigate the anti-proliferative effect of ZST316 over three days using the xCELLigence Real-Time quantitative Cell Analysis (RTCA) instrument.

VeraVecs were treated with supraphysiological concentration of ZST316, 100 μM , calculated based on 100x K_i , to account for any potential difficulty in cell uptake. In addition to ZST316, we also assessed the effect of L-NMMA (as positive control) and SDMA (as negative control) on tube formation. For these molecules, we chose concentrations that are also considered supraphysiological (1 mM for L-NMMA and 10 μM for SDMA; physiological plasma concentrations of these arginine analogues are 0.05 and 0.5 μM , respectively (Da Boit et al., 2018, Hulin et al., 2019, van Dyk et al., 2015).

The viability and growth rate of VeraVec cells treated with ZST316 was similar to non-treated or vehicle control cells as shown in **Figure 3.9**. These results are in agreement with prior studies

investigating the effect of NO[•] reduction (which is the consequence of DDAH inhibition) on cell proliferation. In these studies, the proliferation of endothelial cells with NO[•] inhibition was similar to control cells (Cartwright et al., 2000). Similarly, as expected, SDMA had no impact on the proliferation rate of VeraVecs as this methylated form of arginine is not a substrate for DDAH nor does it inhibit NOS.

In contrast, L-NMMA, used as a positive control for DDAH1 inhibition, induced a significantly higher proliferation rate than non-treated and vehicle control after 72 hours (**Fig. 3.5**). Prior studies have demonstrated an increase in the number of viable endothelial cells treated with ADMA or DDAH siRNA compared to control cells (Trittmann et al., 2019). Furthermore, based on a large number of studies, L-NMMA is a NOS inhibitor (Olken et al., 1991, Zhang et al., 1997, Caplin and Leiper, 2012). Previous studies have reported that NOS inhibitors increased proliferation (Lopez-Farre et al., 1997). The negative correlation between NO production and cell proliferation rate has also been reported in other studies. For example, the high amounts of endogenous NO produced by iNOS inhibited proliferation of endothelial cells (Cartwright et al., 2000). Similarly, exogenous NO derived from NO donors has also been shown to inhibit endothelial cell proliferation (Yang et al., 1994, Sarkar et al., 1995, RayChaudhury et al., 1996).

The different results with DDAH inhibitors vs. L-NMMA could be related to the amount of NO reduction as NO can exert opposite effects depending on its concentration. While low amounts of NO favour cell proliferation, high levels could lead to senescence, cell cycle arrest, reduced proliferation, or even apoptosis (Napoli et al., 2013).

Although there have been contradictory results in the literature regarding the relation between NO inhibition and cell proliferation, it is possible that DDAH inhibitors, in addition to inhibiting NOS, have off-target effects, even though they have not yet been identified. Moreover, we cannot rule out the possibility that particular pathways through which DDAH inhibitors generate their ultimate impact on cells, may not be involved in growth rate.

3.3.2 The effect of DDAH1 inhibitors on angiogenesis

Several studies have reported that NOS inhibitors block *in vitro* VEGF-induced angiogenesis (Papapetropoulos et al., 1997, Ziche et al., 1997a). As L-NMMA, a DDAH1 substrate, has previously been shown to inhibit eNOS activity (Rossiter et al., 2005), we speculated that DDAH1 is an essential mediator of angiogenesis. However, the functional significance of DDAH1 inhibition which leads to the accumulation of L-NMMA in endothelial cells has not been previously

CHAPTER 3

documented. We hypothesised that DDAH inhibition would attenuate the formation of capillary-like structures in endothelial cells in a dose-dependent manner.

The potential anti-angiogenic effect of our most potent DDAH1 inhibitor, ZST316 was investigated in HUVECs (Human umbilical vein endothelial cells) and engineered VeraVec cells. These cells were designed and kept in a state of activity with the ability to simulate *in vivo* inductive angiogenesis (Gori et al., 2017). According to a recent study in our lab using UPLC-MS, DDAH1 inhibitors did not demonstrate high cell uptake in an epithelial human breast cancer cell line, MDA-MB-231 cells (Hulin et al., 2019). Based on that information, DDAH1 inhibitor concentrations were selected from different ranges, starting from 5 times K_i , and up to 100 times K_i – concentrations previously shown in our lab to be sufficient to inhibit tube formation in MDA-MB-231 cell line (Hulin et al., 2017).

The effect of ZST316 was compared to L-257 (reference DDAH inhibitor), non-treated, or vehicle control by the *in vitro* Matrigel® tube formation assay. This quantitative method uses a growth factor-reduced Matrigel to assess the angiogenic activity of vascular endothelial cells *in vitro* (Shao et al., 2009, Ribeiro et al., 1995).

Preliminary experiments with ZST316, similar to L-257, showed a significant reduction in the formation of capillary-like structures with 5 μ M. Interestingly, increasing concentrations to 100 μ M did not have an increasing anti-angiogenic effect *in vitro*. 100 μ M DDAH1 inhibitor did not significantly affect angiogenesis in HUVEC cells as demonstrated by the number of tubes, loops, and branches compared to their vehicle control (**Fig. 3.10**). However, these initial experiments with HUVECs were performed once. Repeating the *in vitro* Matrigel tube formation experiments with VeraVec cells showed that ZST316 5 and 100 μ M, significantly suppressed both tube and loop formation compared to vehicle control (**Fig 3.11**). Notably, the inhibitory effect of 100 μ M of ZST316 on loop (but not tube) formation was greater than 5 μ M (**Fig 3.11, C**), suggesting the presence of a dose-dependent effect.

Previous experiments with ZST316 and ZST152 by other lab members showed similar results in cancer cell models, with suppression of vasculogenic mimicry, i.e., the formation of vessel-like structures, on Matrigel at concentrations > 1 μ M (Hulin et al., 2019). Furthermore, studies on microvascular endothelial cells also revealed that siRNA-mediated knockdown of DDAH1, or treatment with ADMA, led to reduction of NO synthesis and consequent reduced tube formation vs. controls (Trittmann et al., 2019). Another recent study suggests that DDAH deficient HUVEC

cells expressed less VEGF, and showed less cell proliferation and angiogenesis (Zhang et al., 2013). This proposed mechanism underlying the anti-angiogenic effect of DDAH inhibition is different from earlier research showing no significant impact on NOS after DDAH inhibition (Rossiter et al., 2005). Future experiments should examine whether the effect of DDAH inhibition is mediated by NOS and/or VEGF.

3.3.3 The potential effect of DDAH1 inhibitors on eNOS protein expression: Was there a protein expression change involved in the DDAH1-dependent angiogenesis?

Our DDAH1 inhibitors have shown to inhibit angiogenesis *in vitro*, which suggests that the accumulation of DDAH substrates (ADMA and L-NMMA), and the subsequent eNOS inhibition, could have led to angiogenesis attenuation. This is in line with prior studies that have shown that DDAH1 silencing in cultured vascular endothelial cells result in reduced NO synthesis by NOS, due to ADMA accumulation (Hu et al., 2011a). Similarly, inhibition of DDAH1 by ZST316 increased the concentrations of the substrates ADMA and L-NMMA, which directly inhibit NOS activity (Hulin et al., 2020). Although presumably, there would be no significant change in eNOS protein expression.

To test this hypothesis, we initially assessed and confirmed the presence of DDAH1 and eNOS in VeraVec endothelial cells (**Fig. 3.12**). To investigate the effect of DDAH1 inhibitors on eNOS protein expression levels, quantitative immunoblot assays were performed on lysates from treated cells with our most potent DDAH1 inhibitor, ZST316, at 5 and 100 μ M. ZST316 did not significantly change eNOS protein expression, similar to L-NMMA (positive control for NOS activity inhibition), and SDMA (negative control) (**Fig. 3.13**).

Similarly, DDAH1 knockout mice have previously been shown to have significant elevations in plasma and tissue ADMA and L-NMMA, without alterations in the expression of eNOS (Hu et al., 2011a). Furthermore, DDAH1 gene silencing using siRNA silencing, while reducing NO production in microvascular endothelial cells or HUVEC cells, did not influence eNOS protein levels (Trittman et al., 2019, Zhang et al., 2011).

Additional experiments assessing the expression of other proteins potentially involved in the ADMA/DDAH/NOS pathway showed a non-specific antibody binding on the DDAH2 blot. This makes it difficult to robustly determine whether DDAH2 protein is expressed in VeraVec cells (**Appendix 1, A**). No protein expression was detected for VEGF-A, nNOS, or iNOS (**Appendix 1, B, C, D**). Multiple non-specific bands and/or high background on DDAH2, VEGF, and iNOS blots may be

due to poor-quality antibodies (**Appendix 1, A, B, and D**). For more information on antibodies, refer to **Chapter 2, Table 2.7**.

3.4 Conclusion

Our DDAH1 inhibitors did not exert significant toxic effects in neuronal or endothelial cells and, unexpectedly, showed some protection against MPP⁺-induced toxicity in neuronal cells.

Inhibition of angiogenesis is currently perceived as a promising strategy in treating disorders with excessive angiogenesis, such as cancer. In Matrigel tube formation assays, treatment with our DDAH1 inhibitor ZST316 (5 and 100 μ M) exerted significant anti-angiogenic effects in VeraVec cells compared to vehicle control. This effect is likely mediated by the DDAH/ADMA/NOS pathway, particularly inhibition of eNOS activity, but not changes in eNOS protein expression. Moreover, many of angiogenic-related responses in endothelial cells are mediated through ROS (Ushio-Fukai and Nakamura, 2008). Therefore, this effect could also be due to ROS-induced quenching of NO[•], at least in part and the mechanism is thought to be NOS-independent pathways (Paolucci et al., 2001). Other studies have suggested that NADPH (ROS)-dependent inhibition of angiogenesis could occur through VEGF signalling inhibition (Ushio-Fukai and Nakamura, 2008). According to another research, ROS generation could be a potential consequence of ADMA accumulation following DDAH1 inhibition (Wells and Holian, 2007).

Therefore, DDAH1 might represent a potential therapeutic target for disorders characterized by excessive angiogenesis. However, it is important to note that the observed results in immortalised cultured endothelial cells may not necessarily reflect those *in vivo* due to the altered expression patterns of key markers in cell models (Galley et al., 2000).

CHAPTER 4. DEVELOPING MODELS OF VEGF-A MODULATION AND THEIR EFFECT ON DDAH1 EXPRESSION

4.1 Introduction

Vascular endothelial growth factor-A (VEGF-A) is a member of a family of growth factors and the key driver of the biochemical pathways involved in the process of angiogenesis (Loureiro and D'Amore, 2005). Hypoxia is the primary pathophysiological stimulus for increased VEGF-A expression via the accumulation of transcription factor, hypoxia-inducible factor-1 α (HIF-1 α) (Berra et al., 2006, Weidemann and Johnson, 2008, Liu et al., 1995, Liao and Johnson, 2007). HIF-1 α stimulates the production of VEGF, which binds to, and activates VEGF receptors (VEGFRs) on neighbouring endothelial cells (ECs). This promotes vascular endothelial cell permeability and protease production, leading to cell migration, proliferation, and subsequent formation of new blood vessels (Bautch, 2012, Liao and Johnson, 2007, Berra et al., 2006).

In Chapter 3, it was observed that pharmacological DDAH1 inhibition significantly reduced tube formation *in vitro*. Since VEGF is an essential mediator of angiogenesis, the presence of a positive correlation between DDAH1 and VEGF-A was hypothesised. To test this hypothesis, in this chapter, it was attempted to modulate VEGF-A using hypoxia and small interfering RNA (siRNA) gene silencing to investigate the effect of VEGF-A up- (hypoxia) and down-regulation (siRNA) on DDAH1 expression. For this purpose, a cell culture model of hypoxia-induced VEGF-A upregulation was first developed to investigate whether this elevates DDAH1 expression. Then, a model of VEGF-A knockdown by siRNA was created to see whether this reduces DDAH1 expression.

Finally, it was investigated whether the DDAH1-mediated inhibition of angiogenesis (previously observed in **chapter 3**) is VEGF-dependent. As the selectivity profile of our DDAH1 inhibitors has yet to be fully explored, a model of DDAH1 knockdown by siRNA was created to investigate the effect of specific inhibition of DDAH1 on VEGF-A expression. It was hypothesised that siRNA-mediated knockdown of DDAH1 reduces VEGF-A expression. The outcome could describe the possible mechanism of action of our DDAH1 inhibitors and whether their potential therapeutic anti-angiogenic property is through VEGF-A inhibition.

Several cell models can be used to investigate the interplay between VEGF-A and DDAH1. VEGF is expressed in nearly every adult tissue. The retina is one of the most metabolically active tissues in the body and VEGF is the major regulator of retinal angiogenesis (Campochiaro et al., 2016, Penn

et al., 2008, Schlingemann and van Hinsbergh, 1997). Hypoxia stimulates VEGF-A expression in all organs, including the retina (Witmer et al., 2003, Aiello et al., 1995). Retinal hypoxia and HIF-mediated upregulation of VEGF are the leading causes of vision impairment in several ocular disorders characterised by excessive formation of new abnormal vessels inside the retina, e.g., diabetic retinopathy, age-related macular degeneration, and retinopathy of prematurity (Dombrow and Adelman, 2011, Kaur et al., 2008). Retinal pigment epithelial (RPE) cells are the most functionally and metabolically active cells within the retina. These cells are an important source of various angiogenic factors, including VEGF (Xiao et al., 2006). Consequently, they have the potential to contribute to retinal angiogenesis (Ikeda et al., 2006, Forooghian et al., 2007, Aiello et al., 1995, Miller et al., 1997). Moreover, these cells have been shown to contain DDAH1 protein (Gu et al., 2012, Lange et al., 2016).

Therefore, in this study, cultured, immortalized human RPE (ARPE-19) cells were used to modulate VEGF-A, and investigate its potential effects on DDAH1. ARPE-19 cells are commercially available, easy to culture, and have retained most of their native characteristics (Dunn et al., 1996).

4.2 Results

4.2.1 Basal expression of DDAH1

4.2.1.1 Basal mRNA expression of DDAH1

The basal mRNA levels of the two transcript variants of human DDAH1 was tested (**Refer to the discussion section 4.3.1, page 123**). Other genes involved in the DDAH/NOS pathway were also assessed: DDAH2, VEGF-A, NOSs, and cationic transporter 2 (CAT-2) (**Refer to the discussion section 4.3.1, page 125**). Complementary DNA (cDNA) amplified by PCR was visualised by agarose gel electrophoresis. The expression of selected genes in ARPE-19 cells were screen-checked and compared to those in HEK-293T cells (used as an indicator cell), positive controls (plasmid with the desired DNA), and the negative control (RNA-free water).

DNA fragments at the correct size (expected sizes are shown on **Fig. 4.1**, next to their names) were detected for ARPE-19 cDNA (marked as “R” in **Fig. 4.1**), on gel electrophoresis for two transcript variants of DDAH1: variant 1 (n=1), and variant 2 (n=2), and VEGF-A (n=2), compared to the positive control, where available (marked as “+”), or the indicator cDNA from HEK-293T (marked as “H” in **Fig. 4.1**). 18S was used as the housekeeping gene (**Fig. 4.1, B, purple**).

CHAPTER 4

DDAH2, NOSs, and CAT-2 transporter genes were also checked. Whilst DDAH2 (n=2) was expressed when compared with their positive control (**Appendix 3, A, grey**) no DNA band was visualised for nNOS (n=1), iNOS (n=1), eNOS (n=1), or CAT-2 (n=1) genes (**Appendix 3**).

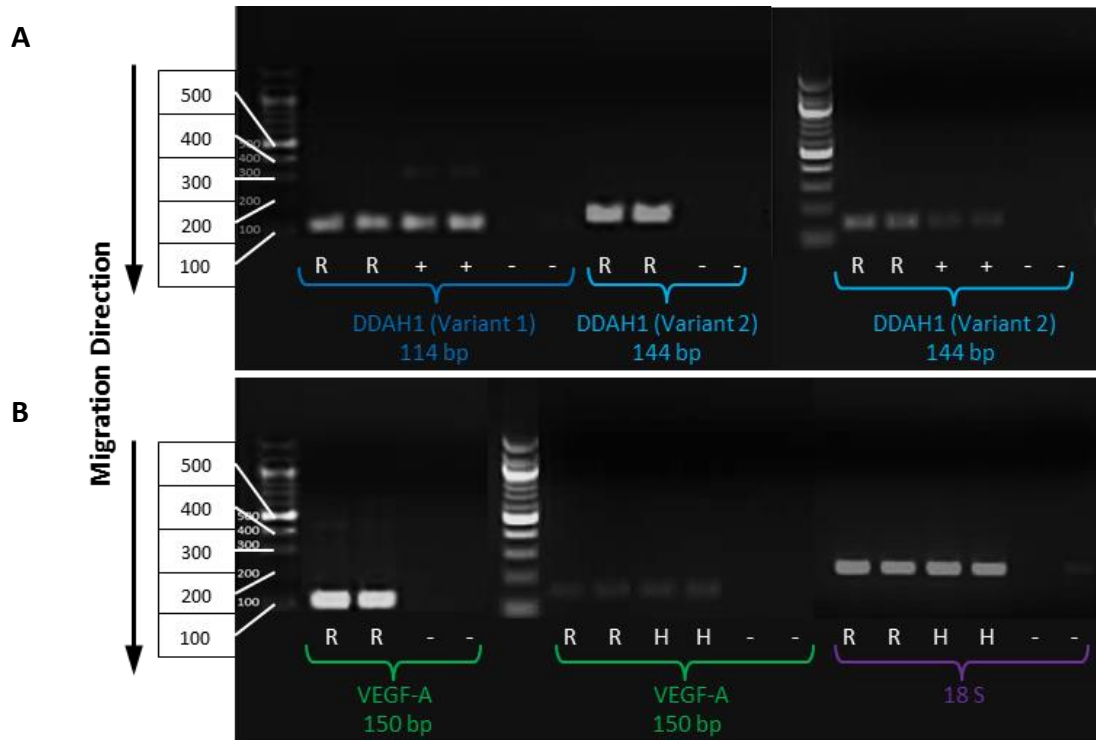


Figure 4.1. Agarose gel (2%) electrophoresis of PCR amplified cDNA template from ARPE-19 cells.

Gel electrophoresis image of DNA fragments, showing expression of DDAH1, variant 1, DDAH1, variant 2, DDAH2, VEGF-A, and 18S housekeeping gene. 1000bp ladder was applied as a reference. “R” represents the corresponding cDNA from human RPE cells (ARPE-19), “H” represents cDNA from HEK-293T cells, used as an indicator cell, “+” serves as the positive control where available, which is HEK-293T cells transfected with the gene of interest, and “-” represents negative control, which is the nuclease-free water with the primer. DNA samples for DDAH1 (variant 1) (n=1), DDAH1 (variant 2) (n=2), DDAH2 (n=2), and VEGF-A (n=2), were loaded on the gel, and the presence or absence of the selected genes was visualised and confirmed. All the above genes were present in ARPE-19 cells. Downward arrows indicate the direction of migration of the samples. The expected gene sizes (in base pair(bp)) are also indicated below their names.

4.2.1.2 Basal protein expression of DDAH1

Qualitative western blot analysis showed the presence of DDAH1 protein in ARPE-19 lysates but not in HEK293T lysates (negative control) (**Fig. 4.2**).

In addition, protein expression of DDAH2, eNOS, iNOS, and nNOS was examined. No band was detected in eNOS, nNOS, or iNOS blots at the expected molecular weights (**Appendix 4, A, B, C**). However, a protein band for DDAH2 was detected at 30 kDa, although slightly lower than the band

generated for our positive control (Flag-tagged DDAH2-HEK293T cells). Interestingly, the negative control intact HEK293T cells also generated a band of the same molecular weight for DDAH2, 30 kDa (See Appendix 4, D).

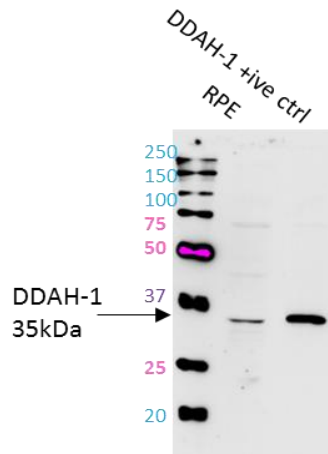


Figure 4.2. Qualitative western blot analysis showing basal protein expression in ARPE-19 cells.

Endogenous expression of DDAH1 (n=3) was detected and compared with the positive control (transiently transfected DDAH1-HEK293T cells with the gene of interest) and negative controls (intact HEK-293T lysates) (n=1).

4.2.2 Model 1: DDAH1 Expression changes during hypoxia-mediated VEGF-A upregulation

To develop a model of VEGF-A upregulation and determine the potential effect on DDAH1 expression, ARPE-19 cells were cultured and exposed to hypoxia for increasing periods (1, 4, 8, 16, 24-hour). The effect of hypoxia on VEGF-A and DDAH1 message and protein expression was tested by real-time q-RT-PCR (Real-Time Quantitative Reverse Transcription PCR) and immunoblotting, respectively, and compared to normoxic cells.

4.2.2.1 DDAH1 and VEGF-A message expression changes during hypoxia

After exposing cells to 18 and 24 hours of hypoxia, mRNA expression levels of VEGF-A significantly increased (**Fig 4.3, A**). Interestingly, this increase was more significant after 18 hours of hypoxia compared to all other time points (**Fig 4.3, A**). Similarly, DDAH1 mRNA also showed a significant elevation after 18 and 24 hours of hypoxia (**Fig 4.3, B**).

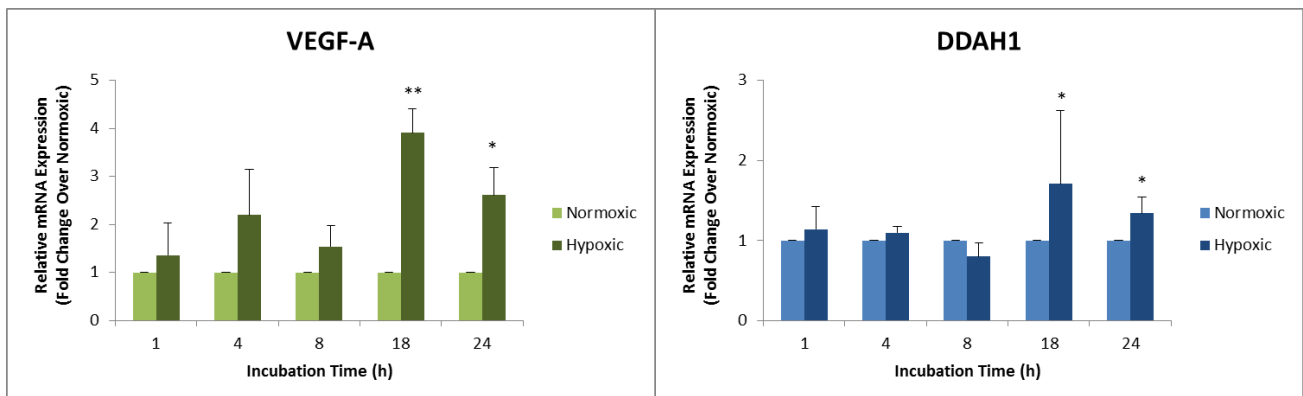


Figure 4.3. Quantitative real-time PCR analysis of VEGF-A and DDAH1 mRNA levels in hypoxic vs. normoxic ARPE-19 cells.

Quantitative real-time PCR data showing (A) VEGF-A gene and (B) DDAH1 gene expression normalised to β -actin in ARPE-19 cells exposed to hypoxia for increasing time periods: 1h (n=2), 4h (n=2), 8h (n=2), 18h (n=4), and 24h (n=2), compared to normoxia. Parametric unpaired Student's t-test was used to compare the hypoxic and normoxic groups at each time-point. *P < 0.05, ** P < 0.01, Error bar = SEM.

To confirm whether 18-hour hypoxia had the maximum effect on VEGF-A mRNA upregulation and to investigate its effect on DDAH1 upregulation, a further experiment was performed; these experiments were focused on 18 hours of hypoxia versus normoxia and DDAH1 (variant 1 and variant 2), DDAH2 and VEGF-A genes were tested. Following RNA extraction and quality check, PCR amplification revealed that both VEGF-A and DDAH1 long mRNA levels were significantly higher than that of the normoxic cells (**Fig. 4.4**). By contrast, DDAH1 variant 2 and DDAH2 mRNA did not show any significant change compared to normoxic cells.

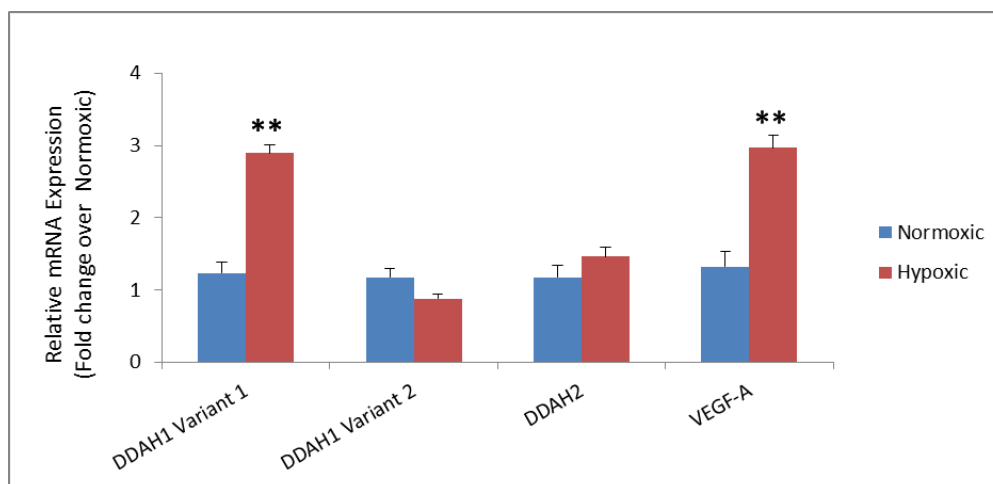


Figure 4.4. Quantitative real-time PCR analysis of mRNA levels in 18 h hypoxic vs normoxic ARPE-19 cells.

mRNA expression of genes of interest normalised to β -actin in ARPE-19 cells under 18 hour hypoxic or normoxic condition. DDAH1 long (n=3), DDAH1 short (n=3), DDAH2 (n=3) and VEGF-A (n=2) were measured by q-PCR. Parametric unpaired Student's t-test was used to compare two groups. **P < 0.01. Error bar = SEM.

4.2.2.2 DDAH1 and VEGF-A protein expression changes during hypoxia

In the next set of experiments, changes in protein expression of VEGF-A and DDAH1 were examined during hypoxia. To measure VEGF-A protein expression, secreted VEGF into the media was measured by enzyme-linked immunoassay (ELISA). Again, 18-hour, but not 24-hour, hypoxia, significantly increased VEGF protein expression in ARPE-19 compared to normoxic cells.

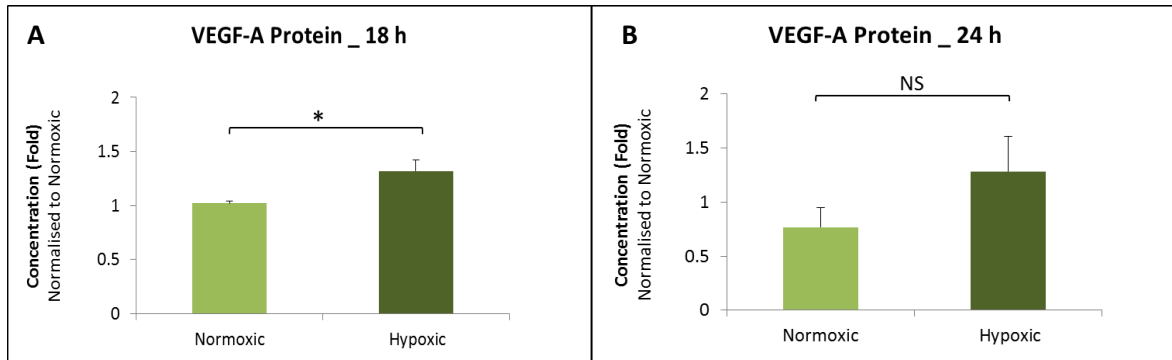


Figure 4.5. The effect of 18 and 24 h hypoxia on VEGF-A in ARPE-19 cells.

ARPE-19 cells were incubated for (A) 18 hours and (B) 24 hours under hypoxia or normoxia, and average VEGF-A protein expression was measured by ELISA on media and compared (n=3). Parametric unpaired Student's t-test was used to compare two groups. *P < 0.05, NS= not significant, Error bar = SEM.

Subsequently, the DDAH1 protein levels under hypoxia compared to normoxic conditions were measured, using western blot analysis. Contrary to expectations, 18-hour hypoxia caused a significant decrease $56.1 \pm 7.25\%$ in DDAH1 protein.

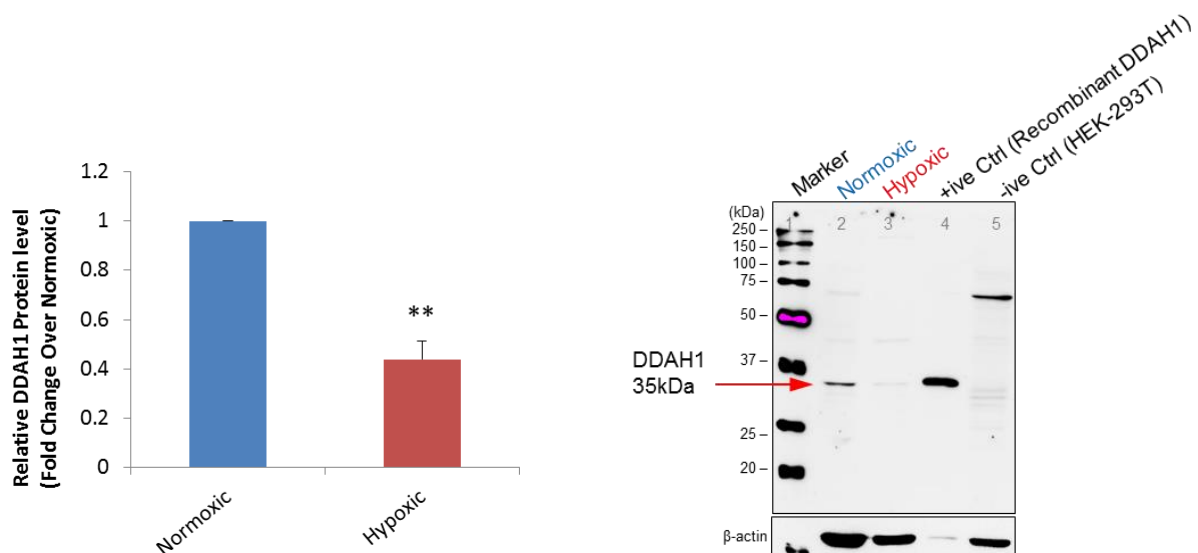


Figure 4.6. DDAH1 protein levels in hypoxic vs. normoxic ARPE-19 cell lysate.

Western blot analysis of DDAH1 protein expression normalised to β -actin in ARPE-19 cells after 18-hour hypoxia vs. normoxia (n=5). ** P \leq 0.01, Error bar = SEM. One-way ANOVA followed by Bonferroni post hoc test was used to compare hypoxic cells to normoxic.

4.2.3 Model 2: DDAH1 expression changes during siRNA-mediated VEGF-A knockdown

At 72 hours after the transfection of ARPE-19 cells, VEGF-A siRNA significantly reduced the VEGF levels: VEGF-A message showed a reduction when q-RT-PCR data was normalised to β -actin housekeeping gene (n=2) (**Fig. 4.7, A**). ELISA assay on the VEGF-A protein released into the culture media also confirmed VEGF-A knockdown by transfection efficiency of 86% (**Fig. 4.7, B**).

VEGF-A knockdown had no significant effect on DDAH1 message compared to control cells (**Fig. 4.7, C**), while DDAH1 protein was affected. Densitometry analysis on western blot results showed an increase in DDAH1 protein expression in cells transfected with VEGF-A siRNA, compared to controls; siRNA-mediated knockdown of VEGF-A, increased DDAH1 protein expression by 3.9-fold (**Fig. 4.7, D and E**).

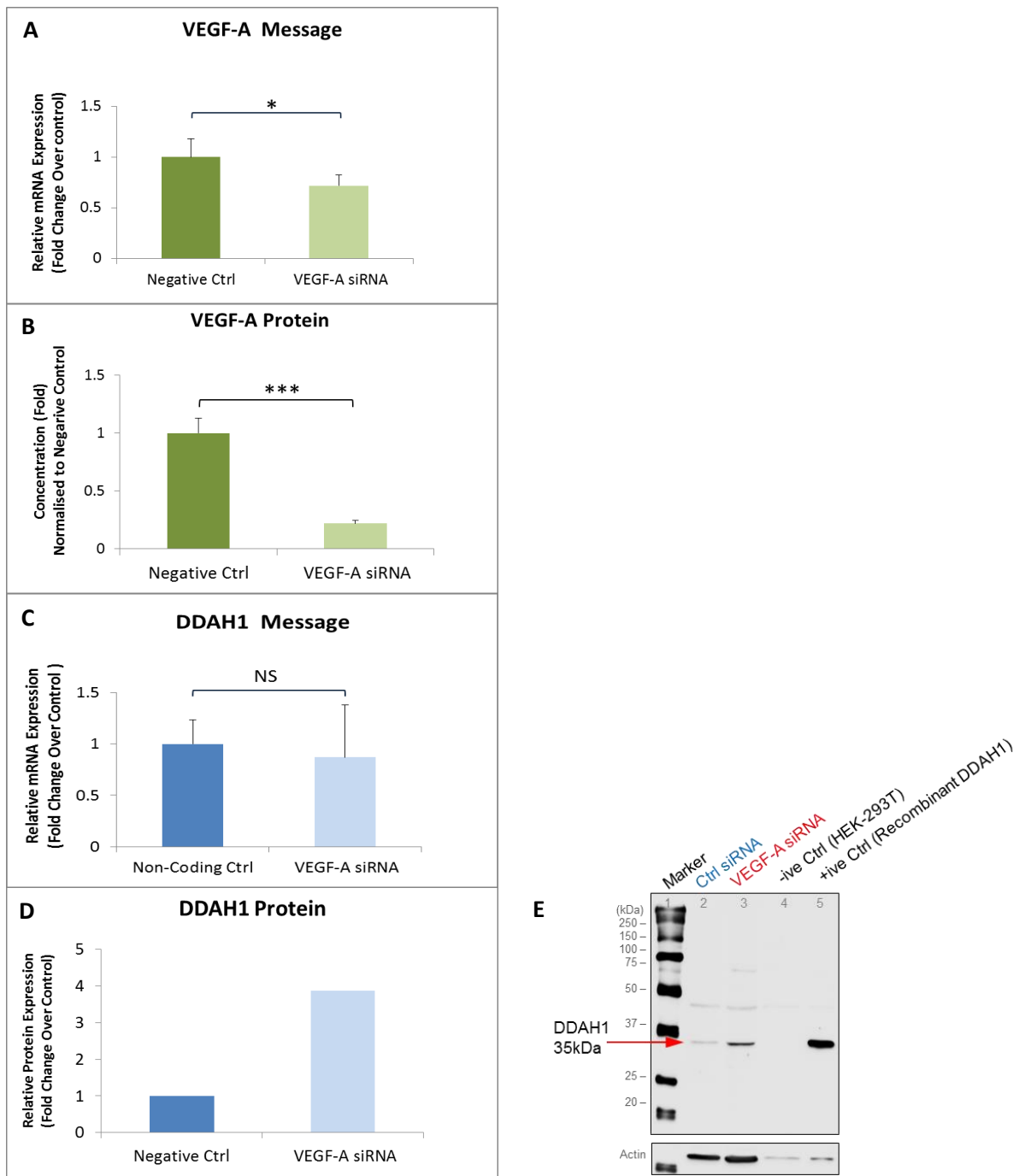


Figure 4.7. Quantitative real-time PCR analysis of VEGF-A and DDAH1 mRNA levels in hypoxic vs. normoxic ARPE-19 cells, and the effect of VEGF-A knockdown on DDAH1 message and protein.

Transfection efficiency (VEGF-A gene knockdown (siRNA)) was determined by measuring (A) VEGF-A message (n=1, with 5 technical replicates) and (B) VEGF-A protein in the media (ELISA) (n=2). Effect of VEGF knockdown on (C) DDAH1 gene expression was measured by q-PCR (n=3 technical replicates) and (D) DDAH1 protein (western Blot) (n=1). The expression of each mRNA and protein was normalised to β -actin. (E) Representative image showing protein intensity before and after VEGF knockdown. *P < 0.05, ***P < 0.001 and NS = not significant. Error bar = SEM.

4.2.4 Examining the crosstalk between DDAH1 and VEGF-A: VEGF-A expression changes during siRNA-mediated DDAH1 knockdown

A pilot experiment was conducted to determine whether DDAH1 inhibition affects VEGF-A expression (as one of the main factors affected by angiogenesis).

Transfection of ARPE-19 cells with DDAH1 siRNA, successfully knocked down the DDAH1 gene, by 82% at 72 hours (**Fig. 4.8, A**). Next, the effect of DDAH1 inhibition on VEGF-A message and protein were tested.

Silencing DDAH1 gene had no effect on the expression levels of VEGF-A gene (**Fig. 4.8, B**). Similarly, ELISA experiments displayed no significant change in VEGF protein content in media from DDAH1-knockdown ARPE-19 cells, compared to negative control (non-targeting) siRNA cells (**Fig. 4.8, C**).

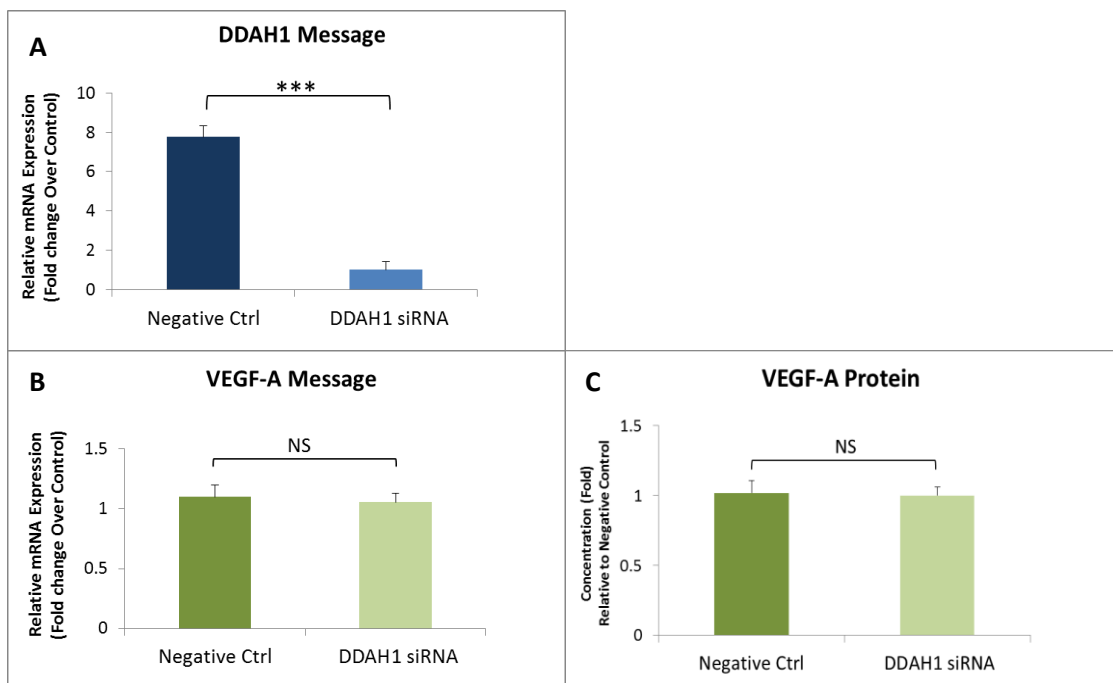


Figure 4.8. Quantitative real-time PCR analysis of VEGF-A and DDAH1 mRNA levels in hypoxic vs normoxic ARPE-19 cells and the effect of DDAH1 knockdown on VEGF-A gene and protein expression.

(A) Transfection of DDAH1 siRNA into ARPE-19 cells effectively knocked down DDAH1 message; DDAH1 gene was significantly knocked down by siRNA (n=3). (B) VEGF-A mRNA expression (qPCR) (n=3) and (C) VEGF-A protein Expression (ELISA) (n=5) of RPE cells were measured. ***P < 0.001 and NS = not significant. Error bar = SEM.

4.3 Discussion

In this chapter, two *in vitro* experimental models of VEGF-A modulation (hypoxia-mediated VEGF-A upregulation and siRNA-mediated VEGF-A knockdown) were developed to examine whether there is a positive correlation between VEGF-A and DDAH1 expression levels.

4.3.1 Basal Expression of DDAH

Basal DDAH1 mRNA expression was initially assessed in ARPE-19 cells. According to the National Centre of Biotechnology Information database, two transcript variations of DDAH1 gene have been identified: Variant 1 (NM_012137.3), which encodes the longest isoform, and variant 2 (NM_001134445.1), which encodes a truncated isoform at the N-terminus compared to variant 1 (NCBI, 2021) (available at <https://www.ncbi.nlm.nih.gov/gene/23576>). It is known that variant 1 is the essential active isoform in ADMA metabolism (Leiper et al., 2007, Murray-Rust et al., 2001) and variant 2 is catalytically inactive. Nevertheless, data collected within our laboratory suggests that variant 2 might be involved in ADMA metabolism through synergistic activation of variant 1 (unpublished data). Therefore, the expression levels of the two variants in ARPE-19 cells were determined, and for this purpose, two transcript variants-specific primer sets that specifically amplify the two variants were used.

Gene expression patterns were compared with those in non-transfected HEK-293T, initially used as a negative control. Stably transfected HEK-293T cells with the gene of interest were used as the positive control, where available. Sterile nuclease-free water with the primer was used as the negative control to check for contamination. The housekeeping gene 18S ribosomal RNA was used to normalise sample-to-sample variation of PCR assays (**Fig. 4.1**).

cDNA fragments separated by size on agarose gel electrophoresis were apparent at the expected size for DDAH1 variants 1 and 2 in ARPE-19 samples, similar to their positive controls (**Fig. 4.1, A**). Similarly, basal protein expression in ARPE-19 cells indicated the presence of DDAH1 protein (**Fig. 4.2**). Protein expression of DDAH1 has been previously found in mice retinal tissues by immunohistochemistry and ARPE-19 cell lysate tested by immunoblotting (Lange et al., 2016). Therefore, our results are in line with the available evidence.

Both PCR replicas of ARPE-19 showed that VEGF-A mRNA was expressed in these cells (**Fig. 4.1, B, green**). However, unfortunately, no positive control for VEGF-A gene was available in these experiments and thus, the expression levels were only compared with those in HEK-293T cells at

CHAPTER 4

the second PCR run (**Fig. 4.1, B, green**). Due to not having access to a reliable anti-human VEGF-A antibody or ELISA kit, the basal expression of VEGF-A in ARPE-19 was not tested. Previous evidence suggests that VEGF expression in unstimulated cells remains at basal levels (Wang et al., 2019).

In addition to DDAH1 and VEGF-A, other genes involved in the DDAH/NOS pathway associated with VEGF-mediated angiogenesis were tested: DDAH2 and the three NOS isoforms (nNOS, iNOS, and eNOS), along with the cellular transporter CAT-2. The amplified PCR product for DDAH2 in ARPE19 cells was observed at the expected size range, generating a band with the same size as the positive control, around 143 bp (**Appendix 3, A, grey**). This indicates the presence of DDAH2 mRNA in ARPE-19 cells, and unexpectedly, in HEK-293T cells (our negative control cells) as well (**Appendix 3, A, grey**). Similarly, a single protein band was detected at the predicted molecular weight for DDAH2 (30 kDa) in ARPE-19 lysate (**Appendix 4, D**). Again, for HEK-293T cell lysate, used as our negative control, an unexpected protein band occurred at the same size as DDAH2 (**Appendix 4, D, lanes 1 and 3**). Based on previous studies in our lab, showing the absence of DDAH2 protein expression in HEK-293T cells (Tommasi, 2015), these cells were used as our negative control. However, our results disproved prior studies. Furthermore, Western Blot images from a recent study also confirmed the endogenous expression of DDAH2 protein in HEK-293T cells (Huang et al., 2021).

Notably, the recombinant DDAH2 protein lysate used as the positive control (DDAH2-HEK293T stably transfected cell lysate) had an additional protein tag. This octapeptide or FLAG epitope is used for recombinant protein identification (Sequence motif DYKDDDDK (D=aspartic acid, Y=tyrosine, and K=lysine), with 1012 Da (Hopp et al., 1988). Therefore, it is expected that the generated band is slightly higher (larger molecular weight) than that of the intact DDAH2 protein, similar to the band generated on the DDAH2 blot (**Appendix 4, D, lane 2**). Hence it does not indicate the correct size for DDAH2 protein. Further investigations using untagged DDAH2-HEK293T controls are required to clarify these results. However, since DDAH2 was not the main focus of our studies, it was not investigated further. Prior research has found DDAH2 protein expression in both RPE tissue and cell line (ARPE-19) (Lange et al., 2016).

None of the three NOS genes were expressed in ARPE-19 cells, while they were expressed in HEK-293T samples, similar to the positive controls (**Appendix 3, red, orange, and pink**). Similarly, protein eNOS was not expressed (**Appendix 4, A**), perhaps due to antibody-related issues (Cell

Signalling, 49G3), as it did not generate an intense band for the positive control either (**lane 3**). nNOS and iNOS proteins were not expressed in ARPE-19 cells either, even though multiple non-specific bindings were apparent in all lanes, including the positive controls (**Appendix 4, B and C**). Therefore, the western blotting assay results were not reliable. This may be related to the quality of the antibodies (nNOS antibody (Abcam, Ab76067), and iNOS antibody (Santa Cruz, H-174 sc-8310)), or the positive controls (recombinant proteins produced in HEK-293T). The stably transfected cells were made before these experiments and could have been degraded over time, as a common problem reported in the literature (Robert et al., 2009).

Previous studies showed that basal message and protein levels of eNOS in ARPE-19 cells were at minimal levels (approximately 5 times less than hypoxia-induced cells) (Wang et al., 2019), which perhaps explains the absence of a band for eNOS protein in our ARPE-19 lysate. Other studies also showed that unstimulated ARPE-19 cells expressed no iNOS mRNA or protein either (Fang et al., 2012, Sripathi et al., 2012). Studies by Wang *et al.* suggested that NOS proteins followed a similar pattern as VEGF and were not expressed in unstimulated ARPE-19 cells (Wang et al., 2019). To the best of our knowledge, no evidence of nNOS expression exists in the literature for ARPE-19.

The last gene examined in ARPE-19 cells was the CAT-2 transporter (SLC7A2). CAT-2 is a member of solute carriers (SLC)-7 family of transporters, and one of the transporters of methylarginines across cell membranes (Kittel and Maas, 2014, Closs et al., 2004). This CAT family member is highly expressed in cells with a high demand for L-Arg (Verrey et al., 2004). The lack of this transporter significantly impairs L-Arg transport and NO production, and therefore it is required for sustained NOS activity (Nicholson et al., 2001). The experimental data showed no evidence of the CAT-2 transporter gene in ARPE-19 cells, while this transporter was expressed in HEK-293T. However, no positive control for this gene was available to confirm the results (**Appendix 3, B, yellow**).

RPE transporters can be critical in ocular drug distribution. A recent study on expression and localisation of transporter proteins in human fetal RPE cells demonstrated the presence of SLC7 transporters (including SLC7A1 (CAT-1)) using QTAP and SWATH-Mass Spectrometry analysis (Hellinen et al., 2019) but not CAT-2. It has been reported that CAT-2 expression was induced in iNOS-stimulated cells (Bozkus et al., 2015). Moreover, previous studies showed that while both CAT-1 and CAT-2 proteins transport L-Arg through the cell membrane, the transport of L-Arg by CAT-1 is slower compared to CAT-2, and therefore cells with a high demand for L-Arg express more CAT-2 (Verrey et al., 2004). The specific functions of CAT-3 and CAT-4 are not well characterised.

Based on the previous information, the absence of CAT-2 in our unstimulated ARPE-19 was expected. However, it cannot necessarily create any issue for cellular L-Arg transport, as firstly, CAT2 can get activated in stimulated ARPE-19, and secondly, CAT-1 transporter could also be expressed in these cells.

4.3.2 Model 1: DDAH1 expression changes during hypoxia-mediated VEGF-A upregulation

To determine the role of DDAH1 in angiogenic pathways and to assess whether a positive correlation exists between the expression of DDAH1 and VEGF-A (the major pro-angiogenic factor), a cell culture model of VEGF-A upregulation was developed using hypoxia. According to prior research, hypoxia may increase DDAH1 expression, which is associated with increased angiogenic factors, including VEGF (Buijs et al., 2017).

Previous investigations in cultured ARPE-19 cells under various hypoxia time-points suggested a self-regulated feedback loop for HIF-1 α regulation; mRNA levels of HIF-1 α fluctuated during the first 24 hours, similar to VEGF mRNA, while HIF-1 α protein increased after this time before returning to baseline at 36 hours hypoxia (Forooghian et al., 2007). Therefore, experiments at different hypoxia time points were performed to determine when hypoxia has the highest impact on VEGF-A gene in ARPE-19 cells. The expression of each mRNA was normalised to β -actin.

The results showed no significant increase in VEGF-A gene expression before 18 hours of hypoxia. However, both 18 and 24 hours hypoxia elevated VEGF-A mRNA. The highest VEGF-A message was observed when cells were exposed to hypoxia for 18 hours. Incubation of cells for a further six hours under hypoxia (24 hours) slightly suppressed the increase in VEGF-A mRNA, even though the latter remained significantly higher compared to the normoxic group (**Fig. 4.3, A**). When the 18-hour hypoxia experiments were repeated, results confirmed the significant upregulation of VEGF-A, with the highest expression at 18 hour-hypoxia. Importantly, this upregulation coordinated with DDAH1 (variant 1) mRNA upregulation, with highest expression level after 18 hours of hypoxia (**Fig. 4.3, B, and Fig. 4.4**).

Quantitative RT-PCR is a powerful and highly sensitive technique used to measure gene expression. However the accuracy of this method is dependent upon the normalisation of different mRNA samples to stably expressed genes, known as housekeeping genes (Silver et al., 2006). During hypoxia, the expression of some housekeeping genes, such as GAPDH has been shown to change (Kozera and Rapacz, 2013, Zhong and Simons, 1999). Therefore, the expression of a number of potential housekeeping genes was assessed under hypoxic conditions. In the

CHAPTER 4

current studies, 18S, β -actin, and PPIA were measured as potential housekeeping gene candidates, previously validated to be suitable and stable reference genes for hypoxia experiments (Thellin et al., 1999, Tan et al., 2012, Liu et al., 2016). In contrast to past research, hypoxia induced an increase in PPIA gene expression. However, both 18S and β -actin showed relatively stable expressions in hypoxia preconditioned ARPE-19 cells. Nevertheless, throughout the whole study, the sample replicates with 18S was not always sufficient for statistical analysis. Furthermore, β -actin showed a closer cycle threshold (Ct) value to our target genes (DDAH1 and VEGF-A). According to the literature, suitable reference genes are recommended to have a similar cycle threshold (Ct) value to the gene of interest (Kozera and Rapacz, 2013). Therefore, β -actin was selected to normalise the mRNA expression of the genes. However, protein expression measurements are more physiologically relevant compared to gene expression measurements.

VEGF-A protein levels significantly increased only at 18-hour hypoxia (**Fig. 4.5, A**). 24-hour hypoxia had no significant effect on VEGF-A protein expression compared to normoxia (**Fig. 4.5, B**). Contrary to expectation, after 18 hours of hypoxia and a significant rise in VEGF message and protein, DDAH1 protein decreased significantly (**Fig. 4.6**).

The strong VEGF-A elevation observed for RPE cells under hypoxia was in accordance to previous reports in various cells including RPE cells (Shweiki et al., 1992, Wang et al., 2019, Punglia et al., 1997, Geisen et al., 2006, Lin et al., 2013, Wu et al., 2007, Bento et al., 2010, Watkins et al., 2013). A recent study reported an 8-fold increase in VEGF-A gene after 24-hour hypoxia induction by cobalt chloride (CoCl_2) (Wu et al., 2016). In our study, using hypoxic gas mixtures, the effect of hypoxia on VEGF-A message was greater over 18 hours compared to 24 hours, with an increase of up to 4.5-times normoxia (**Fig. 4.5, A**).

Similar to total VEGF mRNA levels, 12 or 24-hour hypoxia increase secreted protein in all retinal cells types, including RPE cells (Watkins et al., 2013). A recent study has established an *in vitro* hypoxia model using CoCl_2 to induce ARPE-19 cells, indicating an upregulation of HIF-1 α , VEGF, VEGFR-2, and eNOS protein expression over 24 hours, analysed by both ELISA and western blotting assays (Wang et al., 2019). Our experiment produced different results; while no significant change was observed for VEGF-A protein over 24 hours of hypoxia (**Fig. 4.5, B**), 18-hour hypoxia elevated VEGF-A protein amount (**Fig. 4.5, A**). An older study suggested a self-regulatory feedback loop for HIF-1 α , which also affected VEGF production by ARPE-19 (Forooghian et al., 2007). This might explain the maximum hypoxia-mediated VEGF upregulation at 18-hour versus 24-hour hypoxia.

Therefore, since at 18-hours hypoxia, both VEGF-A gene (**Fig. 4.3, A, and 4.4**) and protein (**Fig. 4.5, A**) were upregulated, western blot experiments to test the DDAH1 protein expression changes was performed over 18-hour hypoxia.

Western blot results revealed that although DDAH1 was directly correlated to VEGF-A at the mRNA level (both were upregulated under hypoxia) (**Fig. 4.4**), at the protein level, the expression of DDAH1 was reduced by 56.1 ± 7.2 % after 18-hour hypoxia versus normoxic ARPE-19 cells (**Fig. 4.6**). Therefore, our hypothesis was disproven; our cell culture model of hypoxia-induced VEGF-A overexpression could not upregulate DDAH1 expression. It is worth mentioning that in low expressing protein samples, such as DDAH1, the signal-to-noise ratio is low. Therefore, caution is required when presenting percent changes as they might erroneously inflate the real protein expression in the sample (Bass et al., 2017).

In a previous *ex-vivo* study, hypoxia exposure significantly lowered DDAH1 protein expression and activity in tissues by 37% when compared to the normoxic group (Millatt et al., 2003), which was in agreement with our findings. Another study showed a significant reduction in both DDAH1 mRNA and protein during chronic hypoxia (Hannemann et al., 2020a); a correlation that was not found in our study (**Fig 4.4 vs. 4.6**).

Interestingly, a recent study in human hepatocellular carcinoma (HCC) reported that DDAH1 is the key regulator in angiogenesis. The authors suggested that hypoxia initially upregulated DDAH1, which was then accompanied by an increase in VEGF protein, leading to angiogenesis stimulation in a time-dependent fashion (Buijs et al., 2017). Nevertheless, other researchers believe that the effect of hypoxia on gene and consequently protein expression profile is cell-type specific (D'Alessandro et al., 2019). In their studies, while hypoxia induction increased VEGF-A in all types of cells tested, other genes expressed differently in different cells (D'Alessandro et al., 2019). To the best of our knowledge, there is no evidence in the literature for DDAH1 expression changes in hypoxia-induced ARPE-19 cells. This is because while RPE cells are known to secrete VEGF in response to hypoxia, they may not be the highest expressing cells for DDAH1 in the retina, based on a previous study on DDAH1 expression in different layers of the retina (Lange et al., 2016). DDAH1 was found to be expressed in the ganglion cell layer, the inner nuclear layer, and the photoreceptor layer of the retina (Lange et al., 2016). Interestingly, these researchers claimed that the role of DDAH2 in ADMA accumulation and retinal angiogenesis is much higher than that of DDAH1 (Lange et al., 2016). Another study has indicated increased ADMA levels (a potential

indication of low or inhibited DDAH1 levels) in monkeys' choroid-retinal endothelial cells (RF/6A) pre-treated with hypoxia and also in the retinal tissue of rat models of diabetic retinopathy (Du et al., 2018). Therefore, combining different layers of the retina through co-culture techniques (for modelling retinal angiogenesis), could create a better platform to investigate the crosstalk on the expression pattern of VEGF-A and DDAH1 under hypoxia.

Furthermore, hypoxia can affect many other genes and proteins in the signalling pathway; hence, the correlation does not necessarily imply causation. Therefore, to better understand the crosstalk between DDAH1 and VEGF-A and the potential regulation of VEGF-A on DDAH1, a second model of VEGF-A modulation was developed, in which specific gene silencing experiments were conducted.

4.3.3 Model 2: DDAH1 expression changes during siRNA-mediated VEGF-A knockdown

During this set of experiments, the hypothesis of DDAH1 downregulation after siRNA-mediated VEGF-A knockdown was tested.

The high transfection efficiency of siRNA is crucial for gene silencing in transfected cells. Efficient downregulation of VEGF-A by siRNA was determined in ARPE-19 cells in earlier studies (>75% for protein) (Zuo et al., 2010, Chen et al., 2013). In this study, the suppressive effect of siRNA silencing of VEGF-A gene after 72 hours was observed, and statistical significance was calculated at the mRNA level (**Fig. 4.7, A**). To measure the effect of protein inhibition ELISA assay was used. The amount of VEGF released into the medium showed a significant reduction (> 85 %) in transfected cells versus controls (**Fig. 4.7, B**). Based on the VEGF-A protein level and the high transfection efficacy, VEGF-A gene silencing was efficient. Following experiments revealed that siRNA-mediated VEGF-A gene knockdown had no effect on DDAH1 message (**Fig. 4.7, C**). Despite that, an increase in DDAH1 protein expression was detected in VEGF-A-deficient cells (**Fig. 4.7, D**). Indeed, it has to be considered that western blot experiments were conducted by an N of 1; thus, the statistical analysis of data was not feasible. To our best knowledge, no studies have been conducted on DDAH1 changes by modulation of VEGF (overexpression or knockdown).

4.3.4 Examining the crosstalk between DDAH1 and VEGF-A

To assess the effect of DDAH1 in biological aspects of angiogenesis and to see how DDAH-deficiency affects VEGF-A expression (as a major factor affected by angiogenesis), siRNA silencing of DDAH1 gene was conducted.

CHAPTER 4

Previous studies have shown that DDAH1 silencing by siRNA in HUVEC, over 24, 48, or 72 hours, decreased DDAH1 mRNA and protein levels (Zhang et al., 2011). Comparably, transfection of DDAH1 siRNA successfully knocked down DDAH1 gene in ARPE-19 cells after 72 hours (**Fig. 4.8, A**). However, gene silencing of DDAH1 did not affect expression levels of VEGF-A gene (**Fig. 4.8, B**), or protein (**Fig. 4.8, C**) as demonstrated by RT-PCR and ELISA assays, respectively.

A previous study demonstrated that DDAH1 knockdown by siRNA, attenuated VEGF protein expression in primary HUVEC cells, measured by immunoblot assay (Zhang et al., 2013). These researchers found that DDAH1 gene silencing affects multiple signalling pathways, including VEGF, NO/cGMP/PKG, and Ras/PI3K/Akt pathways, impairing proliferation and angiogenesis of vascular endothelial cells (Zhang et al., 2013). Another study has also shown that DDAH overexpressing murine endothelial cells secreted less ADMA, enhanced tube formation on Matrigel, and over 2-folds higher VEGF mRNA expression compared to non-transfected cells (Smith et al., 2003). The positive correlation between DDAH1 and VEGF is also evident from previous studies in rat C6 glioma cells; DDAH1 overexpression led to upregulation of VEGF mRNA in cell lysates (by Northern blot analysis), and VEGF protein in the media (by ELISA) (Kostourou et al., 2002). However, this positive correlation between DDAH1 and VEGF was not confirmed in another study, in which the overexpression of DDAH1 in HUVEC and bovine endothelial cells did not increase VEGF levels in the medium (Hasegawa et al., 2006).

Recently, the effect of siRNA-mediated DDAH1 knockdown on VEGF-mediated angiogenesis and also on ADMA levels in cell supernatant was assessed in monkeys' choroid-retina endothelial cells (RF/6A) (Du et al., 2018). DDAH1 deficiency significantly increased both ADMA secretion in cell media and the *in vitro* tube formation (Du et al., 2018). These researchers stated that the DDAH1/ADMA pathway might be the key regulator of angiogenesis in the retina through other pro-angiogenic factors than VEGF. They supported their claim by referring to the approximate 50% unsuccessful cases of diabetic retinopathy during anti-VEGF therapies (Ojha et al., 2017). In addition, they suggested an important regulatory role for EphrinB2 protein (a membrane-associated ligand that binds to Ephrin receptors, the most prominent family of tyrosine kinases) in the regulation of retinal angiogenesis (Du et al., 2018).

Hence, the last two findings may be taken together with ours to suggest that DDAH1 levels do not regulate VEGF-A production.

4.4 Conclusion

The developed models of VEGF-A modulation (hypoxia-mediated VEGF-A overexpression and siRNA-mediated VEGF-A knockdown) revealed contradictory findings regarding the effect of VEGF on DDAH1 regulation. 18-hour hypoxia resulted in maximum VEGF-A gene and protein expression levels in ARPE-19 cells. Under the same hypoxic conditions, while DDAH1 gene was upregulated, the protein was significantly downregulated. Since protein expression (rather than message) is the ultimate determinant of the potential influence of a factor on cellular pathways, based on DDAH1 protein reduction, it can be concluded that hypoxia-mediated VEGF-A overexpression suppresses DDAH1 expression. However, according to previous studies, hypoxia can affect several signalling pathways, including VEGF-A, which could have caused DDAH1 alteration. Therefore, the changes observed in DDAH1 expression under hypoxia cannot be limited to the effects of VEGF-A overexpression. Selective gene silencing targeting VEGF-A, and studying the changes in DDAH1, could further clarify the regulatory role of VEGF-A on DDAH1. The model of siRNA-mediated VEGF-A knockdown resulted in upregulation of DDAH1 protein. Therefore, our results from both models of VEGF-A modulation showed a negative correlation between VEGF-A and DDAH1 protein expression.

The final aim of this chapter was to investigate the cellular pathway through which DDAH1 inhibitor inhibited angiogenesis. Moreover, this study aimed to investigate whether VEGF-A had a role in this process. Since VEGF (VEGF-A) is the key mediator of angiogenesis, any change in its expression could be translated to a change in angiogenesis pattern, and vice versa. If this claim is valid, the previously observed angiogenesis inhibition by DDAH1 inhibitors will reflect reduced VEGF-A expression. The hypothesis of positive regulation of VEGF-A by DDAH1 was tested via selective silencing of DDAH1 gene and measuring VEGF-A expression changes. Knockdown of DDAH1 gene did not affect VEGF-A expression. This suggests that there might be a VEGF-independent pathway involved in the process of angiogenesis downregulation by DDAH1 inhibitors.

Further proteomics analysis by Mass Spectrometry on treated versus non-treated cells with DDAH1 inhibitors would clarify the affected pathways.

CHAPTER 5. INVESTIGATING THE IMPACT OF THE DDAH1 INHIBITOR ZST316 ON INTRACELLULAR BIOCHEMICAL PATHWAYS USING MASS SPECTROMETRY ANALYSIS

5.1 Introduction

DDAH1 is a key enzyme involved in the metabolism of the endogenous NOS inhibitors, ADMA and L-NMMA. Increased DDAH1 expression and subsequent increased NO production have been linked to excessive angiogenesis which plays a key role in several disease states, such as cancer, retinal disorders, psoriasis, atherosclerosis, rheumatoid arthritis, and Alzheimer's disease (Carmeliet, 2003, Carmeliet and Jain, 2011). Therefore, compounds with antiangiogenic properties could be an attractive option to inhibit excessive angiogenesis and its associated pathologies.

There are a number of steps to bring putative drug candidates, such as the novel DDAH1 inhibitors, through human studies and, eventually, to the market. The initial phase involves laboratory analysis, using computer and human cells models, testing the efficacy, toxicity and physiochemical properties. If drugs pass this initial step, they are then tested on animal models before being investigated in humans. Human testing consists of several phases: phase 1, in a relatively small number of healthy volunteers to evaluate the safety of the dose range; phase 2, in patients to further investigate efficacy and dose; phase 3, in a larger number of patients to demonstrate efficacy and rule out significant toxicity. After the results of these phases are reviewed and approved by the regulatory authorities, phase 4 (post-marketing surveillance) is conducted by the manufacturer, monitoring the long-term effects in the population (Therapeutic Goods Administration, 2020, The University of Queensland, 2017).

A novel class of small molecule DDAH1 inhibitors was initially designed and synthesised within the Department of Clinical Pharmacology at Flinders University, and their derived kinetic parameters (IC_{50} and K_i) for the inhibition of DDAH1 enzyme overexpression in HEK-293T cell lysate were reported and compared to the reference and selective DDAH1 inhibitor, L-257 (Tommasi et al., 2015, Leiper et al., 2007). One such compound, ZST316, is the most potent human DDAH1 inhibitor reported to date.

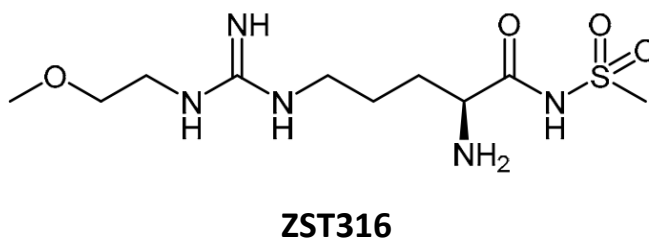
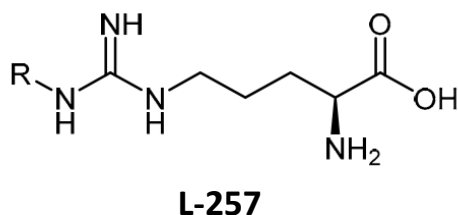


Figure 5.1. Chemical structure of the DDAH1 inhibitor, ZST316, relative to L-257 (the reference selective DDAH1 inhibitor).

Further experiments demonstrated the ability of ZST316 to inhibit endogenous DDAH1 activity in an *in vitro* model of triple negative breast cancer, MDA-MB-231 cells (Hulin et al., 2019). Following a 48-hour incubation with 100 μ M ZST316 in culture medium, MDA-MB-231 cell lysate displayed a 40% increase in the DDAH1 substrate ADMA, and a 38% decrease in the DDAH1 product L-citrulline (Hulin et al., 2019). Moreover, ZST316 caused a dose-dependent impairment in the formation of capillary-like tube structures in an *in vitro* model of vasculogenic mimicry. This effect was not associated with cellular toxicity or alterations in proliferation (Hulin et al., 2019). Similarly, cell culture experiments showed the absence of clear effects on cell viability and proliferation of these compounds in endothelial (**Chapter 3, Fig. 3.9**) and non-endothelial cells (**Chapter 3, Fig. 3.1 and 3.5**). Moreover, the results of the experiments on endothelial cells treated with ZST316 at 5 and 100 μ M were in line with previous findings, confirming the inhibition of tube formation in treated cells, although the inhibitory effect of the 5 μ M compound was greater than 100 μ M (**Chapter 3, Fig. 3.10 and 3.11**). However, the presence of off-target effects with DDAH1 inhibitors has not been investigated at the biochemical level.

ZST316 is an arginine-based analogue that could also potentially inhibit NOS enzymes. It should be noted that the low levels of NO released from the constitutive forms of NOS enzyme (eNOS and nNOS), are beneficial and play an important role in normal physiology and homeostasis, as

opposed to the high amounts of iNOS-derived NO (Kubes, 2000). Therefore, direct inhibition of eNOS or nNOS could affect physiological function or cause unwarranted toxicity.

Designing drugs with a restricted number of targets is a key challenge in drug discovery. Small molecule compounds, including the DDAH1 inhibitors synthesised locally, have the potential to interact with other small molecules such as proteins and metabolites. These interactions are either undesired, leading to adverse side effects, or sometimes advantageous (e.g. anti-inflammatory effects of statin therapy, mediated by changes in the gut microbiome (Kim et al., 2019)). A better understanding of the mechanisms of drug action, common biological pathways and drug targets should allow for more efficient utilisation of compounds with desirable selectivity profiles.

5.1.1 Aims and hypotheses

The original aim was studying the effects of our most potent DDAH1 inhibitor, ZST316, in endothelial VeraVec cells to assess which angiogenesis pathways are altered by the inhibitors and to investigate the cellular changes in components of the DDAH/ADMA/NOS pathway. These findings could identify the biological processes, molecular mechanisms, and signalling pathways behind the anti-angiogenic activity of ZST316 that was previously observed in endothelial cells (**Chapter 3**). Unfortunately, the VeraVec cell line is no longer available since their production and commercialization has been discontinued by the relevant biotechnology company (Angiocrine Bioscience, Inc.).

An alternative aim was therefore pursued, i.e., to elucidate the differential protein expression in ZST316-treated cells. This would provide novel information regarding the observed anti-angiogenic effect of ZST316 and also highlight any potential off-target effects. For this purpose, HEK293T cells were chosen as the cell model to assess the changes in protein abundance following treatment with 5 and 100 μ M ZST316 versus untreated (vehicle) control.

A mass spectrometry approach was used and a relative quantification on a significant number (thousands) of proteins from ZST316-treated samples and vehicle control were performed to measure those that were differentially expressed, upregulated, and/or downregulated, in each group.

It was hypothesised that ZST316 inhibits the enzymatic activity of DDAH1 without directly altering the protein expression of DDAH1 and other proteins within the ADMA/DDAH1/NOS axis after 24 hours.

To further interrogate differentially expressed protein datasets, and their potential effect on the cells, pathway analysis was performed to examine if any biological pathway was significantly altered in HEK-293T cells treated with 5 and 100 μ M ZST316. This would elucidate whether the treatment with the DDAH1 inhibitor might induce homeostatic alterations that are not morphologically evident with standard methods investigating proliferation and viability, used in previous experiments.

Therefore, these experiments sought to identify the potential mechanism behind the observed anti-angiogenic effect of ZST316, as well as the presence of additional effects on other biochemical pathways.

5.1.2 HEK-293: The cell line used for these drug discovery experiments

The ideal target for an anti-angiogenic compound should have high expression in endothelial cells at sites of angiogenesis, while having low expression in non-endothelial cell types. Therefore, VeraVec cells (with proven high DDAH1 expression) were a robust model to test the anti-angiogenic effects of the compound at molecular level. However, as these cells are no longer available, non-endothelial cells were used. In this context, HEK-293 cells are a suitable non-endothelial cell type that expresses DDAH1 at low levels (Mishima et al., 2004, Palm et al., 2007, Tran et al., 2000). The negative Western blot data generated from these cells (**Chapter 3, Fig. 3.12, and Chapter 4, Fig. 4.7**, indicated as –ive Ctrl) also suggests that the protein expression in HEK-293 cells is markedly low. Immunostaining of kidney tissue has shown that DDAH1 is located in the kidney (Palm et al., 2007) although no information is available for specific cell types.

The HEK-293 cell line and its variants originated from embryonal kidney and are frequently used in cell culture-based studies due to their rapid growth rate, high protein yield, and ease of transfection (Yuan et al., 2018, Stepanenko and Dmitrenko, 2015). Their fast-growing property is due to an adenovirus gene introduced by a researcher in the same lab where HEK cells had been originally isolated from and this result was from his 293rd experiment (Graham et al., 1977). Owing to this adenoviral DNA, they express viral promoters that encode for E1A/E1B proteins that initiate replication of the host cell and result in high levels of protein production (Lin et al., 2014, Stepanenko and Dmitrenko, 2015). Specifically, the HEK-293T variant, carrying a temperature-sensitive allele of the SV40 large T antigen, allows for amplification of the transfected plasmid, and thereby, a considerable increase and prolonged expression of the gene of interest. Therefore, they are a common vector for transfection (Abaandou et al., 2021, Yuan et al., 2018). The HEK-293T

cells are also an attractive option for drug development studies due to their human origin (Abaandou et al., 2021), ease of growth, rapid doubling time (36 hours), and ability to exhibit fully human-like posttranslational modifications in their proteins (Hu et al., 2018, Dumont et al., 2016).

5.1.3 Mass Spectrometry

Mass Spectrometry (MS) is an increasingly utilised technique to study a broad range of analytes including lipids (Frick and Schmidt, 2019), sugars (Kailemia et al., 2014), metabolites (Gowda and Djukovic, 2014) and proteins (Alfaro et al., 2017). This technique is being increasingly used to assess the differential protein expression in pathological states (Kim et al., 2021, Zhang et al., 2018, Aslam et al., 2017, Lim and Elenitoba-Johnson, 2004) or in response to drugs (Wingfield and Wilson, 2016, van Breemen, 2003). The current generation of instruments, in skilled hands, can identify and quantify thousands of proteins from a single injection of less than one μg of peptides. For protein analysis, proteins must be cleaved into peptides for mass spectrometry analysis as electrospray MS is generally limited to sequencing peptides of less than 40 amino acids (Coon et al., 2005). This is because the mass spectrometer must fragment each peptide and measure the mass of the fragment ions in order to determine the amino acid sequence. Peptides of more than forty amino acids do not fragment as efficiently as smaller peptides making it difficult to determine the amino acid sequence. Consequently, samples are cleaved with a protease, most commonly trypsin (Burkhart et al., 2012, Gundry et al., 2010), to generate peptides that can be sequenced by the instrument. Software packages such as Mascot, Proteome Discoverer, and PEAKS, analyse the MS data and match the mass of the fragment ions with the expected mass of the fragment ions determined from a specific database to produce peptide sequences. The peptides from each protein are then combined to determine the sequence coverage of each protein (Orsburn, 2021). Mass spectrometry is considered the gold standard for identifying proteins as it sequences peptides to make the identification. Previous techniques such as Western Blotting require the use of antibodies which can cross-react with other proteins and give false positives.

Mass spectrometry of proteins uses positive ion mode whereby the peptides are positively charged as a consequence of 0.1% formic acid present in all buffers, which protonates the primary amino at the amino terminus of peptides and also the primary amine present on lysine or arginine residues which lie at the C-terminus of tryptic peptides (Steckel and Schlosser, 2019). The negatively charged instrument draws the positively charged peptides in the gas phase into the instrument and utilizes the positive charge of the peptide ion to manipulate it through ion guides

CHAPTER 5

and quadrupoles into the collision cell and then into the mass analyser. Mass spectrometry instruments consequently utilize mass to charge (m/z , where m =mass and z =charge) ratios to control ions in the instrument and not mass alone as it requires the positive charge on the peptide for control of the ion. A doubly charged peptide (positive charge on both amino and C termini) will have half the apparent mass as a single charged ion e.g. a doubly charged ion of mass to charge ratio (m/z) of 553 will have an actual mass of approximately 1016 Daltons.

Mass spectrometers can be operated in data dependent mode (DDA) which is used principally for the identification of proteins. DDA uses an initial scan (MS1) to measure the mass of all positively charged ions entering the mass spectrometer at that time. It then performs a second series of MS called MS2 whereby it isolates multiply charged ions (peptides of charge state +2 to +6) iteratively in a collision cell. For example, if the MS1 scan identified 4 multiply charged ions, it would first accumulate the most intense multiply charged ion into the collision cell by setting voltages on the quadrupole which lies upstream of the collision cell so that it acts as a mass filter so that it only allows ions of this m/z through to the collision cell. Once inside the collision cell, these peptides are accelerated using RF frequency and DC (direct current) voltages so that the peptides collide with an inert collision gas (e.g. nitrogen, helium, argon). This collision fragments the peptides between the C=O and N-H atoms of the peptide bond that links each amino acid in the peptide generating a series of b and y fragment ions. B ions fragment from the N terminus and y ions fragment from the C terminus (Pappireddi et al., 2019). The fragment ions are transferred to the mass analyzer and the m/z of the fragment ions determined. The instrument then isolates the second most abundant ion (peptide) in the collision cell and fragments the ion. Once all peptides that are detectable in the MS1 scan (depending on instrument settings) have been fragmented, another MS1 scan is performed, and the process repeated. This is a simplification of the process as there are many instrument settings that control this process such as the number of peptides per cycle, exclusion lists, cycle time and injection time. These parameters and others allow a skilled operator to program the instrument to optimise the process for each type of sample. The MS1/MS2 process is also called tandem mass spectrometry and it is called data dependent because the MS2 scans are dependent on the ions identified in the MS1 scans (Pappireddi et al., 2019, Steckel and Schlosser, 2019). This process, for an Orbitrap type of instrument, is outlined in **Figure 5.3**.

Relatively recently, data independent acquisition (DIA) methods have been developed which have been instrumental in increasing the number of proteins that can be quantified in a single analysis.

DIA uses a single MS1 scan to determine the precursor mass and charge state of all peptides entering the instrument. An MS2 scan is then performed, but instead of isolating a single peptide at a time, it uses sequential windows of typically 20 m/z Dalton width across a mass range usually from m/z 350 to approximately 1,000 to 1,200 to place a mixture of peptides into the collision cell and fragment them. Therefore, each MS1 scan is followed by around 30-40 MS2 scans. This MS1/MS2 cycle is continuously repeated for the entire run. The principle is that this technique aims to fragment all peptides that are entering the instrument rather than selecting individual peptides for fragmentation which is likely to only fragment the most intense peptides. This process increases both the number of peptides fragmented and the number of times that each peptide is fragmented. Ideally, each peptide is fragmented at least 10 times as it is eluted from the C18 column into the instrument increasing the likelihood of achieving an accurate peak elution shape. The software then compares all the MS1/ MS2 data with a library generated by DDA analysis to correlate the b/y ions with the precursor peptides to determine the sequence and identity of the peptides. It is called data independent because the MS2 scans are independent of the MS1 scans because fixed MS2 windows have been used. The software integrates the chromatographic peak that the fragment ions generate over time as they elute from the column into the instrument which produces a relative quantity for each peptide present. This process is similar to integrating peaks generated by conventional protein purification chromatography. However, DIA generates relative abundance data only as no standards are used.

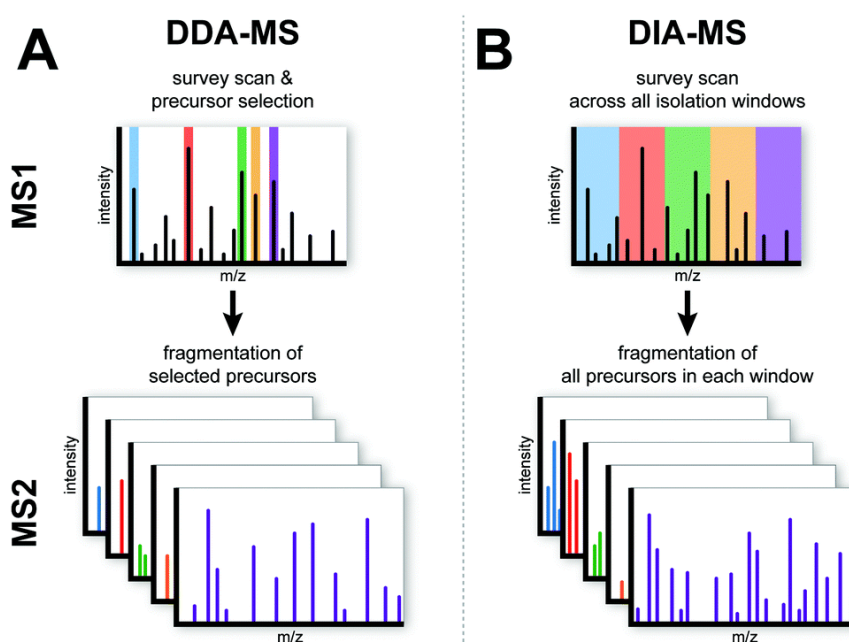


Figure 5.2. Schematic overview of the data-dependent acquisition mass spectrometry (DDA-MS) and data-independent acquisition mass spectrometry (DIA-MS).

(A) DDA analysis isolates a single peptide precursor following MS1 into the collision cell for MS2 whereas (B) DIA allows multiple peptides in a defined m/z range into the collision cell. The MS2 spectra are therefore more complex in DIA than for DDA. Adapted from (Krasny and Huang, 2021).

5.1.4 Pathway analysis

Pathway analysis helps to identify the relationship between the differentially expressed proteins in each treatment group and the biological signalling pathways that regulate cellular functions. This approach allows the identification of the biological pathways that are the most important and enriched and those that are likely insignificant. This study aimed to identify the size and the directions of the effects that differentially expressed proteins in each treatment group can have on cells. To continue the study on the effect of DDAH1 inhibitors on cell viability and proliferation as well as angiogenesis in previous chapters, this chapter specifically focused on angiogenic and apoptotic pathways analysis.

5.1.4.1 An introduction to apoptosis pathways

Cells can die via three main types of processes: type I or programmed cell death, also known as apoptosis (the main pathway), type II or the degradation process of autophagy to remove damaged proteins, and type III or unprogrammed and accidental necrosis (Elmore, 2007, Green and Llambi, 2015).

Apoptosis is a tightly controlled mechanism of cell death that occurs via two main pathways: intrinsic (mitochondrial), or extrinsic (via expressing tumour necrosis factor (TNF) receptors and ligand-binding), in addition to a third endoplasmic reticulum (ER)- stress pathway (regulated by molecular chaperons, e.g. the heat shock proteins (Hsp) family) (Shen et al., 2002). Intrinsic pathways are mitochondrial events that occur in the context of intracellular injury, which causes changes in the inner mitochondrial membrane, and release of pro-apoptotic proteins (cytochrome c) from the mitochondria intermembrane space into the cytosol (Elmore, 2007). These proteins activate apoptotic protease activating factor 1, caspase-9 and caspase-3, which ultimately lead to apoptotic cell death (Elmore, 2007). The extrinsic pathway initiates with stimulation of death receptors and ligands-binding, which activates caspases (cysteine-dependent proteases), specifically caspase-8 (Sauerwald et al., 2011), leading to intracellular protein degradation and irreversible cell death (Sauerwald et al., 2011, Elmore, 2007). The third pathway is activated by the accumulation of misfolded proteins in the ER via alteration in Ca^{2+} homeostasis, causing ER-stress, which in the long-term leads to apoptotic caspase activation and cell death (Elmore, 2007).

5.1.4.2 *The importance of testing angiogenesis and apoptosis pathways for ZST316 drug discovery experiments*

An anti-angiogenic agent is considered valid when the drug characterisation data guarantee over-representation or enrichment of several angiogenic-related pathways in endothelial cells at sites of angiogenesis, and under-representation or inhibition of apoptotic-related pathways, in all cell types. Hundreds of anti-angiogenic compounds, targeting different angiogenic factors, have been investigated for their potential to combat excessive vessel growth in pathologies such as cancer, ocular neovascularisation, and rheumatoid arthritis. Nevertheless, the overall benefits of anti-angiogenic therapy are often limited by toxicity. Therefore, highly sensitive analytical techniques might assist in the discovery of new anti-angiogenic therapies by identifying the exact mechanisms of action involved, including the interaction with apoptosis-related pathways. By performing a pathway analysis on the significantly upregulated and downregulated list of proteins as input, the angiogenic- or apoptotic-associated pathways in which the differentially expressed proteins are over-represented or under-represented can be identified.

HEK-293T cells contain proteins involved in angiogenesis, e.g., VEGF and DDAH isoforms. Therefore, their study can provide useful initial information on the regulation of these pathways by DDAH1 inhibitors, and for designing future experiments on other cell types, particularly endothelial cells.

5.1.4.3 *Rationale for using InnateDB*

Protein expression profiles and interactions can be assessed using different pathway analysis platforms such as InnateDB, Ingenuity Pathway Analysis (IPA), STRING, etc., each with their strengths and weaknesses. In this study, InnateDB was used for the signalling pathway analysis of the mass spectrometry data.

InnateDB (publicly available at <http://www.innatedb.com>) is a database specifically designed for analysis of mammalian innate immunity networks, signalling pathways, genes, and proteins (Lynn et al., 2008, Lynn et al., 2010). Although this database was initially designed to investigate pathways involved in human and mouse innate immune response, it has aggregated detailed information that is sourced from several databases including the Kyoto Encyclopaedia of Genes and Genomes (KEGG), Reactome, NetPath, the Integrating Network Objects with Hierarchies (INOH), BioCarta, and the Pathway Interaction Database (PID). Furthermore, several external datasets have been imported into InnateDB from a wide range interaction and pathway databases including the Molecular Interaction database (MINT) (Chatr-Aryamontri et al., 2007), IntAct

database (Kerrien et al., 2007), the Database of Interacting Proteins (DIP) (Salwinski et al., 2004), the General Repository for Interaction Datasets (BioGRID) (Breitkreutz et al., 2007), and the Biomolecular Interaction Network Database (BIND) (Alfarano et al., 2005). Therefore, InnateDB is one of the most comprehensive databases that incorporates over 300,000 molecular interactions and >3,000 pathways relevant to human and mouse cellular systems (Breuer et al., 2013). Hence, it can be easily adapted to other biological and cellular processes, e.g., in this project, analysing the effects of pharmacological DDAH1 inhibition on cell signalling and pathway regulation, focusing on angiogenesis and apoptosis pathways. In this study, ZST316 was investigated for its enrichment in KEGG pathways using InnateDB software.

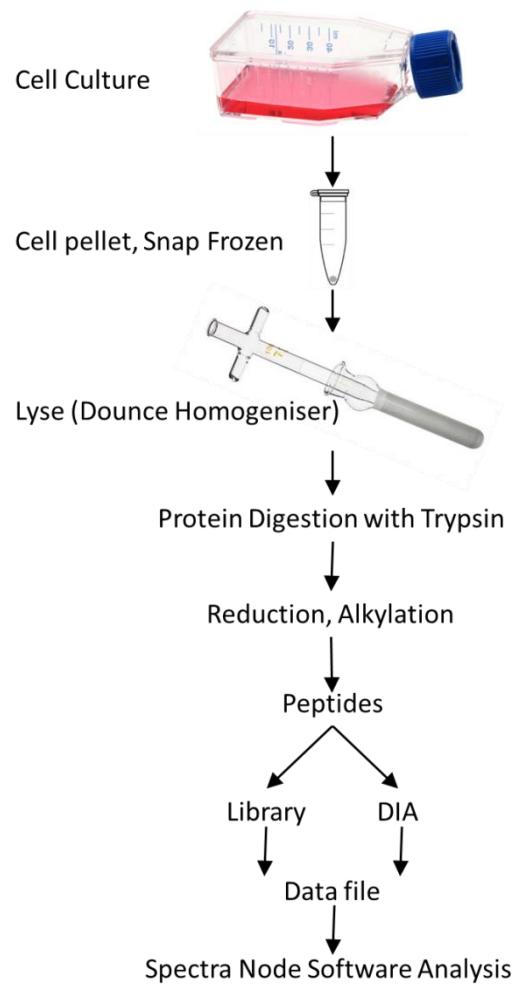
5.2 Methods

5.2.1 Experimental Workflow

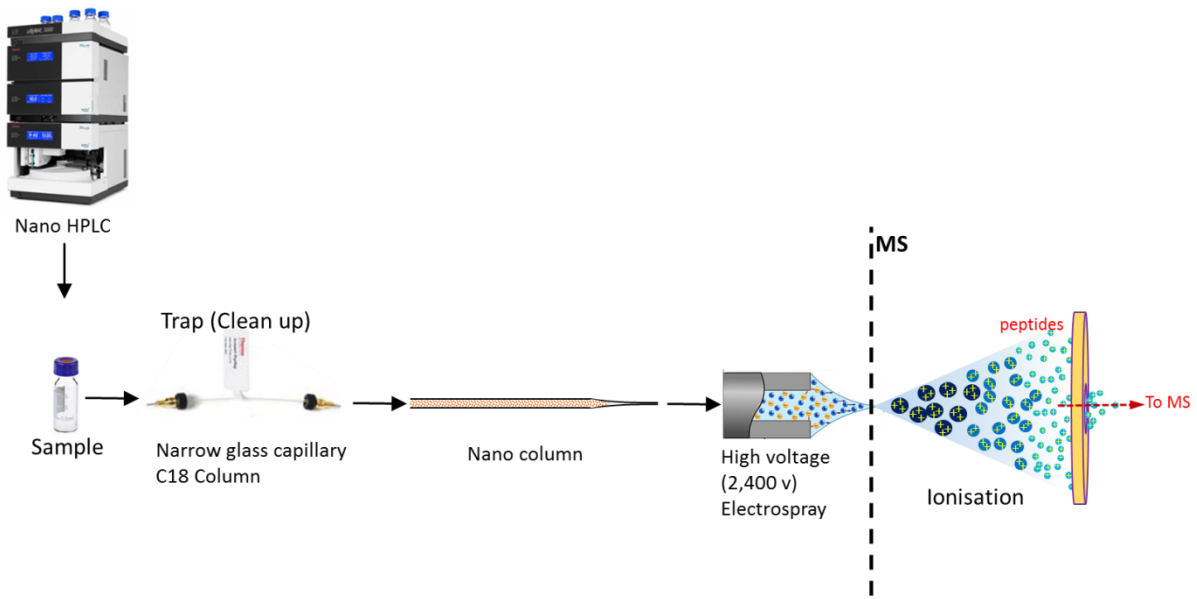
Cultured HEK-293T cells were treated with vehicle, 5 μ M or 100 μ M ZST316, each with four biological replicates (4 flasks), for 24 hours (The rationale of choosing the selected concentrations and incubation time is described in the **discussion section 5.4.1, page 162**). Cells were harvested and, in order to provide high quality pellets suitable for MS, the cell pellets were snap-frozen in liquid nitrogen and kept in -80°C until they were lysed, trypsin digested and prepared for MS procedure. Samples were then injected into the HPLC and analysed by MS. **Figure 5.3** illustrates the workflow of the experiment. For detailed information on cell culture process, sample preparation, and MS procedure refer to the Materials and Methods (**Chapter 2, section 2.10**).

CHAPTER 5

A. Sample Preparation



B. Nano HPLC



C. Mass Spectrometer

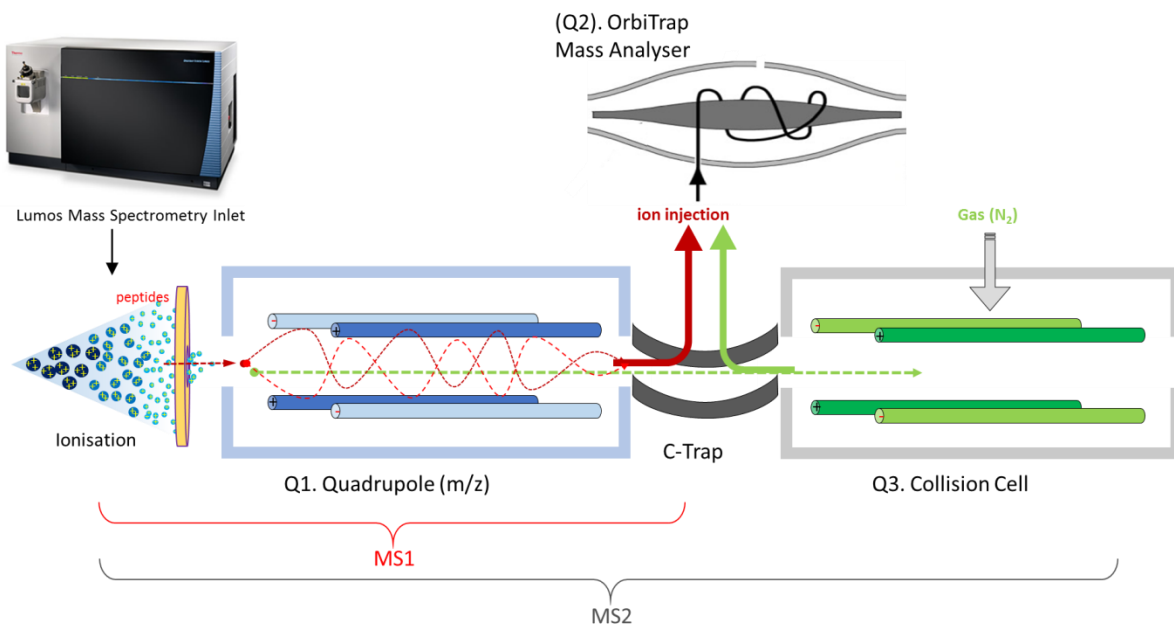


Figure 5.3. Schematic outline of the MS workflow established for ZST316-treated or non-treated HEK-293T cells.

(A) Sample preparation, (B) Diagram illustrating the injection HPLC component of the mass spectrometry analysis (Thermo Dionex Ultimate 3000 nano uHPLC), (C) Diagram illustrating the manipulation of ions inside the Thermo Exploris Fusion Lumos mass spectrometry (DDA analysis). Red dashed line represents ions going through MS1, and green dashed line represent the ions during the second round of MS (MS2).

5.2.2 Pathway Analysis Methods

Functional relationships between the proteins identified in HEK-293T cells treated with vehicle (water), 5 and 100 μM ZST316 and angiogenesis and apoptosis pathways were bioinformatically determined using InnateDB ORA tool (the rationale for choosing the two compound concentrations has been explained earlier in this chapter, **section 5.2.1**).

The lists of differentially expressed proteins, with a $\log_2\text{Fold-change} \geq 0.6$ (equivalent to a 50% increase or decrease in abundance) and a Q-value < 0.05 as a cut-off criterion, was used to perform InnateDB pathway analysis (**see Appendices 5-7**). The protein IDs (Uniprot IDs) from each list (5 μM ZST316 vs control, 100 μM ZST316 vs control, and the overlap of differentially expressed proteins between the two doses) were uploaded.

5.3 Results

5.3.1 DIA analysis

A small proportion (5 μg) from each of the 12 samples were pooled and a spectral library constructed using high pH reversed phase fractionation and DDA analysis as well as gas phase fractionation and DIA analysis to make the HEK-293T cell library. This library contained 6,203 protein groups. Proteins are determined by the presence of peptide sequences that are derived from the intact protein. A protein group is a master protein which contains peptides that are not present in any other protein group. For example, there are multiple isoforms of haemoglobin that contain peptides common to all isoforms but also unique peptides. Therefore, if multiple peptides were identified from the common region and one peptide from haemoglobin gamma, then all of the isoforms of haemoglobin could be listed in proteins identified, but only haemoglobin gamma would be listed in the protein groups as this single protein could potentially generate all of the peptides detected. However, it is possible that other isoforms of haemoglobin are present but only generate peptides that were common to all isoforms. Therefore, the list of protein groups is more stringent than the list of proteins and consists of the minimum set of proteins which could justify the presence of the peptides sequence (the list of all identified protein groups in the library is available on request). Throughout the thesis, the term proteins, instead of protein groups, will be used for simplicity.

The differentially expressed proteins in all groups (listed in **Appendices 5-7**) were selected using a cut-off of $\log_2\text{Fold-change} \geq 0.6$ and Q-value ≤ 0.05 .

5.3.1.1 Identification of differentially expressed proteins at the baseline level

Instruments with extremely high sensitivity can be subject to significant run to run variation when analysing samples near the limit of its sensitivity. For example, this issue can be seen when performing mRNA differential quantification using PCR due to its extreme sensitivity. This background variation is sometimes called noise. To determine the background level of noise for identifying differentially expressed proteins using the DIA method for quantification, control HEK-293T samples from two biological replicates were selected and prepared for MS. Each replicate was injected into the mass spectrometer four times (four technical replicates) using DIA (**Fig. 5.4, A, “Experiment 1”**). As the samples were replicates of control samples, there should theoretically be no differences between the samples. However, biological replicates might contain subtle differences in seeding density or degree of confluence while technical replicates might suffer from instrument variations in measuring identical samples. These eight samples were the background change candidates, and the four technical replicates from biological replicate one were compared with the four technical replicates from biological replicate two (**Fig. 5.4, B, “Experiment 2”**).

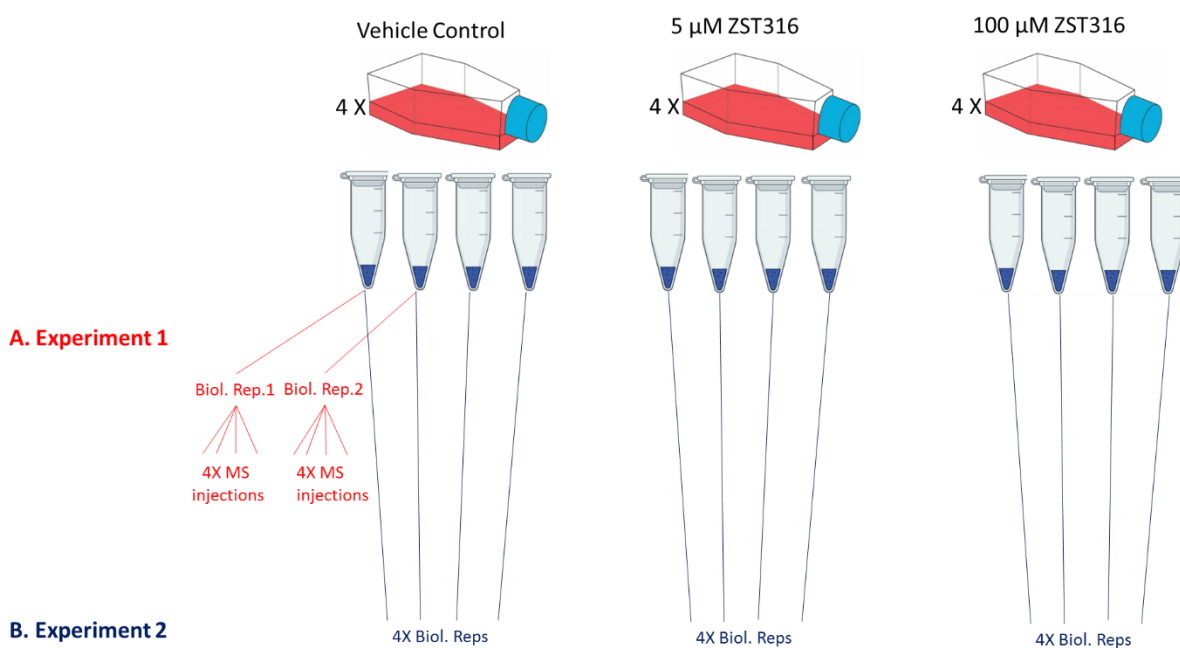


Figure 5.4. Overview of the MS experimental design.

HEK-293T cells were cultured and treated with vehicle (water), ZST316 at 5 and 100 μ M in quadruplicate. (A) During “experiment 1”, two replicates of the vehicle control samples were selected and ran by MS to test the differentially expressed proteins as baseline of changes. (B) During “experiment 2”, all the four replicates from each sample set were ran by MS to quantify differentially expressed proteins in them.

When comparing background candidates (vehicle control) from biological replicate 1 to 2, 150 proteins were differentially expressed (out of the approximately 5,500 proteins quantified in each run (**Table 5.2A**)), with 72 (48%) significantly upregulated and 78 (52%) significantly downregulated (**Fig. 5.5, left bar**). The total number of proteins quantified in each MS analysis, 5,500 (**Table 5.1, A**), was approximately 88% of the 6,203 protein groups identified in the library.

“Experiment 1” was conducted under the same conditions as for vehicle, 5 and 100 μM ZST316-treated cells.

5.3.1.2 Identification of differentially expressed proteins with ZST316 treatment

Next, vehicle (water) control and the treated (5 and 100 μM ZST316) samples were analysed by MS (**Fig. 5.4, B**, “Experiment 2”). Protein abundance for the 5 and 100 μM ZST316-treated groups were compared to vehicle controls.

In “experiment 2”, the number of proteins significantly upregulated in 5 and 100 μM ZST316 treatments were 77 and 97 (**Fig. 5.5, red bar**), compared to vehicle only, while the number of significantly downregulated proteins were 117 and 118 (**Fig. 5.5, green bar**), respectively.

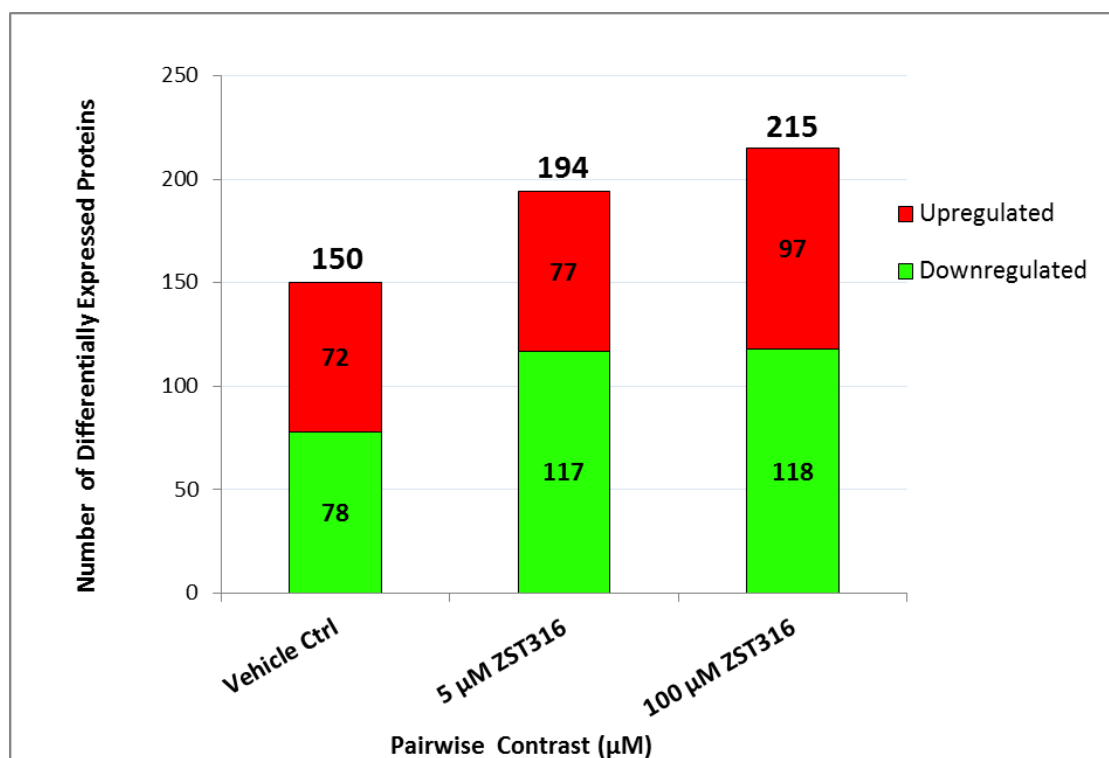


Figure 5.5. Stacked-bar graph showing the abundance of upregulated (red portion of bar) and downregulated (green portion of bar) proteins in HEK-293T cells treated with vehicle, 5, and 100 μM ZST316.

The stacked-bar graph provides the number of differentially expressed proteins at baseline in “experiment 1” (first bar on the left) which indicates the background noise, and “in experiments 2” in 5 and 100 μM ZST316-treated cells

CHAPTER 5

compared to vehicle-treated cells (second and third bars respectively).

Notably, these figures represent only 1.3-2.2% of the 5,500 proteins quantified in each MS analysis. The proportion of changes compared to the library is calculated in **Table 5.1**. In Chi-square analysis (<https://www.socscistatistics.com/tests/chisquare2/default2.aspx>) there was a significant difference between the downregulated proteins in both ZST316-treated groups vs vehicle control, but not between the upregulated proteins in treated vs vehicle (**Table 5.1, C**).

CHAPTER 5

Table 5.1. Quantified proteins by Spectronaut in each sample set and the proportion of changes compared to the library.

(A) Number of proteins quantified in each sample. Spectronaut reports the number of proteins identified and quantified in each sample. Note that the library contained 6,203 proteins. (B) Proportion of differentially expressed proteins compared to the number of proteins quantified in each sample. (C) The contingency table provides information on the observed cell totals: (the expected cell totals) in the brackets and [the chi-square statistic for each cell] in square brackets. The chi-square statistic, p-value and statement of significance appear beneath the table. (Blue means you're dealing with dependent variables; red, independent).

A. Treatment group	Vehicle Ctrl	ZST316 5 μ M	ZST316 100 μ M
Rep. 1	5451	5558	5471
Rep. 2	5542	5530	5482
Rep. 3	5474	5476	5387
Rep. 4	5503	5489	5451
Average	5493	5513	5448

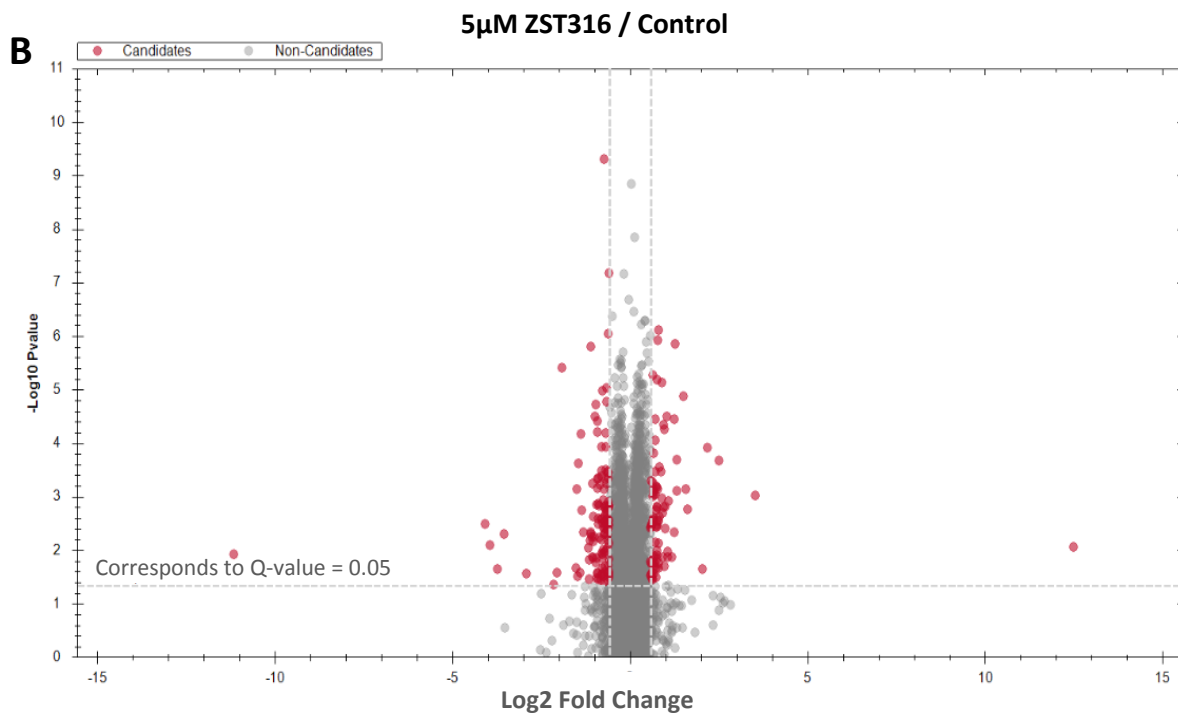
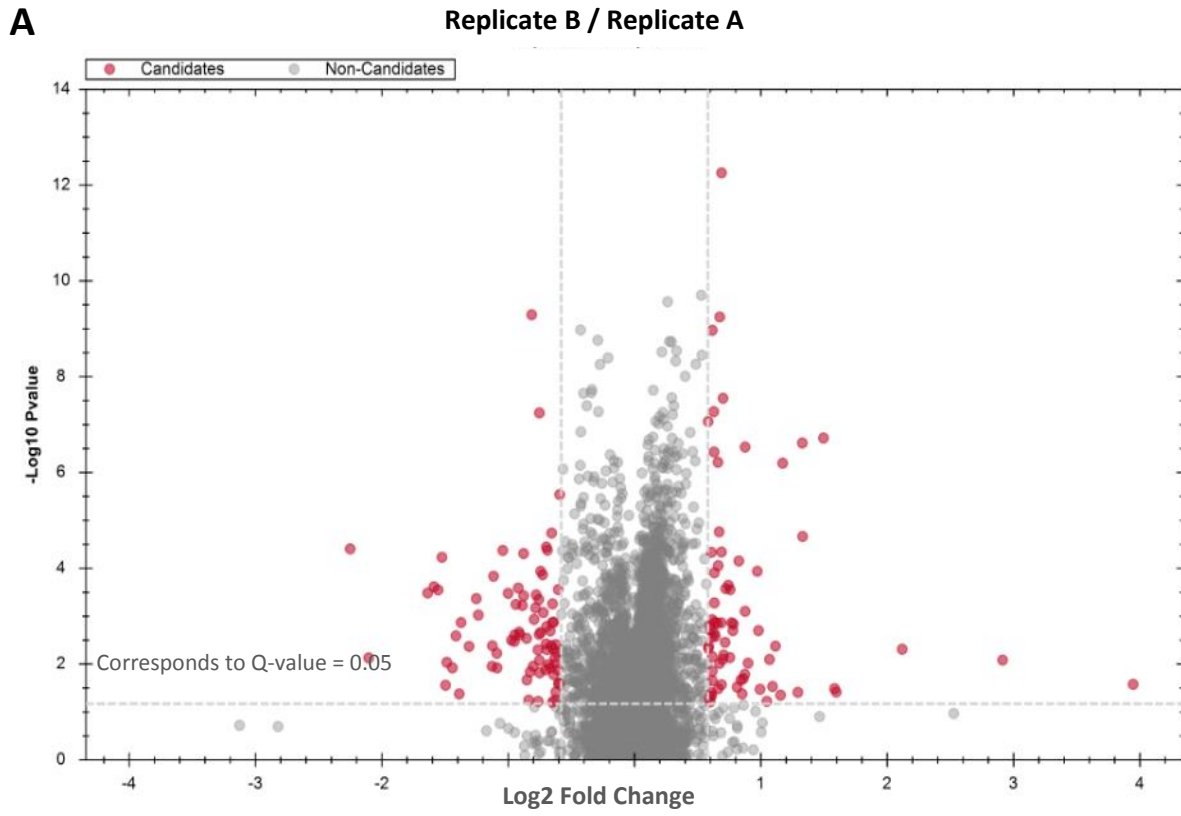
B. Treatment group	Vehicle Ctrl	ZST316 5 μ M	ZST316 100 μ M
Upregulated	72/5493 = 1.3%	77/5513 = 1.4%	97/5448 = 1.8%
Downregulated	78/5493 = 1.4%	117/5513 = 2.1%	118/5448 = 2.2%

C. Chi-square Statistic	Vehicle Ctrl	ZST316 5 μ M	ZST316 100 μ M	Raw Totals
Upregulated	72 (82.23) [1.25]	77 (82.42) [0.36]	97 (81.45) [2.97]	246
Total	5421 (5410.88) [0.02]	5436 (5430.58) [0.01]	5351 (5366.55) [0.05]	16208
Column Totals	5493	5513	5448	16454 (Grand Total)
The chi-square statistic is 4.6425. The p-value is .098153. The result is not significant at p < .05.				
Downregulated	78 (104.49) [6.72]	117 (104.87) [1.40]	118 (103.64) [1.99]	313
Total	5415 (5388.51) [0.13]	5396 (5408.13) [0.03]	5330 (5344.36) [0.04]	16141
Column Totals	4593	5513	5448	16454 (Grand Total)
The chi-square statistic is 10.3059. The p-value is .005782.				

Figure 5.6 shows the volcano plots from the differentially expressed proteins in “experiment 1” between the two vehicle control replicates (**Fig. 5.6.A**), and “in experiment 2” for 5 μ M ZST316 vs vehicle control (**Fig. 5.6, B**), and 100 μ M ZST316 vs vehicle control (**Fig. 5.6, C**). The differentially expressed proteins were selected using the following criteria: Q- value \leq 0.05 (above the horizontal dash lines), $|\text{Log}_2\text{Foldchange}| \geq 0.6$ (outside the two vertical dash lines) (**See**

CHAPTER 5

Appendices 5, 6, and 7). The red dots and grey dots indicate the proteins that are or are not differentially expressed at the significance level, respectively. The red dots on the right of the volcano plots are significantly upregulated while those on the left are significantly downregulated. The total number of dots represents the number of proteins quantified, approximately 5,500.



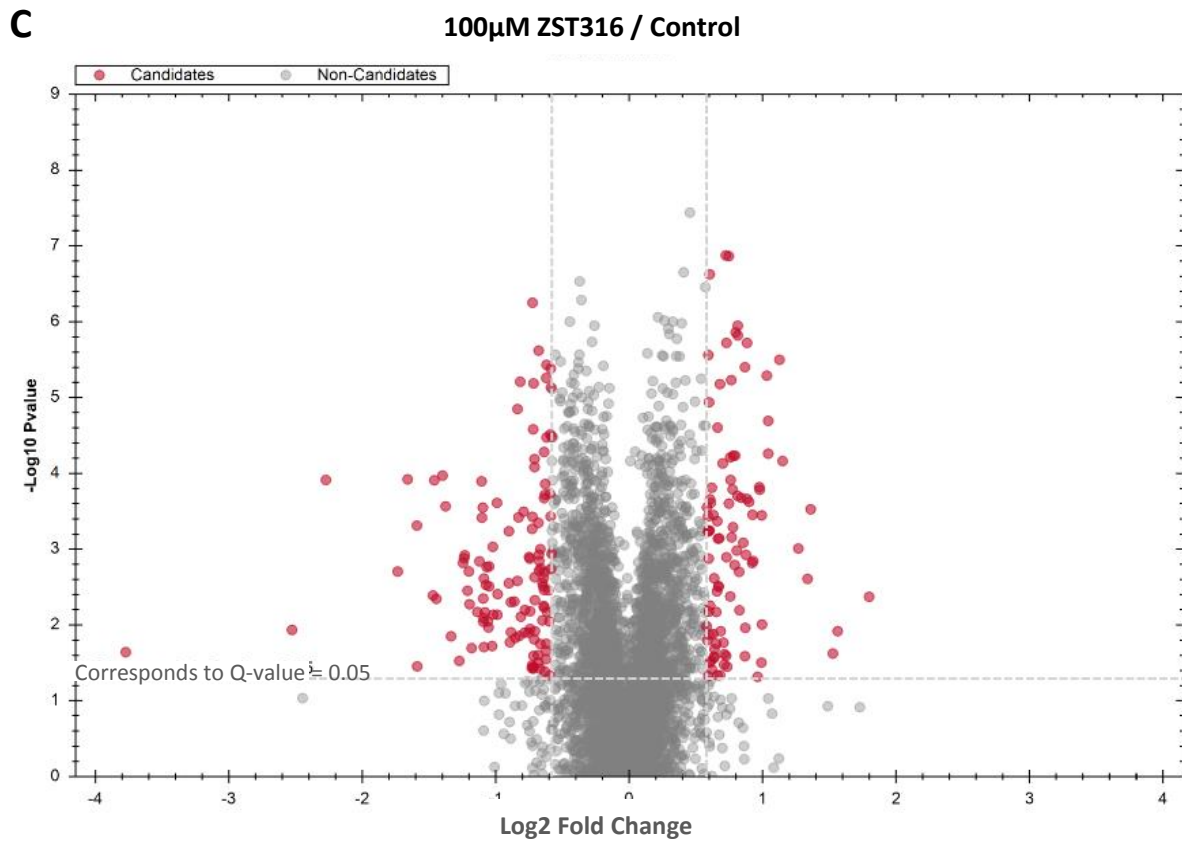


Figure 5.6. Volcano plots for proteomic profiling of HEK-293T cells treated with vehicle, 5 and 100 μ M ZST316.

Red dots represent differentially expressed proteins (candidates) and grey dots represent proteins with no significant change (non-candidates): Volcano plot (A) plots differentially expressed proteins in the baseline experiment comparing replicates from untreated HEK293T cells. Volcano plots (B) and (C) display differentially expressed proteins in 5 μ M and 100 μ M ZST316 treated cells compared to vehicle control treated cells respectively. The volcano plots were generated Spectronaut. Y axis represents $-\log_{10} (q \text{ value})$ and x axis represents $\log_2 \text{fold change}$. Differentially expressed proteins identified with the cut-offs of $Q \leq 0.05$ and $0.6 \leq \text{Log}_2 \text{fold-change} \leq -0.6$.

Looking at the differentially expressed proteins, a small number were concomitantly upregulated in both the 5 μ M and 100 μ M ZST316-treated cells. The Venn diagram below illustrates the 23 overlapping upregulated (**Fig. 5.7, A**) and 16 overlapping downregulated (**Fig. 5.7, B**) proteins in the 5 and 100 μ M ZST316-treated cells (dashed lines in **Figure 5.7**, and described in **Table 5.2**). A complete description of these proteins can be found in **Appendices 8 and 9**. Of note, DDAH2 is among the proteins that were upregulated with both doses of ZST316 (**bold text in Table 5.2, A and B**).

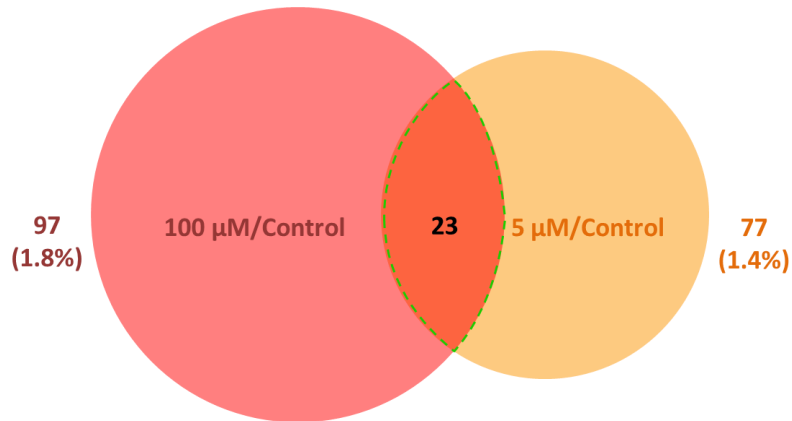
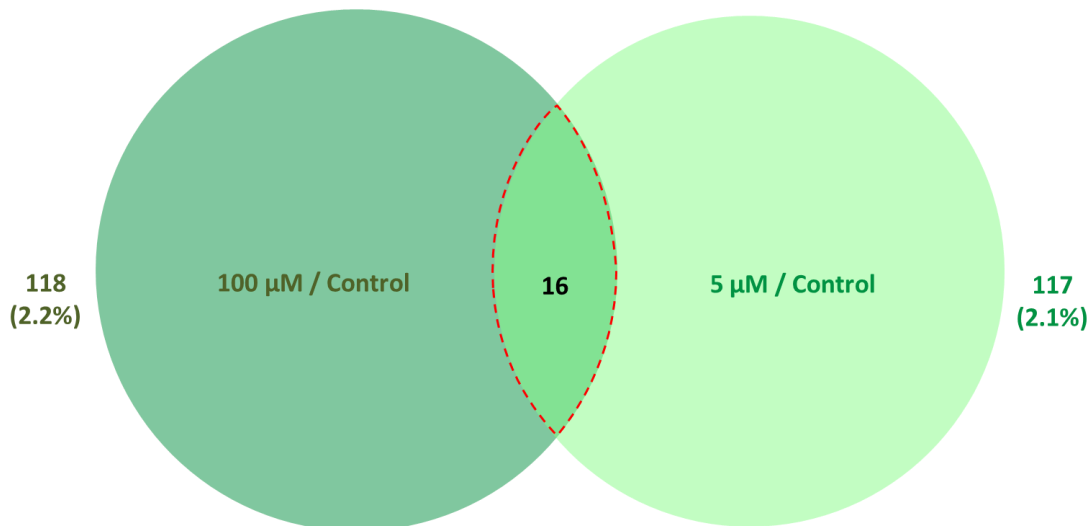
A. Upregulated Proteins**B. Downregulated Proteins**

Figure 5.7. Venn diagrams represent comparisons made from two pairwise contrasts of HEK-293T cells treated with 5 and 100 μM ZST316 versus control cells.

The Venn diagrams show the number of unique proteins and the number of commonly shared proteins found in pairwise contrasts of vehicle control or ZST316-treated HEK-293T cells, out of the total number of 6,203 proteins quantified in the library (Percentage values indicate how small the values are). The Venn diagram in Panel (A) compares all upregulated proteins of 5 μM vs control (orange) with 100 μM vs control (red). Panel (B) compares all downregulated proteins of 5 μM vs control (dark green) with 100 μM vs control (light green). Dashed-lines mark the number of concomitant up- or down-regulated proteins in 5 and 100 μM treatments.

CHAPTER 5

Table 5.2. List of overlapping (A) 23 upregulated and (B) 16 downregulated protein descriptions (and their related genes if available) between 5 and 100 μ M ZST316-treated HEK-293T cells.

A. 23 Overlapping Upregulated Proteins	
Gene ID	Protein Descriptions
MYO9B	MYO9B variant protein; (Unconventional myosin-IXb))
hCG_21651	HCG21651, isoform CRA_a, (Protein FAM92A)
JMJD4	2-oxoglutarate and iron-dependent oxygenase JMJD4
HSP90AB4P	Putative heat shock protein HSP 90-beta 4
N/A	cDNA FLJ16452 fis, clone BRAWH3002467, highly similar to RAB GDP DISSOCIATION INHIBITOR BETA
N/A LIMD5	cDNA FLJ54018, highly similar to PDZ and LIM domain protein 5
DDAH2	N(G),N(G)-dimethylarginine dimethylaminohydrolase 2;DDAH2
RASAL2	cDNA FLJ77041, highly similar to Homo sapiens RAS protein activator like 2 (RASAL2), transcript variant 1, mRNA, (Ras GTPase-activating protein nGAP)
HACL1	cDNA FLJ55041, highly similar to 2-hydroxyphytanoyl-CoA lyase
ZNF654	Zinc finger protein 654
HSD17B12	Very-long-chain 3-oxoacyl-CoA reductase
HSPA8	Heat shock cognate 71 kDa protein (Fragment)
FKBP1	FK506 binding protein like, isoform CRA_a
PRKRIP1	PRKR interacting protein 1 (IL11 inducible), isoform CRA_a
TUBE1	Tubulin epsilon chain
SLC7A6	Solute carrier family 7 (Cationic amino acid transporter, γ^+ system), member 6, isoform SLC7A6
PALM	Paralemmin, isoform CRA_a
MRP63	Mitochondrial ribosomal protein 63, isoform CRA_a
PPP3CC	Serine/threonine-protein phosphatase 2B catalytic subunit gamma isoform
SPIRE1	Protein spire homolog 1
GOT2	Aspartate aminotransferase; mitochondrial
RAB23	RAB23, member RAS oncogene family, isoform CRA_a;Ras-related protein Rab-23
PTPMT1	cDNA FLJ57723, moderately similar to Protein-tyrosine phosphatase mitochondrial 1, mitochondrial

B. 16 Overlapping Downregulated Proteins	
Gene ID	Protein Descriptions
RPF2	Ribosome production factor 2 homolog
SNW1	SNW domain-containing protein 1; SNW1 protein
CTNNBIP1	Catenin, beta interacting protein 1, isoform CRA_a
KNOP1	Lysine-rich nucleolar protein 1
SETMAR	Histone-lysine N-methyltransferase SETMAR
PYGO2	Pygopus homolog 2 (Drosophila), isoform CRA_a
PAN3	PAN2-PAN3 deadenylation complex subunit PAN3
REXO4	RNA exonuclease 4
NDUFAF8	NADH dehydrogenase [ubiquinone] 1 alpha subcomplex assembly factor 8
TIMM10	Mitochondrial import inner membrane translocase subunit Tim10
CDC42EP1	CDC42 effector protein (Rho GTPase binding) 1, isoform CRA_a
BUD13	cDNA FLJ76180; BUD13 homolog
N/A	cDNA FLJ55706; Tetratricopeptide repeat protein 30A
GTPBP6	Putative GTP-binding protein 6
THYN1	Thymocyte nuclear protein 1, isoform CRA_a
N/A	p231

5.3.2 Pathway Analysis

The protein differential expression lists for each set contained at least one protein that was present in the pathways listed in **Appendices 10 to 12**, and in some cases the number of differentially expressed proteins that were present in a pathway reached a statistically significant level of enrichment. These proteins and the list of enriched pathways are listed on **Tables 5.4 to 5.6**. The terms gene and protein are interchangeable for the purpose of pathway analysis tables.

5.3.2.1 Identification of the differentially expressed proteins present in a signalling pathway and the enriched pathways in response to ZST316 treatment in HEK-293T compared to control cells

To examine which biological pathways were altered in HEK-293T cells treated with 5 and 100 μM ZST316 versus vehicle control group, the biochemical pathways were extracted from the Kyoto Encyclopedia of Genes and Genomes (KEGG) and pathway analysis was performed for the differentially expressed proteins with Q-value ≤ 0.05 in each set, using InnateDB pathway analysis (Lynn et al., 2008).

Both upregulated and downregulated proteins in each set of differentially expressed proteins recognised by mass spectrometry for vehicle, 5 and 100 μM ZST316-treated HEK cells (**Appendices 5-7**) were subjected to KEGG pathway enrichment analysis. The associated pathways with the genes (linked with the Uniprot IDs) are shown in **Appendix 10, 11, and 12** for vehicle, 5, and 100 μM ZST316, respectively.

KEGG pathway analysis of the vehicle control revealed that upregulated and downregulated proteins were present in 12 and 20 pathways, respectively (**Appendix 10**). No KEGG pathway was found to be enriched when subjected to ORA for the upregulated proteins. By contrast, three pathways were enriched with downregulated proteins (**shown on Table 5.4**).

CHAPTER 5

Table 5.4. Enriched KEGG pathways over-represented with vehicle control HEK-293T cells, and the associated genes related to differentially expressed downregulated proteins.

(ORA showed no enriched KEGG pathway that was over-represented with control cells by the upregulated proteins).

Pathway Name (Enriched by down-regulated proteins)	Pathway Id	Pathway uploaded gene count	Genes in InnateDB for this entity	% Associated genes	Pathway p-value (corrected)	(Down-regulated) Gene Symbols
Ribosome	474	6	137	4.38	1.35E-05	MRPS5; MRPS6; RPL8; RPS27; RPS3A; RPS7;
Spliceosome	8120	3	133	2.26	0.0041	EFTUD2; PRPF3; SNRPD2;
Fc gamma R-mediated phagocytosis	4359	2	93	2.15	0.0215	MARCKS; MARCKSL1;

KEGG pathway analysis of upregulated and downregulated proteins by 5 μ M ZST316 resulted in 32 and 43 pathways, respectively (**Appendix 11**), where three pathways in each group were shown to be enriched when subjected for further ORA analyses. These pathways included Wnt signalling pathway, proteins processing in endoplasmic reticulum and calcium signalling pathways for upregulated proteins (**Table 5.5, A**), and RNA transport, RNA degradation and Insulin signalling pathways for downregulated proteins (**Table 5.5, B**).

Table 5.5. Enriched KEGG pathways over-represented with 5 μ M ZST316 treatments of HEK-293T cells and the associated genes related to differentially expressed (A. upregulated, B. downregulated) proteins.

A. Pathway Name (Enriched by upregulated proteins)	Pathway Id	Pathway uploaded gene count	Genes in InnateDB for this entity	% Associated genes	Pathway p-value (corrected)	(Upregulated) Gene Symbols
Wnt signalling pathway	445	2	140	1.43	0.0129	GPC4; PPP3CC;
Protein processing in endoplasmic reticulum	10363	2	171	1.17	0.0143	CANX; RPN1;
Calcium signalling pathway	594	2	183	1.09	0.0145	PPP3CC; VDAC3;

B. Pathway Name (Enriched by down-regulated proteins)	Pathway Id	Pathway uploaded gene count	Genes in InnateDB for this entity	% Associated genes	Pathway p-value (corrected)	(Down-regulated) Gene Symbols
RNA transport	10361	3	170	1.76	0.0080	EIF4E2; POP4; RPP14;
RNA degradation	5710	2	74	2.70	0.0153	ENO3; PAN3;
Insulin signalling pathway	531	2	143	1.40	0.0368	EIF4E2; NRAS;

CHAPTER 5

For 100 μ M ZST316 treated cells, KEGG pathway analysis showed 59 pathways associated with upregulated proteins (**Appendix 12**). The enriched pathway analysis identified 9 over-represented pathways: B cell receptor signalling pathway with the highest (4%) term significance ($P= 0.001$) with 3 genes from 74 total genes listed in the pathway, followed by Long-term potentiation, VEGF and MAPK signalling pathways, T cell receptor signalling pathway, natural killer signalling pathway, Wnt signalling, purine metabolism and calcium signalling pathway (p-values sorted in ascending order, **Table 5.6, A**). Pathway analysis revealed that at least one protein from the list of downregulated proteins was present in 17 pathways (**Appendix 12**), in which three were found to be over-represented: Spliceosome, Ribosome and Pyrimidine metabolism pathways (**Table 5.6, B**). The p-values were corrected using the Benjamini and Hochberg correction for the false discovery rate (as recommended by the software) (Benjamini and Hochberg, 1995), although similar results were obtained using the more stringent Bonferroni correction.

Table 5.6. Enriched KEGG pathways over-represented with 100 μ M ZST316 treatments of HEK-293T cells and the associated genes related to differentially expressed (A. upregulated, B. downregulated) proteins.

A. Pathway Name (Enriched by upregulated proteins)	Pathway Id	Pathway uploaded gene count	Genes in InnateDB for this entity	% Associated genes	Pathway p-value (corrected)	(Upregulate) Gene Symbols
B cell receptor signalling pathway	532	3	74	4.05	0.001	BCL10; PPP3CC; PRKCB;
Long-term potentiation	507	2	67	2.99	0.003	PPP3CC; PRKCB;
VEGF signalling pathway	432	2	62	3.23	0.004	PPP3CC; PRKCB;
MAPK signalling pathway	487	3	257	1.17	0.004	LAMTOR3; PPP3CC; PRKCB;
T cell receptor signalling pathway	563	2	107	1.87	0.007	BCL10; PPP3CC;
Natural killer cell mediated cytotoxicity	578	2	130	1.54	0.010	PPP3CC; PRKCB;
Wnt signalling pathway	445	2	140	1.43	0.011	PPP3CC; PRKCB;
Purine metabolism	503	2	174	1.15	0.014	PDE6D; PNP;
Calcium signalling pathway	594	2	183	1.09	0.015	PPP3CC; PRKCB;

B. Pathway Name (Enriched by downregulated proteins)	Pathway Id	Pathway uploaded gene count	Genes in InnateDB for this entity	% Associated genes	Pathway p-value (corrected)	(Down-regulated) Gene Symbols
Spliceosome	8120	3	133	2.26	0.031	EFTUD2; RBM22; SNW1;

Ribosome	474	2	137	1.46	0.035	RPS20; RPS29;
Pyrimidine metabolism	409	2	104	1.92	0.036	POLR3K; UPP1;

5.3.2.2 Identification of the differentially expressed proteins that overlapped between 5 and 100 μ M ZST316 that were present in a signalling pathway and the associated enriched pathways

Overlapped upregulated (16) and downregulated (23) proteins (see Table 5.2) were extracted from differentially expressed proteins of HEK-293T cells treated with 5 and 100 μ M subjected to InnateDB pathway analysis tool. Fifteen pathways were found to be regulated by the overlapping upregulated proteins. However, only one target gene (PPP3CC) was present in 14 of these pathways (Table 5.7). Three of the 16 overlapping downregulated proteins were present in four pathways (Table 5.7, B), none of which were found to be enriched.

Table 5.7. Identification of significantly (A) upregulated, or (B) downregulated proteins overlapped between 5 and 100 μ M ZS316 that were present in biological pathways. (The enriched pathways are marked with an asterisk sign).

A.	InnateDB ID	(Upregulated) Gene Symbol	Pathway Name (Over-representation*)
	485	PPP3CC	Apoptosis
	563	PPP3CC	T cell receptor signalling pathway
	487	PPP3CC	MAPK signalling pathway
	8113	PPP3CC	Oocyte meiosis
	10367	PPP3CC	Osteoclast differentiation
	507	PPP3CC	Long-term potentiation
	532	PPP3CC	B cell receptor signalling pathway
	4377	SPIRE1	Dorso-ventral axis formation
	578	PPP3CC	Natural killer cell mediated cytotoxicity
	494	PPP3CC	Axon guidance
	2798	PPP3CC	Amyotrophic lateral sclerosis (ALS)
	432	PPP3CC	VEGF signalling pathway
	594	PPP3CC	Calcium signalling pathway
	445	PPP3CC	Wnt signalling pathway
	521	PPP3CC	Alzheimer's disease
B.	InnateDB ID	(Downregulated) Gene Symbol	Pathway Name (Over-representation*)
	558	SETMAR	Lysine degradation
	5710	PAN3	RNA degradation
	8120	SNW1	Spliceosome
	491	SNW1	Notch signalling pathway

5.3.2.3 Regulation of angiogenesis and apoptosis pathways in response to ZST316 treatment of HEK-293T cells

The biochemical pathways related to angiogenesis and apoptosis were extracted from the KEGG database (<https://www.genome.jp/kegg/pathway.html>). Then, the lists of over-represented pathways by each treatment group was compared to the KEGG lists to see if any of them existed within the KEGG angiogenesis or apoptosis pathways.

5.3.2.3.1 Regulation of angiogenesis pathway in response to ZST316 treatment of HEK-293T cells

KEGG database introduced 30 signalling pathways classified as angiogenesis-related pathways (Table 5.8).

Table 5.8. 30 KEGG signalling pathways classified as angiogenesis-related pathways. (hsa stands for homo sapiens).

Entry	Pathway Name
hsa05205	Proteoglycans in cancer
hsa05323	Rheumatoid arthritis
hsa04060	Cytokine-cytokine receptor interaction
hsa04370	VEGF signalling pathway
hsa04371	Apelin signalling pathway
hsa05202	Transcriptional misregulation in cancer
hsa05203	Viral carcinogenes
hsa04926	Relaxin signalling pathway
hsa05163	Human cytomegalovirus infection
hsa05167	Kaposi sarcoma-associated herpesvirus infection
hsa05206	MicroRNAs in cancer
hsa05208	Chemical carcinogenesis - reactive oxygen species
hsa05211	Renal cell carcinoma
hsa01521	EGFR tyrosine kinase inhibitor resistance
hsa04012	ErbB signalling pathway
hsa04066	HIF-1 signalling pathway
hsa04115	p53 signalling pathway
hsa04151	PI3K-Akt signalling pathway
hsa04350	TGF-beta signalling pathway
hsa04919	Thyroid hormone signalling pathway
hsa04933	AGE-RAGE signalling pathway in diabetic complications
hsa05165	Human papillomavirus infection
hsa05200	Pathways in cancer
hsa05207	Chemical carcinogenesis - receptor activation
hsa05212	Pancreatic cancer
hsa05219	Bladder cancer
hsa05222	Small cell lung cancer
hsa05224	Breast cancer
hsa05231	Choline metabolism in cancer
hsa05418	Fluid shear stress and atherosclerosis

KEGG-based angiogenic-related pathways were compared with the lists of over-represented pathways by the differentially expressed proteins (Tables 5.4- 5.6). The VEGF signalling pathway was found to be among the enriched pathways with the upregulated proteins by 100 μ M ZST316 (Table 5.6, A). Among the whole 62 proteins involved in the VEGF pathway, the enriched pathway

revealed that two VEGF pathway proteins, including CALN and PKC (related to genes PPP3CC and PRKCB respectively) were significantly amplified in HEK-293T cells (**Table 5.6, A**). The description of these genes, their related proteins, and their upregulation levels with 100 μ M ZST316 are as follows:

- Protein ID P48454 belongs to serine/threonine-protein phosphatase 2B catalytic subunit gamma isoform (also known as Calmodulin-dependent calcineurin A subunit gamma isoform (CALN-A3), related to gene PPP3CC, was upregulated by 55% with 100 μ M ZST316 treatment.
- Protein ID P05771 belongs to protein kinase C (KPC) beta type, related to PRKCB gene, was upregulated by 57% with 100 μ M ZST316 treatment.

The involvement of CALN and PKC proteins in VEGF pathway is demonstrated on the KEGG VEGF signalling pathway diagram in **Figure 5.8**. (<https://www.genome.jp/pathway/hsa04370>)

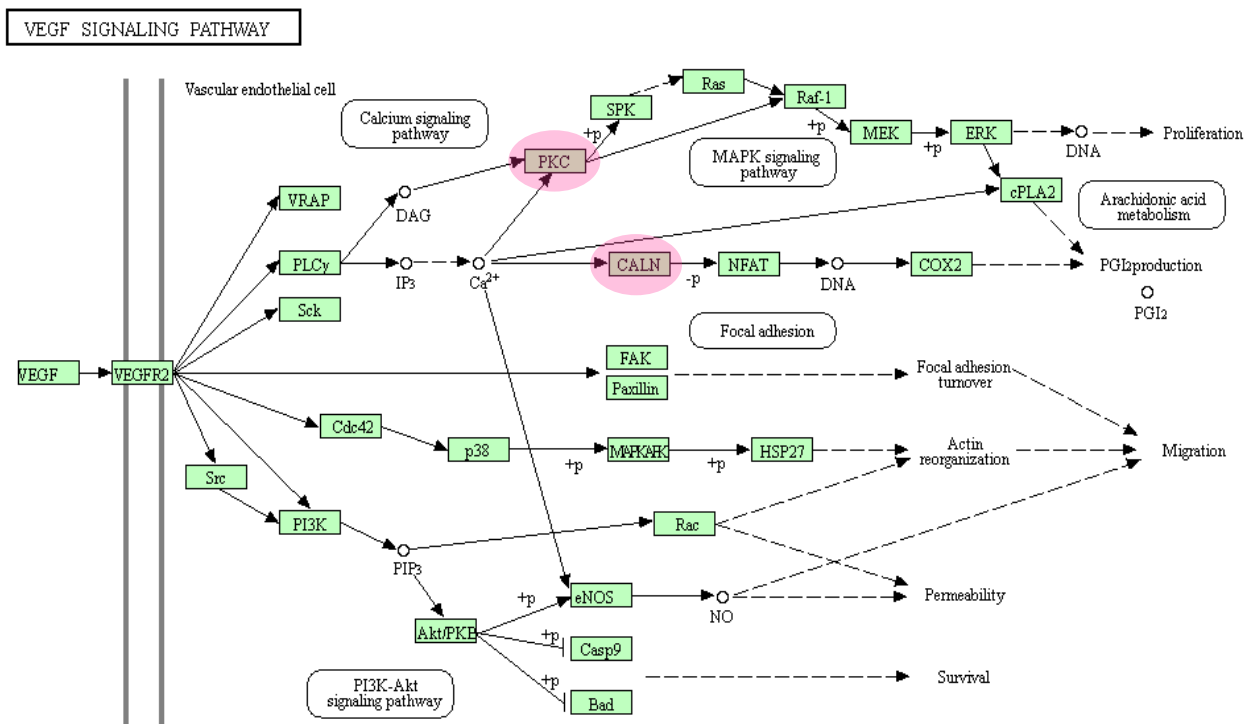


Figure 5.8. VEGF signalling pathway map adapted from KEGG (ID: hsa04379) with significantly enriched differentially expressed proteins.

In the figure, pink circles indicate the two differentially upregulated proteins by 100 μ M ZST316: CALN and PKC, and their involvement in VEGF pathway.

5.3.2.3.2 Regulation of apoptosis pathway in response to ZST316 treatment of HEK-293T cells

KEGG database introduced an apoptosis signalling pathway (<https://www.genome.jp/pathway/hsa04210>), showed as a diagram in **Figure 5.9**. However, this

CHAPTER 5

pathway was not identified as being enriched or over-represented by the differentially expressed protein in any of the control or treated samples. The KEGG pathway map for apoptosis (Entry: has04210) is available at <https://www.genome.jp/pathway/hsa04210>).

In addition, there are eight other pathways integrated with the apoptosis pathway also introduced as apoptosis-related pathways, listed in **Table 5.9**.

Table 5.9. Signalling pathways related to KEGG apoptosis pathway. (hsa stands for homo sapiens).

Entry	Pathway Name
hsa04010	MAPK signalling pathway
hsa04020	Calcium signalling pathway
hsa04064	NF-kappa B signalling pathway
hsa04115	p53 signalling pathway
hsa04141	Protein processing in endoplasmic reticulum
hsa04151	PI3K-Akt signalling pathway
hsa04650	Natural killer cell mediated cytotoxicity
hsa04668	TNF signalling pathway

Upregulated proteins by 5 μ M ZST316 over-represented two of these pathways: Protein processing in endoplasmic reticulum and Calcium signalling pathway. Upregulated proteins by 100 μ M ZST316 also over-represented three of these pathways: MAPK signalling, calcium signalling and natural killer cell mediated cytotoxicity. However, none of the pathways were among the list of over-represented pathways by the vehicle control samples.

5.4 Discussion

5.4.1 Cell culture and sample preparation

In these experiments, HEK-293T cells were treated with vehicle (water), 5 and 100 μ M ZST316. The 5 μ M concentration was selected based on a 5-fold higher than the K_i value of the inhibitor (Fowler and Zhang, 2008) (ZST316 K_i value =1 μ M), whereas the 100 μ M was chosen as supraphysiological (i.e. pharmacological), to account for potential issues with intracellular transportation and drug uptake, based on existing recommendations (Kittel and Maas, 2014). These concentrations have previously been shown to inhibit angiogenesis in endothelial cells *in vitro* (**Fig. 3.10 and 3.11**), without concomitantly affecting cell viability or proliferation, **Fig. 3.2, and 3.5, Chapter 3**). However, the use of a highly sensitive mass spectrometry technique allows the identification of more subtle modifications in proteins that do not necessarily translate into changes in proliferation, viability, or death. Therefore, in this chapter, MS analysis was used to detect subtle changes of biochemical pathways following treatment with the DDAH1 inhibitor, ZST316.

HEK-293T cells were treated over a 24-hour incubation period with ZST316. Previous *in-vitro* experiments investigating angiogenesis (**Chapter 3**), and toxicity (assessed by looking at cell viability and/or proliferation, **Chapter 2**), used a similar timeframe, which was considered adequate to investigate protein changes in terms of transcription and translation. The

investigation of additional time points (6, 12, 24, 48 hours), to better capture early or late drug-related effects, could not be performed within existing resources.

5.4.2 DIA analysis

The first step in MS-based proteomics analysis is to generate a library of peptides that provides peptide reference data for mass spectrometry. This was obtained from pooling all vehicle- and ZST316-treated samples to get a snapshot of existing cell proteins, by employing the high-pH reversed-phase (HpH-RP) fractionation in combination with gas-phase fractionation (GPF) to generate a DIA library. By combining the data from the two methods (DIA and DDA), a relatively comprehensive Spectronaut reference library was generated. The Spectronaut quant identified a total of 6,203 proteins in HEK-293T cells (pooled vehicle- and ZST316-treated samples), which set the theoretical maximum of proteins that could be quantified in each sample (**Table 5.1**).

The abundance of proteins was then measured as a surrogate to investigate possible on- and off-target effects of DDAH1 inhibition, with particular emphasis on the mechanisms involved in tube formation, observed in **chapter 3**.

5.4.2.1 Identification of differentially expressed proteins at the baseline level

To design a robust quantitative proteomics study, it is important to have an insight into the potential variability from at least three different sources: 1) biological variations when comparing identically treated flasks, due to differences in cell confluence in each flask. 2) Instrument variations involving column performance and downstream processes. 3) Temporal variations of the biological replicates of control flasks at the time of harvest, snap freezing, or homogenizing. These variations will provide valuable information regarding the background noise level vs. the inhibitor-related effects.

Therefore, a small-scale experiment (“experiment 1”, **Fig. 5.4**) was performed with two biological replicates of the vehicle-treated (control) cells to measure differentially expressed proteins between the two samples, indicating the baseline level of change in protein expression. If similar changes were also detected in cells treated with ZST316, they could not be accounted as a genuine effect of the inhibitor. By contrast, if the changes were markedly greater in the presence of the inhibitor, then they would likely reflect an effect of the drug.

The Spectronaut used a cut-off of $\text{Log}_2\text{fold-change} \geq 0.6$ and $Q\text{-value} \leq 0.05$ for the list of differentially expressed proteins in each sample set (**Appendices 5-7**). Spectronaut tests the

differential expression of thousands of proteins simultaneously (multiple hypothesis testing) which invalidates the use of a p value. In statistical multiple hypothesis testing, a Q-value is a p value with an adjustment for estimating the False Discovery Rate (FDR), a statistical approach to correct for multiple comparisons that represents the proportion of false positives (or false “significant” results) expected from a test.

When samples from two biological replicates of vehicle-treated cells were compared (**Appendix 5**), 150 proteins (out of a total of 6,203) were differentially expressed, with nearly equal proteins and percentages, 72 proteins (48%) and 78 proteins (52%), significantly upregulated and downregulated, respectively (**Fig. 5.5, first bar**). The volcano plot visualising the relative number of significantly upregulated (red dots on the right) and downregulated (red dots on the left) proteins in experiment 1 (**Fig. 5.6, A**) and experiments 2 (**Fig. 5.6, B and C**), compared to the total number of proteins quantified in HEK-293T cells for that sample group (grey dots) (**Table 5.1, A**), indicated that the number of changes in protein expression was relatively low (1.3-2.2 %).

5.4.2.2 Identification of differentially expressed proteins with ZST316 treatment

Vehicle control and treated samples with 5 and 100 μ M ZST316 were analysed by MS to identify the differentially expressed proteins in the treated groups compared to the vehicle control group (“experiment 2”, **Figure 5.4**).

A total of 194 and 215 proteins were differentially expressed in 5 and 100 μ M treated samples, 129% and 143%, respectively, compared to the 150 (100%) differentially expressed in the vehicle control samples (**Fig. 5.5**). This suggests that 70-77% of the changes observed with ZST316 (at 100 and 5 μ M respectively) could be attributed to background noise. At the same time, a smaller percentage of these changes (30% for 100 μ M and 23% for 5 μ M) were likely a genuine effect of the inhibitor.

A total of 77 (51%) and 97 (65%) proteins were significantly upregulated with 5 and 100 μ M ZST316, respectively, compared to 72 (48%) in control cells (**Fig. 5.5, red bars**). However, a similar number of proteins were significantly downregulated, 117 (78%) and 118 (79%), with 5 and 100 μ M ZST316, respectively. This suggests an equivalent effect from both concentrations in downregulating proteins. Compared to the vehicle control group, the number of downregulated proteins with either dose of ZST316 was 1.5-fold higher than that of the vehicle control (117-118 over 78) (**Fig. 5.5, green bars**).

CHAPTER 5

Comparing the number of downregulated proteins with that of the upregulated ones with 5 and 100 μM ZST316 (**green bars vs. red bars in Fig. 5.5**), it is apparent that the former outnumbered the latter, with either dose; while 55-60% of the total differentially expressed proteins in ZST316-treated samples showed a significant downregulation, only around 40-45% of them were upregulated. This proportion was greater with 5 μM ZST316. The volcano plots (**Fig. 5.6, B and C**) also depicted the relation of the differentially expressed protein numbers between ZST316-treated samples (**red dots**) to the total number of quantified proteins (**grey dots**).

It should be noted that the proportion of changes compared to the whole library clearly conveys that relatively minimal changes were observed with 5 or 100 μM ZST316, similar to the control samples, around 1-2% of the total identified proteins in the library for each group (**Table 5.1, B**). However, statistical analysis using the Chi squared (χ^2) test revealed that while there was no statistical difference between the upregulated protein numbers in treated samples vs vehicle control, downregulated proteins by ZST316-treated samples significantly outnumbered those in the vehicle control group (**P-value < .05, Table 5.1, C**). This suggests that ZST316 at high (100 μM) or low (5 μM) dose, has the ability to significantly downregulate protein abundance compared to the vehicle. In spite of that, identifying statistical significance may not necessarily reflect the presence of significant biological changes. Pathway analysis on differentially expressed proteins (specifically on downregulated proteins) may further clarify if the changes observed are expected to cause any biological or pathological response.

Furthermore, repeating these experiments with pre-defined biological replicates that give sufficient statistical power would determine the validity and reproducibility of these results and detect any effects if they truly occurred.

Among the differentially expressed proteins, a relatively small number were concomitantly upregulated (**Fig. 5.7, A**) or downregulated (**Fig. 5.7, B**) (23 and 16 proteins respectively) in 5 and 100 μM ZST316-treated groups (**Table 5.2, and Venn diagrams, Fig. 5.7**). This means that approximately 24% of the total upregulated proteins by 100 μM , and 30% by 5 μM , were also upregulated by their counterpart (**Fig. 5.7, A**). When assessing the downregulated protein list, the Venn diagram showed an even smaller overlap (approximately 13.5%) between the two treated groups (**Fig. 5.7, B**). The relatively small number of overlapping proteins between the two concentrations of ZST316 indicates that the majority of the differentially expressed proteins were

unique and dose specific. This suggests that different concentrations of the compound affect different proteins (**Table 5.1**).

Small-molecule drugs commonly interact with more than a single protein target. The extent of this interaction may depend on the drug concentration, whereby drug targets at low doses could be different to those at higher doses. Dose-specific metabolomics studies have recently reported that drugs at different doses have a unique binding affinity to different proteins (Yao et al., 2019). Therefore, it is not unexpected to see varying protein expressions in 5 and 100 μ M of ZST316 treated samples. Although again, it is worth mentioning that these changes are too small to be accounted as a genuine effect from the compound. Future dose-response experiments should include varying concentrations of ZST316 and different time periods to cover the potential changes over time to identify the dose at which the maximum drug-target (ZST316-DDAH1) binding affinity is achieved with minimal off-target sites.

5.4.2.3 Identification of differentially expressed proteins with ZST316 treatment related to ADMA/DDAH/NOS pathway

The MS results indicated the presence of both DDAH isoforms 1 and 2 in HEK-293T cells in the library data (generated from both ZST316- and vehicle-treated cells).

Interestingly, while preliminary evidence using routine MS analysis only identified around 1,900 proteins and no DDAH1 or DDAH2 peptide capture, fractionation and DIA analysis detected these isoforms in HEK-293T cells, along with all the fragment ions (the list of identified proteins in the library is available on request). This suggests low expression of both DDAH1 and DDAH2 in these cells, with a likely higher expression of DDAH1 protein, according to the number of unique peptides identified for each of the DDAH isoforms (Shown on **Table 5.3, A vs. B**). Nevertheless, the six unique peptides found for DDAH2 (**Table 5.3, B**) also provide robust evidence for the detection of DDAH2 isoform in this cell line.

In previous Western Blot experiments where HEK-293T cells were used as a negative control, DDAH1 protein was undetected (**Chapter 3, Fig. 3.12, A, and Chapter 4, Fig. 4.7, E**, indicated as –ive Ctrl). While the DDAH2 protein band was not observed in these cells in one experiment (**Appendix 1, A, well #2**, indicted as –ive Ctrl), another displayed a faint band at around the molecular weight of DDAH2 (**Appendix 4, D**, indicted as –ive Ctrl). Of note, DDAH2 message has also been detected in these cells (**Appendix 3, A**, annotated as H). This presumably suggests a relatively small expression of DDAH2 isoform in the cells. However, mass spectrometry is a

considerably more advanced technique due to the high sensitivity in protein quantification compared to Western Blotting.

The expression of DDAH1 and DDAH2 isoforms has been shown to be tissue specific. The kidney cortex has been shown to have the highest expression of DDAH enzymes (Palm et al., 2007). Western blot analysis of kidney lysates also demonstrated protein expression of both isoforms (Wetzel et al., 2020). DDAH1 protein expression has also been detected in the kidney embryo (Mishima et al., 2004, Palm et al., 2007, Tran et al., 2000). Moreover, a recent study has also shown protein (by immunoblotting) expression of DDAH2 at baseline level in HEK-293 cells (Li et al., 2021). Nevertheless, these cells have been used as negative controls for protein expression in previous studies (Tommasi et al., 2015, Tommasi, 2015).

To the best of my knowledge, the activity of DDAH enzymes has not been determined in HEK-293 cells. These cells have previously been used within our research group as the negative control for DDAH1-transfected cells in activity assays. The result from these experiments revealed minor (baseline level) activity from non-transfected cells (Qualitative analysis depends on the sensitivity of the assay) (The unpublished data for these experiments performed by Dr. Sara Tommasi are available on request). Therefore, both the expression and the activity of DDAH1 are markedly low in HEK-293T cells.

Prior studies have shown that both DDAH1 and DDAH2 regulate NO production by hydrolysing ADMA and L-NMMA, the major endogenous inhibitors of NOS enzymes (Pope et al., 2009, Kittel and Maas, 2014). However, there are inconsistencies in the literature regarding the relative importance of DDAH2 in ADMA metabolism (Leone et al., 1992, Wang et al., 2007). Some studies provide strong evidence that the mechanisms of action of the two isoforms are different (Hu et al., 2011a). For example, DDAH1 knockout mice displayed no DDAH activity in several tissues. DDAH1 was the only enzyme responsible for ADMA and L-NMMA degradation and DDAH2 showed no role *in vivo*. Notably DDAH2 expression was unaffected (Hu et al., 2011a). This suggests that there are no feedback mechanisms *in vivo* and/or DDAH2 was not driving DDAH1 activity. In another study, DDAH1 and DDAH2 siRNA-mediated gene silencing significantly increased ADMA concentrations in cultured endothelial cells (Du et al., 2018). Notably, the role of DDAH1 was greater than DDAH2 in ADMA accumulation (Du et al., 2018). Nevertheless, the specific role of the DDAH2 isoform in ADMA regulation and NO production is yet to be fully understood, due to the lack of a specific activity assay to measure DDAH2 function.

Following exposure to 5 and 100 μ M ZST316, DDAH1 protein expression remained unchanged compared to vehicle control (as evidenced by missing from the table of differentially expressed proteins, **Appendices 6 or 7**). This was expected because ZST316 competitively inhibits DDAH1 activity by occupying its active site (The kinetic characterisation of DDAH1 inhibition by ZST316 was previously reported) (Tommasi et al., 2015)). Therefore, they are not expected to change the expression level of DDAH1 protein. Moreover, these MS investigations focused on protein abundance changes.

Interestingly, both 5 and 100 μ M of ZST316 upregulated DDAH2 protein expression by two-fold, with no statistical difference between the two doses (**Appendices 6 and 7**). Considering that the time point was 24 hours, it is speculated that this was a sustained steady state increase.

DDAH2 is known to co-express with eNOS in kidney vascular cells (Welch et al., 2000), and with nNOS in the macula densa (Wilcox et al., 1992, Welch et al., 2000, Onozato et al., 2008). However, NOS enzymes (eNOS, nNOS or iNOS) were not detected in the current study using mass spectrometry (whether due to their absence, or their low expression levels undetectable by MS). This aligns with previous work (Tran et al., 2003).

5.4.2.3.1 Possible mechanisms for DDAH2 overexpressed following DDAH1 inhibition

A significant increase in DDAH2 protein was recently reported in DDAH1 knockout mice (Hannemann et al., 2020b). It is plausible that DDAH2 has a supportive role for DDAH1, and in situations where DDAH1 is inhibited, cells might overexpress DDAH2 to compensate for DDAH1 deficiency. However, the compensatory role of DDAH2 for the loss of DDAH1 had been disproven by earlier research. Hu and colleagues (Hu et al., 2011b) observed that DDAH1 knockout mice inhibited DDAH1 activity, while DDAH2 expression remained unaffected (cited by (Cooke and Ghebremariam, 2011)). Nevertheless, our results were in line with the recent findings by Hannemann *et al.* (Hannemann et al., 2020b), supporting the upregulation of DDAH2 protein as a consequence of DDAH1 protein inhibition.

VEGF protein, a hallmark of angiogenesis, might also be related to the ADMA/DDAH/NOS pathway. The expression changes of VEGF-A message and protein in response to DDAH1 knockdown were previously investigated in the retinal pigment epithelial cell model (**Chapter 4, Fig. 4.8**). Hence, it was worthwhile looking at its differential expression changes in our samples.

VEGF-A protein was not present. This protein was either not expressed in HEK-293T cells, or the expression level was too low for detections by the mass spectrometer. The issue with MS detection for low molecular weight proteins, such as VEGF (19~22 kDa (monomer)), is the lack of ionisable tryptic peptides. Since the trypsin enzyme digests proteins at lysine and/or arginine, when it cuts small proteins, the size of the peptides could be too short to be detectable by MS. Low levels of VEGF-A gene expression have been reported in HEK-293 cells (**Chapter 4, Fig. 4.1, B**), and in previous studies (Lin et al., 2010). However, MS data suggest that this is not reflected at the protein level. Nevertheless, a positive correlation between mRNA and protein expression is not always present. In contrast to our findings, studies have shown VEGF-A protein expression in HEK-293 cells lysate (by immunoblotting) and cell supernatants (by ELISA) (Lin et al., 2010, Sun et al., 2021).

5.4.3 Pathway analysis

In order to analyse the data by InnateDB, the protein IDs from each set were first uploaded to see whether any of the proteins are present in a biological pathway. The protein differential expression lists contained at least one protein that was present in a pathway (**Appendices 10-12**). For KEGG enrichment analysis, identified pathways containing ≥ 1 differentially expressed proteins, were subjected to an Over Representation Analysis (ORA). This analysis was used to identify the main biochemical metabolic pathways in which the number of differentially expressed proteins reached a statistically significant level of enrichment.

However, following this analysis and to confirm the results, using a second tool Enrichr (available at <http://amp.pharm.mssm.edu/Enrichr>) was also considered. This software uses gene symbols for data analysis. Therefore, in a further round, the Entrez genes were uploaded to investigate whether the software recognises the same pathways in each set. For this purpose, the Database for Annotation, Visualization and Integration Discovery (DAVID) Functional Annotation tool (<https://david.ncifcrf.gov/>, version 6.8) (Huang et al., 2009) was used to convert the differentially expressed gene symbols related to the Uniprot IDs, to Entrez genes. Notably, not all the Uniprot IDs were linked to a gene symbol within the Uniprot database and therefore those proteins that were missing out a gene symbol were inevitably excluded from the analysis (**see Appendix 13, Table A**). Moreover, among the available gene symbols, some were not found in DAVID database and consequently, again, a few Entrez genes were missing from the list (**see Appendix 13, Table B**). When the Entrez genes extracted from DAVID database (**see Appendix 13, Table C**) were uploaded to InnateDB for second-round pathway analysis, the associated pathways and those

indicated as over-represented ones were slightly different between the two tests. Therefore, the initial approach (using Uniprot IDs) was preferred for pathway analysis. The results for Uniprot IDs conversion to Entrez genes using DAVID database tool can be found in **Appendix 13**.

The KEGG (Kyoto Encyclopedia of Genes and Genomes) pathway database (Kanehisa et al., 2012) integrates genomic, molecular, and functional level information in biological systems including cells and includes the highest number of drug targets (Mora and Donaldson, 2012). This database (InnateDB software) was utilised for the pathway analysis in this study, where Q-values < 0.05 were considered significant.

5.4.3.1 Identification of the differentially expressed proteins present in a signalling pathway and the enriched pathways in response to ZST316 treatment in HEK-293T compared to control cells

InnateDB pathway analysis of the significantly upregulated proteins in the vehicle-treated biological replicates (experiment 1) revealed their presence in 12 biological pathways (**Appendix 10, A**). Among these, none were enriched when the over-representation analysis (ORA) was performed. Significantly downregulated proteins by this group were present in 20 pathways (**Appendix 10, B**), where three of them were enriched. These pathways included ribosome, spliceosome and Fc gamma R-mediated phagocytosis, in which the gene association was only 2-4.4% (**Table 5.4**).

In a past study where KEGG pathway of ribosome was found to be enriched, 18 associated proteins were differentially expressed (Yu et al., 2015). Similarly, Fc gamma R-mediated pathway has previously shown to be enriched by 17 proteins differentially expressed (Choudhary and Singh, 2018), compared to the only 2 found downregulated with the enriched pathway. This suggests that the gene involvement in the identified enriched pathways in this study is not high enough to expect a change in the overall regulation of such pathways.

The same analytical method was repeated for the ZST316-treated samples. Pathway analysis on differentially expressed proteins by 5 μ M ZST316 treated HEK-293T cells identified a list of 32 and 43 pathways for both up- and down-regulated proteins sets (**Appendix 11, A and B, respectively**). However, only three in each set were identified to be over-represented; Wnt signalling, protein processing in ER, and calcium signalling pathways were enriched by upregulated proteins, while RNS transport, RNA degradation and insulin signalling pathways were enriched by downregulated proteins with 5 μ M ZST316-treated HEK-293T cells (**Table 5.5**). However, the gene involvement in these pathways was as low as \sim 1-2.7%. Notably, no similarity was found between the present and

enriched pathways with differentially expressed proteins in 5 μ M ZST316-treated groups and those identified for the vehicle control group.

KEGG Pathway analysis on differentially expressed proteins by 100 μ M ZST316-treated HEK cells identified 59 pathways for upregulated proteins, and 17 for downregulated proteins (**Appendix 12, A and B, respectively**). Accordingly, nine pathways were identified to be enriched (**listed in Table 5.6, A**). Among these, the B cell receptor signalling pathway had the highest term significance (~4% = three upregulated proteins out of the total 74 genes associated with this entry according to InnateDB) (**Table 5.6, A**). Recent studies have shown high protein target involvement (16) in an enriched B cell receptor signalling pathway (Choudhary and Singh, 2018).

Other interesting identified pathways over-represented by the upregulated proteins with 100 μ M ZST316 were the VEGF pathway (with just over 3% (2/62) gene associations), calcium signalling (1% (2/183) gene association), T cell receptor (1.8% (2/107) gene association), natural killer cell mediated cytotoxicity (only 1.5% (2/130) gene association), and MAPK signalling (with 1.2% (3/257) gene association).

MAPK proteins are Ser/Thr kinases that relay extracellular signals into a wide range of cellular processes, including gene expression, cell cycle, metabolism, motility, cell survival, apoptosis and differentiation (Dhillon et al., 2007). Recent pathway analysis studies have shown that the MAPK pathway was over-represented with 49 genes (Chen et al., 2021b), and in another study, with 8 (23.5% gene involvement) (Chen et al., 2021a). A past study also indicated that the majority of the proteins involved in calcium signalling were differentially expressed after drug treatment (You et al., 2013). Enriched VEGF pathway in our study displayed a 3% gene association, compared to a study that found 14.7% (5) genes in the pathway (Chen et al., 2021a). Natural killer cell mediated cytotoxicity has been shown to be enriched with 13 differentially expressed genes (Choudhary and Singh, 2018), and T cell receptor signalling with 28 (Choudhary and Singh, 2018), and 6 (17.6% gene involvement) (Chen et al., 2021a), and in a cancer-related pathway study, by only 5 differentially expressed genes (Bhat et al., 2015).

The list of significantly downregulated proteins by 100 μ M ZST316 also over-represented three pathways: spliceosome, ribosome and pyrimidine metabolism, where protein-coding gene association were only approximately 1.5-2.3% (**Table 5.6, B**). Two pathways (ribosome and spliceosome) were also detected in the list of over-represented pathways by downregulated proteins by control samples (**see Table 5.4**). Although the affected related genes were slightly

different in the two groups. This suggests that the change observed in these pathways by 100 μM ZST316 may be non-significant due to the similarity with the control group.

5.4.3.2 Identification of the differentially expressed proteins overlapped between 5 and 100 μM ZST316 that were present in a signalling pathway and the associated enriched pathways

Next, the significantly upregulated and downregulated proteins in both 5 and 100 μM ZST316 - treated samples (**Appendices 8 and 9**) were subjected to pathway analysis. **Table 5.7** shows the identified 15 and 4 KEGG pathways for the 23 concomitantly upregulated and 16 concomitantly downregulated proteins, respectively. Notably, the results identified the involvement of one target gene in the majority of these pathways, PPP3CC. This gene is related to the protein serine/threonine-protein phosphatase 2B catalytic subunit gamma isoform, also known as calmodulin-dependent calcineurin A subunit gamma isoform (CALN-A3). This reveals that the function of this potential target is related to many biological pathways. The protein numbers in this list did not reach a statistically significant level of enrichment, thus none of these pathways were enriched.

As previously discussed, the list of overlapping significantly expressed proteins represented a small proportion of the total proteins differentially expressed in each group (24-30% for upregulated, and 13.5% for downregulated proteins) (**Fig. 5.7, Table 5.2**). Nevertheless, this could have shortlisted the key proteins involved in DDAH1 inhibition process, hypothetically leading to significant effects from ZST316 treatment. Yet, the pathway analysis invalidated this hypothesis; none of the overlapping differentially expressed protein had a marked effect on biological pathways. Therefore, activation or inhibition of these proteins by the two doses of the compound tested is unlikely to play a significant role in the overall maintenance of cellular homeostasis.

5.4.3.3 Identification of proteins involved in angiogenesis or apoptosis pathways

In the previous chapters, tube formation assay on HUVEC and VeraVec endothelial cells revealed anti-angiogenic effects of 5 and 100 μM of ZST316 (**Chapter 3, Fig. 3.10 and 3.11**). Also, DDAH1 inhibitors showed no significant change in cell viability (determined by colorimetric assays) and/or proliferation (determined by live-cell imaging), processes that are related to apoptosis (**Chapter 3, Fig. 3.1, 3.5, and 3.9**). However, those experiments could only demonstrate the subsequent morphological changes in cells, rather than a thorough investigation into the changes in biochemical pathways by the compounds that could potentially lead to cell death in the long term or could translate into apoptosis signalling in another cell. Using MS approach combined with

pathway enrichment analysis, this study aimed to examine if any of the differentially expressed proteins found in the treated sample sets could contribute to any significant alteration in angiogenic- or apoptotic-related pathways in non-endothelial cells like HEK-293T cells.

5.4.3.3.1 Regulation of angiogenesis pathway in response to ZST316 treatment of HEK-293T cells

Within the list of 30 angiogenesis-related pathways in the KEGG database, only one (VEGF signalling pathway) was found in our lists of enriched pathways; VEGF pathway was over-represented by the significant upregulated proteins with 100 μ M ZST316 (indicated in **Table 5.6, A**). However, among the 62 proteins involved in the VEGF pathway, only two (demonstrated by gene symbols PPP3CC and PRKCB, related to target proteins CALN and PKC) were significantly upregulated. This denotes a gene-association of just over 3% (**Table 5.6, A**). Notably, the VEGF protein itself was not detected in HEK-293T cells. Pathway analysis studies focusing on angiogenesis using similar approaches (Gene Ontology and KEGG pathway enrichment analysis) found amplification of many of the angiogenesis-related pathways, including the VEGF pathway with multiple targets enriched (5-14). Importantly the enriched pathways also covered the main members of the studied processes, e.g. VEGF protein was highly enriched in the VEGF pathway (Ji et al., 2021, Guo et al., 2020, Chen et al., 2021a).

Furthermore, other indirect angiogenic pathways are further derived from each of the 30 angiogenesis pathways listed in **Table 5.8**. The indirect pathways can be found by clicking on the entry number for each pathway on **table 5.8**. As an example, pathways in cancer (Entry: hsa05200) include a list of 21 other pathways that are therefore indirectly connected to angiogenesis, including Wnt signalling, calcium signalling, HIF-1 signalling, PI3K-Akt, VEGF, MAPK, mTOR, P53, and apoptosis. Comparing our lists of enriched pathways to the indirectly related pathways to angiogenesis, the MAPK pathway was enriched by upregulated proteins with 100 μ M ZST316. Upregulated proteins with both 5 and 100 μ M ZST316 enriched Wnt signalling and calcium signalling pathways. However, still, the number of proteins involved in the pathways is minimal. Moreover, none of the target proteins was among the known angiogenic-factors of the pathways. Therefore, one cannot be convinced that the effect of ZST316 on the overall angiogenesis process is significant.

This was expected from ZST316 treatment of non-endothelial HEK-293T cells, which are not the most suitable cell line to express angiogenic factors and changes in angiogenesis pathways. By

using endothelial cells in future experiments, perhaps more of the angiogenic proteins and pathways would be over-represented following treatment with DDAH1 inhibitors.

5.4.3.3.2 Regulation of apoptosis pathway in response to ZST316 treatment of HEK-293T cells

KEGG-based pathway analysis did not identify apoptosis pathways among the enriched ones in either of the vehicle or ZST316-treated groups (**Fig. 5.9**). However, there were eight other pathways introduced within KEGG database that are related to the apoptosis pathway, listed on **Table 5.9**. While none of these pathways were found among the enriched ones in the control group, ZST316-treated group enriched a number of the apoptosis-related pathways. Upregulated proteins by 5 μ M compound enriched two pathways: protein processing in endoplasmic reticulum (by association of 2 targets out of the total 171 involved genes) and calcium signalling (by 2 targets out of the total 183 genes). Therefore, the target association in both pathways were as small as just over 1% (**Table 5.5, A**). Similarly, upregulated proteins by 100 μ M compound enriched three of these pathways: MAPK signalling (3 genes out of the total 257 involved genes), calcium signalling (2 genes out of the total 183) and natural killer cell mediated cytotoxicity (2 genes out of the total 130). The percentages of gene association in these pathways were between 1.1-1.5%. Previous studies have shown MAPK pathway amplification with 49 targets (Chen et al., 2021b), natural killer cell mediated cytotoxicity pathway with 13 (Choudhary and Singh, 2018). Another study also indicated upregulation of 45 proteins involved in KEGG apoptotic signalling pathway, albeit based on GSEA database (Going et al., 2018).

In addition, the KEGG dataset also contains a list of 101 signalling pathways classified as apoptosis-related pathways, including TNF signalling, viral carcinogenesis, Alzheimer's disease, Foxo, and P53. Therefore, further analysis of our data might identify indirect relationships with such pathways. However, since the genes association in the identified pathways is very small, it is not expected to markedly change the overall regulation of the pathway. Therefore, this investigation was limited to the direct KEGG apoptosis pathway.

In conclusion, KEGG apoptosis pathway analysis revealed that this pathway was not enriched by the differentially expressed proteins. Further investigations to look at the indirect apoptotic-related pathways showed a few of our enriched pathway among this list. However, the number of target proteins enriched in these pathways is too small to suggest significant effect in the overall pathway regulation and consequently cell apoptosis.

5.5 Conclusion

5.5.1 Overall interpretation of data and future perspective

In this chapter, the fundamental molecular mechanisms underlying the effect of ZST316 treatment were investigated at the protein level, including proteins that were studied in previous experiments, particularly DDAH1, DDAH2, NOSs and VEGF. The vast majority (98-99%) of the investigated proteins did not show any tangible changes and only a very small fraction of them were significantly upregulated or downregulated.

While no expression of NOSs or VEGF was detected by MS, DDAH1 and DDAH2 proteins were expressed in HEK-293T cells although at low levels. As expected, by inhibiting DDAH1 with ZST316, the protein expression remained unchanged. Interestingly, the DDAH2 isoform was significantly upregulated with low- and high-dose ZST316. The DDAH1 substrates and biochemical pathways are well established. By contrast, the substrate(s) and the biological role of DDAH2 are currently unknown, although there might be some crossover between the isoforms substrates. However, as observed from our data, and also recently reported by a German group (Hannemann et al., 2020b), DDAH1 inhibition caused DDAH2 upregulation. Therefore, the possibility that DDAH2 elevation compensates for the inhibition of DDAH1 cannot be excluded. A plausible explanation would be to consider a substrate crossover between DDAH1 and DDAH2, whereby both enzymes metabolise ADMA. Therefore, DDAH2 upregulation might compensate for the loss of DDAH1 function in our experiment, and explain the small change observed at the signalling pathway level, and consequently on cellular function.

A series of experiments are required to confirm this hypothesis. For example, the effect of the DDAH1 inhibitor could be investigated after knocking out DDAH2, using cell models that also include endothelial cells, where angiogenesis pathways are more important. It was previously observed that DDAH1 inhibition in endothelial cells inhibited tube formation (**Chapter 3, Fig. 3.10 and 3.11**). Therefore, the compensatory role of DDAH2 for DDAH1 inhibition in these cells (if any) could be minimal or partial.

Moreover, the 24 hour treatment period selected for cell treatment, not only gives sufficient time for changes in protein expression (in this case upregulation of DDAH2) and function (compensation for DDAH1 inhibition), but also allows for the system to return back to equilibrium. Further studies are warranted to investigate the presence of possible changes within this 24-hour period.

CHAPTER 5

The information regarding the differentially expressed proteins in vehicle- and ZST316- groups was used for pathway analysis using the InnateDB software. KEGG analysis of the differentially expressed proteins identified pathways that were over-represented. Other studies investigated new chemical entities using a similar approach (Mass spectrometry analysis followed by KEGG-based pathway analysis). These studies have also reported some potential changes in the regulation of the biological pathways according to the target proteins that were significantly expressed in those pathways. This is an attractive option to investigate the presence of subtle biochemical, rather than morphological, changes. The results of these experiments provide solid preliminary data for the conduct of further studies.

KEGG enrichment analysis of the differentially expressed proteins revealed association of only a small proportion of these targets out of the total proteins involved in the pathway. This suggests that there is a minimal effect of ZST316 on the biological pathways of HEK-293T cells. Identifying statistical significance should not always be counted as significant biological effects. Therefore, it is likely that ZST316 has no significant effect on HEK-293T cells.

Studies that have used similar approaches (regardless of the cells, samples, or the drug), have identified around 5 to over 20 target proteins significantly expressed in the enriched pathways. In our study, ORA revealed that the number of up and downregulated proteins in the enriched pathways ranged between 2 to 6, with the majority of the pathways being enriched with only 2 or 3 target proteins.

Overall, one message arising from these data is that the two doses of ZST316 do not significantly influence key cellular homeostatic mechanisms and regulatory pathways, including those involved in angiogenesis and apoptosis. Although the underlying mechanisms of action for ZST316 from this set of experiments on HEK-293T cells remain unclear, nevertheless, it is reassuring that no major perturbations in key biochemical pathways were observed in non-endothelial cell lines. Such minimal effects on proteins suggest that ZST316 is likely to target DDAH1 without significant off-target effects. These results are in line with those for the characterisation of marketed drugs such as aspirin (Maurer et al., 2014), amlodipine (Norvasc) (Perchenet et al., 2000), and Pfizer and Moderna COVID-19 vaccines (Corbett et al., 2020).

In this study, HEK-293T cells have been used as a template. Applying this methodology, these experiments can be continued on a cell line that is more reflective of changes occurring in angiogenesis that comprise proteins related to the ADMA/DDAH/NOS pathway to investigate the

effect of ZST316 (and other DDAH1 inhibitors) on the protein profile in these cells. The protein data set collected from these cells can be further used for a comprehensive pathway analysis by using a more sophisticated software (such as QIAGEN Ingenuity Pathway Analysis (IPA)), with specific focus on angiogenic-related pathways. These experiments can be followed by Gene Ontology analysis, to identify those biological processes, cellular components and molecular functions that are impacted in these cells. These studies will pave the way for discovering the best potential of DDAH1 inhibitor drugs in regulating angiogenesis pathways in the body and possible changes on endothelial cells.

Furthermore, testing the drugs over separate time-points is of extreme importance for future experiments on ZST316 or any other DDAH1 inhibitors. Future dose-response experiments should include varying concentrations of ZST316, performed at different time points to capture potential changes over time and identify the dose at which the maximum drug-target (ZST316-DDAH1) binding affinity is achieved, with minimal non-specific binding sites. Through serial experiments, it is possible to identify early or late drug-associated changes in the expression patterns of DDAH2, and any potential off-targets of the compound. Repeating these experiments using endothelial cells, where the proteins of interest are highly expressed, might better reflect the conditions in which the compound delivers its maximum efficacy. These experiments will allow the identification of the most appropriate, safe and effective dose, with minimal off-target effects.

5.5.2 Limitations of this work

The first limitation of the current study was the use of HEK-293T cells. Although the cell line has been extensively used as a human cell model in *in vitro* experiments, there is also evidence in the literature of genotypic and phenotypic variations that are different to primary human cells (Lin et al., 2014, Stepanenko and Dmitrenko, 2015). Therefore, these results should be confirmed in other non-endothelial cells that also express DDAH proteins as a more suitable model to investigate potential off-target effects of the compound on human body.

Another limitation was that following the MS approach, the abundance of the differentially expressed proteins were measured, and not their activity; the changes in proteins expression were used as a surrogate for activity. However, the observed changes in protein abundance do not necessarily mean a change in the activity; doubling of an enzyme may or may not double its enzymatic activity, depending on how it is regulated.

CHAPTER 5

In terms of a threshold for differentially expressed proteins, the Spectronaut software sets a default threshold as a 50% increase or a 50% decrease (using log base 2 values of 0.6 = 1.5 fold for cut-offs, which equates to increase or decrease of 50%). However, a 10% change in some proteins may elicit a significant change in activity while doubling another, may not be significant. But one cannot set different thresholds for every protein. Therefore, in general, a maximum 50% increase or decrease is widely used as a threshold.

Regarding the pathway analysis of the data, a limitation was that these experiments did not include a positive (e.g. a cell line where the system could detect the presence of a genuine change) or a negative control (e.g. the same cells treated with the vehicle).

It is worth emphasising that these preliminary experiments did not involve a comprehensive pathway analysis, as this was not the aim of the chapter. Rather, the aim was to perform an exploratory analysis of whether patterns of protein upregulation and downregulations can be identified according to the different doses of the compound, and to further interpret the changes in differentially expressed proteins in relation to specific pathways. To this end, the potential to use this combined technique of mass spectrometry and pathway analysis for drug discovery was successfully demonstrated.

CHAPTER 6. GENERAL CONCLUSIONS AND FUTURE DIRECTIONS

6.1 General conclusions

Angiogenesis is the formation of new blood vessels from pre-existing vasculature. In recent years, there has been growing evidence for the contribution of excessive angiogenesis to the pathophysiology of a variety of diseases including Alzheimer's, AIDS, obesity, ocular diseases, cancer, arthritis, and psoriasis.

The DDAH/ADMA/NOS pathway plays a key role in angiogenesis (Cooke, 2003, Fiedler et al., 2009). In particular, increased NOS activity and excessive NO production promote angiogenesis. Overexpression of DDAH1, the enzyme responsible for the clearance of the endogenous NOS inhibitors ADMA and L-NMMA, could also enhance angiogenesis by reducing the concentrations of these substrates (Jacobi et al., 2005).

Therefore, the inhibition of DDAH1 using small molecules might reduce excessive angiogenesis, via increasing ADMA and L-NMMA accumulation, representing a promising strategy in conditions such as angiogenesis, characterized by NO overproduction.

Our lab has designed 12 novel small molecule inhibitors against human DDAH1 (Tommasi et al., 2015). Among these, ZST316 and ZST152 exhibited a greater inhibitory effect compared to the reference DDAH1 inhibitor, L-257, whereas the potency of ZST086 was similar to L-257. These inhibitors were selected to investigate their anti-angiogenic potential *in vitro*.

Cell viability and proliferation assays have a pivotal role in drug discovery studies. Such assays were used to assess the safety profile of DDAH1 inhibitors in endothelial and non-endothelial cell lines.

Cell viability by endpoint colorimetric assays and proliferation by real-time quantitative analysis of neuronal cell models showed that treatment of PC-12 cells with a range of ZST152 concentrations of up to 100 μM had no tangible cell toxicity effect over four days compared to the vehicle control. Similarly, crystal violet assays revealed that treating SH-SY5Y cells with ZST316, ZST152, and ZST086 between 5 and 125 μM had no significant effect for 48 hours.

DDAH1 inhibitors were then tested in neuronal cells exposed to the neurotoxin MPP⁺ to see whether they would augment MPP⁺-mediated toxicity. Unexpectedly, in these experiments,

CHAPTER 6

ZST316, ZST152, ZST086, and L-257 prevented the toxic effects of MPP⁺. The protective effect of DDAH1 inhibitors against MPP⁺-induced toxicity could be mediated by the inhibition of NOS and/or NADPH oxidase.

In the next group of experiments, we investigated the potential toxicity and anti-angiogenic effect of our most potent DDAH inhibitor, ZST316, in HUVEC and Human VeraVec endothelial cells. Treated cells remained viable and proliferated to levels comparable to those of non-treated cells. In contrast, the growth rate of VeraVec cells treated with the selective NOS inhibitor, L-NMMA (used as our positive control) was significantly augmented compared to the control cells. The different results obtained with ZST316 and L-NMMA could be related to the extent of reduced NO synthesis by these compounds. While low amounts of NO favour cell proliferation, high amounts could lead to senescence, cell cycle arrest, reduced proliferation, or even apoptosis (Napoli et al., 2013). It is also possible that DDAH1 inhibitors, in addition to NOS inhibition, have off-target effects that maintain cell viability.

The administration of 5 μ M ZST316 significantly reduced the formation of capillary-like structures in HUVEC cells. However, 100 μ M ZST316 failed to affect angiogenesis. Similar results were observed using the reference inhibitor L-257. By contrast, the administration of 5 and 100 μ M ZST316 significantly suppressed both tube and loop formation in VeraVec cells, with the higher dose exerting a greater effect.

The reduction in endothelial cell tube formation following inhibition of NO production via siRNA-mediated DDAH1 knockout, or ADMA treatment, has previously been reported (Trittmann et al., 2019). Furthermore, decreased cell proliferation and angiogenesis in DDAH deficient HUVEC cells has been associated with reduced VEGF expression (Zhang et al., 2013).

In this context, the potential effect of DDAH1 inhibition on eNOS protein expression was also examined to test whether the consequent ADMA and L-NMMA accumulation could have any subsequent impact on the amount of eNOS protein, ultimately affecting angiogenesis. However, treatment with 5 or 100 μ M ZST316 had no significant effect on eNOS protein expression, similar to the positive (L-NMMA) and negative (SDMA) controls for NOS activity inhibition. These results were in line with several previous studies on DDAH1 knockout mice, gene silencing, or pharmacological inhibition of DDAH1 where significant elevations in plasma and tissue ADMA and L-NMMA concentrations and/or reduced NO production in endothelial cells did not influence

CHAPTER 6

eNOS protein expression (Hu et al., 2011a, Leiper et al., 2007, MacAllister et al., 1996, Trittman et al., 2019, Zhang et al., 2011).

As vascular endothelial growth factor-A (VEGF-A) is the master regulatory protein in angiogenic-related pathways (Loureiro and D'Amore, 2005) we then investigated the relationship between DDAH1 and VEGF-A using hypoxia to upregulate VEGF-A and siRNA gene silencing to knockdown VEGF-A in human retinal pigment epithelial (RPE) (ARPE-19) cells. This cell line is a major source of VEGF (Xiao et al., 2006) and also expresses DDAH1 protein (Gu et al., 2012, Lange et al., 2016). To develop a model of VEGF-A upregulation, RPE cells were exposed to hypoxia to investigate whether this increases DDAH1 expression. ARPE-19 cells showed a significant upregulation of VEGF-A mRNA at 18 and 24 hours of hypoxia induction compared to the normoxic group. This upregulation was accompanied by DDAH1 message upregulation. Importantly, both VEGF-A and DDAH1 mRNA expression levels were the highest after 18 hours of hypoxia. However, contrary to expectation, despite increasing protein expression of VEGF-A at 18 hours of hypoxia, DDAH1 protein significantly decreased.

The strong VEGF-A elevation observed in hypoxia-induced RPE cells was in line with several previous reports (Shweiki et al., 1992, Wang et al., 2019, Punglia et al., 1997, Geisen et al., 2006, Lin et al., 2013, Wu et al., 2007, Bento et al., 2010, Watkins et al., 2013). Hypoxia-induced reductions in DDAH1 mRNA, protein, and/or activity have also been observed in previous studies (Millatt et al., 2003, Hannemann et al., 2020a). However, such correlation between DDAH1 mRNA and protein changes was not observed in our study. The effect of hypoxia on gene and protein expression is cell-type specific and while VEGF-A upregulation under hypoxia is observed in most cell types, the regulation pattern of other genes can vary in different cells (D'Alessandro et al., 2019). In particular, ARPE-19 cells may not be the highest expressing cells for DDAH1 in the retina, based on a previous immunohistochemistry study on different retinal layers (Lange et al., 2016). Moreover, increased ADMA concentrations have been reported in hypoxia-induced choroid-retinal endothelial cells and diabetic retinal tissue, suggesting a relatively low expression and/or activity of DDAH1 (Du et al., 2018). Therefore, retinal co-culture models that reflect retinal angiogenesis may represent a more robust system to investigate the crosstalk between VEGF-A and DDAH1 under hypoxia.

As hypoxia can influence numerous target genes and proteins, and therefore various signalling pathways, we conducted further experiments with a specific gene silencing technique, siRNA, to

CHAPTER 6

better understand the crosstalk between VEGF-A and DDAH1. To develop a model of VEGF-A knockdown, genes silencing by siRNA was conducted in RPE cells to investigate whether this reduces DDAH1 expression. siRNA-mediated VEGF-A knockdown resulted in upregulation of DDAH1 protein, while it did not affect DDAH1 message, in contrast to our hypothesis of a positive correlation between DDAH1 and VEGF-A. To investigate whether the DDAH1-mediated angiogenesis inhibition observed in **chapter 3** is VEGF-dependent, specific inhibition of DDAH1 by siRNA was performed in RPE cells. However, DDAH1 knockdown did not affect VEGF-A message or protein expression, again in contrast with our hypothesis that DDAH1 knockdown reduces VEGF-A expression (as a major factor affected by angiogenesis).

The positive correlation between DDAH1 and VEGF has been reported in previous studies where siRNA-mediated knockdown of DDAH1 reduced VEGF protein and impaired angiogenesis (Zhang et al., 2013), and DDAH1 overexpression increased VEGF mRNA and stimulated angiogenesis (Kostourou et al., 2002, Smith et al., 2003). However, another study reported no significant changes in VEGF concentrations with DDAH1 overexpression (Hasegawa et al., 2006).

Recent studies on the effect of siRNA-mediated DDAH1 knockdown on VEGF-mediated angiogenesis in choroid-retina endothelial cells showed a significant reduction in tube-formation (Du et al., 2018). The DDAH1/ADMA pathway might be the key regulator of retinal angiogenesis however this process is likely to be regulated by pro-angiogenic factors other than VEGF.

Although the observed ZST316-mediated anti-angiogenic effects in HUVEC and VeraVec endothelial cells were not associated with significant alterations in cell viability or proliferation, studying the morphological changes in cells is not sufficient to rule out the presence of subtle effects in biochemical pathways associated with angiogenesis and/or apoptosis.

MS techniques play a key role in modern drug discovery and development due to their ability to identify the mechanisms of action of small molecule drugs, including their target and off-target effects (Leurs U., 2016, Yan et al., 2020, Going et al., 2018). Such techniques include MALDI MSI, nLC-MS, stable isotope ratio (IR)-MS, and gas chromatography (GC)-MS or LC-MS/MS as their Mass Spectrometer approach for drug characterization. However, the first three techniques are not protein-discovery instruments and thus, their MS techniques are different from the LC-MS/MS method. The first-time use of an HPLC technique coupled with mass spectrometry (MS) allowed for a thorough investigation of the mechanism of the action of the DDAH1 inhibitor ZST316 and its impact at the cellular level. Proteomics analysis allowed identifying not only the mechanism of

CHAPTER 6

ZST316 action as anti-angiogenic agent, but also new proteins as off-target effects of the compound.

Quantitative proteomics by MS was initially planned on VeraVec endothelial cells. However, as these cells are no longer commercially available, we used HEK-293T cells instead to perform an exploratory analysis of molecular targets of ZST316. These cells have extensively been used in drug development studies due to their human origin, ease of growth, and rapid doubling time (Abaandou et al., 2021, Hu et al., 2018, Dumont et al., 2016). Furthermore, they express our proteins of interest (DDAH1 and 2) albeit at relatively low levels (Li et al., 2021, Mishima et al., 2004, Palm et al., 2007, Tran et al., 2000).

Data independent acquisition (DIA) targeting all ions within a selected m/z range, was used to identify and quantify the proteins affected by ZST316. Quantitative proteomics analysis by MS measured a list of proteins that were significantly upregulated or downregulated by two biological replicates of vehicle-treated HEK-293T samples (experiment 1) and high and low dose (100 and 5 μ M) of ZST316-treated compared to the vehicle-treated samples (experiment 2). "Experiment 1" revealed that in the vehicle-treated samples several proteins (\sim 150) were significantly upregulated and/or downregulated. These results indicated the level of non-specific baseline changes in protein expression. "Experiment 2" also revealed that in ZST316-treated samples (5 and 100 μ M vs control) several proteins (\sim 200) were significantly upregulated or downregulated. The total number of downregulated proteins with ZST316 treatment was significantly higher than that of upregulated proteins (almost 60% vs just over 40%) compared to the control group. However, this represents only 1-2% of all analysed proteins.

Only a small number of proteins were concomitantly upregulated or downregulated with both doses of ZST316. Further pathway analysis failed to identify specific biological pathways that were enriched with these protein sets.

ZST316 treatment did not cause any change in DDAH1 expression. This suggests that ZST316 inhibited the enzymatic activity of DDAH1, by occupying its active site, without affecting the abundance of the enzyme. Interestingly, both 5 and 100 μ M ZST316 caused an almost two-fold upregulation of DDAH2 protein. This, in the presence of pharmacological DDAH1 inhibition, might represent a compensatory effect of the other isoform to ensure some degree of ADMA metabolism. Similar results have been recently reported by other groups, although the exact mechanism involved remains to be identified (Hannemann et al., 2020b).

CHAPTER 6

Following MS experiments, the lists of differentially expressed proteins from each group (vehicle or ZST316-treated) were used as an input for pathway analysis by InnateDB software. These lists contained at least one protein that was present in a KEGG pathway. Over-representation analysis (ORA) was performed to identify the main biochemical pathways enriched by the differentially expressed proteins, whereby the number of target proteins present in a pathway reached a statistically significant level of enrichment.

The differentially expressed proteins from both experiments contained at least one protein that was present in the pathways and, in some cases, the number of differentially expressed proteins that were present in a pathway reached a statistically significant level of enrichment. These small numbers (varying between 2 to 6), although statistically significant for enriching some pathways, are unlikely to be sufficient for a significant biological effect. The limited changes observed in the signalling pathway profile of HEK-293T cells might be due to a DDAH2-mediated compensatory effect following DDAH1 inhibition. Overall, the minimal effect of ZST316 treatment on the biological pathways of HEK-293T cells rules out the presence of tangible off-target effects at least in this cell line.

The differentially expressed proteins did not enrich any apoptotic-related pathways, while VEGF signalling pathway relevant to angiogenesis was enriched with upregulated proteins by 100 μ M ZST316, but the gene association in the pathway enrichment was small (~3%). Besides, VEGF protein, as the main angiogenic factor in this pathway, was undetected. Pathway analysis studies focusing on angiogenesis using similar approaches (Gene Ontology and KEGG pathway enrichment analysis) found amplification of many of the angiogenesis-related pathways, including the VEGF pathway with multiple target proteins enriched (5-14). Importantly, the enriched pathways also covered the main members of the processes; for instance, VEGF protein was highly enriched in the VEGF pathway (Ji et al., 2021, Guo et al., 2020, Chen et al., 2021a). This suggests that ZST316 treatment had no significant effect on the regulation of biochemical pathways related to angiogenesis in non-endothelial cells such as HEK-293T.

In conclusion, ZST316 does not seem to significantly influence the main homeostatic biochemical pathways in the cell, including those investigated in our previous experiments (apoptosis and angiogenesis).

These exploratory studies used HEK-293T cells as a template for future research on endothelial cells, a cell type that is fully involved in angiogenic processes and expresses proteins involved in

the ADMA/DDAH/NOS pathway targeted by ZST316 (and other DDAH1 inhibitors). Furthermore, designing experiments with different time points and a wide range of ZST316 doses will provide more robust information regarding the optimal dose and treatment duration in terms of efficacy and safety.

6.2 Future directions

The results of these experiments provide necessary background information for the conduct of further studies to confirm the lack of a major effect of pharmacological DDAH1 inhibition on the viability and proliferation of other endothelial and non-endothelial cell lines. In this context, complementing such studies with MS methodology will provide a comprehensive assessment of the effects on key homeostatic pathways that regulate angiogenesis and/or apoptosis.

Moreover, the possible neuroprotective effect of DDAH1 inhibitors in SH-SY5Y cells, albeit not the focus of this project, warrants further investigation. In this context, ADMA has been shown to exert protective effects against MPP⁺-induced neurotoxicity via inhibiting oxidative stress generated by ROS overproduction in a cell model of Parkinson's disease, PC-12 (Tang et al., 2011). Furthermore, the reported stimulatory effect of MPP⁺ on iNOS expression in experimental Parkinson's disease suggest that DDAH1-inhibition induced ADMA accumulation might attenuate the iNOS-mediated excess NO synthesis and associated negative effects on cell homeostasis (Ye et al., 2017). Additional experiments are needed to explore the potential effects of DDAH1 inhibitors on iNOS, NO, ROS production and oxidative stress in experimental models of Parkinson's disease.

The observed anti-angiogenic effects of DDAH1 inhibitors should be further investigated in different endothelial cell lines, also using proteomic analysis to identify the exact mechanisms involved, e.g. NOS inhibition and/or VEGF-A or related pathways, and unravel the complex interplay between DDAH1, NOS, and VEGF.

Such experiments should also be conducted in disease cell models with different degrees of ROS production and NO production, from overexpressed iNOS or other stimuli, to investigate whether the relationship between DDAH and VEGF and the anti-angiogenic effects of DDAH1 inhibitors are affected by specific experimental conditions.

According to many previous studies, blocking NOS with ADMA initiates a cascade of events associated with many pathological disorders, including inflammation (Evans, 1995, Tripathi et al., 2007). However, this hypothesis has been recently challenged due to the growing recognition of

the adverse effects of iNOS-derived NO. Therefore, in disease states with NO overproduction (whether induced by eNOS such as in solid tumours, or by iNOS during inflammation), DDAH1 inhibitors targeting NO synthesis might represent a novel therapeutic strategy. An increase in ADMA and L-NMMA levels has previously been shown to inhibit iNOS (Pekarova et al., 2013).

Importantly, DDAH1 inhibition not only targets the traditional angiogenesis process in ECs, but also the vasculogenic mimicry that has recently been discovered as an alternative blood supply strategy used by tumour cells. Our DDAH1 inhibitors have previously been shown to inhibit vasculogenic mimicry *in vitro* in a triple-negative cancer cell model (Hulin et al., 2019). In future *in vivo* experiments, targeting DDAH1 by our compounds in combination with an anti-VEGF drug could increase the efficacy of anti-angiogenic therapy by restricting vasculogenic mimicry of solid tumours and angiogenesis in the surrounding endothelial cells.

Of note, the systemic administration of ADMA or L-NMMA (similar to the application of DDAH1 inhibitors) may cause hypertension. However, in a septic shock patient with hypotension, iNOS-mediated circulating NO, superoxide (O_2^-), and other free radicals, a NOS inhibitor such as ADMA might restore a physiological blood pressure. It is important to emphasise that hypertension, also a side effect with anti-VEGF drugs used in cancer, has been shown to be a marker of anti-angiogenic efficacy of these drugs and predict favourable outcomes. Future animals and human should investigate whether elevations in blood pressure might similarly represent a marker of effective DDAH1 inhibition.

In our studies, we mainly focused on the effects of our most potent DDAH1 inhibitor, ZST316. This compound has been shown to have the highest potency in terms of DDAH1 inhibition (based on its K_i). However other DDAH1 inhibitors should be tested assess their relative efficacy and safety in different cell types.

The results of these experiments suggest a promising role for DDAH1 inhibition as a novel therapeutic strategy to suppress excessive angiogenesis. However, it is important to highlight that *in vitro* results may not necessarily reflect *in vivo* responses due to the altered expression patterns of key markers in cell models compared to cells *in vivo* (Galley et al., 2000). Consequently, future experiments necessitate *in vivo* studies to confirm the presence of tangible anti-angiogenic effects without overt systemic toxicity.

REFERENCES

- ABAANDOU, L., QUAN, D. & SHILOACH, J. 2021. Affecting HEK293 Cell Growth and Production Performance by Modifying the Expression of Specific Genes. *Cells*, 10, 1667.
- ACHAN, V., BROADHEAD, M., MALAKI, M., WHITLEY, G., LEIPER, J., MACALLISTER, R. & VALLANCE, P. 2003. Asymmetric dimethylarginine causes hypertension and cardiac dysfunction in humans and is actively metabolized by dimethylarginine dimethylaminohydrolase. *Arteriosclerosis, thrombosis, and vascular biology*, 23, 1455-1459.
- ACHAN, V., HO, H., HEESCHEN, C., STUEHLINGER, M., JANG, J., KIMOTO, M., VALLANCE, P. & COOKE, J. P. 2005. ADMA regulates angiogenesis: genetic and metabolic evidence. *Vascular Medicine*, 10, 7-14.
- ADAIR, T. & MONTANI, J. 2010. Angiogenesis. 2010. *Morgan & Claypool Life Sciences: San Rafael, CA*.
- ADAIR, T. H. 2004. An emerging role for adenosine in angiogenesis. *Am Heart Assoc*.
- AGANI, F. & JIANG, B.-H. 2013. Oxygen-independent regulation of HIF-1: novel involvement of PI3K/AKT/mTOR pathway in cancer. *Current cancer drug targets*, 13, 245-251.
- AIELLO, L. P., NORTHRUP, J. M., KEYT, B. A., TAKAGI, H. & IWAMOTO, M. A. 1995. Hypoxic regulation of vascular endothelial growth factor in retinal cells. *Archives of ophthalmology*, 113, 1538-1544.
- AL-LATAYFEH, M., SILVA, P. S., SUN, J. K. & AIELLO, L. P. 2012. Antiangiogenic therapy for ischemic retinopathies. *Cold Spring Harbor perspectives in medicine*, 2, a006411.
- ALFARANO, C., ANDRADE, C., ANTHONY, K., BAHROOS, N., BAJEC, M., BANTOFT, K., BETEL, D., BOBECHKO, B., BOUTILIER, K. & BURGESS, E. 2005. The biomolecular interaction network database and related tools 2005 update. *Nucleic acids research*, 33, D418-D424.
- ALFARO, J. A., IGNATCHENKO, A., IGNATCHENKO, V., SINHA, A., BOUTROS, P. C. & KISLINGER, T. 2017. Detecting protein variants by mass spectrometry: a comprehensive study in cancer cell-lines. *Genome medicine*, 9, 1-12.
- ALLEN, T. 2004. *Dorland's Illustrated Medical Dictionary*: WB Saunders, Philadelphia, 2003. ISBN 0-721-60146-4, Hardcover, pp xxvii+ 2190, AUD \$82.50. Taylor & Francis.
- AMOUR, J., BRZEZINSKA, A. K., WEIHRAUCH, D., BILLSTROM, A. R., ZIELONKA, J., KROLIKOWSKI, J. G., BIENENGRAEBER, M. W., WARLTIER, D. C., PRATT, P. F. & KERSTEN, J. R. 2009. Role of heat shock protein 90 and endothelial nitric oxide synthase during early anesthetic and ischemic preconditioning. *The Journal of the American Society of Anesthesiologists*, 110, 317-325.
- AMROUNI, D., MEILLER, A., GAUTIER-SAUVIGNÉ, S., PIRAUD, M., BOUTEILLE, B., VINCENDEAU, P., BUGUET, A. & CESPUGLIO, R. 2011. Cerebral changes occurring in arginase and dimethylarginine dimethylaminohydrolase (DDAH) in a rat model of sleeping sickness. *PLoS One*, 6, e16891.
- ANANTHARAM, V., KAUL, S., SONG, C., KANTHASAMY, A. & KANTHASAMY, A. G. 2007. Pharmacological inhibition of neuronal NADPH oxidase protects against 1-methyl-4-phenylpyridinium (MPP⁺)-induced oxidative stress and apoptosis in mesencephalic dopaminergic neuronal cells. *Neurotoxicology*, 28, 988-997.
- ANDERSON, J. M. & VAN ITALLIE, C. M. 2009. Physiology and function of the tight junction. *Cold Spring Harbor perspectives in biology*, 1, a002584.
- ANDREW, P. J. & MAYER, B. 1999. Enzymatic function of nitric oxide synthases. *Cardiovascular research*, 43, 521-531.
- ARNOULD, T., MICHIELS, C., ALEXANDRE, I. & REMACLE, J. 1992. Effect of hypoxia upon intracellular calcium concentration of human endothelial cells. *Journal of cellular physiology*, 152, 215-221.
- ARSHAD, A., CHEN, X., CONG, Z., QING, H. & DENG, Y. 2014. TRPC1 protects dopaminergic SH-SY5Y cells from MPP⁺, salsolinol, and N-methyl-(R)-salsolinol-induced cytotoxicity. *Acta Biochim Biophys Sin*, 46, 22-30.
- ASLAM, B., BASIT, M., NISAR, M. A., KHURSHID, M. & RASOOL, M. H. 2017. Proteomics: technologies and their applications. *Journal of chromatographic science*, 55, 182-196.
- ASLANTÜRK, Ö. S. 2018. *In vitro cytotoxicity and cell viability assays: principles, advantages, and disadvantages*, InTech.
- AVERY, R. L., PEARLMAN, J., PIERAMICI, D. J., RABENA, M. D., CASTELLARIN, A. A., MA'AN, A. N., GIUST, M. J., WENDEL, R. & PATEL, A. 2006. Intravitreal bevacizumab (Avastin) in the treatment of proliferative diabetic retinopathy. *Ophthalmology*, 113, 1695-1705. e6.
- BABAEI, S. & STEWART, D. J. 2002. Overexpression of endothelial NO synthase induces angiogenesis in a co-culture model. *Cardiovascular research*, 55, 190-200.
- BABAEI, S., TEICHERT-KULISZEWSKA, K., MONGE, J.-C., MOHAMED, F., BENDECK, M. P. & STEWART, D. J. 1998. Role of nitric oxide in the angiogenic response in vitro to basic fibroblast growth factor. *Circulation Research*, 82, 1007-1015.
- BÁCSKAY, I., NEMES, D., FENYVESI, F., VÁRADI, J., VASVÁRI, G., FEHÉR, P., VECSENYÉS, M. & UJHELYI, Z. 2018. *Role of cytotoxicity experiments in pharmaceutical development*, InTech: London, UK.

REFERENCES

- BALARATNASINGAM, C., DHRAMI-GAVAZI, E., MCCANN, J. T., GHADIALI, Q. & FREUND, K. B. 2015. Aflibercept: a review of its use in the treatment of choroidal neovascularization due to age-related macular degeneration. *Clinical ophthalmology (Auckland, NZ)*, 9, 2355.
- BAO, B., ZHANG, M. Q., CHEN, Z. Y., WU, X. B., XIA, Z. B., CHAI, J. Y. & YIN, X. P. 2019. Sulforaphane prevents PC12 cells from oxidative damage via the Nrf2 pathway. *Molecular medicine reports*, 19, 4890-4896.
- BASS, J. J., WILKINSON, D. J., RANKIN, D., PHILLIPS, B. E., SZEWCZYK, N. J., SMITH, K. & ATHERTON, P. J. 2017. An overview of technical considerations for Western blotting applications to physiological research. *Scandinavian journal of medicine & science in sports*, 27, 4-25.
- BAUTCH, V. L. 2012. VEGF-directed blood vessel patterning: from cells to organism. *Cold Spring Harbor perspectives in medicine*, 2, a006452.
- BEDFORD, M. T. & RICHARD, S. 2005. Arginine methylation: an emerging regulator of protein function. *Molecular cell*, 18, 263-272.
- BELCIK, J. T., QI, Y., KAUFMANN, B. A., XIE, A., BULLENS, S., MORGAN, T. K., BAGBY, S. P., KOLUMAM, G., KOWALSKI, J. & OYER, J. A. 2012. Cardiovascular and systemic microvasculature effects of anti-vascular endothelial growth factor therapy for cancer. *Journal of the American College of Cardiology*, 60, 618-625.
- BENJAMINI, Y. & HOCHBERG, Y. 1995. Controlling the false discovery rate: a practical and powerful approach to multiple testing. *Journal of the Royal statistical society: series B (Methodological)*, 57, 289-300.
- BENTLEY, K., MARIGGI, G., GERHARDT, H. & BATES, P. A. 2009. Tipping the balance: robustness of tip cell selection, migration and fusion in angiogenesis. *PLoS Comput Biol*, 5, e1000549.
- BENTO, C., FERNANDES, R., MATAFOME, P., SENA, C., SEICA, R. & PEREIRA, P. J. E. P. 2010. Methylglyoxal-induced imbalance in the ratio of vascular endothelial growth factor to angiotensin 2 secreted by retinal pigment epithelial cells leads to endothelial dysfunction. *Experimental physiology*, 95, 955-970.
- BERRA, E., GINOUVÈS, A. & POUYSSÉGUR, J. J. E. R. 2006. The hypoxia-inducible-factor hydroxylases bring fresh air into hypoxia signalling. *Embo reports*, 7, 41-45.
- BHAT, A., HEINZEL, A., MAYER, B., PERCO, P., MÜHLBERGER, I., HUSI, H., MERSEBURGER, A. S., ZOIDAKIS, J., VLAHOU, A. & SCHANSTRA, J. P. 2015. Protein interactome of muscle invasive bladder cancer. *PLoS One*, 10, e0116404.
- BISHT, M., DHASMANA, D. & BIST, S. 2010. Angiogenesis: Future of pharmacological modulation. *Indian journal of pharmacology*, 42, 2.
- BOOCCOCK, C. A., CHARNOCK-JONES, D. S., SHARKEY, A. M., MCLAREN, J., BARKER, P. J., WRIGHT, K. A., TWENTYMAN, P. R. & SMITH, S. K. 1995. Expression of Vascular Endothelial Growth Factor and Its Receptors VEGFR-1 and KDR in Ovarian Carcinoma. *JNCI: Journal of the National Cancer Institute*, 87, 506-516.
- BOZKUS, C. C., ELZEY, B. D., CRIST, S. A., ELLIES, L. G. & RATLIFF, T. L. 2015. Expression of cationic amino acid transporter 2 is required for myeloid-derived suppressor cell-mediated control of T cell immunity. *The Journal of Immunology*, 195, 5237-5250.
- BREITKREUTZ, B.-J., STARK, C., REGULY, T., BOUCHER, L., BREITKREUTZ, A., LIVSTONE, M., OUGHTRED, R., LACKNER, D. H., BÄHLER, J. & WOOD, V. 2007. The BioGRID interaction database: 2008 update. *Nucleic acids research*, 36, D637-D640.
- BREUER, K., FOROUSHANI, A. K., LAIRD, M. R., CHEN, C., SRIBNAIA, A., LO, R., WINSOR, G. L., HANCOCK, R. E., BRINKMAN, F. S. & LYNN, D. J. 2013. InnateDB: systems biology of innate immunity and beyond—recent updates and continuing curation. *Nucleic acids research*, 41, D1228-D1233.
- BRUIX, J., QIN, S., MERLE, P., GRANITO, A., HUANG, Y.-H., BODOKY, G., PRACHT, M., YOKOSUKA, O., ROSMORDUC, O. & BREDER, V. 2017. Regorafenib for patients with hepatocellular carcinoma who progressed on sorafenib treatment (RESORCE): a randomised, double-blind, placebo-controlled, phase 3 trial. *The Lancet*, 389, 56-66.
- BUIJS, N., OOSTERINK, J. E., JESSUP, M., SCHIERBEEK, H., STOLZ, D. B., HOUDIJK, A. P., GELLER, D. A. & VAN LEEUWEN, P. A. J. A. 2017. A new key player in VEGF-dependent angiogenesis in human hepatocellular carcinoma: dimethylarginine dimethylaminohydrolase 1. *Angiogenesis*, 20, 557-565.
- BURKHART, J. M., SCHUMBRUTZKI, C., WORTELKAMP, S., SICKMANN, A. & ZAHEDI, R. P. 2012. Systematic and quantitative comparison of digest efficiency and specificity reveals the impact of trypsin quality on MS-based proteomics. *Journal of proteomics*, 75, 1454-1462.
- CAMPINHO, P., VILFAN, A. & VERMOT, J. 2020. Blood flow forces in shaping the vascular system: a focus on endothelial cell behavior. *Frontiers in Physiology*, 11.
- CAMPOCHIARO, P. A., AIELLO, L. P. & ROSENFELD, P. J. 2016. Anti-vascular endothelial growth factor agents in the treatment of retinal disease: from bench to bedside. *Ophthalmology*, 123, S78-S88.
- CAMPOCHIARO, P. A., LAUER, A. K., SOHN, E. H., MIR, T. A., NAYLOR, S., ANDERTON, M. C., KELLEHER, M., HARROP, R., ELLIS, S. & MITROPHANOUS, K. A. 2017. Lentiviral vector gene transfer of endostatin/angiostatin for macular degeneration (GEM) study. *Human gene therapy*, 28, 99-111.
- CANNELL, I. G., KONG, Y. W. & BUSHHELL, M. 2008. How do microRNAs regulate gene expression? *Biochemical Society Transactions*, 36, 1224-1231.

REFERENCES

- CAPLIN, B. & LEIPER, J. 2012. Endogenous nitric oxide synthase inhibitors in the biology of disease: markers, mediators, and regulators? *Arteriosclerosis, thrombosis, and vascular biology*, 32, 1343-1353.
- CARMELIET, P. 2000. Mechanisms of angiogenesis and arteriogenesis. *Nature medicine*, 6, 389-396.
- CARMELIET, P. 2003. Angiogenesis in health and disease. *Nature medicine*, 9, 653-660.
- CARMELIET, P. 2005. Angiogenesis in life, disease and medicine. *Nature*.
- CARMELIET, P. & JAIN, R. K. 2011. Molecular mechanisms and clinical applications of angiogenesis. *Nature*, 473, 298-307.
- CARREAU, A., HAFNY-RAHBI, B. E., MATEJUK, A., GRILLON, C. & KIEDA, C. 2011. Why is the partial oxygen pressure of human tissues a crucial parameter? Small molecules and hypoxia. *Journal of cellular and molecular medicine*, 15, 1239-1253.
- CARTWRIGHT, J. E., JOHNSTONE, A. P. & WHITLEY, G. S. J. 2000. Endogenously produced nitric oxide inhibits endothelial cell growth as demonstrated using novel antisense cell lines. *British journal of pharmacology*, 131, 131-137.
- CHATR-ARYAMONTRI, A., CEOL, A., PALAZZI, L. M., NARDELLI, G., SCHNEIDER, M. V., CASTAGNOLI, L. & CESARENI, G. 2007. MINT: the Molecular INTERaction database. *Nucleic acids research*, 35, D572-D574.
- CHEN, C.-W., YE, M.-K., SHIAU, C.-Y., CHIANG, C.-H. & LU, D.-W. 2013. Efficient downregulation of VEGF in retinal pigment epithelial cells by integrin ligand-labeled liposome-mediated siRNA delivery. *International journal of nanomedicine*, 8, 2613.
- CHEN, H. X. & CLECK, J. N. 2009. Adverse effects of anticancer agents that target the VEGF pathway. *Nature reviews Clinical oncology*, 6, 465.
- CHEN, J.-X. & MEYRICK, B. 2004. Hypoxia increases Hsp90 binding to eNOS via PI3K-Akt in porcine coronary artery endothelium. *Laboratory investigation*, 84, 182-190.
- CHEN, S., YANG, X., WEI, Z., ZHANG, Y., HUANG, Y., SHI, Z., ZHANG, Z., WANG, J., ZHANG, H. & MA, J. 2021a. Establishment of an anti-inflammation-based bioassay for the quality control of the 13-component TCM formula (Lianhua Qingwen). *Pharmaceutical Biology*, 59, 537-545.
- CHEN, Y., DONG, J., YANG, D., QIAN, Q., WANG, P., YANG, X., LI, W., LI, G., SHEN, X. & WANG, F. 2021b. Synergistic Network Pharmacology for Traditional Chinese Medicine Liangxue Tongyu Formula in Acute Intracerebral Hemorrhagic Stroke. *Neural plasticity*, 2021.
- CHOI, Y.-K. & KIM, K.-W. 2008. Blood-neural barrier: its diversity and coordinated cell-to-cell communication. *BMB reports*, 41, 345-352.
- CHOUDHARY, N. & SINGH, V. 2018. A census of *P. longum*'s phytochemicals and their network pharmacological evaluation for identifying novel drug-like molecules against various diseases, with a special focus on neurological disorders. *PLoS One*, 13, e0191006.
- CIBOR, D., DOMAGALA-RODACKA, R., RODACKI, T., JURCZYŚZYŃ, A., MACH, T. & OWCZAREK, D. 2016. Endothelial dysfunction in inflammatory bowel diseases: pathogenesis, assessment and implications. *World Journal of Gastroenterology*, 22, 1067.
- CILLERO-PASTOR, B., MATEOS, J., FERNÁNDEZ-LÓPEZ, C., OREIRO, N., RUIZ-ROMERO, C. & BLANCO, F. J. 2012. Dimethylarginine dimethylaminohydrolase 2, a newly identified mitochondrial protein modulating nitric oxide synthesis in normal human chondrocytes. *Arthritis & Rheumatism*, 64, 204-212.
- CLOSS, E. I., SIMON, A., VÉKONY, N. & ROTMANN, A. 2004. Plasma membrane transporters for arginine. *The Journal of nutrition*, 134, 2752S-2759S.
- COOK, K. M. & FIGG, W. D. 2010. Angiogenesis inhibitors: current strategies and future prospects. *CA: a cancer journal for clinicians*, 60, 222-243.
- COOKE, J. P. 2003. NO and angiogenesis. *Atherosclerosis Supplements*, 4, 53-60.
- COOKE, J. P. 2004. Asymmetrical Dimethylarginine The Über Marker? *Circulation*, 109, 1813-1818.
- COOKE, J. P. & GHEBREMARIAM, Y. T. 2011. DDAH says NO to ADMA. *Arteriosclerosis, Thrombosis, and Vascular Biology*.
- COON, J. J., SYKA, J. E., SHABANOWITZ, J. & HUNT, D. F. 2005. Tandem mass spectrometry for peptide and protein sequence analysis. *Biotechniques*, 38, 519-523.
- CORBETT, K. S., EDWARDS, D. K., LEIST, S. R., ABIONA, O. M., BOYOGLU-BARNUM, S., GILLESPIE, R. A., HIMANSU, S., SCHÄFER, A., ZIWAWO, C. T. & DIPIAZZA, A. T. 2020. SARS-CoV-2 mRNA vaccine design enabled by prototype pathogen preparedness. *Nature*, 586, 567-571.
- CRIVELLATO, E., NICO, B., VACCA, A., DJONOV, V., PRESTA, M. & RIBATTI, D. 2004. Recombinant human erythropoietin induces intussusceptive microvascular growth in vivo. *Leukemia*, 18, 331-336.
- CZESNIKIEWICZ-GUZIŁ, M., LORKOWSKA, B., ZAPALA, J., CZAJKA, M., SZUTA, M., LOSTER, B., GUZIŁ, T. & KORBUT, R. 2008. NADPH oxidase and uncoupled nitric oxide synthase are major sources of reactive oxygen species in oral squamous cell carcinoma. Potential implications for immune regulation in high oxidative stress conditions. *Journal of physiology and pharmacology*, 59, 139.

REFERENCES

- D'AMICO, G., MUÑOZ-FÉLIX, J. M., PEDROSA, A. R. & HODIVALA-DILKE, K. M. 2020. "Splitting the matrix": intussusceptive angiogenesis meets MT 1-MMP. *EMBO Molecular Medicine*, 12, e11663.
- D'ANDREA, L. D., ROMANELLI, A., DI STASI, R. & PEDONE, C. 2010. Bioinorganic aspects of angiogenesis. *Dalton Transactions*, 39, 7625-7636.
- D'MELLO, R., SAND, C. A., PEZET, S., LEIPER, J. M., GAURILCIKAITE, E., MCMAHON, S. B., DICKENSON, A. H. & NANDI, M. 2015. Dimethylarginine dimethylaminohydrolase 1 is involved in spinal nociceptive plasticity. *Pain*, 156, 2052.
- D'ALESSANDRO, S., MAGNAVACCA, A., PEREGO, F., FUMAGALLI, M., SANGIOVANNI, E., PRATO, M., DELL'AGLI, M. & BASILICO, N. 2019. Effect of hypoxia on gene expression in cell populations involved in wound healing. *BioMed Research International*, 2019.
- DA BOIT, M., TOMMASI, S., ELLIOT, D., ZINELLU, A., SOTGIA, S., SIBSON, R., MEAKIN, J. R., ASPDEN, R. M., CARRU, C. & MANGONI, A. A. 2018. Sex differences in the associations between L-arginine pathway metabolites, skeletal muscle mass and function, and their responses to resistance exercise, in old age. *The journal of nutrition, health & aging*, 22, 534-540.
- DANN, C. E., BRUICK, R. K. & DEISENHOFER, J. 2002. Structure of factor-inhibiting hypoxia-inducible factor 1: an asparaginyl hydroxylase involved in the hypoxic response pathway. *Proceedings of the National Academy of Sciences*, 99, 15351-15356.
- DAYAL, S. & LENTZ, S. R. 2005. ADMA and hyperhomocysteinemia. *Vascular Medicine*, 10, S27-S33.
- DE SPIEGELAERE, W., CASTELEYN, C., VAN DEN BROECK, W., PLENDL, J., BAHRAMSOLTANI, M., SIMOENS, P., DJONOV, V. & CORNILLIE, P. 2012. Intussusceptive angiogenesis: a biologically relevant form of angiogenesis. *Journal of vascular research*, 49, 390-404.
- DECICCO-SKINNER, K. L., HENRY, G. H., CATAISSON, C., TABIB, T., GWILLIAM, J. C., WATSON, N. J., BULLWINKLE, E. M., FALKENBURG, L., O'NEILL, R. C. & MORIN, A. 2014. Endothelial cell tube formation assay for the in vitro study of angiogenesis. *Journal of visualized experiments: JoVE*.
- DEVASAGAYAM, T., TILAK, J., BOLOOR, K., SANE, K. S., GHASKADBI, S. S. & LELE, R. 2004. Free radicals and antioxidants in human health: current status and future prospects. *Japi*, 52, 4.
- DHILLON, A. S., HAGAN, S., RATH, O. & KOLCH, W. 2007. MAP kinase signalling pathways in cancer. *Oncogene*, 26, 3279-3290.
- DJONOV, V., ANDRES, A. C. & ZIEMIECKI, A. 2001. Vascular remodelling during the normal and malignant life cycle of the mammary gland. *Microscopy research and technique*, 52, 182-189.
- DJONOV, V. G., KURZ, H. & BURRI, P. H. 2002. Optimality in the developing vascular system: branching remodeling by means of intussusception as an efficient adaptation mechanism. *Developmental dynamics: an official publication of the American Association of Anatomists*, 224, 391-402.
- DOMBROW, M. & ADELMAN, R. A. 2011. Ocular Angiogenesis: The Science Behind the Symptoms. *Retinal Physician*, January.
- DU, M.-R., YAN, L., LI, N.-S., WANG, Y.-J., ZHOU, T. & JIANG, J.-L. 2018. Asymmetric dimethylarginine contributes to retinal neovascularization of diabetic retinopathy through EphrinB2 pathway. *Vascular pharmacology*, 108, 46-56.
- DUDA, D. G., FUKUMURA, D. & JAIN, R. K. 2004. Role of eNOS in neovascularization: NO for endothelial progenitor cells. *Trends in molecular medicine*, 10, 143-145.
- DULAK, J. & JÓZKOWICZ, A. 2003. Regulation of vascular endothelial growth factor synthesis by nitric oxide: facts and controversies. *Antioxidants and Redox Signaling*, 5, 123-132.
- DULAK, J., JÓZKOWICZ, A., DEMBINSKA-KIEC, A., GUEVARA, I., ZDZIENICKA, A., ZMUDZINSKA-GROCHOT, D., FLOREK, I., WÓJTOWICZ, A., SZUBA, A. & COOKE, J. P. 2000. Nitric oxide induces the synthesis of vascular endothelial growth factor by rat vascular smooth muscle cells. *Arteriosclerosis, thrombosis, and vascular biology*, 20, 659-666.
- DUMONT, J., EUWART, D., MEI, B., ESTES, S. & KSHIRSAGAR, R. 2016. Human cell lines for biopharmaceutical manufacturing: history, status, and future perspectives. *Critical reviews in biotechnology*, 36, 1110-1122.
- DUNN, K., AOTAKI-KEEN, A., PUTKEY, F. & HJELMELAND, L. M. 1996. ARPE-19, a human retinal pigment epithelial cell line with differentiated properties. *Experimental eye research*, 62, 155-170.
- DWORAKOWSKI, R., ANILKUMAR, N., ZHANG, M. & SHAH, A. 2006. Redox signalling involving NADPH oxidase-derived reactive oxygen species. *Biochemical society transactions*.
- EGGINTON, S., HUDLICKA, O., BROWN, M., WALTER, H., WEISS, J. & BATE, A. 1998. Capillary growth in relation to blood flow and performance in overloaded rat skeletal muscle. *Journal of applied physiology*, 85, 2025-2032.
- EGGINTON, S., ZHOU, A.-L., BROWN, M. & HUDLICKA, O. 2001. Unorthodox angiogenesis in skeletal muscle. *Cardiovascular research*, 49, 634-646.
- EILKEN, H. M. & ADAMS, R. H. 2010. Dynamics of endothelial cell behavior in sprouting angiogenesis. *Current opinion in cell biology*, 22, 617-625.
- ELMORE, S. 2007. Apoptosis: a review of programmed cell death. *Toxicologic pathology*, 35, 495-516.

REFERENCES

- ESCUADERO, C., ROBERTS, J. M., MYATT, L. & FEOKTISTOV, I. 2014. Impaired adenosine-mediated angiogenesis in preeclampsia: potential implications for fetal programming. *Frontiers in pharmacology*, 5, 134.
- ESSER, S., LAMPUGNANI, M. G., CORADA, M., DEJANA, E. & RISAU, W. 1998. Vascular endothelial growth factor induces VE-cadherin tyrosine phosphorylation in endothelial cells. *Journal of cell science*, 111, 1853-1865.
- EVANS, C. 1995. Nitric oxide: what role does it play in inflammation and tissue destruction? *Agents and actions. Supplements*, 47, 107-116.
- FALLAH, A., SADEGHINIA, A., KAHROBA, H., SAMADI, A., HEIDARI, H. R., BRADARAN, B., ZEINALI, S. & MOLAVI, O. 2019. Therapeutic targeting of angiogenesis molecular pathways in angiogenesis-dependent diseases. *Biomedicine & Pharmacotherapy*, 110, 775-785.
- FANG, I.-M., YANG, C.-H., YANG, C.-M. & CHEN, M.-S. 2012. The expression of inducible nitric oxide synthase in human retinal pigment epithelial cells under stimulation of proinflammatory cytokine tumor necrosis factor- α . *Taiwan Journal of Ophthalmology*, 2, 13-17.
- FAVARO, E., RAMACHANDRAN, A., MCCORMICK, R., GEE, H., BLANCHER, C., CROSBY, M., DEVLIN, C., BLICK, C., BUFFA, F. & LI, J.-L. 2010. MicroRNA-210 regulates mitochondrial free radical response to hypoxia and krebs cycle in cancer cells by targeting iron sulfur cluster protein ISCU. *PLoS One*, 5, e10345.
- FAVERO, G., PAGANELLI, C., BUFFOLI, B., RODELLA, L. F. & REZZANI, R. 2014. Endothelium and its alterations in cardiovascular diseases: life style intervention. *BioMed Research International*, 2014.
- FÉLÉTOU, M. 2011. *The Endothelium: part 1: multiple functions of the endothelial cells-focus on endothelium-derived vasoactive mediators*, rafael (CA): Morgan & Claypool Life Sciences.
- FEOKTISTOVA, M., GESERICK, P., KELLERT, B., DIMITROVA, D. P., LANGLAIS, C., HUPE, M., CAIN, K., MACFARLANE, M., HÄCKER, G. & LEVERKUS, M. 2011. cIAPs block Ripoptosome formation, a RIP1/caspase-8 containing intracellular cell death complex differentially regulated by cFLIP isoforms. *Molecular cell*, 43, 449-463.
- FERRARA, N. & ADAMIS, A. P. 2016. Ten years of anti-vascular endothelial growth factor therapy. *Nature Reviews Drug Discovery*, 15, 385-403.
- FERRARA, N., DAMICO, L., SHAMS, N., LOWMAN, H. & KIM, R. 2006. Development of ranibizumab, an anti-vascular endothelial growth factor antigen binding fragment, as therapy for neovascular age-related macular degeneration. *Retina*, 26, 859-870.
- FERRARA, N., HILLAN, K. J., GERBER, H.-P. & NOVOTNY, W. 2004. Discovery and development of bevacizumab, an anti-VEGF antibody for treating cancer. *Nature Reviews Drug Discovery*, 3, 391-400.
- FIEDLER, L. 2008. The DDAH/ADMA pathway is a critical regulator of NO signalling in vascular homeostasis. *Cell adhesion & migration*, 2, 149-150.
- FIEDLER, L. R., BACHETTI, T., LEIPER, J., ZACHARY, I., CHEN, L., RENNÉ, T. & WOJCIAK-STOTHARD, B. 2009. The ADMA/DDAH pathway regulates VEGF-mediated angiogenesis. *Arteriosclerosis, thrombosis, and vascular biology*, 29, 2117-2124.
- FIEDLER, L. R. & WOJCIAK-STOTHARD, B. 2009. The DDAH/ADMA pathway in the control of endothelial cell migration and angiogenesis. *Biochemical Society Transactions*, 37, 1243-1247.
- FLAMME, I., FRÖLICH, T. & RISAU, W. 1997. Molecular mechanisms of vasculogenesis and embryonic angiogenesis. *Journal of cellular physiology*, 173, 206-210.
- FLEMING, I. & BUSSE, R. 2003. Molecular mechanisms involved in the regulation of the endothelial nitric oxide synthase. *American Journal of Physiology-Regulatory, Integrative and Comparative Physiology*, 284, R1-R12.
- FLEMING, I., FISSLTHALER, B., DIMMELER, S., KEMP, B. E. & BUSSE, R. 2001. Phosphorylation of Thr495 regulates Ca²⁺/calmodulin-dependent endothelial nitric oxide synthase activity. *Circulation Research*, 88, e68-e75.
- FOLKMAN, J. 1971. Tumor angiogenesis: therapeutic implications. *The New England Journal of Medicine*, 285, 1182-1186.
- FOLKMAN, J. 1995. Angiogenesis in cancer, vascular, rheumatoid and other disease. *Nature medicine*, 1, 27-30.
- FOLKMAN, J. 2007. Angiogenesis: an organizing principle for drug discovery? *Nature reviews Drug discovery*, 6, 273-286.
- FOROOGHIAN, F., RAZAVI, R. & TIMMS, L. 2007. Hypoxia-inducible factor expression in human RPE cells. *British Journal of Ophthalmology*, 91, 1406-1410.
- FÖRSTERMANN, U., BOISSEL, J. P. & KLEINERT, H. 1998. Expressional control of the 'constitutive' isoforms of nitric oxide synthase (NOS I and NOS III). *The FASEB Journal*, 12, 773-790.
- FÖRSTERMANN, U. & SESSA, W. C. 2012. Nitric oxide synthases: regulation and function. *European heart journal*, 33, 829-837.
- FOWLER, S. & ZHANG, H. 2008. In vitro evaluation of reversible and irreversible cytochrome P450 inhibition: current status on methodologies and their utility for predicting drug-drug interactions. *The AAPS journal*, 10, 410-424.
- FRAISL, P., MAZZONE, M., SCHMIDT, T. & CARMELIET, P. 2009. Regulation of angiogenesis by oxygen and metabolism. *Developmental cell*, 16, 167-179.

REFERENCES

- FRANCESCONI III, R. A., FAIBISH, M. & SHAO, R. 2011. A Matrigel-based tube formation assay to assess the vasculogenic activity of tumor cells. *Journal of visualized experiments: JoVE*.
- FRICK, M. & SCHMIDT, C. 2019. Mass spectrometry—A versatile tool for characterising the lipid environment of membrane protein assemblies. *Chemistry and physics of lipids*, 221, 145-157.
- FU, Z. & XIANG, J. 2020. Aptamers, the nucleic acid antibodies, in cancer therapy. *International Journal of Molecular Sciences*, 21, 2793.
- FUKUMURA, D., GOHONGI, T., KADAMBI, A., IZUMI, Y., ANG, J., YUN, C.-O., BUERK, D. G., HUANG, P. L. & JAIN, R. K. 2001. Predominant role of endothelial nitric oxide synthase in vascular endothelial growth factor-induced angiogenesis and vascular permeability. *Proceedings of the National Academy of Sciences*, 98, 2604-2609.
- FULTON, D., GRATTON, J.-P., MCCABE, T. J., FONTANA, J., FUJIO, Y., WALSH, K., FRANKE, T. F., PAPAPETROPOULOS, A. & SESSA, W. C. 1999. Regulation of endothelium-derived nitric oxide production by the protein kinase Akt. *Nature*, 399, 597-601.
- FURCHGOTT, R. F. 1984. The role of endothelium in the responses of vascular smooth muscle to drugs. *Annual review of pharmacology and toxicology*, 24, 175-197.
- FURCHGOTT, R. F. 1999. Endothelium-derived relaxing factor: discovery, early studies, and identification as nitric oxide. *Bioscience reports*, 19, 235-251.
- FURCHGOTT, R. F. & ZAWADZKI, J. V. 1980. The obligatory role of endothelial cells in the relaxation of arterial smooth muscle by acetylcholine. *Nature*, 288, 373-376.
- GALLEY, H., BLAYLOCK, M., DUBBELS, A. & WEBSTER, N. 2000. Variability in E-selectin expression, mRNA levels and sE-selectin release between endothelial cell lines and primary endothelial cells. *Cell biology international*, 24, 91-99.
- GALLEY, H. F. & WEBSTER, N. R. 2004. Physiology of the endothelium. *British journal of anaesthesia*, 93, 105-113.
- GARIANO, R. F. & GARDNER, T. W. 2005. Retinal angiogenesis in development and disease. *Nature*, 438, 960-966.
- GEISEN, P., MCCOLM, J. R., KING, B. M. & HARTNETT, M. E. 2006. Characterization of barrier properties and inducible VEGF expression of several types of retinal pigment epithelium in medium-term culture. *Current eye research*, 31, 739-748.
- GERHARDT, H., GOLDING, M., FRUTTIGER, M., RUHRBERG, C., LUNDKVIST, A., ABRAMSSON, A., JELTSCH, M., MITCHELL, C., ALITALO, K. & SHIMA, D. 2003. VEGF guides angiogenic sprouting utilizing endothelial tip cell filopodia. *The Journal of cell biology*, 161, 1163-1177.
- GHEBREMARIAM, Y. T., ERLANSON, D. A. & COOKE, J. P. 2014. A novel and potent inhibitor of dimethylarginine dimethylaminohydrolase: A modulator of cardiovascular nitric oxide. *Journal of Pharmacology and Experimental Therapeutics*, 348, 69-76.
- GHISO, N., ROHAN, R. M., AMANO, S., GARLAND, R. & ADAMIS, A. P. 1999. Suppression of hypoxia-associated vascular endothelial growth factor gene expression by nitric oxide via cGMP. *Investigative ophthalmology & visual science*, 40, 1033-1039.
- GIANNI-BARRERA, R., BARTOLOMEO, M., VOLLMAR, B., DJONOV, V. & BANFI, A. 2014. Split for the cure: VEGF, PDGF-BB and intussusception in therapeutic angiogenesis. Portland Press Ltd.
- GIANNI-BARRERA, R., TRANI, M., FONTANELLAZ, C., HEBERER, M., DJONOV, V., HLUSHCHUK, R. & BANFI, A. 2013. VEGF over-expression in skeletal muscle induces angiogenesis by intussusception rather than sprouting. *Angiogenesis*, 16, 123-136.
- GIANNI-BARRERA, R., TRANI, M., REGINATO, S. & BANFI, A. 2011. To sprout or to split? VEGF, Notch and vascular morphogenesis. *Biochemical Society Transactions*, 39, 1644-1648.
- GOING, C. C., TAILOR, D., KUMAR, V., BIRK, A. M., PANDRALA, M., RICE, M. A., STOYANOVA, T., MALHOTRA, S. & PITTERI, S. J. 2018. Quantitative proteomic profiling reveals key pathways in the anticancer action of methoxychalcone derivatives in triple negative breast cancer. *Journal of proteome research*, 17, 3574-3585.
- GORI, J. L., BUTLER, J. M., KUNAR, B., POULOS, M. G., GINSBERG, M., NOLAN, D. J., NORGAARD, Z. K., ADAIR, J. E., RAFII, S. & KIEM, H. P. 2017. Endothelial cells promote expansion of long-term engrafting marrow hematopoietic stem and progenitor cells in primates. *Stem cells translational medicine*, 6, 864-876.
- GOWDA, G. N. & DJUKOVIC, D. 2014. Overview of mass spectrometry-based metabolomics: opportunities and challenges. *Mass Spectrometry in Metabolomics*, 3-12.
- GRAHAM, F. L., SMILEY, J., RUSSELL, W. & NAIRN, R. 1977. Characteristics of a human cell line transformed by DNA from human adenovirus type 5. *Journal of general virology*, 36, 59-72.
- GRECO, R., FERRIGNO, A., DEMARTINI, C., ZANABONI, A., MANGIONE, A. S., BLANDINI, F., NAPPI, G., VAIRETTI, M. & TASSORELLI, C. 2015. Evaluation of ADMA-DDAH-NOS axis in specific brain areas following nitroglycerin administration: study in an animal model of migraine. *The journal of headache and pain*, 16, 1-8.
- GREEN, D. R. & LLAMBI, F. 2015. Cell death signaling. *Cold Spring Harbor perspectives in biology*, 7, a006080.
- GREENBERG, D. A. & JIN, K. 2005. From angiogenesis to neuropathology. *Nature*, 438, 954-959.
- GREENE, L. A. & TISCHLER, A. S. 1976. Establishment of a noradrenergic clonal line of rat adrenal pheochromocytoma cells which respond to nerve growth factor. *Proceedings of the National Academy of Sciences*, 73, 2424-2428.

REFERENCES

- GRIENDLING, K. 2004. Novel NAD (P) H oxidases in the cardiovascular system. *Heart*, 90, 491-493.
- GROTHEY, A., VAN CUTSEM, E., SOBRERO, A., SIENA, S., FALCONE, A., YCHOU, M., HUMBLET, Y., BOUCHÉ, O., MINEUR, L. & BARONE, C. 2013. Regorafenib monotherapy for previously treated metastatic colorectal cancer (CORRECT): an international, multicentre, randomised, placebo-controlled, phase 3 trial. *The Lancet*, 381, 303-312.
- GROUP, E. S. 2002. Preclinical and phase 1A clinical evaluation of an anti-VEGF pegylated aptamer (EYE001) for the treatment of exudative age-related macular degeneration. *Retina*, 22, 143-152.
- GU, X., NERIC, N. J., CRABB, J. S., CRABB, J. W., BHATTACHARYA, S. K., RAYBORN, M. E., HOLLYFIELD, J. G. & BONILHA, V. L. 2012. Age-related changes in the retinal pigment epithelium (RPE). *PLoS One*, 7, e38673.
- GUERAUD, F., ATALAY, M., BRESGEN, N., CIPAK, A., ECKL, P. M., HUC, L., JOUANIN, I., SIEMS, W. & UCHIDA, K. 2010. Chemistry and biochemistry of lipid peroxidation products. *Free radical research*, 44, 1098-1124.
- GUIJARRO-MUNOZ, I., COMPTE, M., ALVAREZ-VALLINA, L. & SANZ, L. 2013. Antibody gene therapy: getting closer to clinical application? *Current gene therapy*, 13, 282-290.
- GUNDRY, R. L., WHITE, M. Y., MURRAY, C. I., KANE, L. A., FU, Q., STANLEY, B. A. & VAN EYK, J. E. 2010. Preparation of proteins and peptides for mass spectrometry analysis in a bottom-up proteomics workflow. *Current protocols in molecular biology*, 90, 10.25. 1-10.25. 23.
- GUO, M.-F., DAI, Y.-J., GAO, J.-R. & CHEN, P.-J. 2020. Uncovering the mechanism of Astragalus membranaceus in the treatment of diabetic nephropathy based on network pharmacology. *Journal of Diabetes Research*, 2020.
- GUZY, R. D. & SCHUMACKER, P. T. 2006. Oxygen sensing by mitochondria at complex III: the paradox of increased reactive oxygen species during hypoxia. *Experimental physiology*, 91, 807-819.
- HAMANAKA, R. B. & CHANDEL, N. S. 2009. Mitochondrial reactive oxygen species regulate hypoxic signaling. *Current opinion in cell biology*, 21, 894-899.
- HANNEMANN, J., APPEL, D., SEEBERGER-STEINMEISTER, M., BRÜNING, T., ZUMMACK, J. & BÖGER, R. 2020a. Sequence Variation in the DDAH1 Gene Predisposes for Delayed Cerebral Ischemia in Subarachnoidal Hemorrhage. *Journal of Clinical Medicine*, 9, 3900.
- HANNEMANN, J., GLATZEL, A., HILLIG, J., ZUMMACK, J., SCHUMACHER, U., LÜNEBURG, N., HARBAUM, L. & BÖGER, R. 2020b. Upregulation of DDAH2 limits pulmonary hypertension and right ventricular hypertrophy during chronic hypoxia in Ddah1 knockout mice. *Frontiers in Physiology*, 11, 1524.
- HASEGAWA, K., WAKINO, S., KIMOTO, M., MINAKUCHI, H., FUJIMURA, K., HOSOYA, K., KOMATSU, M., KANEKO, Y., KANDA, T. & TOKUYAMA, H. 2013. The hydrolase DDAH2 enhances pancreatic insulin secretion by transcriptional regulation of secretogogin through a Sirt1-dependent mechanism in mice. *The FASEB Journal*, 27, 2301-2315.
- HASEGAWA, K., WAKINO, S., TANAKA, T., KIMOTO, M., TATEMATSU, S., KANDA, T., YOSHIOKA, K., HOMMA, K., SUGANO, N. & KURABAYASHI, M. 2006. Dimethylarginine dimethylaminohydrolase 2 increases vascular endothelial growth factor expression through Sp1 transcription factor in endothelial cells. *Arteriosclerosis, thrombosis, and vascular biology*, 26, 1488-1494.
- HAYYAN, M., HASHIM, M. A. & ALNASHEF, I. M. 2016. Superoxide ion: generation and chemical implications. *Chemical reviews*, 116, 3029-3085.
- HEISS, E. H. & M DIRSCH, V. 2014. Regulation of eNOS enzyme activity by posttranslational modification. *Current pharmaceutical design*, 20, 3503-3513.
- HELLINEN, L., SATO, K., REINISALO, M., KIDRON, H., RILLA, K., TACHIKAWA, M., UCHIDA, Y., TERASAKI, T. & URTTI, A. 2019. Quantitative protein expression in the human retinal pigment epithelium: Comparison between apical and basolateral plasma membranes with emphasis on transporters. *Investigative ophthalmology & visual science*, 60, 5022-5034.
- HELLSTROM, M., LINDAHL, P., ABRAMSSON, A. & BETSHOLTZ, C. 1999. Role of PDGF-B and PDGFR-beta in recruitment of vascular smooth muscle cells and pericytes during embryonic blood vessel formation in the mouse. *Development*, 126, 3047-3055.
- HELLSTRÖM, M., PHNG, L.-K., HOFMANN, J. J., WALLGARD, E., COULTAS, L., LINDBLOM, P., ALVA, J., NILSSON, A.-K., KARLSSON, L. & GAIANO, N. 2007. Dll4 signalling through Notch1 regulates formation of tip cells during angiogenesis. *Nature*, 445, 776-780.
- HIELSCHER, A. & GERECHT, S. 2015. Hypoxia and free radicals: role in tumor progression and the use of engineering-based platforms to address these relationships. *Free Radical Biology and Medicine*, 79, 281-291.
- HLUSHCHUK, R., EHRBAR, M., REICHMUTH, P., HEINIMANN, N., STYP-REKOWSKA, B., ESCHER, R., BAUM, O., LIENEMANN, P., MAKANYA, A. & KESHET, E. 2011. Decrease in VEGF expression induces intussusceptive vascular pruning. *Arteriosclerosis, thrombosis, and vascular biology*, 31, 2836-2844.
- HOLDEN, D. P., CARTWRIGHT, J. E., NUSSEY, S. S. & WHITLEY, G. S. J. 2003. Estrogen stimulates dimethylarginine dimethylaminohydrolase activity and the metabolism of asymmetric dimethylarginine. *Circulation*, 108, 1575-1580.

REFERENCES

- HOLZER, T. R., FULFORD, A. D., NEDDERMAN, D. M., UMBERGER, T. S., HOZAK, R. R., JOSHI, A., MELEMED, S. A., BENJAMIN, L. E., PLOWMAN, G. D. & SCHADE, A. E. 2013. Tumor cell expression of vascular endothelial growth factor receptor 2 is an adverse prognostic factor in patients with squamous cell carcinoma of the lung. *PLoS One*, 8, e80292.
- HOOD, J. D., MEININGER, C. J., ZICHE, M. & GRANGER, H. J. 1998. VEGF upregulates ecNOS message, protein, and NO production in human endothelial cells. *American Journal of Physiology-Heart and Circulatory Physiology*, 274, H1054-H1058.
- HOPP, T. P., PRICKETT, K. S., PRICE, V. L., LIBBY, R. T., MARCH, C. J., CERRETTI, D. P., URDAL, D. L. & CONLON, P. J. 1988. A short polypeptide marker sequence useful for recombinant protein identification and purification. *Nature Biotechnology*, 6, 1204-1210.
- HORVATH, S. 1980. Cytotoxicity of drugs and diverse chemical agents to cell cultures. *Toxicology*, 16, 59-66.
- HOTER, A., EL-SABBAN, M. E. & NAIM, H. Y. 2018. The HSP90 family: structure, regulation, function, and implications in health and disease. *International Journal of Molecular Sciences*, 19, 2560.
- HU, J., HAN, J., LI, H., ZHANG, X., LAN LIU, L., CHEN, F. & ZENG, B. 2018. Human embryonic kidney 293 cells: a vehicle for biopharmaceutical manufacturing, structural biology, and electrophysiology. *Cells Tissues Organs*, 205, 1-8.
- HU, X., ATZLER, D., XU, X., ZHANG, P., GUO, H., LU, Z., FASSETT, J., SCHWEDHELM, E., BÖGER, R. H. & BACHE, R. J. 2011a. Dimethylarginine dimethylaminohydrolase-1 is the critical enzyme for degrading the cardiovascular risk factor asymmetrical dimethylarginine. *Arteriosclerosis, thrombosis, and vascular biology*, 31, 1540-1546.
- HU, X., ATZLER, D., XU, X., ZHANG, P., GUO, H., LU, Z., FASSETT, J., SCHWEDHELM, E., BÖGER, R. H. & BACHE, R. J. 2011b. Global DDAH1 gene deficient mice reveal that DDAH1 is the critical enzyme for degrading the cardiovascular risk factor ADMA. *Arteriosclerosis, thrombosis, and vascular biology*, 31, 1540.
- HUA, Z., LV, Q., YE, W., WONG, C.-K. A., CAI, G., GU, D., JI, Y., ZHAO, C., WANG, J. & YANG, B. B. 2006. MiRNA-directed regulation of VEGF and other angiogenic factors under hypoxia. *PLoS One*, 1, e116.
- HUANG, D. W., SHERMAN, B. T. & LEMPICKI, R. A. 2009. Bioinformatics enrichment tools: paths toward the comprehensive functional analysis of large gene lists. *Nucleic acids research*, 37, 1-13.
- HUANG, S.-P., WU, M.-S., SHUN, C.-T., WANG, H.-P., LIN, M.-T., KUO, M.-L. & LIN, J.-T. 2004. Interleukin-6 increases vascular endothelial growth factor and angiogenesis in gastric carcinoma. *Journal of biomedical science*, 11, 517-527.
- HUANG, S., LI, Z., WU, Z., LIU, C., YU, M., WEN, M., ZHANG, L. & WANG, X. 2021. DDAH2 suppresses RLR-MAVS-mediated innate antiviral immunity by stimulating nitric oxide-activated, Drp1-induced mitochondrial fission. *Science Signaling*, 14.
- HUDLICKA, O. & BROWN, M. D. 2009. Adaptation of skeletal muscle microvasculature to increased or decreased blood flow: role of shear stress, nitric oxide and vascular endothelial growth factor. *Journal of vascular research*, 46, 504-512.
- HULIN, J.-A., GUBAREVA, E. A., JARZEBSKA, N., RODIONOV, R. N., MANGONI, A. A. & TOMMASI, S. 2020. Inhibition of dimethylarginine dimethylaminohydrolase (DDAH) enzymes as an emerging therapeutic strategy to target angiogenesis and vasculogenic mimicry in cancer. *Frontiers in oncology*, 9, 1455.
- HULIN, J.-A., TOMMASI, S., ELLIOT, D., HU, D. G., LEWIS, B. C. & MANGONI, A. A. 2017. MiR-193b regulates breast cancer cell migration and vasculogenic mimicry by targeting dimethylarginine dimethylaminohydrolase 1. *Scientific reports*, 7, 1-15.
- HULIN, J.-A., TOMMASI, S., ELLIOT, D. & MANGONI, A. A. 2019. Small molecule inhibition of DDAH1 significantly attenuates triple negative breast cancer cell vasculogenic mimicry in vitro. *Biomedicine & Pharmacotherapy*, 111, 602-612.
- IKEDA, Y., YONEMITSU, Y., ONIMARU, M., NAKANO, T., MIYAZAKI, M., KOHNO, R.-I., NAKAGAWA, K., UENO, A., SUEISHI, K. & ISHIBASHI, T. 2006. The regulation of vascular endothelial growth factors (VEGF-A, -C, and -D) expression in the retinal pigment epithelium. *Experimental eye research*, 83, 1031-1040.
- IRESON, C. R. & KELLAND, L. R. 2006. Discovery and development of anticancer aptamers. *Molecular cancer therapeutics*, 5, 2957-2962.
- ISAACS, J. S., JUNG, Y.-J., MIMNAUGH, E. G., MARTINEZ, A., CUTTITTA, F. & NECKERS, L. M. 2002. Hsp90 regulates a von Hippel Lindau-independent hypoxia-inducible factor-1 α -degradative pathway. *Journal of Biological Chemistry*, 277, 29936-29944.
- ISOGAI, S., LAWSON, N. D., TORREALDAY, S., HORIGUCHI, M. & WEINSTEIN, B. M. 2003. Angiogenic network formation in the developing vertebrate trunk. *Development*, 130, 5281-5290.
- ITAKURA, J., ISHIWATA, T., SHEN, B., KORNMANN, M. & KORC, M. 2000. Concomitant over-expression of vascular endothelial growth factor and its receptors in pancreatic cancer. *International journal of cancer*, 85, 27-34.
- JACOBI, J., SYDOW, K., VON DEGENFELD, G., ZHANG, Y., DAYOUB, H., WANG, B., PATTERSON, A. J., KIMOTO, M., BLAU, H. M. & COOKE, J. P. 2005. Overexpression of dimethylarginine dimethylaminohydrolase reduces tissue asymmetric dimethylarginine levels and enhances angiogenesis. *Circulation*, 111, 1431-1438.

REFERENCES

- JAG, R., BOHR, D. & SPARKS, H. 1980. Architecture of the vessel wall. *American Physiological Soc.*
- JAGER, R. D., MIELER, W. F. & MILLER, J. W. 2008. Age-related macular degeneration. *New England Journal of Medicine*, 358, 2606-2617.
- JAIN, R. K. 2003. Molecular regulation of vessel maturation. *Nature medicine*, 9, 685-693.
- JAIN, R. K., FINN, A. V., KOLODZIE, F. D., GOLD, H. K. & VIRMANI, R. 2007. Antiangiogenic therapy for normalization of atherosclerotic plaque vasculature: a potential strategy for plaque stabilization. *Nature Reviews Cardiology*, 4, 491.
- JARVIS, S. 2018. Vascular system 1: anatomy and physiology. *Nursing Times*, 114, 40-44.
- JÁSZAI, J. & SCHMIDT, M. H. 2019. Trends and challenges in tumor anti-angiogenic therapies. *Cells*, 8, 1102.
- JEONG, K. H., JEON, M.-T., KIM, H. D., JUNG, U. J., JANG, M. C., CHU, J. W., YANG, S. J., CHOI, I. Y., CHOI, M.-S. & KIM, S. R. 2015. Nobiletin protects dopaminergic neurons in the 1-methyl-4-phenylpyridinium-treated rat model of Parkinson's disease. *Journal of medicinal food*, 18, 409-414.
- JI, M., WANG, C., YANG, T., MENG, X., WANG, X. & LI, M. 2021. Integrated phytochemical analysis based on UPLC–MS/MS and network pharmacology approaches to explore the effect of *Odontites vulgaris* Moench on rheumatoid arthritis. *Frontiers in pharmacology*, 12.
- JOURDE-CHICHE, N., FAKHOURI, F., DOU, L., BELLIE, J., BURTEY, S., FRIMAT, M., JARROT, P.-A., KAPLANSKI, G., LE QUINTREC, M. & PERNIN, V. 2019. Endothelium structure and function in kidney health and disease. *Nature Reviews Nephrology*, 15, 87-108.
- JUSTICE, J. M., TANNER, M. A. & MYERS, P. R. 2000. Endothelial cell regulation of nitric oxide production during hypoxia in coronary microvessels and epicardial arteries. *Journal of cellular physiology*, 182, 359-365.
- KAILEMIA, M. J., RUHAAK, L. R., LEBRILLA, C. B. & AMSTER, I. J. 2014. Oligosaccharide analysis by mass spectrometry: a review of recent developments. *Analytical chemistry*, 86, 196-212.
- KAMBA, T. & MCDONALD, D. 2007. Mechanisms of adverse effects of anti-VEGF therapy for cancer. *British journal of cancer*, 96, 1788-1795.
- KANEHISA, M., GOTO, S., SATO, Y., FURUMICHI, M. & TANABE, M. 2012. KEGG for integration and interpretation of large-scale molecular data sets. *Nucleic acids research*, 40, D109-D114.
- KAUR, C., FOULDS, W. S. & LING, E.-A. 2008. Hypoxia-ischemia and retinal ganglion cell damage. *Clinical ophthalmology (Auckland, NZ)*, 2, 879.
- KEEFE, A. D., PAI, S. & ELLINGTON, A. 2010. Aptamers as therapeutics. *Nature Reviews Drug Discovery*, 9, 537-550.
- KEEFE, D., BOWEN, J., GIBSON, R., TAN, T., OKERA, M. & STRINGER, A. 2011. Noncardiac vascular toxicities of vascular endothelial growth factor inhibitors in advanced cancer: a review. *The oncologist*, 16, 432-444.
- KERRIEN, S., ALAM-FARUQUE, Y., ARANDA, B., BANCARZ, I., BRIDGE, A., DEROW, C., DIMMER, E., FEUERMAN, M., FRIEDRICHSEN, A. & HUNTLEY, R. 2007. IntAct—open source resource for molecular interaction data. *Nucleic acids research*, 35, D561-D565.
- KHWANRAJ, K., PHRUKSANIYOM, C., MADLAH, S. & DHARMASAROJA, P. 2015. Differential expression of tyrosine hydroxylase protein and apoptosis-related genes in differentiated and undifferentiated SH-SY5Y neuroblastoma cells treated with MPP+. *Neurology research international*, 2015.
- KIM, J., LEE, H., AN, J., SONG, Y., LEE, C.-K., KIM, K. & KONG, H. 2019. Alterations in gut microbiota by statin therapy and possible intermediate effects on hyperglycemia and hyperlipidemia. *Frontiers in microbiology*, 10, 1947.
- KIM, J. A., VETRIVEL, P., KIM, S. M., HA, S. E., KIM, H. H., BHOSALE, P. B., HEO, J. D., LEE, W. S., SENTHIL, K. & KIM, G. S. 2021. Quantitative Proteomics Analysis for the Identification of Differential Protein Expression in Calf Muscles between Young and Old SD Rats Using Mass Spectrometry. *ACS omega*, 6, 7422-7433.
- KIM, L. A. & D'AMORE, P. A. 2012. A brief history of anti-VEGF for the treatment of ocular angiogenesis. *The American journal of pathology*, 181, 376-379.
- KIM, S. H., JEONG, J. H., LEE, S. H., KIM, S. W. & PARK, T. G. 2006. PEG conjugated VEGF siRNA for anti-angiogenic gene therapy. *Journal of Controlled Release*, 116, 123-129.
- KIM, Y.-W. & BYZOVA, T. V. 2014. Oxidative stress in angiogenesis and vascular disease. *Blood, The Journal of the American Society of Hematology*, 123, 625-631.
- KIM, Y.-W., WEST, X. Z. & BYZOVA, T. V. 2013. Inflammation and oxidative stress in angiogenesis and vascular disease. *Journal of molecular medicine*, 91, 323-328.
- KIMURA, H. & ESUMI, H. 2003. Reciprocal regulation between nitric oxide and vascular endothelial growth factor in angiogenesis. *Acta biochemica polonica-English edition*, 50, 49-60.
- KIMURA, K., HASHIGUCHI, T., DEGUCHI, T., HORINOUCI, S., UTO, T., OKU, H., SETOYAMA, S., MARUYAMA, I., OSAME, M. & ARIMURA, K. 2007. Serum VEGF—as a prognostic factor of atherosclerosis. *Atherosclerosis*, 194, 182-188.
- KINARIVALA, N., SHAH, K., ABBRUSCATO, T. J. & TRIPPIER, P. C. 2017. Passage variation of PC12 cells results in inconsistent susceptibility to externally induced apoptosis. *ACS chemical neuroscience*, 8, 82-88.

REFERENCES

- KINASEWITZ, G. T., PRIVALLE, C. T., IMM, A., STEINGRUB, J. S., MALCYNKI, J. T., BALK, R. A. & DEANGELO, J. 2008. Multicenter, randomized, placebo-controlled study of the nitric oxide scavenger pyridoxalated hemoglobin polyoxyethylene in distributive shock. *Critical care medicine*, 36, 1999-2007.
- KITTEL, A. & MAAS, R. 2014. Pharmacology and clinical pharmacology of methylarginines used as inhibitors of nitric oxide synthases. *Current pharmaceutical design*, 20, 3530-3547.
- KNIPP, M., CHARNOCK, J. M., GARNER, C. D. & VAŠÁK, M. 2001. Structural and Functional Characterization of the Zn (II) Site in Dimethylargininase-1 (DDAH-1) from Bovine Brain Zn (II) release activates DDAH-1. *Journal of Biological Chemistry*, 276, 40449-40456.
- KNOWLES, R. G. & MONCADA, S. 1994. Nitric oxide synthases in mammals. *Biochemical Journal*, 298, 249.
- KOLTE, D., MCCLUNG, J. A. & ARONOW, W. S. 2016. Vasculogenesis and angiogenesis. *Translational Research in Coronary Artery Disease*. Elsevier.
- KONE, B. C., KUNCEWICZ, T., ZHANG, W. & YU, Z.-Y. 2003. Protein interactions with nitric oxide synthases: controlling the right time, the right place, and the right amount of nitric oxide. *American Journal of Physiology-Renal Physiology*, 285, F178-F190.
- KONERDING, M. A., TURHAN, A., RAVNIC, D. J., LIN, M., FUCHS, C., SECOMB, T. W., TSUDA, A. & MENTZER, S. J. 2010. Inflammation-induced intussusceptive angiogenesis in murine colitis. *The Anatomical Record: Advances in Integrative Anatomy and Evolutionary Biology*, 293, 849-857.
- KONISHI, H., SYDOW, K. & COOKE, J. P. 2007. Dimethylarginine dimethylaminohydrolase promotes endothelial repair after vascular injury. *Journal of the American College of Cardiology*, 49, 1099-1105.
- KOPIN, I. 1987. MPTP: an industrial chemical and contaminant of illicit narcotics stimulates a new era in research on Parkinson's disease. *Environmental health perspectives*, 75, 45-51.
- KOSTOUROU, V., ROBINSON, S., CARTWRIGHT, J. & WHITLEY, G. S. J. 2002. Dimethylarginine dimethylaminohydrolase I enhances tumour growth and angiogenesis. *British journal of cancer*, 87, 673-680.
- KOTTHAUS, J., SCHADE, D., KOTTHAUS, J. & CLEMENT, B. 2012. Designing modulators of dimethylarginine dimethylaminohydrolase (DDAH): A focus on selectivity over arginase. *Journal of enzyme inhibition and medicinal chemistry*, 27, 24-28.
- KOTTHAUS, J., SCHADE, D., MUSCHICK, N., BEITZ, E. & CLEMENT, B. 2008. Structure–activity relationship of novel and known inhibitors of human dimethylarginine dimethylaminohydrolase-1: alkenyl-amidines as new leads. *Bioorganic & medicinal chemistry*, 16, 10205-10209.
- KOZERA, B. & RAPACZ, M. 2013. Reference genes in real-time PCR. *Journal of applied genetics*, 54, 391-406.
- KRASNY, L. & HUANG, P. H. 2021. Data-independent acquisition mass spectrometry (DIA-MS) for proteomic applications in oncology. *Molecular omics*, 17, 29-42.
- KROCK, B. L., SKULI, N. & SIMON, M. C. 2011. Hypoxia-induced angiogenesis: good and evil. *Genes & cancer*, 2, 1117-1133.
- KROLL, J. & WALTENBERGER, J. 1998. VEGF-A induces expression of eNOS and iNOS in endothelial cells via VEGF receptor-2 (KDR). *Biochemical and biophysical research communications*, 252, 743-746.
- KUBES, P. 2000. Inducible nitric oxide synthase: a little bit of good in all of us. *Gut*, 47, 6-9.
- KUMAR, S., RAO, N., VENUGOPAL, S. & GE, R. 2012. Endogenous angiogenesis inhibitors: is the list ever ending. *Advances in medicine and biology. Berhradt LV, ed. NY: Nova Sci Publs*, 38, 1-48.
- LAHAM-KARAM, N., LALLI, M., LEINONEN, N. & YLÄ-HERTTUALA, S. 2015. Differential regulation of vascular endothelial growth factors by promoter-targeted shRNAs. *Molecular Therapy-Nucleic Acids*, 4, e243.
- LAMB DEN, S., KELLY, P., AHMETAJ-SHALA, B., WANG, Z., LEE, B., NANDI, M., TORONDEL, B., DELAHAYE, M., DOWSETT, L. & PIPER, S. 2015. Dimethylarginine dimethylaminohydrolase 2 regulates nitric oxide synthesis and hemodynamics and determines outcome in polymicrobial sepsis. *Arteriosclerosis, thrombosis, and vascular biology*, 35, 1382-1392.
- LANGE, C., MOWAT, F., SAYED, H., MEHAD, M., DULUC, L., PIPER, S., LUHMANN, U., NANDI, M., KELLY, P. & SMITH, A. 2016. Dimethylarginine dimethylaminohydrolase-2 deficiency promotes vascular regeneration and attenuates pathological angiogenesis. *Experimental eye research*, 147, 148-155.
- LEE, C. S., PARK, S. Y., KO, H. H., SONG, J. H., SHIN, Y. K. & HAN, E. S. 2005. Inhibition of MPP⁺-induced mitochondrial damage and cell death by trifluoperazine and W-7 in PC12 cells. *Neurochemistry international*, 46, 169-178.
- LEIPER, J., MURRAY-RUST, J., MCDONALD, N. & VALLANCE, P. 2002. S-nitrosylation of dimethylarginine dimethylaminohydrolase regulates enzyme activity: further interactions between nitric oxide synthase and dimethylarginine dimethylaminohydrolase. *Proceedings of the National Academy of Sciences*, 99, 13527-13532.
- LEIPER, J. & NANDI, M. 2011. The therapeutic potential of targeting endogenous inhibitors of nitric oxide synthesis. *Nature Reviews Drug Discovery*, 10, 277-291.
- LEIPER, J., NANDI, M., TORONDEL, B., MURRAY-RUST, J., MALAKI, M., O'HARA, B., ROSSITER, S., ANTHONY, S., MADHANI, M. & SELWOOD, D. 2007. Disruption of methylarginine metabolism impairs vascular homeostasis. *Nature medicine*, 13, 198-203.

REFERENCES

- LEIPER, J., SANTA MARIA, J., CHUBB, A., MACALLISTER, R., CHARLES, I., WHITLEY, G. & VALLANCE, P. 1999. Identification of two human dimethylarginine dimethylaminohydrolases with distinct tissue distributions and homology with microbial arginine deiminases. *Biochem. J*, 343, 209-214.
- LEIVA, E., WEHINGER, S., GUZMÁN, L. & ORREGO, R. 2015. Role of oxidized LDL in atherosclerosis. *Hypercholesterolemia*, 55-78.
- LEMOINE, A. Y., LEDOUX, S. & LARGER, E. 2013. Adipose tissue angiogenesis in obesity. *Thrombosis and haemostasis*, 110, 661-669.
- LEONE, A., MONCADA, S., VALLANCE, P., CALVER, A. & COLLIER, J. 1992. Accumulation of an endogenous inhibitor of nitric oxide synthesis in chronic renal failure. *The Lancet*, 339, 572-575.
- LEONE, P., BUONAVOGLIA, A., FASANO, R., SOLIMANDO, A. G., DE RE, V., CICCIO, S., VACCA, A. & RACANELLI, V. 2019. Insights into the Regulation of Tumor Angiogenesis by Micro-RNAs. *Journal of Clinical Medicine*, 8, 2030.
- LEURS U., M. U. H., RAND K.D. 2016. Applications of Mass Spectrometry in Drug Development Science. *Analytical Techniques in the Pharmaceutical Sciences*. Springer.
- LEVINE, A. B., PUNIHAOLE, D. & LEVINE, T. B. 2012. Characterization of the role of nitric oxide and its clinical applications. *Cardiology*, 122, 55-68.
- LI, H., RAMAN, C., GLASER, C. B., BLASKO, E., YOUNG, T. A., PARKINSON, J. F., WHITLOW, M. & POULOS, T. L. 1999. Crystal Structures of Zinc-free and-bound Heme Domain of Human Inducible Nitric-oxide Synthase *Journal of Biological Chemistry*, 274, 21276-21284.
- LI, J.-M. & SHAH, A. M. 2004. Endothelial cell superoxide generation: regulation and relevance for cardiovascular pathophysiology. *American Journal of Physiology-Regulatory, Integrative and Comparative Physiology*, 287, R1014-R1030.
- LI, J., SUN, L. & LI, Y. 2021. Regulation of dimethylarginine dimethylaminohydrolase 2 expression by NF- κ B acetylation. *Experimental and Therapeutic Medicine*, 21, 1-1.
- LI, Y., SUN, R., ZOU, J., YING, Y. & LUO, Z. 2019. Dual roles of the AMP-activated protein kinase pathway in angiogenesis. *Cells*, 8, 752.
- LIAO, D. & JOHNSON, R. S. 2007. Hypoxia: a key regulator of angiogenesis in cancer. *Cancer and Metastasis Reviews*, 26, 281-290.
- LIAUDET, L., VASSALLI, G. & PACHER, P. 2009. Role of peroxynitrite in the redox regulation of cell signal transduction pathways. *Frontiers in bioscience: a journal and virtual library*, 14, 4809.
- LIEKENS, S., DE CLERCQ, E. & NEYTS, J. 2001. Angiogenesis: regulators and clinical applications. *Biochemical pharmacology*, 61, 253-270.
- LIM, M. S. & ELENITIBA-JOHNSON, K. S. 2004. Proteomics in pathology research. *Laboratory investigation*, 84, 1227-1244.
- LIMA, B., FORRESTER, M. T., HESS, D. T. & STAMLER, J. S. 2010. S-nitrosylation in cardiovascular signaling. *Circulation Research*, 106, 633-646.
- LIN, C.-H., LI, C., LIAO, P., TSE, L., HUANG, W., CHENG, H. & CHENG, Y. J. B. J. O. P. 2013. Silibinin inhibits VEGF secretion and age-related macular degeneration in a hypoxia-dependent manner through the PI-3 kinase/Akt/mTOR pathway. 168, 920-931.
- LIN, C.-L., WANG, F.-S., HSU, Y.-C., CHEN, C.-N., TSENG, M.-J., SALEEM, M. A., CHANG, P.-J. & WANG, J.-Y. 2010. Modulation of Notch-1 signaling alleviates vascular endothelial growth factor-mediated diabetic nephropathy. *Diabetes*, 59, 1915-1925.
- LIN, Y.-C., BOONE, M., MEURIS, L., LEMMENS, I., VAN ROY, N., SOETE, A., REUMERS, J., MOISSE, M., PLAISANCE, S. & DRMANAC, R. 2014. Genome dynamics of the human embryonic kidney 293 lineage in response to cell biology manipulations. *Nature communications*, 5, 1-12.
- LINSKY, T. & FAST, W. 2011. A continuous, fluorescent, high-throughput assay for human dimethylarginine dimethylaminohydrolase-1. *Journal of biomolecular screening*, 16, 1089-1097.
- LIU, X., LIU, Z., GONG, Q., TIAN, R. & SU, G. 2016. Identification and validation of reference genes for quantitative RT-PCR analysis of retinal pigment epithelium cells under hypoxia and/or hyperglycemia. *Gene*, 580, 41-46.
- LIU, Y., COX, S. R., MORITA, T. & KOUREMBANAS, S. 1995. Hypoxia regulates vascular endothelial growth factor gene expression in endothelial cells identification of a 5' enhancer. *Circulation research*, 77, 638-643.
- LIVAK, K. J. & SCHMITTGEN, T. D. 2001. Analysis of relative gene expression data using real-time quantitative PCR and the 2- $\Delta\Delta$ CT method. *Methods*, 25, 402-408.
- LLUIS, J. M., BURICCHI, F., CHIARUGI, P., MORALES, A. & FERNANDEZ-CHECA, J. C. 2007. Dual role of mitochondrial reactive oxygen species in hypoxia signaling: activation of nuclear factor- κ B via c-SRC-and oxidant-dependent cell death. *Cancer Research*, 67, 7368-7377.
- LOBOV, I., RENARD, R., PAPADOPOULOS, N., GALE, N., THURSTON, G., YANCOPOULOS, G. & WIEGAND, S. 2007. Delta-like ligand 4 (Dll4) is induced by VEGF as a negative regulator of angiogenic sprouting. *Proceedings of the National Academy of Sciences*, 104, 3219-3224.

REFERENCES

- LOHELA, M., BRY, M., TAMMELA, T. & ALITALO, K. 2009. VEGFs and receptors involved in angiogenesis versus lymphangiogenesis. *Current opinion in cell biology*, 21, 154-165.
- LOPEZ-FARRE, A., SÁNCHEZ DE MIGUEL, L., CARAMELO, C., GOMEZ-MACIAS, J., GARCIA, R., MOSQUERA, J., DE FRUTOS, T., MILLAS, I., RIVAS, F. & ECHEZARRETA, G. 1997. Role of nitric oxide in autocrine control of growth and apoptosis of endothelial cells. *American Journal of Physiology-Heart and Circulatory Physiology*, 272, H760-H768.
- LÓPEZ, A., LORENTE, J. A., STEINGRUB, J., BAKKER, J., MCLUCKIE, A., WILLATTS, S., BROCKWAY, M., ANZUETO, A., HOLZAPFEL, L. & BREEN, D. 2004. Multiple-center, randomized, placebo-controlled, double-blind study of the nitric oxide synthase inhibitor 546C88: effect on survival in patients with septic shock. *Critical care medicine*, 32, 21-30.
- LOUREIRO, R. M. & D'AMORE, P. A. 2005. Transcriptional regulation of vascular endothelial growth factor in cancer. *Cytokine & growth factor reviews*, 16, 77-89.
- LYNN, D. J., CHAN, C., NASEER, M., YAU, M., LO, R., SRIBNAIA, A., RING, G., QUE, J., WEE, K. & WINSOR, G. L. 2010. Curating the innate immunity interactome. *BMC systems biology*, 4, 1-14.
- LYNN, D. J., WINSOR, G. L., CHAN, C., RICHARD, N., LAIRD, M. R., BARSKY, A., GARDY, J. L., ROCHE, F. M., CHAN, T. H. & SHAH, N. 2008. InnateDB: facilitating systems-level analyses of the mammalian innate immune response. *Molecular systems biology*, 4, 218.
- MACALLISTER, R. J., PARRY, H., KIMOTO, M., OGAWA, T., RUSSELL, R. J., HODSON, H., WHITLEY, G. S. J. & VALLANCE, P. 1996. Regulation of nitric oxide synthesis by dimethylarginine dimethylaminohydrolase. *British journal of pharmacology*, 119, 1533-1540.
- MAHENDRA, G., KUMAR, S., ISAYEVA, T., MAHASRESHTI, P. J., CURIEL, D. T., STOCKARDT, C. R., GRIZZLE, W. E., ALAPATI, V., SINGH, R. & SIEGAL, G. P. 2005. Antiangiogenic cancer gene therapy by adeno-associated virus 2-mediated stable expression of the soluble FMS-like tyrosine kinase-1 receptor. *Cancer gene therapy*, 12, 26-34.
- MAKANYA, A. N., HLUSHCHUK, R., BAUM, O., VELINOV, N., OCHS, M. & DJONOV, V. 2007. Microvascular endowment in the developing chicken embryo lung. *American journal of physiology-lung cellular and molecular physiology*, 292, L1136-L1146.
- MAKANYA, A. N., HLUSHCHUK, R. & DJONOV, V. G. 2009. Intussusceptive angiogenesis and its role in vascular morphogenesis, patterning, and remodeling. *Angiogenesis*, 12, 113.
- MALOY, S. & HUGHES, K. 2013. *Brenner's Encyclopedia of Genetics*, Academic Press.
- MARONGIU, M., PICCARDI, M., BERNARDI, F., CORSINI, G. U. & DEL ZOMPO, M. 1988. Evaluation of the toxicity of the dopaminergic neurotoxins MPTP and MPP+ in PC12 pheochromocytoma cells: binding and biological studies. *Neuroscience letters*, 94, 349-354.
- MARTI, C. N., GHEORGHIADE, M., KALOGEROPOULOS, A. P., GEORGIPOULOU, V. V., QUYYUMI, A. A. & BUTLER, J. 2012. Endothelial dysfunction, arterial stiffness, and heart failure. *Journal of the American College of Cardiology*, 60, 1455-1469.
- MASOUD, G. N. & LI, W. 2015. HIF-1 α pathway: role, regulation and intervention for cancer therapy. *Acta Pharmaceutica Sinica B*, 5, 378-389.
- MAURER, K., BINZEN, U., MÖRZ, H., BUGERT, P., SCHEDEL, A., TREEDE, R.-D. & GREFFRATH, W. 2014. Acetylsalicylic acid enhances tachyphylaxis of repetitive capsaicin responses in TRPV1-GFP expressing HEK293 cells. *Neuroscience letters*, 563, 101-106.
- MCCABE, T. J., FULTON, D., ROMAN, L. J. & SESSA, W. C. 2000. Enhanced electron flux and reduced calmodulin dissociation may explain "calcium-independent" eNOS activation by phosphorylation. *Journal of Biological Chemistry*, 275, 6123-6128.
- MCQUILLAN, L., LEUNG, G., MARSDEN, P., KOSTYK, S. & KOUREMBANAS, S. 1994. Hypoxia inhibits expression of eNOS via transcriptional and posttranscriptional mechanisms. *American Journal of Physiology-Heart and Circulatory Physiology*, 267, H1921-H1927.
- MENTZER, S. J. & KONERDING, M. A. 2014. Intussusceptive angiogenesis: expansion and remodeling of microvascular networks. *Angiogenesis*, 17, 499-509.
- MILLATT, L. J., WHITLEY, G. S., LI, D., LEIPER, J. M., SIRAGY, H. M., CAREY, R. M. & JOHNS, R. A. 2003. Evidence for dysregulation of dimethylarginine dimethylaminohydrolase I in chronic hypoxia-induced pulmonary hypertension. *Circulation*, 108, 1493-1498.
- MILLER, J. W., ADAMIS, A. P. & AIELLO, L. P. 1997. Vascular endothelial growth factor in ocular neovascularization and proliferative diabetic retinopathy. *Diabetes/metabolism reviews*, 13, 37-50.
- MINET, E., ARNOULD, T., MICHEL, G., ROLAND, I., MOTTET, D., RAES, M., REMACLE, J. & MICHIELS, C. 2000. ERK activation upon hypoxia: involvement in HIF-1 activation. *FEBS letters*, 468, 53-58.
- MISHIMA, T., HAMADA, T., UI-TEI, K., TAKAHASHI, F., MIYATA, Y., IMAKI, J., SUZUKI, H. & YAMASHITA, K. 2004. Expression of DDAH1 in chick and rat embryos. *Developmental brain research*, 148, 223-232.

REFERENCES

- MORA, A. & DONALDSON, I. M. 2012. Effects of protein interaction data integration, representation and reliability on the use of network properties for drug target prediction. *BMC bioinformatics*, 13, 1-17.
- MÜNDEL, T., FEIL, R., MÜLSCH, A., LOHMANN, S. M., HOFMANN, F. & WALTER, U. 2003. Physiology and pathophysiology of vascular signaling controlled by cyclic guanosine 3', 5'-cyclic monophosphate-dependent protein kinase. *Circulation*, 108, 2172-2183.
- MUROHARA, T. & ASAHARA, T. 2002. Nitric oxide and angiogenesis in cardiovascular disease. *Antioxidants and Redox Signaling*, 4, 825-831.
- MUROHARA, T., WITZENBICHLER, B., SPYRIDOPOULOS, I., ASAHARA, T., DING, B., SULLIVAN, A., LOSORDO, D. W. & ISNER, J. M. 1999. Role of endothelial nitric oxide synthase in endothelial cell migration. *Arteriosclerosis, thrombosis, and vascular biology*, 19, 1156-1161.
- MURPHY, M. P. 1999. Nitric oxide and cell death. *Biochimica et Biophysica Acta (BBA)-Bioenergetics*, 1411, 401-414.
- MURRAY-RUST, J., LEIPER, J., MCALISTER, M., PHELAN, J., TILLEY, S., SANTA MARIA, J., VALLANCE, P. & MCDONALD, N. 2001. Structural insights into the hydrolysis of cellular nitric oxide synthase inhibitors by dimethylarginine dimethylaminohydrolase. *Nature Structural & Molecular Biology*, 8, 679-683.
- MURTHY, R. C., MCFARLAND, T. J., YOKEN, J., CHEN, S., BARONE, C., BURKE, D., ZHANG, Y., APPUKUTTAN, B. & STOUT, J. T. 2003. Corneal transduction to inhibit angiogenesis and graft failure. *Investigative ophthalmology & visual science*, 44, 1837-1842.
- MUZ, B., DE LA PUENTE, P., AZAB, F. & AZAB, A. K. 2015. The role of hypoxia in cancer progression, angiogenesis, metastasis, and resistance to therapy. *Hypoxia*, 3, 83.
- NANDI, M., KELLY, P., TORONDEL, B., WANG, Z., STARR, A., MA, Y., CUNNINGHAM, P., STIDWILL, R. & LEIPER, J. 2012. Genetic and pharmacological inhibition of dimethylarginine dimethylaminohydrolase 1 is protective in endotoxemic shock. *Arteriosclerosis, thrombosis, and vascular biology*, 32, 2589-2597.
- NAPOLI, C., PAOLISSO, G., CASAMASSIMI, A., AL-OMRAN, M., BARBIERI, M., SOMMESE, L., INFANTE, T. & IGNARRO, L. J. 2013. Effects of nitric oxide on cell proliferation: novel insights. *Journal of the American College of Cardiology*, 62, 89-95.
- NATHAN, C. & XIE, Q.-W. 1994. Nitric oxide synthases: roles, tolls, and controls. *Cell*, 78, 915-918.
- NCBI, D. 2021. Available: <https://www.ncbi.nlm.nih.gov/gene/23576> [Accessed].
- NEGRE-SALVAYRE, A., AUGÉ, N., AYALA, V., BASAGA, H., BOADA, J., BRENKE, R., CHAPPLE, S., COHEN, G., FEHER, J. & GRUNE, T. 2010. Pathological aspects of lipid peroxidation. *Free radical research*, 44, 1125-1171.
- NG, E. W., SHIMA, D. T., CALIAS, P., CUNNINGHAM, E. T., GUYER, D. R. & ADAMIS, A. P. 2006. Pegaptanib, a targeted anti-VEGF aptamer for ocular vascular disease. *Nature Reviews Drug Discovery*, 5, 123-132.
- NICHOLSON, B., MANNER, C. K., KLEEMAN, J. & MACLEOD, C. L. 2001. Sustained nitric oxide production in macrophages requires the arginine transporter CAT2. *Journal of Biological Chemistry*, 276, 15881-15885.
- NUZZI, R. & TRIDICO, F. Local and systemic complications after intravitreal administration of anti-vascular endothelial growth factor agents in the treatment of different ocular diseases: a five-year retrospective study. *Seminars in Ophthalmology*, 2015. Taylor & Francis, 129-135.
- OGAWA, Y. 1977. On the fine structural changes of the microvascular beds in the skeletal muscle. *Journal of Sports Science and Medicine*, 6, 1-19.
- OJHA, S., BALAJI, V., SADEK, B. & RAJESH, M. 2017. Beneficial effects of phytochemicals in diabetic retinopathy: experimental and clinical evidence. *European Review for Medical and Pharmacological Sciences*, 21, 2769-83.
- OLKEN, N. M., RUSCHE, K. M., RICHARDS, M. K. & MARLETTA, M. A. 1991. Inactivation of macrophage nitric oxide synthase activity by NG-methyl-L-arginine. *Biochemical and biophysical research communications*, 177, 828-833.
- OLSSON, A.-K., DIMBERG, A., KREUGER, J. & CLAESSEON-WELSH, L. 2006. VEGF receptor signalling? In control of vascular function. *Nature reviews Molecular cell biology*, 7, 359-371.
- ONOZATO, M. L., TOJO, A., LEIPER, J., FUJITA, T., PALM, F. & WILCOX, C. S. 2008. Expression of DDAH and PRMT isoforms in the diabetic rat kidney; effects of angiotensin II receptor blockers. *Diabetes*, 57, 172-180.
- ORSBURN, B. C. 2021. Proteome Discoverer—A Community Enhanced Data Processing Suite for Protein Informatics. *Proteomes*, 9, 15.
- OSANAI, T., SAITOH, M., SASAKI, S., TOMITA, H., MATSUNAGA, T. & OKUMURA, K. 2003. Effect of shear stress on asymmetric dimethylarginine release from vascular endothelial cells. *Hypertension*, 42, 985-990.
- OUCHI, N., KOBAYASHI, H., KIHARA, S., KUMADA, M., SATO, K., INOUE, T., FUNAHASHI, T. & WALSH, K. 2004. Adiponectin stimulates angiogenesis by promoting cross-talk between AMP-activated protein kinase and Akt signaling in endothelial cells. *Journal of Biological Chemistry*, 279, 1304-1309.
- OUCHI, N., SHIBATA, R. & WALSH, K. 2005. AMP-activated protein kinase signaling stimulates VEGF expression and angiogenesis in skeletal muscle. *Circulation Research*, 96, 838-846.
- PACHER, P., BECKMAN, J. S. & LIAUDET, L. 2007. Nitric oxide and peroxynitrite in health and disease. *Physiological reviews*, 87, 315-424.

REFERENCES

- PALM, F., ONOZATO, M. L., LUO, Z. & WILCOX, C. S. 2007. Dimethylarginine dimethylaminohydrolase (DDAH): expression, regulation, and function in the cardiovascular and renal systems. *American Journal of Physiology-Heart and Circulatory Physiology*, 293, H3227-H3245.
- PAOLOCCI, N., BIONDI, R., BETTINI, M., LEE, C.-I., BERLOWITZ, C. O., ROSSI, R., XIA, Y., AMBROSIO, G., ABBATE, A. L., KASS, D. & ZWEIER, J. L. 2001. Oxygen Radical-mediated Reduction in Basal and Agonist-evoked NO Release in Isolated Rat Heart. 33, 671-679.
- PAPADIMITRIOU, M., HATZIDAKI, E. & PAPASOTIRIOU, I. 2019. Linearity comparison of three colorimetric cytotoxicity assays. *Journal of Cancer Therapy*, 10, 580.
- PAPAPETROPOULOS, A., GARCÍA-CARDEÑA, G., MADRI, J. A. & SESSA, W. C. 1997. Nitric oxide production contributes to the angiogenic properties of vascular endothelial growth factor in human endothelial cells. *The Journal of clinical investigation*, 100, 3131-3139.
- PAPETTI, M. & HERMAN, I. M. 2002. Mechanisms of normal and tumor-derived angiogenesis. *American Journal of Physiology-Cell Physiology*, 282, C947-C970.
- PAPPIREDDI, N., MARTIN, L. & WÜHR, M. 2019. A review on quantitative multiplexed proteomics. *ChemBioChem*, 20, 1210-1224.
- PATEL-HETT, S. & D'AMORE, P. A. 2011. Signal transduction in vasculogenesis and developmental angiogenesis. *The International journal of developmental biology*, 55, 353.
- PATTON, K. T. & THIBODEAU, G. A. 2018. *Anthony's Textbook of Anatomy & Physiology-E-Book*, Elsevier Health Sciences.
- PAULUS, Y. M. & SODHI, A. 2016. Anti-angiogenic therapy for retinal disease. *Pharmacologic Therapy of Ocular Disease*. Springer.
- PEKAROVA, M., KUBALA, L., MARTISKOVA, H., BINO, L., TWAROGOVA, M., KLINKE, A., RUDOLPH, T. K., KUCHTOVA, Z., KOLAROVA, H. & AMBROZOVA, G. 2013. Asymmetric dimethylarginine regulates the lipopolysaccharide-induced nitric oxide production in macrophages by suppressing the activation of NF-kappaB and iNOS expression. *European journal of pharmacology*, 713, 68-77.
- PENN, J., MADAN, A., CALDWELL, R. B., BARTOLI, M., CALDWELL, R. & HARTNETT, M. 2008. Vascular endothelial growth factor in eye disease. *Progress in retinal and eye research*, 27, 331-371.
- PEPPER, M. S. 1997. Manipulating angiogenesis: from basic science to the bedside. *Arteriosclerosis, thrombosis, and vascular biology*, 17, 605-619.
- PERCHENET, L., BÉNARDEAU, A. & ERTEL, E. A. 2000. Pharmacological properties of Ca v 3.2, a low voltage-activated Ca 2+ channel cloned from human heart. *Naunyn-Schmiedeberg's archives of pharmacology*, 361, 590-599.
- POPE, A. J., KARRUPIAH, K., KEARNS, P. N., XIA, Y. & CARDOUNEL, A. J. 2009. Role of dimethylarginine dimethylaminohydrolases in the regulation of endothelial nitric oxide production. *Journal of Biological Chemistry*, 284, 35338-35347.
- POTENTE, M., URBICH, C., SASAKI, K.-I., HOFMANN, W. K., HEESCHEN, C., AICHER, A., KOLLIPARA, R., DEPINHO, R. A., ZEIHNER, A. M. & DIMMELER, S. 2005. Involvement of Foxo transcription factors in angiogenesis and postnatal neovascularization. *The Journal of clinical investigation*, 115, 2382-2392.
- POZZI, C., CUOMO, A., SPADONI, I., MAGNI, E., SILVOLA, A., CONTE, A., SIGISMUND, S., RAVENDA, P. S., BONALDI, T. & ZAMPINO, M. G. 2016. The EGFR-specific antibody cetuximab combined with chemotherapy triggers immunogenic cell death. *Nature medicine*, 22, 624.
- PRIOR, B. M., YANG, H. & TERJUNG, R. L. 2004. What makes vessels grow with exercise training? *Journal of applied physiology*, 97, 1119-1128.
- PUGH, C. W. & RATCLIFFE, P. J. 2003. Regulation of angiogenesis by hypoxia: role of the HIF system. *Nature medicine*, 9, 677-684.
- PUNGLIA, R. S., LU, M., HSU, J., KUROKI, M., TOLENTINO, M. J., KEOUGH, K., LEVY, A. P., LEVY, N. S., GOLDBERG, M. A. & D'AMATO, R. J. 1997. Regulation of vascular endothelial growth factor expression by insulin-like growth factor I. *Diabetes*, 46, 1619-1626.
- RADOMSKI, M. W. & SALAS, E. 1995. Nitric oxide—biological mediator, modulator and factor of injury: its role in the pathogenesis of atherosclerosis. *Atherosclerosis*, 118, S69-S80.
- RAJABI, M. & MOUSA, S. A. 2017. The role of angiogenesis in cancer treatment. *Biomedicines*, 5, 34.
- RAO, Y. K., FANG, S.-H., WU, W.-S. & TZENG, Y.-M. 2010. Constituents isolated from *Cordyceps militaris* suppress enhanced inflammatory mediator's production and human cancer cell proliferation. *Journal of Ethnopharmacology*, 131, 363-367.
- RAPISARDA, A. & MERRILL, G. 2012. Role of the VEGF/VEGFR axis in cancer biology and therapy. *Guidance Molecules in Cancer and Tumor Angiogenesis*, 114, 237.
- RAYCHAUDHURY, A., FRISCHER, H. & MALIK, A. B. 1996. Inhibition of endothelial cell proliferation and bFGF-induced phenotypic modulation by nitric oxide. *Journal of cellular biochemistry*, 63, 125-134.
- REUTER, S., GUPTA, S. C., CHATURVEDI, M. M. & AGGARWAL, B. B. 2010. Oxidative stress, inflammation, and cancer: how are they linked? *Free Radical Biology and Medicine*, 49, 1603-1616.

REFERENCES

- RIBATTI, D. & DJONOV, V. 2012. Intussusceptive microvascular growth in tumors. *Cancer letters*, 316, 126-131.
- RIBEIRO, M. J., PHILLIPS, D. J., BENSON, J. M., EVATT, B. L., ADES, E. W. & HOOPER, W. C. 1995. Hemostatic properties of the SV-40 transfected human microvascular endothelial cell line (HMEC-1): a representative in vitro model for microvascular endothelium. *Thrombosis research*, 79, 153-161.
- RISAU, W. 1991. Embryonic angiogenesis factors. *Pharmacology & Therapeutics*, 51, 371-376.
- RISAU, W. 1997. Mechanisms of angiogenesis. *Nature*, 386, 671-674.
- RISAU, W. & LEMMON, V. 1988. Changes in the vascular extracellular matrix during embryonic vasculogenesis and angiogenesis. *Developmental biology*, 125, 441-450.
- ROBERT, F., BIERAU, H., ROSSI, M., AGUGIARO, D., SORANZO, T., BROLY, H. & MITCHELL-LOGEAN, C. 2009. Degradation of an Fc-fusion recombinant protein by host cell proteases: Identification of a CHO cathepsin D protease. *Biotechnology and bioengineering*, 104, 1132-1141.
- ROSSITER, S., SMITH, C. L., MALAKI, M., NANDI, M., GILL, H., LEIPER, J. M., VALLANCE, P. & SELWOOD, D. L. 2005. Selective substrate-based inhibitors of mammalian dimethylarginine dimethylaminohydrolase. *Journal of medicinal chemistry*, 48, 4670-4678.
- RUHRBERG, C., GERHARDT, H., GOLDING, M., WATSON, R., IOANNIDOU, S., FUJISAWA, H., BETSHOLTZ, C. & SHIMA, D. T. 2002. Spatially restricted patterning cues provided by heparin-binding VEGF-A control blood vessel branching morphogenesis. *Genes & development*, 16, 2684-2698.
- RUPAIMOOLE, R. & SLACK, F. J. 2017. MicroRNA therapeutics: towards a new era for the management of cancer and other diseases. *Nature Reviews Drug Discovery*, 16, 203.
- SALWINSKI, L., MILLER, C. S., SMITH, A. J., PETTIT, F. K., BOWIE, J. U. & EISENBERG, D. 2004. The database of interacting proteins: 2004 update. *Nucleic acids research*, 32, D449-D451.
- SANG, N., STIEHL, D. P., BOHENSKY, J., LESHCHINSKY, I., SRINIVAS, V. & CARO, J. 2003. MAPK signaling up-regulates the activity of hypoxia-inducible factors by its effects on p300. *Journal of Biological Chemistry*, 278, 14013-14019.
- SANHUEZA, C., WEHINGER, S., BENNETT, J. C., VALENZUELA, M., OWEN, G. & QUEST, A. 2015. The twisted survivin connection to angiogenesis. *Molecular cancer*, 14, 198.
- SANZ, L., BLANCO, B. & ALVAREZ-VALLINA, L. 2004. Antibodies and gene therapy: teaching old 'magic bullets' new tricks. *Trends in immunology*, 25, 85-91.
- SARKAR, R., WEBB, R. C. & STANLEY, J. C. 1995. Nitric oxide inhibition of endothelial cell mitogenesis and proliferation. *Surgery*, 118, 274-279.
- SAUERWALD, T., LEWIS, A., DORAI, H. & BETENBAUGH, M. 2011. Apoptosis: The Signaling Pathways and Their Control. In: MOO-YOUNG, M. (ed.) *Comprehensive Biotechnology*. 2 ed.
- SCAPPATICCI, F. A., SMITH, R., PATHAK, A., SCHLOSS, D., LUM, B., CAO, Y., JOHNSON, F., ENGLEMAN, E. G. & NOLAN, G. P. 2001. Combination angiostatin and endostatin gene transfer induces synergistic antiangiogenic activity in vitro and antitumor efficacy in leukemia and solid tumors in mice. *Molecular Therapy*, 3, 186-196.
- SCHLATTER, P., KÖNIG, M., KARLSSON, L. & BURRI, P. 1997. Quantitative study of intussusceptive capillary growth in the chorioallantoic membrane (CAM) of the chicken embryo. *Microvascular research*, 54, 65-73.
- SCHLINGEMANN, R. O. & VAN HINSBERGH, V. W. 1997. Role of vascular permeability factor/vascular endothelial growth factor in eye disease. *British Journal of Ophthalmology*, 81, 501-512.
- SCHNABEL, R., BLANKENBERG, S., LUBOS, E., LACKNER, K. J., RUPPRECHT, H. J., ESPINOLA-KLEIN, C., JACHMANN, N., POST, F., PEETZ, D. & BICKEL, C. 2005. Asymmetric Dimethylarginine and the Risk of Cardiovascular Events and Death in Patients With Coronary Artery Disease Results from the AtheroGene Study. *Circulation Research*, 97, e53-e59.
- SEMENZA, G. L. 2000. HIF-1 and human disease: one highly involved factor. *Genes & development*, 14, 1983-1991.
- SERVOS, S., ZACHARY, I. & MARTIN, J. 1999. VEGF modulates NO production: the basis of a cytoprotective effect? *Cardiovascular Research*, 41, 509-510.
- SEWDUTH, R. & SANTORO, M. M. 2016. "Decoding" angiogenesis: new facets controlling endothelial cell behavior. *Frontiers in Physiology*, 7, 306.
- SHAO, R. & GUO, X. 2004. Human microvascular endothelial cells immortalized with human telomerase catalytic protein: a model for the study of in vitro angiogenesis. *Biochemical and biophysical research communications*, 321, 788-794.
- SHAO, R., HAMEL, K., PETERSEN, L., CAO, Q., ARENAS, R. B., BIGELOW, C., BENTLEY, B. & YAN, W. 2009. YKL-40, a secreted glycoprotein, promotes tumor angiogenesis. *Oncogene*, 28, 4456-4468.
- SHEN, J., CHEN, X., HENDERSHOT, L. & PRYWES, R. 2002. ER stress regulation of ATF6 localization by dissociation of BiP/GRP78 binding and unmasking of Golgi localization signals. *Developmental cell*, 3, 99-111.
- SHIBUYA, M. 2011. Vascular endothelial growth factor (VEGF) and its receptor (VEGFR) signaling in angiogenesis: a crucial target for anti-and pro-angiogenic therapies. *Genes & cancer*, 2, 1097-1105.
- SHIBUYA, M. 2013. Vascular endothelial growth factor and its receptor system: physiological functions in angiogenesis and pathological roles in various diseases. *The Journal of Biochemistry*, 153, 13-19.

REFERENCES

- SHIH, T. & LINDLEY, C. 2006. Bevacizumab: an angiogenesis inhibitor for the treatment of solid malignancies. *Clinical therapeutics*, 28, 1779-1802.
- SHWEIKI, D., ITIN, A., SOFFER, D. & KESHET, E. 1992. Vascular endothelial growth factor induced by hypoxia may mediate hypoxia-initiated angiogenesis. *Nature*, 359, 843-845.
- SIBAL, L., C AGARWAL, S., D HOME, P. & H BOGER, R. 2010. The role of asymmetric dimethylarginine (ADMA) in endothelial dysfunction and cardiovascular disease. *Current cardiology reviews*, 6, 82-90.
- SILVER, N., BEST, S., JIANG, J. & THEIN, S. L. 2006. Selection of housekeeping genes for gene expression studies in human reticulocytes using real-time PCR. *BMC molecular biology*, 7, 1-9.
- ŚLIWKA, L., WIKTORSKA, K., SUCHOCKI, P., MILCZAREK, M., MIELCZAREK, S., LUBELSKA, K., CIERPIAŁ, T., ŁYŻWA, P., KIEŁBASIŃSKI, P. & JAROMIŃ, A. 2016. The comparison of MTT and CVS assays for the assessment of anticancer agent interactions. *PLoS One*, 11, e0155772.
- SMITH, C. L., BIRDSEY, G. M., ANTHONY, S., ARRIGONI, F. I., LEIPER, J. M. & VALLANCE, P. 2003. Dimethylarginine dimethylaminohydrolase activity modulates ADMA levels, VEGF expression, and cell phenotype. *Biochemical and biophysical research communications*, 308, 984-989.
- SOLDNER, F., WELLER, M., HAID, S., BEINROTH, S., MILLER, S. W., WÜLLNER, U., DAVIS, R. E., DICHGANS, J., KLOCKGETHER, T. & SCHULZ, J. B. 1999. MPP+ inhibits proliferation of PC12 cells by a p21WAF1/Cip1-dependent pathway and induces cell death in cells lacking p21WAF1/Cip1. *Experimental cell research*, 250, 75-85.
- SRIPATHI, S. R., HE, W., UM, J.-Y., MOSER, T., DEHNBOSTEL, S., KINDT, K., GOLDMAN, J., FROST, M. C. & JAHNG, W. J. 2012. Nitric oxide leads to cytoskeletal reorganization in the retinal pigment epithelium under oxidative stress. *Advances in bioscience*
- biotechnology*, 3, 1167.
- STANEL, S. C., SJÖBERG, J., SALMONSON, T., FOGGI, P., CALENO, M., MELCHIORRI, D., GRAVANIS, I., TZOGANI, K. & PIGNATTI, F. 2017. European Medicines Agency approval summary: Zaltrap for the treatment of patients with oxaliplatin-resistant metastatic colorectal cancer. *ESMO open*, 2, e000190.
- STECKEL, A. & SCHLOSSER, G. 2019. An organic chemist's guide to electrospray mass spectrometric structure elucidation. *Molecules*, 24, 611.
- STEMPEL, A. J., PAN, Y., SMITH, J. R. & APPUKUTTAN, B. 2012. Hypoxia-Induced Autophagy in Human Retinal Endothelial Cells. *Investigative ophthalmology & visual science*, 53, 4288-4288.
- STEPANENKO, A. & DMITRENKO, V. 2015. HEK293 in cell biology and cancer research: phenotype, karyotype, tumorigenicity, and stress-induced genome-phenotype evolution. *Gene*, 569, 182-190.
- STRATMAN, A. N. & DAVIS, G. E. 2012. Endothelial cell-pericyte interactions stimulate basement membrane matrix assembly: influence on vascular tube remodeling, maturation and stabilization. *Microscopy and microanalysis: the official journal of Microscopy Society of America, Microbeam Analysis Society, Microscopical Society of Canada*, 18, 68.
- STRIJDOM, H., JACOBS, S., HATTINGH, S., PAGE, C. & LOCHNER, A. 2006. Nitric oxide production is higher in rat cardiac microvessel endothelial cells than ventricular cardiomyocytes in baseline and hypoxic conditions: a comparative study. *The FASEB Journal*, 20, 314-316.
- SUÁREZ, Y. & SESSA, W. C. 2009. MicroRNAs as novel regulators of angiogenesis. *Circulation Research*, 104, 442-454.
- SUCHTING, S., FREITAS, C., LE NOBLE, F., BENEDITO, R., BRÉANT, C., DUARTE, A. & EICHMANN, A. 2007. The Notch ligand Delta-like 4 negatively regulates endothelial tip cell formation and vessel branching. *Proceedings of the National Academy of Sciences*, 104, 3225-3230.
- SUN, B., LIU, Y., HUANG, W., ZHANG, Q., LIN, J., LI, W., ZHANG, J. & CHEN, F. 2021. Functional identification of a rare vascular endothelial growth factor a (VEGFA) variant associating with the nonsyndromic cleft lip with/without cleft palate. *Bioengineered*, 12, 1471-1483.
- SUND, M., ZEISBERG, M. & KALLURI, R. 2005. Endogenous stimulators and inhibitors of angiogenesis in gastrointestinal cancers: basic science to clinical application. *Gastroenterology*, 129, 2076-2091.
- SUNDERKÖTTER, C., STEINBRINK, K., GOEBELER, M., BHARDWAJ, R. & SORG, C. 1994. Macrophages and angiogenesis. *Journal of leukocyte biology*, 55, 410-422.
- TAKEMOTO, M., SUN, J., HIROKI, J., SHIMOKAWA, H. & LIAO, J. K. 2002. Rho-kinase mediates hypoxia-induced downregulation of endothelial nitric oxide synthase. *Circulation*, 106, 57-62.
- TAN, S. C., CARR, C. A., YEOH, K. K., SCHOFIELD, C. J., DAVIES, K. E. & CLARKE, K. 2012. Identification of valid housekeeping genes for quantitative RT-PCR analysis of cardiosphere-derived cells preconditioned under hypoxia or with prolyl-4-hydroxylase inhibitors. *Molecular biology reports*, 39, 4857-4867.
- TANG, J., FRANKEL, A., COOK, R. J., KIM, S., PAIK, W. K., WILLIAMS, K. R., CLARKE, S. & HERSCHMAN, H. R. 2000. PRMT1 is the predominant type I protein arginine methyltransferase in mammalian cells. *Journal of Biological Chemistry*, 275, 7723-7730.

REFERENCES

- TANG, X.-Q., FANG, H.-R., LI, Y.-J., ZHOU, C.-F., REN, Y.-K., CHEN, R.-Q., WANG, C.-Y. & HU, B. 2011. Endogenous hydrogen sulfide is involved in asymmetric dimethylarginine-induced protection against neurotoxicity of 1-methyl-4-phenyl-pyridinium ion. *Neurochemical research*, 36, 2176-2185.
- TEERLINK, T. 2005. ADMA metabolism and clearance. *Vascular Medicine*, 10, S73-S81.
- THE UNIVERSITY OF QUEENSLAND. 2017. *How drugs go from discovery to the pharmacy shelf* [Online]. Available: <https://chr.centre.uq.edu.au/article/2017/10/how-drugs-go-discovery-pharmacy-shelf> [Accessed 2021, June 30].
- THELLIN, O., ZORZI, W., LAKAYE, B., DE BORMAN, B., COUMANS, B., HENNEN, G., GRISAR, T., IGOUT, A. & HEINEN, E. 1999. Housekeeping genes as internal standards: use and limits. *Journal of biotechnology*, 75, 291-295.
- THERAPEUTIC GOODS ADMINISTRATION. 2020. *Therapeutic Goods Administration, Legislation for Clinical Trials* [Online]. Available: <https://www.tga.gov.au/node/4125> [Accessed July 5, 2021].
- THIEMERMANN, C. 1994. The role of the L-arginine: nitric oxide pathway in circulatory shock. *Advances in pharmacology*, 28, 45-45.
- THOMSEN, L. L. & MILES, D. W. 1998. Role of nitric oxide in tumour progression: lessons from human tumours. *Cancer and Metastasis Reviews*, 17, 107-118.
- TOLENTINO, M. 2011. Systemic and ocular safety of intravitreal anti-VEGF therapies for ocular neovascular disease. *Survey of ophthalmology*, 56, 95-113.
- TOMMASI, S. 2015. *Design and synthesis of human dimethylarginin dimethylaminohydrolase (DDAH) inhibitors and development of a novel DDAH activity assay* Doctor of philosophy, University of Aberdeen.
- TOMMASI, S., ZANATO, C., LEWIS, B. C., NAIR, P. C., DALL'ANGELO, S., ZANDA, M. & MANGONI, A. A. 2015. Arginine analogues incorporating carboxylate bioisosteric functions are micromolar inhibitors of human recombinant DDAH-1. *Organic & biomolecular chemistry*, 13, 11315-11330.
- TONG, W. H. & ROUAULT, T. 2000. Distinct iron-sulfur cluster assembly complexes exist in the cytosol and mitochondria of human cells. *The EMBO journal*, 19, 5692-5700.
- TOUSOULIS, D., KAMPOLI, A.-M., TENTOLOURIS NIKOLAOS PAPAGEORGIOU, C. & STEFANADIS, C. 2012. The role of nitric oxide on endothelial function. *Current vascular pharmacology*, 10, 4-18.
- TRAN, C. T., LEIPER, J. M. & VALLANCE, P. 2003. The ddah/adma/nos pathway. *Atherosclerosis Supplements*, 4, 33-40.
- TRAN, C. T. L., FOX, M. F., VALLANCE, P. & LEIPER, J. M. 2000. Chromosomal Localization, Gene Structure, and Expression Pattern of DDAH1: Comparison with DDAH2 and Implications for Evolutionary Origins. *Genomics*, 68, 101-105.
- TRIGGLE, C. R., SAMUEL, S. M., RAVISHANKAR, S., MAREI, I., ARUNACHALAM, G. & DING, H. 2012. The endothelium: influencing vascular smooth muscle in many ways. *Canadian journal of physiology and pharmacology*, 90, 713-738.
- TRIPATHI, P., TRIPATHI, P., KASHYAP, L. & SINGH, V. 2007. The role of nitric oxide in inflammatory reactions. *FEMS Immunology & Medical Microbiology*, 51, 443-452.
- TRITTMANN, J. K., ALMAZROUE, H., JIN, Y. & NELIN, L. D. 2019. DDAH1 regulates apoptosis and angiogenesis in human fetal pulmonary microvascular endothelial cells. *Physiological reports*, 7, e14150.
- TSURUMI, Y., MUROHARA, T., KRASINSKI, K., CHEN, D., WITZENBICHLER, B., KEARNEY, M., COUFFINHAL, T. & ISNER, J. M. 1997. Reciprocal relation between VEGF and NO in the regulation of endothelial integrity. *Nature medicine*, 3, 879-886.
- TUNG, J. J., TATTERSALL, I. W. & KITAJEWSKI, J. 2012. Tips, stalks, tubes: notch-mediated cell fate determination and mechanisms of tubulogenesis during angiogenesis. *Cold Spring Harbor perspectives in medicine*, 2, a006601.
- UCCELLI, A., WOLFF, T., VALENTE, P., DI MAGGIO, N., PELLEGRINO, M., GÜRKE, L., BANFI, A. & GIANNI-BARRERA, R. 2019. Vascular endothelial growth factor biology for regenerative angiogenesis. *Swiss medical weekly*, 149.
- UEDA, S., KATO, S., MATSUOKA, H., KIMOTO, M., OKUDA, S., MORIMATSU, M. & IMAIZUMI, T. 2003. Regulation of cytokine-induced nitric oxide synthesis by asymmetric dimethylarginine: role of dimethylarginine dimethylaminohydrolase. *Circulation Research*, 92, 226-233.
- USHIO-FUKAI, M. & ALEXANDER, R. W. 2004. Reactive oxygen species as mediators of angiogenesis signaling. Role of NAD (P) H oxidase. *Molecular and cellular biochemistry*, 264, 85-97.
- USHIO-FUKAI, M. & NAKAMURA, Y. 2008. Reactive oxygen species and angiogenesis: NADPH oxidase as target for cancer therapy. *Cancer letters*, 266, 37-52.
- VALKO, M., LEIBFRITZ, D., MONCOL, J., CRONIN, M. T., MAZUR, M. & TELSNER, J. 2007. Free radicals and antioxidants in normal physiological functions and human disease. *The international journal of biochemistry & cell biology*, 39, 44-84.
- VALLANCE, P., BUSH, H. D., MOK, B. J., HURTADO-GUERRERO, R., GILL, H., ROSSITER, S., WILDEN, J. D. & CADDICK, S. 2005. Inhibition of dimethylarginine dimethylaminohydrolase (DDAH) and arginine deiminase (ADI) by pentafluorophenyl (PFP) sulfonates. *Chemical communications*, 5563-5565.
- VALLANCE, P. & LEIPER, J. 2004. Cardiovascular biology of the asymmetric dimethylarginine: dimethylarginine dimethylaminohydrolase pathway. *Arteriosclerosis, thrombosis, and vascular biology*, 24, 1023-1030.

REFERENCES

- VAN BREEMEN, R. B. 2003. Mass spectrometry and drug discovery. *Burger's Medicinal Chemistry and Drug Discovery*, 583-610.
- VAN DYK, M., MANGONI, A. A., MCEVOY, M., ATTIA, J. R., SORICH, M. J. & ROWLAND, A. 2015. Targeted arginine metabolomics: A rapid, simple UPLC-QToF-MSE based approach for assessing the involvement of arginine metabolism in human disease. *Clinica Chimica Acta*, 447, 59-65.
- VANELLA, L., DI GIACOMO, C., ACQUAVIVA, R., SANTANGELO, R., CARDILE, V., BARBAGALLO, I., ABRAHAM, N. G. & SORRENTI, V. 2011. The DDAH/NOS pathway in human prostatic cancer cell lines: antiangiogenic effect of L-NAME. *International Journal of Oncology*, 39, 1303-1310.
- VANPUTTE, C. L., REGAN, J. L. & RUSSO, A. F. 2021. *Seeley's essentials of anatomy & physiology*, University of Iowa.
- VERHEUL, H., HOEKMAN, K., LUYKX-DE BAKKER, S., EEKMAN, C. A., FOLMAN, C. C., BROXTERMAN, H. J. & PINEDO, H. M. 1997. Platelet: transporter of vascular endothelial growth factor. *Clinical cancer research*, 3, 2187-2190.
- VERREY, F., CLOSS, E. I., WAGNER, C. A., PALACIN, M., ENDOU, H. & KANAI, Y. 2004. CATs and HATs: the SLC7 family of amino acid transporters. *Pflügers Archiv*, 447, 532-542.
- VICHAI, V. & KIRTIKARA, K. 2006. Sulforhodamine B colorimetric assay for cytotoxicity screening. *Nature protocols*, 1, 1112.
- VITO, A., EL-SAYES, N. & MOSSMAN, K. 2020. Hypoxia-Driven Immune Escape in the Tumor Microenvironment. *Cells*, 9, 992.
- WACKER, A. & GERHARDT, H. 2011. Endothelial development taking shape. *Current opinion in cell biology*, 23, 676-685.
- WANG, D., GILL, P. S., CHABRASHVILI, T., ONOZATO, M. L., RAGGIO, J., MENDONCA, M., DENNEHY, K., LI, M., MODLINGER, P. & LEIPER, J. 2007. Isoform-specific regulation by NG, N G-dimethylarginine dimethylaminohydrolase of rat serum asymmetric dimethylarginine and vascular endothelium-derived relaxing factor/NO. *Circulation Research*, 101, 627-635.
- WANG, G. L. & SEMENZA, G. L. 1995. Purification and characterization of hypoxia-inducible factor 1. *Journal of Biological Chemistry*, 270, 1230-1237.
- WANG, L.-F., YAN, Z.-Y., LI, Y.-L., WANG, Y.-H., ZHANG, S.-J., JIA, X., LU, L., SHANG, Y.-X., WANG, X. & LI, Y.-H. 2019. Inhibition of Obtusifolin on retinal pigment epithelial cell growth under hypoxia. *International journal of ophthalmology*, 12, 1539.
- WANG, S., QI, Y., YU, L., ZHANG, L., CHAO, F., HUANG, W., HUANG, R., LI, H., LUO, Y. & XIU, Y. 2016. Endogenous nitric oxide regulates blood vessel growth factors, capillaries in the cortex, and memory retention in Sprague-Dawley rats. *American Journal of Translational Research*, 8, 5271.
- WANG, W., MA, Y., LI, J., SHI, H., WANG, L., GUO, F., ZHANG, J., LI, D., MO, B. & WEN, F. 2013. Specificity redirection by CAR with human VEGFR-1 affinity endows T lymphocytes with tumor-killing ability and anti-angiogenic potency. *Gene therapy*, 20, 970-978.
- WANG, Y., WANG, L., CHEN, C. & CHU, X. 2018. New insights into the regulatory role of microRNA in tumor angiogenesis and clinical implications. *Molecular cancer*, 17, 22.
- WANG, Z., LAMBDEN, S., TAYLOR, V., SUJKOVIC, E., NANDI, M., TOMLINSON, J., DYSON, A., MCDONALD, N., CADDICK, S. & SINGER, M. 2014. Pharmacological inhibition of DDAH1 improves survival, haemodynamics and organ function in experimental septic shock. *Biochemical Journal*, 460, 309-316.
- WATKINS, W. M., MCCOLLUM, G. W., SAVAGE, S. R., CAPOZZI, M. E., PENN, J. S. & MORRISON, D. G. 2013. Hypoxia-induced expression of VEGF splice variants and protein in four retinal cell types. *Experimental eye research*, 116, 240-246.
- WATSON, S. P. 2009. Platelet activation by extracellular matrix proteins in haemostasis and thrombosis. *Current pharmaceutical design*, 15, 1358-1372.
- WEIDEMANN, A. & JOHNSON, R. 2008. Biology of HIF-1 α . *Cell Death & Differentiation*, 15, 621-627.
- WEINER, L. M., SURANA, R. & WANG, S. 2010. Monoclonal antibodies: versatile platforms for cancer immunotherapy. *Nature Reviews Immunology*, 10, 317-327.
- WELCH, W. J., TOJO, A. & WILCOX, C. S. 2000. Roles of NO and oxygen radicals in tubuloglomerular feedback in SHR. *American Journal of Physiology-Renal Physiology*, 278, F769-F776.
- WELLS, S. M. & HOLIAN, A. 2007. Asymmetric dimethylarginine induces oxidative and nitrosative stress in murine lung epithelial cells. *American journal of respiratory cell and molecular biology*, 36, 520-528.
- WETZEL, M. D., GAO, T., STANLEY, K., COOPER, T. K., MORRIS JR, S. M. & AWAD, A. S. 2020. Enhancing kidney DDAH-1 expression by adenovirus delivery reduces ADMA and ameliorates diabetic nephropathy. *American Journal of Physiology-Renal Physiology*, 318, F509-F517.
- WILCKEN, D. E., SIM, A. S., WANG, J. & WANG, X. L. 2007. Asymmetric dimethylarginine (ADMA) in vascular, renal and hepatic disease and the regulatory role of L-arginine on its metabolism. *Molecular genetics and metabolism*, 91, 309-317.

REFERENCES

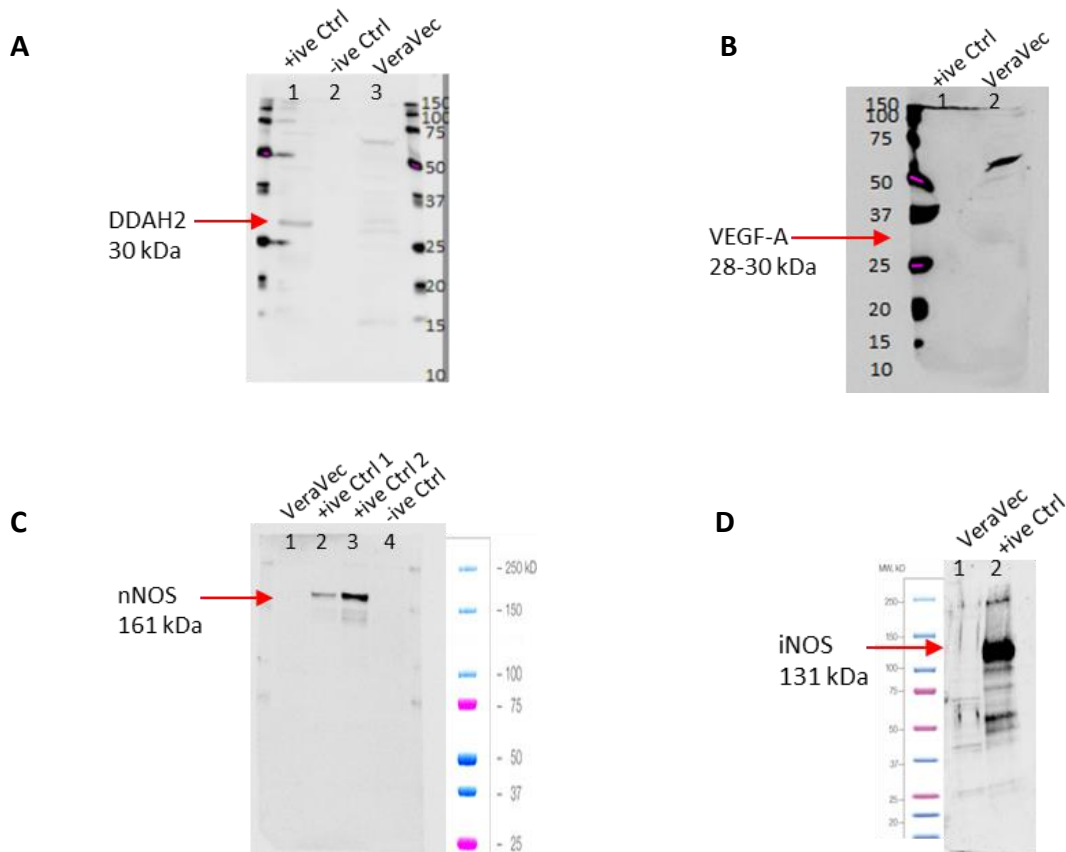
- WILCOX, C. S., WELCH, W. J., MURAD, F., GROSS, S. S., TAYLOR, G., LEVI, R. & SCHMIDT, H. 1992. Nitric oxide synthase in macula densa regulates glomerular capillary pressure. *Proceedings of the National Academy of Sciences*, 89, 11993-11997.
- WILTING, J., BIRKENHÄGER, R., EICHMANN, A., KURZ, H., MARTINY-BARON, G., MARMÉ, D., MCCARTHY, J. E., CHRIST, B. & WEICH, H. A. 1996. VEGF121Induces Proliferation of Vascular Endothelial Cells and Expression of eNOS without Affecting Lymphatic Vessels of the Chorioallantoic Membrane. *Developmental biology*, 176, 76-85.
- WINGFIELD, J. & WILSON, I. D. 2016. Advances in mass spectrometry within drug discovery. *Journal of Biomolecular Screening*, 21, 109-110.
- WITMER, A., VRENSEN, G., VAN NOORDEN, C. & SCHLINGEMANN, R. 2003. Vascular endothelial growth factors and angiogenesis in eye disease. *Progress in retinal and eye research*, 22, 1-29.
- WOJCIAK-STOTHARD, B., TORONDEL, B., TSANG, L. Y. F., FLEMMING, I., FISSLTHALER, B., LEIPER, J. M. & VALLANCE, P. 2007. The ADMA/DDAH pathway is a critical regulator of endothelial cell motility. *Journal of cell science*, 120, 929-942.
- WOLBURG, H., NOELL, S., MACK, A., WOLBURG-BUCHHOLZ, K. & FALLIER-BECKER, P. 2009. Brain endothelial cells and the glio-vascular complex. *Cell and tissue research*, 335, 75-96.
- WU, J., KE, X., FU, W., GAO, X., ZHANG, H., WANG, W., MA, N., ZHAO, M., HAO, X. & ZHANG, Z. 2016. Inhibition of hypoxia-induced retinal angiogenesis by specnuezhenide, an effective constituent of *Ligustrum lucidum* Ait., through suppression of the HIF-1 α /VEGF signaling pathway. *Molecules*, 21, 1756.
- WU, W.-C., KAO, Y.-H., HU, P.-S. & CHEN, J.-H. 2007. Geldanamycin, a HSP90 inhibitor, attenuates the hypoxia-induced vascular endothelial growth factor expression in retinal pigment epithelium cells in vitro. *Experimental eye research*, 85, 721-731.
- XIA, C., MENG, Q., LIU, L.-Z., ROJANASAKUL, Y., WANG, X.-R. & JIANG, B.-H. 2007. Reactive oxygen species regulate angiogenesis and tumor growth through vascular endothelial growth factor. *Cancer Research*, 67, 10823-10830.
- XIAN, D., SONG, J., YANG, L., XIONG, X., LAI, R. & ZHONG, J. 2019. Emerging roles of redox-mediated angiogenesis and oxidative stress in dermatoses. *Oxidative Medicine and Cellular Longevity*, 2019.
- XIAO, Q., ZENG, S., LING, S. & LV, M. 2006. Up-regulation of HIF-1 α and VEGF expression by elevated glucose concentration and hypoxia in cultured human retinal pigment epithelial cells. *Journal of Huazhong University of Science and Technology*, 26, 463-465.
- YAN, Y., XING, T., WANG, S. & LI, N. 2020. Versatile, Sensitive, and Robust Native LC-MS Platform for Intact Mass Analysis of Protein Drugs. *Journal of the American Society for Mass Spectrometry*, 31, 2171-2179.
- YANG, W., ANDO, J., KORENAGA, R., TOYOOKA, T. & KAMIYA, A. 1994. Exogenous nitric oxide inhibits proliferation of cultured vascular endothelial cells. *Biochemical and biophysical research communications*, 203, 1160-1167.
- YANG, Y. & BEDFORD, M. T. 2013. Protein arginine methyltransferases and cancer. *Nature Reviews Cancer*, 13, 37-50.
- YAO, C.-H., WANG, L., STANCLIFFE, E., SINDELAR, M., CHO, K., YIN, W., WANG, Y. & PATTI, G. J. 2019. Dose-response metabolomics to understand biochemical mechanisms and off-target drug effects with the TOXcms software. *Analytical chemistry*, 92, 1856-1864.
- YE, J., COULOURIS, G., ZARETSKAYA, I., CUTCUTACHE, I., ROZEN, S. & MADDEN, T. L. 2012. Primer-BLAST: a tool to design target-specific primers for polymerase chain reaction. *BMC bioinformatics*, 13, 1-11.
- YE, M., YI, Y., WU, S., ZHOU, Y. & ZHAO, D. 2017. Role of paeonol in an astrocyte model of Parkinson's disease. *Medical science monitor: international medical journal of experimental and clinical research*, 23, 4740.
- YE, W., LIU, R., PAN, C., JIANG, W., ZHANG, L., GUAN, Z., WU, J., YING, X., LI, L. & LI, S. 2014. Multicenter randomized phase 2 clinical trial of a recombinant human endostatin adenovirus in patients with advanced head and neck carcinoma. *Molecular Therapy*, 22, 1221-1229.
- YOKOYAMA, Y., DHANABAL, M., GRIFFIOEN, A. W., SUKHATME, V. P. & RAMAKRISHNAN, S. 2000. Synergy between angiostatin and endostatin: inhibition of ovarian cancer growth. *Cancer Research*, 60, 2190-2196.
- YOU, H., MCMANUS, D. P., HU, W., SMOUT, M. J., BRINDLEY, P. J. & GOBERT, G. N. 2013. Transcriptional responses of in vivo praziquantel exposure in schistosomes identifies a functional role for calcium signalling pathway member CamKII. *PLoS pathogens*, 9, e1003254.
- YU, Q., XIONG, Y., GAO, H., LIU, J., CHEN, Z., WANG, Q. & WEN, D. 2015. Comparative proteomics analysis of *Spodoptera frugiperda* cells during *Autographa californica* multiple nucleopolyhedrovirus infection. *Virology journal*, 12, 1-11.
- YUAN, J., XU, W. W., JIANG, S., YU, H. & POON, H. F. 2018. The scattered twelve tribes of HEK293. *Biomedical and Pharmacology Journal*, 11, 621-623.
- ZAKRZEWICZ, D. & EICKELBERG, O. 2009. From arginine methylation to ADMA: a novel mechanism with therapeutic potential in chronic lung diseases. *BMC pulmonary medicine*, 9, 5.
- ZENEBE, W. J., NAZAREWICZ, R. R., PARIHAR, M. S. & GHAFOURIFAR, P. 2007. Hypoxia/reoxygenation of isolated rat heart mitochondria causes cytochrome c release and oxidative stress; evidence for involvement of mitochondrial nitric oxide synthase. *Journal of molecular and cellular cardiology*, 43, 411-419.

REFERENCES

- ZHAN, K., BAI, L., WANG, G., ZUO, B., XIE, L. & WANG, X. 2018. Different angiogenesis modes and endothelial responses in implanted porous biomaterials. *Integrative Biology*, 10, 406-418.
- ZHANG, H. Q., FAST, W., MARLETTA, M. A., MARTASEK, P. & SILVERMAN, R. B. 1997. Potent and selective inhibition of neuronal nitric oxide synthase by N ω -propyl-L-arginine. *Journal of medicinal chemistry*, 40, 3869-3870.
- ZHANG, P., HU, X., XU, X., CHEN, Y. & BACHE, R. J. 2011. Dimethylarginine dimethylaminohydrolase 1 modulates endothelial cell growth through nitric oxide and Akt. *Arteriosclerosis, thrombosis, and vascular biology*, 31, 890-897.
- ZHANG, P., XU, X., HU, X., WANG, H., FASSETT, J., HUO, Y., CHEN, Y. & BACHE, R. J. 2013. DDAH1 deficiency attenuates endothelial cell cycle progression and angiogenesis. *PLoS One*, 8, e79444.
- ZHANG, Q., CHEN, G., LIU, X. & QIAN, Q. 2007. Monoclonal antibodies as therapeutic agents in oncology and antibody gene therapy. *Cell research*, 17, 89-99.
- ZHANG, Q., MA, C., GEARING, M., WANG, P. G., CHIN, L.-S. & LI, L. 2018. Integrated proteomics and network analysis identifies protein hubs and network alterations in Alzheimer's disease. *Acta neuropathologica communications*, 6, 1-19.
- ZHAO, W., ZHAO, T., CHEN, Y., AHOKAS, R. A. & SUN, Y. 2009. Reactive oxygen species promote angiogenesis in the infarcted rat heart. *International journal of experimental pathology*, 90, 621-629.
- ZHONG, H. & SIMONS, J. W. 1999. Direct comparison of GAPDH, β -actin, cyclophilin, and 28S rRNA as internal standards for quantifying RNA levels under hypoxia. *Biochemical and biophysical research communications*, 259, 523-526.
- ZHOU, Q., ANDERSON, C., HANUS, J., ZHAO, F., MA, J., YOSHIMURA, A. & WANG, S. 2016. Strand and cell type-specific function of microRNA-126 in angiogenesis. *Molecular Therapy*, 24, 1823-1835.
- ZICHE, M., MORBIDELLI, L., CHOUDHURI, R., ZHANG, H.-T., DONNINI, S., GRANGER, H. J. & BICKNELL, R. 1997a. Nitric oxide synthase lies downstream from vascular endothelial growth factor-induced but not basic fibroblast growth factor-induced angiogenesis. *Journal of Clinical Investigation*, 99, 2625.
- ZICHE, M., MORBIDELLI, L., MASINI, E., AMERINI, S., GRANGER, H., MAGGI, C., ET AL., GEPPETTI, P. & LEDDA, F. 1994. Nitric oxide mediates angiogenesis in vivo and endothelial cell growth and migration in vitro promoted by substance P. *Journal of Clinical Investigation*, 94, 2036.
- ZICHE, M., PARENTI, A., LEDDA, F., DELL'ERA, P., GRANGER, H. J., MAGGI, C. A. & PRESTA, M. 1997b. Nitric oxide promotes proliferation and plasminogen activator production by coronary venular endothelium through endogenous bFGF. *Circulation Research*, 80, 845-852.
- ZIELLO, J. E., JOVIN, I. S. & HUANG, Y. 2007. Hypoxia-Inducible Factor (HIF)-1 regulatory pathway and its potential for therapeutic intervention in malignancy and ischemia. *The Yale journal of biology and medicine*, 80, 51.
- ZINSER-SIERRA, J. W., RODRÍGUEZ-RAMÍREZ, S., VILLALOBOS-VALENCIA, R. & RAMÍREZ-MÁRQUEZ, M. 2011. Use of Bevacizumab in metastatic colorectal cancer. *Drugs in R & D*, 11, 101-111.
- ZIRLIK, K. & DUYSER, J. 2018. Anti-angiogenics: current situation and future perspectives. *Oncology research and treatment*, 41, 166-171.
- ZOCCALI, C. 2006. Asymmetric dimethylarginine (ADMA): a cardiovascular and renal risk factor on the move. *Journal of hypertension*, 24, 611-619.
- ZUO, L., FAN, Y., WANG, F., GU, Q. & XU, X. 2010. A siRNA targeting vascular endothelial growth factor-A inhibiting experimental corneal neovascularization. *Current eye research*, 35, 375-384.

APPENDICES

Appendix 1. Western blot images of related proteins to ADMA/DDAH/NOS pathway in VeraVec cell lysates.



Western Blot showing basal protein expression in VeraVec endothelial cells.

Endogenous expression of additional proteins potentially involved in the ADMA/DDAH/NOS pathway: (A) DDAH2 (n=1), (B) VEGF-A (n=1), (C) nNOS, representative western blot of three (n=3), and (D) iNOS (n=1), were tested in VeraVec cells by immunoblot analysis.

(A) DDAH2 blot: lane 1: Stably transfected DDAH2-HEK-293T cell lysate used as positive control, Lane 2: Intact HEK293T cell lysate used as negative control, and Lane 3: VeraVec lysate, blotted with DDAH2 antibody (Abcam).

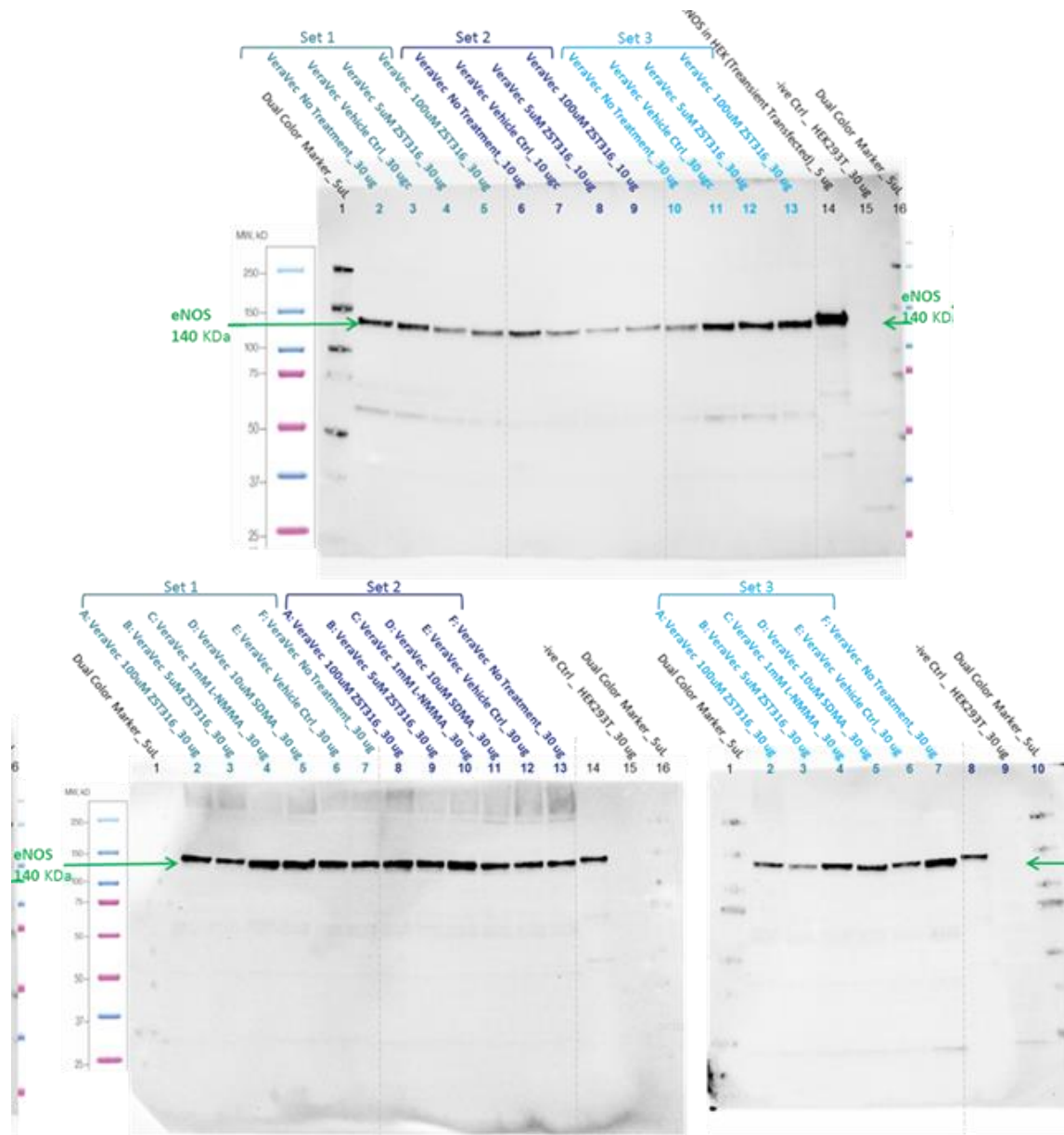
(B) VEGF-A blot, Lane 1: Complete media containing serum used as the positive control, Lane 2: VeraVec lysate, blotted with VEGF-A antibody (US Biological).

(C) Representative nNOS blot of three: lane 1: VeraVec lysate, Lane 2: Transiently transfected nNOS-HEK293T cell lysate used as positive control 1, Lane 3: Intact HEK-293T cell lysate used as negative control, blotted with nNOS antibody (Abcam).

(D) iNOS blot: lane 1: VeraVec lysate, and Lane 2: Stably transfected iNOS-HEK-293T cell lysate used as positive control, blotted with DDAH2 antibody (Santa Cruz).

APPENDICES

Appendix 2. Western blot images of eNOS protein expression in VeraVec cells treated with DDAH1 inhibitor, ZST316, versus non-treated cells.

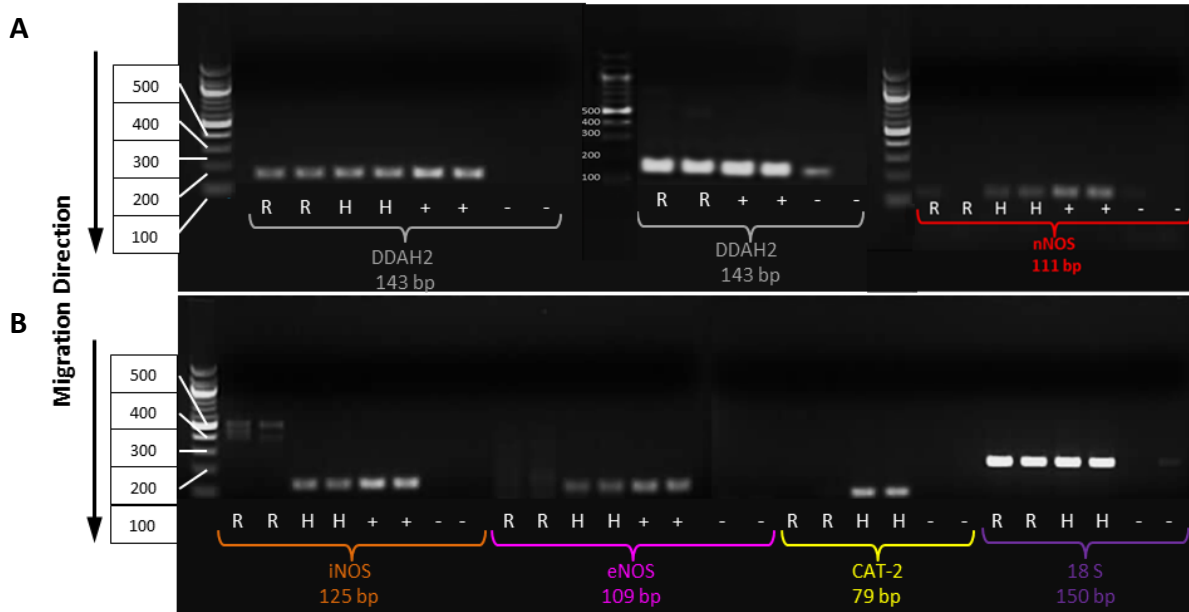


Western blots for eNOS expression demonstrated in treated VeraVec cells with DDAH1 inhibitors.

VeraVec cells from three different batches (set 1, set 2, and set 3) were treated with concentrations of 5 and 100 μM ZST316 (n=6), 1 mM L-NMMA (as positive control for NOS activity inhibition) and 10 μM SDMA (as negative control for NOS activity inhibition) (n=3), for 18 h. The intensities of protein bands were normalised to the total protein.

APPENDICES

Appendix 3. Agarose gel electrophoresis image of cDNA from related genes to ADMA/DDAH/NOS pathway in ARPE-19 cells.

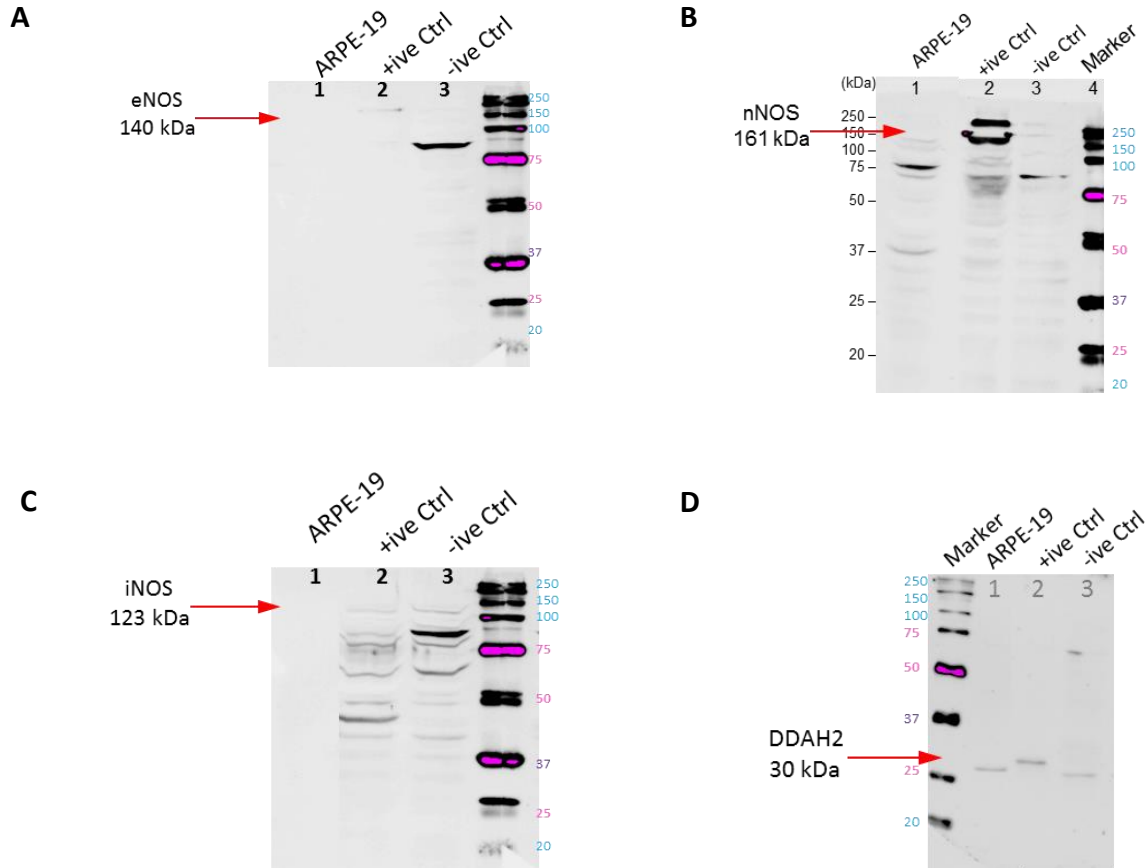


Agarose gel (2%) electrophoresis of PCR amplified cDNA template from ARPE-19 cells.

Gel electrophoresis image of DNA fragments, showing expression of DDAH2 (n=2), nNOS (n=1), iNOS (n=1), eNOS (n=1), CAT-2 (n=1) genes, and 18S housekeeping gene, with reference to 1000bp ladder. “R” represents corresponding cDNA from human RPE cells (ARPE-19), “H” represents cDNA from HEK-293T cells, used as an indicator cell, “+” serves as the positive control where available, which is HEK-293T cells transfected with the gene of interest, and “-” represents negative control, which is the nuclease-free water with the primer. DNA samples for DDAH2, nNOS, iNOS, eNOS, and CAT-2 were loaded on the gel and the presence or absence of the selected genes were visualised and confirmed. Among all, DDAH2 was the only gene that was observed for ARPE-19 cells (similar to HEK-293T and its positive control). Except for DDAH2, none of the other tested genes above were present in ARPE-19 cells. Downward arrows indicate direction of migration of the samples. The expected gene sizes are also indicated below their names.

APPENDICES

Appendix 4. Basal expression of DDAH2 and NOS proteins in ARPE-19 cells.



Qualitative western blot analysis showing basal protein expression in ARPE-19 cells.

Endogenous protein expression of (A) eNOS (n=1), (B) nNOS (n=1), (C) iNOS (n=1), and (D) DDAH2 (n=2), were tested in ARPE-19 cells by immunoblot assays.

(A) eNOS blot: Lane 1, ARPE-19 lysate, lane 2, Stably transfected eNOS-HEK293T cell lysate used as positive control, and lane 3: Intact HEK293T cell lysate used as negative control, blotted with eNOS antibody (Cell Signaling).

(B) nNOS blot: Lane 1, ARPE-19 cell lysate, lane 2, Stably transfected nNOS-HEK293T cell lysate used as positive control, and lane 3, Intact HEK293T cell lysate used as negative control, blotted with nNOS antibody (Abcam).

(C) iNOS blot: : Lane 1, ARPE-19 cell lysate, lane 2, Stably transfected iNOS-HEK293T cell lysate used as positive control, and lane 3, Intact HEK293T cell lysate used as negative control, blotted with nNOS antibody (Santa Cruz).

(D) DDAH2 blot: Lane 1, ARPE-19 cell lysate, lane 2, stably transfected flag-tagged DDAH2-HEK293T cell lysate used as positive control, and lane 3, Intact HEK293T cell lysate used as negative control, blotted with DDAH2 antibody (Abcam).

No eNOS, nNOS (only the final western blot image is shared), or iNOS were detected for ARPE-19 cells. DDAH2 was expressed in ARPE-19 cells, although the controls were not chosen appropriately and are not indicative: positive control (DDAH2-HEK293T stably transfected) was flag-tagged and ran slightly higher than DDAH2 molecular weight of 30kDa, and negative control (intact HEK293T) also expressed DDAH2 (**Refer to Chapter 4 discussion, page 124**).

APPENDICES

A workbook that contains information for Appendices 5 to 9 is available on the link below:

[Supplementary 1 Appendices 5-9 Differentially expressed proteins in ZST316- and vehicle-treated HEK-293T cells.htm](#)

Appendix 5. Differentially expressed proteins with the two biological replicates of vehicle control HEK-293T cells (experiment 1) (Log_2 fold-change ≥ 0.6 , Q-value < 0.05).

Appendix 6. Differentially expressed proteins with 5 μM ZST316 treatment vs. vehicle control in HEK-293T cells (experiment 2) (Log_2 fold-change ≥ 0.6 , Q-value < 0.05).

Appendix 7. Differentially expressed proteins with 100 μM ZST316 treatment vs. vehicle control in HEK-293T cells (experiment 2) (Log_2 fold-change ≥ 0.6 , Q-value < 0.05).

Appendix 8. 23 upregulated proteins that overlapped between 5 and 100 μM ZST316 treatment in HEK-293T cells (Log_2 fold-change ≥ 0.6 , Q-value < 0.05).

Appendix 9. 16 downregulated proteins that overlapped between 5 and 100 μM ZST316-treated HEK-293T cells (Log_2 fold-change ≥ 0.6 , Q-value < 0.05).

APPENDICES

Appendix 10. Identification of significantly (A) upregulated, or (B) downregulated proteins in two biological replicates of vehicle-treated HEK-293T cells (experiment 1) that were present in biological pathways (enriched pathways are marked with an asterisk sign).

A.	InnateDB ID	(Upregulated) Gene Symbol	Pathway Name (Over-representation*)
	503	PNP	Purine metabolism
	558	ASH1L	Lysine degradation
	5713	SIKE1	RIG-I-like receptor signalling pathway
	434	TUBAL3	Pathogenic Escherichia coli infection
	10361	RPP14	RNA transport
	522	ASH1L	Tight junction
	436	TUBAL3	Gap junction
	409	PNP	Pyrimidine metabolism
	8109	null	Vasopressin-regulated water reabsorption
	8110	SLC9A3R2	Aldosterone-regulated sodium reabsorption
	10394	TUBAL3	Phagosome
	496	PNP	Nicotinate and nicotinamide metabolism
B.	InnateDB ID	(Downregulated) Gene Symbol	Pathway Name (Over-representation*)
	4359	MARCKSL1	Fc gamma R-mediated phagocytosis*
	551	COQ5	Ubiquinone and other terpenoid-quinone biosynthesis
	474	MRPS5	Ribosome*
	4386	CHMP4B	Endocytosis
	10394	STX7	Phagosome
	474	RPS3A	Ribosome*
	474	RPS7	Ribosome*
	474	RPS27	Ribosome*
	8120	EFTUD2	Spliceosome*
	10376	UPF2	mRNA surveillance pathway
	4359	MARCKS	Fc gamma R-mediated phagocytosis*
	10361	UPF2	RNA transport
	524	STX7	SNARE interactions in vesicular transport
	8120	PRPF3	Spliceosome*
	474	RPL8	Ribosome*
	8112	SUGT1	NOD-like receptor signalling pathway
	8120	SNRPD2	Spliceosome*
	5710	PAN3	RNA degradation
	10355	MARCKSL1	Leishmaniasis
	474	MRPS6	Ribosome*

APPENDICES

Appendix 11. Identification of significantly (A) upregulated, or (B) downregulated proteins associated with 5 µM ZS316-treated HEK-293T cells that were present in biological pathways (enriched pathways are marked with an asterisk sign).

A.	InnateDB ID	(Upregulated) Gene Symbol	Pathways (Over-representation*)
	563	PPP3CC	T cell receptor signalling pathway
	10367	PPP3CC	Osteoclast differentiation
	594	VDAC3	Calcium signalling pathway*
	10363	CANX	Protein processing in endoplasmic reticulum*
	2805	H2AFY	Systemic lupus erythematosus
	10383	SLC1A5	Protein digestion and absorption
	421	ACP6	Riboflavin metabolism
	2798	PPP3CC	Amyotrophic lateral sclerosis (ALS)
	445	PPP3CC	Wnt signalling pathway*
	4395	EMD	Hypertrophic cardiomyopathy (HCM)
	445	GPC4	Wnt signalling pathway*
	4377	SPIRE1	Dorso-ventral axis formation
	578	PPP3CC	Natural killer cell mediated cytotoxicity
	474	MRPS5	Ribosome
	432	PPP3CC	VEGF signalling pathway
	2812	VDAC3	Parkinson's disease
	493	CANX	Antigen processing and presentation
	8113	PPP3CC	Oocyte meiosis
	532	PPP3CC	B cell receptor signalling pathway
	5714	EMD	Dilated cardiomyopathy
	494	PPP3CC	Axon guidance
	10394	CANX	Phagosome
	10363	RPN1	Protein processing in endoplasmic reticulum*
	4392	VDAC3	Huntington's disease
	594	PPP3CC	Calcium signalling pathway*
	485	PPP3CC	Apoptosis
	487	PPP3CC	MAPK signalling pathway
	507	PPP3CC	Long-term potentiation
	4353	EMD	Arrhythmogenic right ventricular cardiomyopathy (ARVC)
	481	RPN1	N-Glycan biosynthesis
	8110	SLC9A3R2	Aldosterone-regulated sodium reabsorption
	521	PPP3CC	Alzheimer's disease
B.	InnateDB ID	(Downregulated) Gene Symbol	Pathways (Over-representation*)
	461	NRAS	ErbB signalling pathway
	595	NRAS	Melanogenesis
	4397	NRAS	Pathways in cancer
	490	NRAS	Melanoma
	494	NRAS	Axon guidance
	10361	POP4	RNA transport*
	10361	RPP14	RNA transport*

APPENDICES

4389	NRAS	Chemokine signalling pathway
582	NRAS	Chronic myeloid leukemia
483	NRAS	Renal cell carcinoma
487	NRAS	MAPK signalling pathway
4379	NRAS	Neurotrophin signalling pathway
10361	EIF4E2	RNA transport*
491	SNW1	Notch signalling pathway
414	ENO3	Glycolysis / Gluconeogenesis
531	EIF4E2	Insulin signalling pathway*
8120	SNW1	Spliceosome
4386	VPS45	Endocytosis
10404	NRAS	Hepatitis C
405	EIF4E2	mTOR signalling pathway
501	TAF2	Basal transcription factors
523	NRAS	Glioma
5710	ENO3	RNA degradation*
522	NRAS	Tight junction
558	SETMAR	Lysine degradation
531	NRAS	Insulin signalling pathway*
532	NRAS	B cell receptor signalling pathway
507	NRAS	Long-term potentiation
404	NRAS	Regulation of actin cytoskeleton
506	NRAS	Endometrial cancer
500	NRAS	Thyroid cancer
412	NRAS	GnRH signalling pathway
514	NRAS	Bladder cancer
563	NRAS	T cell receptor signalling pathway
424	NRAS	Acute myeloid leukemia
5710	PAN3	RNA degradation*
578	NRAS	Natural killer cell mediated cytotoxicity
432	NRAS	VEGF signalling pathway
436	NRAS	Gap junction
435	NRAS	Fc epsilon RI signalling pathway
544	NRAS	Prostate cancer
444	NRAS	Non-small cell lung cancer
555	NRAS	Long-term depression

APPENDICES

Appendix 12. Identification of significantly (A) upregulated, or (B) downregulated proteins associated with 100 μ M ZS316-treated HEK-293T cells that were present in biological pathways (enriched pathways are marked with an asterisk sign).

A.	InnateDB ID	(Upregulated) Gene Symbol	Pathway Name (Over-representation*)
	10367	PPP3CC	Osteoclast differentiation
	532	BCL10	B cell receptor signalling pathway*
	578	PRKCB	Natural killer cell mediated cytotoxicity*
	2798	PPP3CC	Amyotrophic lateral sclerosis (ALS)
	546	PRKCB	Focal adhesion
	412	PRKCB	GnRH signalling pathway
	405	PRKCB	mTOR signalling pathway
	4377	SPIRE1	Dorso-ventral axis formation
	555	PRKCB	Long-term depression
	420	PRKCB	Vibrio cholerae infection
	503	PDE6D	Purine metabolism*
	432	PRKCB	VEGF signalling pathway*
	435	PRKCB	Fc epsilon RI signalling pathway
	528	PRKCB	Phosphatidylinositol signalling system
	532	PPP3CC	B cell receptor signalling pathway*
	532	PRKCB	B cell receptor signalling pathway*
	513	PTS	Folate biosynthesis
	445	PRKCB	Wnt signalling pathway*
	444	PRKCB	Non-small cell lung cancer
	531	PTPRF	Insulin signalling pathway
	436	PRKCB	Gap junction
	503	PNP	Purine metabolism*
	507	PRKCB	Long-term potentiation*
	507	PPP3CC	Long-term potentiation*
	510	PRKCB	Leukocyte transendothelial migration
	505	PTPRF	Adherens junction
	409	PNP	Pyrimidine metabolism
	461	PRKCB	ErbB signalling pathway
	523	PRKCB	Glioma
	522	PRKCB	Tight junction
	521	PPP3CC	Alzheimer's disease
	563	PPP3CC	T cell receptor signalling pathway*
	8110	PRKCB	Aldosterone-regulated sodium reabsorption
	4397	PRKCB	Pathways in cancer
	487	PRKCB	MAPK signalling pathway*
	445	PPP3CC	Wnt signalling pathway*
	4389	PRKCB	Chemokine signalling pathway
	487	LAMTOR3	MAPK signalling pathway*
	10384	PRKCB	African trypanosomiasis
	10389	PRKCB	Carbohydrate digestion and absorption
	4376	PRKCB	Vascular smooth muscle contraction

APPENDICES

578	PPP3CC	Natural killer cell mediated cytotoxicity*
10370	PRKCB	Pancreatic secretion
432	PPP3CC	VEGF signalling pathway*
10375	PRKCB	Salivary secretion
8113	PPP3CC	Oocyte meiosis
563	BCL10	T cell receptor signalling pathway*
4359	PRKCB	Fc gamma R-mediated phagocytosis
10358	PRKCB	Amoebiasis
494	PPP3CC	Axon guidance
10355	PRKCB	Leishmaniasis
10356	PRKCB	Gastric acid secretion
594	PPP3CC	Calcium signalling pathway
485	PPP3CC	Apoptosis
487	PPP3CC	MAPK signalling pathway*
595	PRKCB	Melanogenesis
594	PRKCB	Calcium signalling pathway
440	PTPRF	Cell adhesion molecules (CAMs)
496	PNP	Nicotinate and nicotinamide metabolism
B.	InnateDB ID	(Downregulated) Gene Symbol
		Pathway Name (Over-representation*)
519	CUL5	Ubiquitin mediated proteolysis
509	POLR3K	RNA polymerase
503	POLR3K	Purine metabolism
491	SNW1	Notch signalling pathway
8117	POLR3K	Cytosolic DNA-sensing pathway
409	UPP1	Pyrimidine metabolism*
2810	UPP1	Drug metabolism
8120	SNW1	Spliceosome*
8120	EFTUD2	Spliceosome*
522	MAGI3	Tight junction
558	SETMAR	Lysine degradation
5710	PAN3	RNA degradation
409	POLR3K	Pyrimidine metabolism*
474	RPS29	Ribosome*
474	RPS20	Ribosome*
588	HLCS	Biotin metabolism
8120	RBM22	Spliceosome*

APPENDICES

Appendix 13. Uniprot IDs of 23 upregulated proteins that overlapped between 5 and 100 μ M ZST316 treatment in HEK-293T cells, conversion to Entrez genes using DAVID database tool.

Table A. Gene symbols of the differentially expressed proteins. Within the 23 Uniprot IDs, one was not linked with any gene (marked with an asterisk sign) and therefore it could not be used in the inversion step.

UniProt Ids	Genes
B0I1T6	MYO9B
A0A024R9A3	hCG_21651
A0A087WT84	JMJD4
58FF6	HSP90AB4P
B3KVE3*	N/A
B7Z481	PDLIM5
O95865	DDAH2
A8K2P3	RASAL2
B4DRJ1	HACL1
A0A1B0GWA0	ZNF654
A0A1B0GV93	HSD17B12
E9PK54	HSPA8
A0A024RCQ6	FKBPL
A0A024QYV5	PRKRIP1
Q9UJT0	TUBE1
A0A024R719	SLC7A6
A0A024R1Y6	PALM
A0A024RDM4	MRP63
P48454	PPP3CC
Q08AE8	SPIRE1
A0A024R6W0	GOT2
A0A024RD41	RAB23
B4DGK8	PTPMT1

Table B. Summary of inversion of gene symbols to Entrez genes in DAVID database. Within the 22 genes, 20 existed in DAVID database, while 2 genes were not found.

Inversion Summary		
ID Count	In DAVID Database	Conversion
<u>20</u>	Yes	Successful
0	Yes	None
<u>2</u>	No	None
0	Ambiguous	Pending
Total Unique User IDs: 22		

APPENDICES

Table C. DAVID conversion. 20 genes were converted to entrez genes using DAVID database.

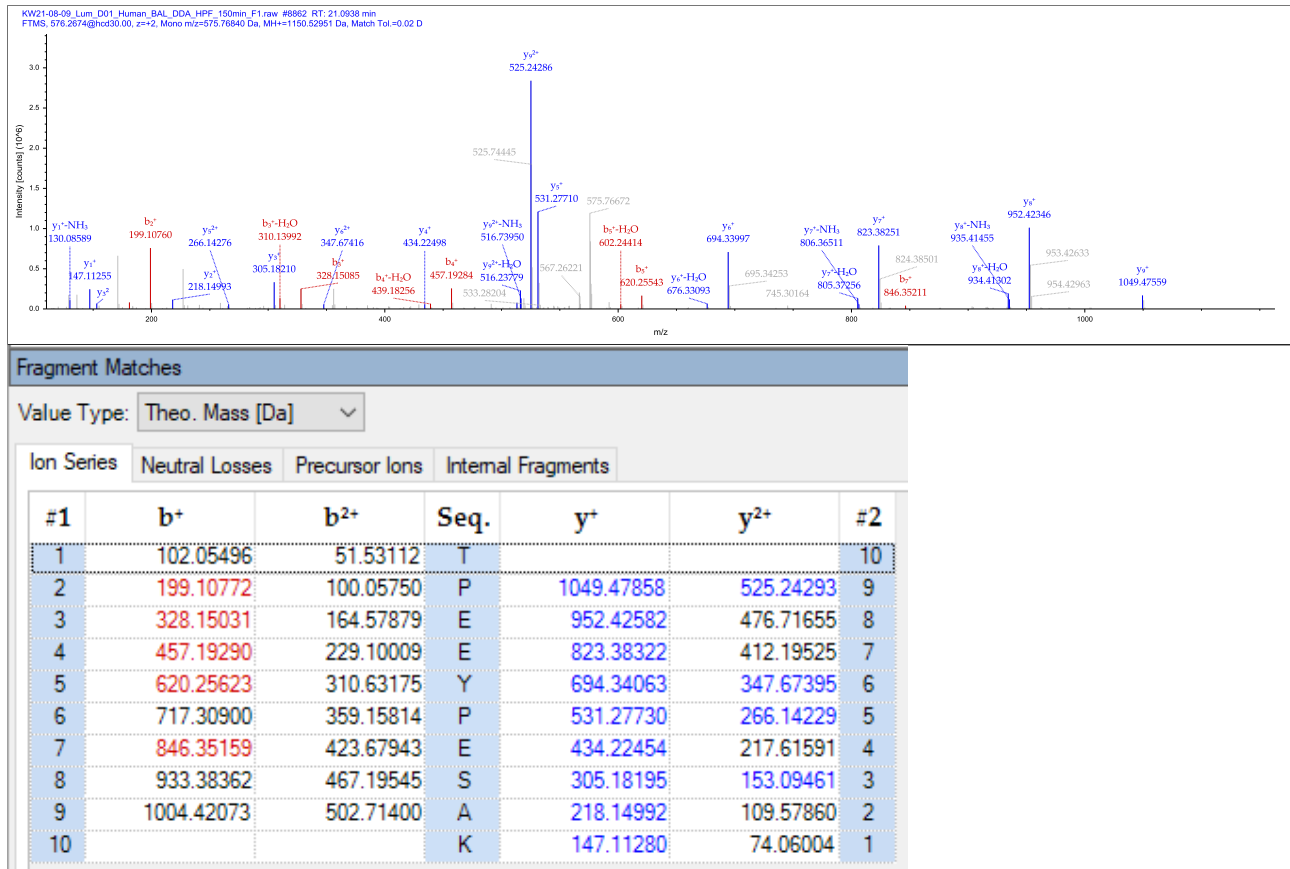
From	To	Species	David Gene Name
JMJD4	65094	Homo sapiens	jumonji domain containing 4(JMJD4)
HSPA8	3312	Homo sapiens	heat shock protein family A (Hsp70) member 8(HSPA8)
HSP90AB4P	664618	Homo sapiens	heat shock protein 90 alpha family class B member 4, pseudogene(HSP90AB4P)
FKBPL	63943	Homo sapiens	FK506 binding protein like(FKBPL)
PRKRIP1	79706	Homo sapiens	PRKR interacting protein 1 (IL11 inducible)(PRKRIP1)
GOT2	2806	Homo sapiens	glutamic-oxaloacetic transaminase 2(GOT2)
TUBE1	51175	Homo sapiens	tubulin epsilon 1(TUBE1)
MYO9B	4650	Homo sapiens	myosin IXB(MYO9B)
RASAL2	9462	Homo sapiens	RAS protein activator like 2(RASAL2)
HSD17B12	51144	Homo sapiens	hydroxysteroid 17-beta dehydrogenase 12(HSD17B12)
SLC7A6	9057	Homo sapiens	solute carrier family 7 member 6(SLC7A6)
PPP3CC	5533	Homo sapiens	protein phosphatase 3 catalytic subunit gamma(PPP3CC)
DDAH2	23564	Homo sapiens	dimethylarginine dimethylaminohydrolase 2(DDAH2)
PTPMT1	114971	Homo sapiens	protein tyrosine phosphatase, mitochondrial 1(PTPMT1)
RAB23	51715	Homo sapiens	RAB23, member RAS oncogene family(RAB23)
PALM	5064	Homo sapiens	paralemmin(PALM)
SPIRE1	56907	Homo sapiens	spire type actin nucleation factor 1(SPIRE1)
HACL1	26061	Homo sapiens	2-hydroxyacyl-CoA lyase 1(HACL1)
ZNF654	55279	Homo sapiens	zinc finger protein 654(ZNF654)
PDLIM5	10611	Homo sapiens	PDZ and LIM domain 5(PDLIM5)

APPENDICES

Appendix 14. Representative spectra of two peptides from (A) DDAH1 and (B) DDAH2.

To provide an indication of the quality of spectra generated by DDA analysis, spectra of two peptides from both DDAH1 and DDAH2 are shown including the sequence of each peptide, fragment ion matching table, MS2 ion window, and basic search settings. Note that the quality of spectra is high despite these peptides being derived from very low abundance proteins.

DDAH1 peptides:



DDAH1 peptide 1 spectra by DDA analysis.

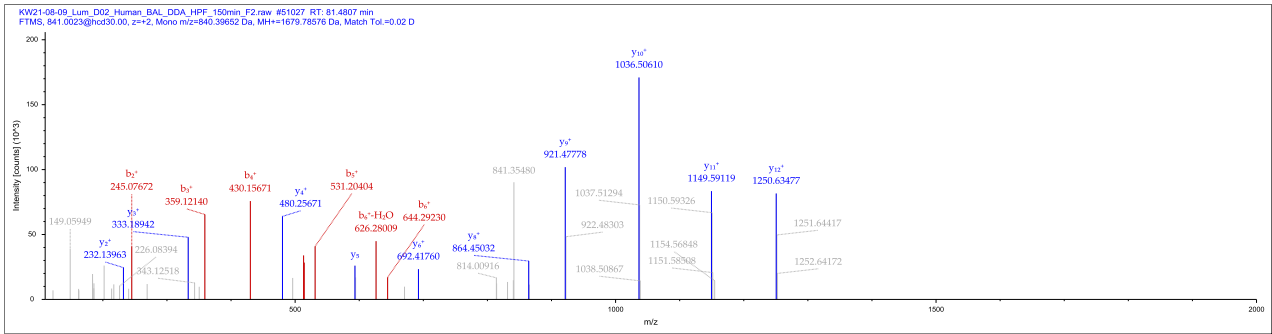
Peptide Sequence: TPEEYPSAK, Charge: +2, Monoisotopic m/z: 575.76840 Da (+1.63 mmu/+2.83 ppm), MH⁺: 1150.52951 Da, RT: 21.0938 min,

Identified with: Sequest HT (v1.17); XCorr: 3.18, Percolator Q-value: 1.1e-4, Percolator PEP: 6.6e-5,

Fragment match tolerance used for search: 0.02 Da

Fragments used for search: -H₂O; y; -NH₃; y; b; b; -H₂O; y.

APPENDICES



Fragment Matches								
Value Type: Theo. Mass [Da]								
Ion Series	Neutral Losses	Precursor Ions	Internal Fragments					
#1	b ⁺	b ²⁺	b ³⁺	Seq.	y ⁺	y ²⁺	y ³⁺	#2
1	116.03422	58.52075	39.34959	D				16
2	245.07681	123.04204	82.36379	E	1564.76018	782.88373	522.25824	15
3	359.11974	180.06351	120.37810	N	1435.71758	718.36243	479.24405	14
4	430.15685	215.58207	144.05714	A	1321.67466	661.34097	441.22974	13
5	531.20453	266.10590	177.73970	T	1250.63754	625.82241	417.55070	12
6	644.28860	322.64794	215.43438	L	1149.58986	575.29857	383.86814	11
7	759.31554	380.16141	253.77670	D	1036.50580	518.75654	346.17345	10
8	816.33700	408.67214	272.78385	G	921.47886	461.24307	307.83114	9
9	873.35847	437.18287	291.79101	G	864.45739	432.73233	288.82398	8
10	988.38541	494.69634	330.13332	D	807.43593	404.22160	269.81683	7
11	1087.45382	544.23055	363.15613	V	692.40899	346.70813	231.47451	6
12	1200.53789	600.77258	400.85081	L	593.34057	297.17392	198.45171	5
13	1347.60630	674.30679	449.87362	F	480.25651	240.63189	160.75702	4
14	1448.65398	724.83063	483.55618	T	333.18809	167.09769	111.73422	3
15	1505.67544	753.34136	502.56333	G	232.14042	116.57385	78.05166	2
16				R	175.11895	88.06311	59.04450	1

DDAH1 peptide 2 spectra by DDA analysis.

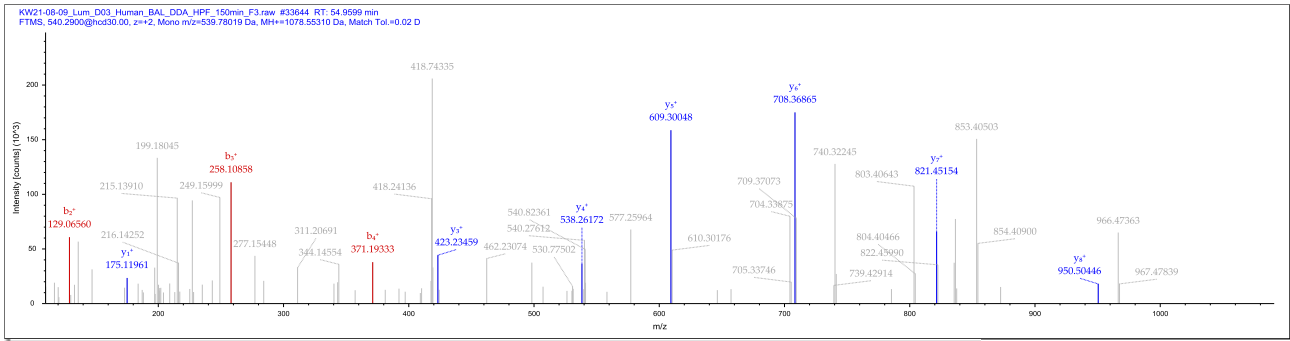
Peptide Sequence: DENATLDGGDVLFTGR, Charge: +2, Monoisotopic m/z: 840.39652 Da (-0.68 mmu/-0.81 ppm), MH+: 1679.78576 Da, RT: 81.4807 min,

Identified with: Sequest HT (v1.17); XCorr: 3.15, Percolator Q-value: 1.1e-4, Percolator PEP: 2.4e-6,

Fragment match tolerance used for search: 0.02 Da

Fragments used for search: -H₂O; y; -NH₃; y; b; b; -H₂O; b; -NH₃; y.

APPENDICES



Fragment Matches						
Value Type: Theo. Mass [Da] ▼						
Ion Series	Neutral Losses	Precursor Ions	Internal Fragments			
#1	b ⁺	b ²⁺	Seq.	y ⁺	y ²⁺	#2
1	58.02874	29.51801	G			10
2	129.06585	65.03657	A	1021.53129	511.26928	9
3	258.10845	129.55786	E	950.49417	475.75072	8
4	371.19251	186.09989	I	821.45158	411.22943	7
5	470.26092	235.63410	V	708.36752	354.68740	6
6	541.29804	271.15266	A	609.29910	305.15319	5
7	656.32498	328.66613	D	538.26199	269.63463	4
8	757.37266	379.18997	T	423.23504	212.12116	3
9	904.44107	452.72418	F	322.18737	161.59732	2
10			R	175.11895	88.06311	1

DDAH2 peptide 2 spectra by DDA analysis.

Peptide Sequence: GAEIVADTFR, Charge: +2, Monoisotopic m/z: 539.78019 Da (+0.17 mmu/+0.32 ppm), MH⁺: 1078.55310 Da, RT: 54.9599 min,

Identified with: Sequest HT (v1.17); XCorr: 2.23, Percolator Q-value: 2.5e-4, Percolator PEP: 1.0e-3,

Fragment match tolerance used for search: 0.02 Da

Fragments used for search: -H₂O; y; -NH₃; y; b; b; -H₂O; y.

APPENDICES

530.4910175-534.4928365
534.4928365-538.4946555
538.4946555-542.4964745
542.4964745-546.4982935
546.4982935-550.5001125
550.5001125-554.5019315
554.5019315-558.5037505
558.5037505-562.5055695
562.5055695-566.5073885
566.5073885-570.5092075
570.5092075-574.5110265
574.5110265-578.5128455
578.5128455-582.5146645
582.5146645-586.5164835
586.5164835-590.5183025
590.5183025-594.5201215
594.5201215-598.5219405
598.5219405-602.5237595

Experiment#4 [MS Full]

Start Time (min): **5**

End Time (min): **150**

Master Scan:

Full Scan

Orbitrap Resolution: **60000**

Scan Range (m/z): **350-1200**

RF Lens (%): **50**

AGC Target: **Custom**

Normalized AGC Target (%): **300**

Maximum Injection Time Mode: **Custom**

Maximum Injection Time (ms): **100**

Microscans: **1**

Data Type: **Profile**

Polarity: **Positive**

Source Fragmentation: **Disabled**

Scan Description:

Experiment#5 [MS 490-610 mz]

Start Time (min): **5**

End Time (min): **150**

Master Scan:

Full Scan

Orbitrap Resolution: **60000**

Scan Range (m/z): **490-610**

RF Lens (%): **40**

AGC Target: **Custom**

Normalized AGC Target (%): **300**

APPENDICES

Maximum Injection Time Mode: **Custom**

Maximum Injection Time (ms): **100**

Microscans: **1**

Data Type: **Profile**

Polarity: **Positive**

Source Fragmentation: **Disabled**

Scan Description:

Experiment#6 [DIA 4mz windows - 500-604 mz]

Start Time (min): **5**

End Time (min): **150**

Master Scan:

DIA

Precursor Mass Range: **500-604**

Multiplex Ions: **False**

Isolation Window (m/z): **4**

Window Overlap (m/z): **0**

Window Placement Optimization: **On**

Mass Defect: **1.0005**

Number Of Scan Events: **25**

Collision Energy Mode: **Fixed**

Collision Energy Type: **Normalized**

Collision Energy (%): **28**

Orbitrap Resolution: **30000**

Scan Range Mode: **Define First Mass**

First Mass (m/z): **110**

RF Lens (%): **70**

AGC Target: **Custom**

Normalized AGC Target (%): **100**

Maximum Injection Time Mode: **Custom**

Maximum Injection Time (ms): **60**

Microscans: **1**

Data Type: **Centroid**

Polarity: **Positive**

Source Fragmentation: **Disabled**

Loop Control: **All**

Scan Description:

DIA m/z window

DIA m/z window
Calculated m/z Window
500.477375-504.479194
504.479194-508.481013
508.481013-512.482832
512.482832-516.484651
516.484651-520.48647
520.48647-524.488289

APPENDICES

524.488289-528.490108
528.490108-532.491927
532.491927-536.493746
536.493746-540.495565
540.495565-544.497384
544.497384-548.499203
548.499203-552.501022
552.501022-556.502841
556.502841-560.50466
560.50466-564.506479
564.506479-568.508298
568.508298-572.510117
572.510117-576.511936
576.511936-580.513755
580.513755-584.515574
584.515574-588.517393
588.517393-592.519212
592.519212-596.521031
596.521031-600.52285
600.52285-604.524669

150min_300nL-GPS_DIA_598-704mz

Method Summary

Method Settings

Application Mode: **Peptide**Method Duration (min): **150**

Global Parameters

Ion Source

Use Ion Source Settings from Tune: **True**FAIMS Mode: **Not Installed**

MS Global Settings

Infusion Mode: **Liquid Chromatography**Expected LC Peak Width (s): **30**Advanced Peak Determination: **True**Default Charge State: **3**Internal Mass Calibration: **Off**

Experiment#1 [MS Full]

Start Time (min): **5**End Time (min): **150**

Master Scan:

Full Scan

Orbitrap Resolution: **60000**Scan Range (m/z): **350-1200**RF Lens (%): **50**AGC Target: **Custom**Normalized AGC Target (%): **300**Maximum Injection Time Mode: **Custom**Maximum Injection Time (ms): **100**Microscans: **1**Data Type: **Profile**Polarity: **Positive**Source Fragmentation: **Disabled**

Scan Description:

Experiment#2 [MS 590-710 mz]

Start Time (min): **5**End Time (min): **150**

Master Scan:

Full Scan

Orbitrap Resolution: **60000**Scan Range (m/z): **590-710**RF Lens (%): **40**AGC Target: **Custom**Normalized AGC Target (%): **300**Maximum Injection Time Mode: **Custom**Maximum Injection Time (ms): **100**

APPENDICES

Microscans: **1**
 Data Type: **Profile**
 Polarity: **Positive**
 Source Fragmentation: **Disabled**

Scan Description:
 Experiment#3 [DIA 4mz windows - 598-702 mz]
 Start Time (min): **5**
 End Time (min): **150**

Master Scan:

DIA

Precursor Mass Range: **598-702**
 Multiplex Ions: **False**
 Isolation Window (m/z): **4**
 Window Overlap (m/z): **0**
 Window Placement Optimization: **On**
 Mass Defect: **1.0005**
 Number Of Scan Events: **25**
 Collision Energy Mode: **Fixed**
 Collision Energy Type: **Normalized**
 Collision Energy (%): **28**
 Orbitrap Resolution: **30000**
 Scan Range Mode: **Define First Mass**
 First Mass (m/z): **110**
 RF Lens (%): **70**
 AGC Target: **Custom**
 Normalized AGC Target (%): **100**
 Maximum Injection Time Mode: **Custom**
 Maximum Injection Time (ms): **60**
 Microscans: **1**
 Data Type: **Centroid**
 Polarity: **Positive**
 Source Fragmentation: **Disabled**
 Loop Control: **All**
 Scan Description:

DIA m/z window

DIA m/z window
Calculated m/z Window
598.5219405-602.5237595
602.5237595-606.5255785
606.5255785-610.5273975
610.5273975-614.5292165
614.5292165-618.5310355
618.5310355-622.5328545
622.5328545-626.5346735
626.5346735-630.5364925

APPENDICES

630.5364925-634.5383115
634.5383115-638.5401305
638.5401305-642.5419495
642.5419495-646.5437685
646.5437685-650.5455875
650.5455875-654.5474065
654.5474065-658.5492255
658.5492255-662.5510445
662.5510445-666.5528635
666.5528635-670.5546825
670.5546825-674.5565015
674.5565015-678.5583205
678.5583205-682.5601395
682.5601395-686.5619585
686.5619585-690.5637775
690.5637775-694.5655965
694.5655965-698.5674155
698.5674155-702.5692345

Experiment#4 [MS Full]

Start Time (min): **5**

End Time (min): **150**

Master Scan:

Full Scan

Orbitrap Resolution: **60000**

Scan Range (m/z): **350-1200**

RF Lens (%): **50**

AGC Target: **Custom**

Normalized AGC Target (%): **300**

Maximum Injection Time Mode: **Custom**

Maximum Injection Time (ms): **100**

Microscans: **1**

Data Type: **Profile**

Polarity: **Positive**

Source Fragmentation: **Disabled**

Scan Description:

Experiment#5 [MS 590-710]

Start Time (min): **5**

End Time (min): **150**

Master Scan:

Full Scan

Orbitrap Resolution: **60000**

Scan Range (m/z): **590-710**

RF Lens (%): **40**

AGC Target: **Custom**

Normalized AGC Target (%): **300**

APPENDICES

Maximum Injection Time Mode: **Custom**

Maximum Injection Time (ms): **100**

Microscans: **1**

Data Type: **Profile**

Polarity: **Positive**

Source Fragmentation: **Disabled**

Scan Description:

Experiment#6 [DIA 4mz windows - 600-704]

Start Time (min): **5**

End Time (min): **150**

Master Scan:

DIA

Precursor Mass Range: **600-704**

Multiplex Ions: **False**

Isolation Window (m/z): **4**

Window Overlap (m/z): **0**

Window Placement Optimization: **On**

Mass Defect: **1.0005**

Number Of Scan Events: **25**

Collision Energy Mode: **Fixed**

Collision Energy Type: **Normalized**

Collision Energy (%): **28**

Orbitrap Resolution: **30000**

Scan Range Mode: **Define First Mass**

First Mass (m/z): **110**

RF Lens (%): **70**

AGC Target: **Custom**

Normalized AGC Target (%): **100**

Maximum Injection Time Mode: **Custom**

Maximum Injection Time (ms): **60**

Microscans: **1**

Data Type: **Centroid**

Polarity: **Positive**

Source Fragmentation: **Disabled**

Loop Control: **All**

Scan Description:

DIA m/z window

DIA m/z window
Calculated m/z Window
600.52285-604.524669
604.524669-608.526488
608.526488-612.528307
612.528307-616.530126
616.530126-620.531945
620.531945-624.533764

APPENDICES

624.533764-628.535583
628.535583-632.537402
632.537402-636.539221
636.539221-640.54104
640.54104-644.542859
644.542859-648.544678
648.544678-652.546497
652.546497-656.548316
656.548316-660.550135
660.550135-664.551954
664.551954-668.553773
668.553773-672.555592
672.555592-676.557411
676.557411-680.55923
680.55923-684.561049
684.561049-688.562868
688.562868-692.564687
692.564687-696.566506
696.566506-700.568325
700.568325-704.570144

150min_300nL-GPS_DIA_698-804mz

Method Summary

Method Settings

Application Mode: **Peptide**

Method Duration (min): **150**

Global Parameters

Ion Source

Use Ion Source Settings from Tune: **True**

FAIMS Mode: **Not Installed**

MS Global Settings

Infusion Mode: **Liquid Chromatography**

Expected LC Peak Width (s): **30**

Advanced Peak Determination: **True**

Default Charge State: **3**

Internal Mass Calibration: **Off**

Experiment#1 [MS Full]

Start Time (min): **5**

End Time (min): **150**

Master Scan:

Full Scan

Orbitrap Resolution: **60000**

Scan Range (m/z): **350-1200**

RF Lens (%): **50**

APPENDICES

AGC Target: **Custom**
Normalized AGC Target (%): **300**
Maximum Injection Time Mode: **Custom**
Maximum Injection Time (ms): **100**
Microscans: **1**
Data Type: **Profile**
Polarity: **Positive**
Source Fragmentation: **Disabled**

Scan Description:

Experiment#2 [MS 690-810 mz]

Start Time (min): **5**

End Time (min): **150**

Master Scan:

Full Scan

Orbitrap Resolution: **60000**
Scan Range (m/z): **690-810**
RF Lens (%): **40**
AGC Target: **Custom**
Normalized AGC Target (%): **300**
Maximum Injection Time Mode: **Custom**
Maximum Injection Time (ms): **100**
Microscans: **1**
Data Type: **Profile**
Polarity: **Positive**
Source Fragmentation: **Disabled**

Scan Description:

Experiment#3 [DIA 4mz windows - 698-802 mz]

Start Time (min): **5**

End Time (min): **150**

Master Scan:

DIA

Precursor Mass Range: **698-802**
Multiplex Ions: **False**
Isolation Window (m/z): **4**
Window Overlap (m/z): **0**
Window Placement Optimization: **On**
Mass Defect: **1.0005**
Number Of Scan Events: **25**
Collision Energy Mode: **Fixed**
Collision Energy Type: **Normalized**
Collision Energy (%): **28**
Orbitrap Resolution: **30000**
Scan Range Mode: **Define First Mass**
First Mass (m/z): **110**
RF Lens (%): **70**

APPENDICES

AGC Target: **Custom**
 Normalized AGC Target (%): **100**
 Maximum Injection Time Mode: **Custom**
 Maximum Injection Time (ms): **60**
 Microscans: **1**
 Data Type: **Centroid**
 Polarity: **Positive**
 Source Fragmentation: **Disabled**
 Loop Control: **All**
 Scan Description:

DIA m/z window

DIA m/z window
Calculated m/z Window
698.5674155-702.5692345
702.5692345-706.5710535
706.5710535-710.5728725
710.5728725-714.5746915
714.5746915-718.5765105
718.5765105-722.5783295
722.5783295-726.5801485
726.5801485-730.5819675
730.5819675-734.5837865
734.5837865-738.5856055
738.5856055-742.5874245
742.5874245-746.5892435
746.5892435-750.5910625
750.5910625-754.5928815
754.5928815-758.5947005
758.5947005-762.5965195
762.5965195-766.5983385
766.5983385-770.6001575
770.6001575-774.6019765
774.6019765-778.6037955
778.6037955-782.6056145
782.6056145-786.6074335
786.6074335-790.6092525
790.6092525-794.6110715
794.6110715-798.6128905
798.6128905-802.6147095

Experiment#4 [MS Full]

Start Time (min): **5**
 End Time (min): **150**

Master Scan:

Full Scan

Orbitrap Resolution: **60000**

APPENDICES

Scan Range (m/z): **350-1200**
RF Lens (%): **50**
AGC Target: **Custom**
Normalized AGC Target (%): **300**
Maximum Injection Time Mode: **Custom**
Maximum Injection Time (ms): **100**
Microscans: **1**
Data Type: **Profile**
Polarity: **Positive**
Source Fragmentation: **Disabled**

Scan Description:

Experiment#5 [MS 690-810]

Start Time (min): **5**

End Time (min): **150**

Master Scan:

Full Scan

Orbitrap Resolution: **60000**
Scan Range (m/z): **690-810**
RF Lens (%): **40**
AGC Target: **Custom**
Normalized AGC Target (%): **300**
Maximum Injection Time Mode: **Custom**
Maximum Injection Time (ms): **100**
Microscans: **1**
Data Type: **Profile**
Polarity: **Positive**
Source Fragmentation: **Disabled**

Scan Description:

Experiment#6 [DIA 4mz windows - 700-804]

Start Time (min): **5**

End Time (min): **150**

Master Scan:

DIA

Precursor Mass Range: **700-804**
Multiplex Ions: **False**
Isolation Window (m/z): **4**
Window Overlap (m/z): **0**
Window Placement Optimization: **On**
Mass Defect: **1.0005**
Number Of Scan Events: **25**
Collision Energy Mode: **Fixed**
Collision Energy Type: **Normalized**
Collision Energy (%): **28**
Orbitrap Resolution: **30000**
Scan Range Mode: **Define First Mass**

APPENDICES

First Mass (m/z): **110**
 RF Lens (%): **70**
 AGC Target: **Custom**
 Normalized AGC Target (%): **100**
 Maximum Injection Time Mode: **Custom**
 Maximum Injection Time (ms): **60**
 Microscans: **1**
 Data Type: **Centroid**
 Polarity: **Positive**
 Source Fragmentation: **Disabled**
 Loop Control: **All**
 Scan Description:

DIA m/z window

DIA m/z window
Calculated m/z Window
700.568325-704.570144
704.570144-708.571963
708.571963-712.573782
712.573782-716.575601
716.575601-720.57742
720.57742-724.579239
724.579239-728.581058
728.581058-732.582877
732.582877-736.584696
736.584696-740.586515
740.586515-744.588334
744.588334-748.590153
748.590153-752.591972
752.591972-756.593791
756.593791-760.59561
760.59561-764.597429
764.597429-768.599248
768.599248-772.601067
772.601067-776.602886
776.602886-780.604705
780.604705-784.606524
784.606524-788.608343
788.608343-792.610162
792.610162-796.611981
796.611981-800.6138
800.6138-804.615619

150min_300nL-GPS_DIA_798-904mz

Method Summary
 Method Settings

APPENDICES

Application Mode: **Peptide**

Method Duration (min): **150**

Global Parameters

Ion Source

Use Ion Source Settings from Tune: **True**

FAIMS Mode: **Not Installed**

MS Global Settings

Infusion Mode: **Liquid Chromatography**

Expected LC Peak Width (s): **30**

Advanced Peak Determination: **True**

Default Charge State: **3**

Internal Mass Calibration: **Off**

Experiment#1 [MS Full]

Start Time (min): **5**

End Time (min): **150**

Master Scan:

Full Scan

Orbitrap Resolution: **60000**

Scan Range (m/z): **350-1200**

RF Lens (%): **50**

AGC Target: **Custom**

Normalized AGC Target (%): **300**

Maximum Injection Time Mode: **Custom**

Maximum Injection Time (ms): **100**

Microscans: **1**

Data Type: **Profile**

Polarity: **Positive**

Source Fragmentation: **Disabled**

Scan Description:

Experiment#2 [MS 790-910 m/z]

Start Time (min): **5**

End Time (min): **150**

Master Scan:

Full Scan

Orbitrap Resolution: **60000**

Scan Range (m/z): **790-910**

RF Lens (%): **40**

AGC Target: **Custom**

Normalized AGC Target (%): **300**

Maximum Injection Time Mode: **Custom**

Maximum Injection Time (ms): **100**

Microscans: **1**

Data Type: **Profile**

Polarity: **Positive**

Source Fragmentation: **Disabled**

APPENDICES

Scan Description:

Experiment#3 [DIA 4mz windows - 798-902 mz]

Start Time (min): **5**

End Time (min): **150**

Master Scan:

DIA

Precursor Mass Range: **798-902**

Multiplex Ions: **False**

Isolation Window (m/z): **4**

Window Overlap (m/z): **0**

Window Placement Optimization: **On**

Mass Defect: **1.0005**

Number Of Scan Events: **25**

Collision Energy Mode: **Fixed**

Collision Energy Type: **Normalized**

Collision Energy (%): **28**

Orbitrap Resolution: **30000**

Scan Range Mode: **Define First Mass**

First Mass (m/z): **110**

RF Lens (%): **70**

AGC Target: **Custom**

Normalized AGC Target (%): **100**

Maximum Injection Time Mode: **Custom**

Maximum Injection Time (ms): **60**

Microscans: **1**

Data Type: **Centroid**

Polarity: **Positive**

Source Fragmentation: **Disabled**

Loop Control: **All**

Scan Description:

DIA m/z window

DIA m/z window
Calculated m/z Window
798.6128905-802.6147095
802.6147095-806.6165285
806.6165285-810.6183475
810.6183475-814.6201665
814.6201665-818.6219855
818.6219855-822.6238045
822.6238045-826.6256235
826.6256235-830.6274425
830.6274425-834.6292615
834.6292615-838.6310805
838.6310805-842.6328995
842.6328995-846.6347185

APPENDICES

846.6347185-850.6365375
850.6365375-854.6383565
854.6383565-858.6401755
858.6401755-862.6419945
862.6419945-866.6438135
866.6438135-870.6456325
870.6456325-874.6474515
874.6474515-878.6492705
878.6492705-882.6510895
882.6510895-886.6529085
886.6529085-890.6547275
890.6547275-894.6565465
894.6565465-898.6583655
898.6583655-902.6601845

Experiment#4 [MS Full]

Start Time (min): **5**

End Time (min): **150**

Master Scan:

Full Scan

Orbitrap Resolution: **60000**

Scan Range (m/z): **350-1200**

RF Lens (%): **50**

AGC Target: **Custom**

Normalized AGC Target (%): **300**

Maximum Injection Time Mode: **Custom**

Maximum Injection Time (ms): **100**

Microscans: **1**

Data Type: **Profile**

Polarity: **Positive**

Source Fragmentation: **Disabled**

Scan Description:

Experiment#5 [MS 790-910]

Start Time (min): **5**

End Time (min): **150**

Master Scan:

Full Scan

Orbitrap Resolution: **60000**

Scan Range (m/z): **790-910**

RF Lens (%): **40**

AGC Target: **Custom**

Normalized AGC Target (%): **300**

Maximum Injection Time Mode: **Custom**

Maximum Injection Time (ms): **100**

Microscans: **1**

Data Type: **Profile**

APPENDICES

Polarity: **Positive**

Source Fragmentation: **Disabled**

Scan Description:

Experiment#6 [DIA 4mz windows - 800-904]

Start Time (min): **5**

End Time (min): **150**

Master Scan:

DIA

Precursor Mass Range: **800-904**

Multiplex Ions: **False**

Isolation Window (m/z): **4**

Window Overlap (m/z): **0**

Window Placement Optimization: **On**

Mass Defect: **1.0005**

Number Of Scan Events: **25**

Collision Energy Mode: **Fixed**

Collision Energy Type: **Normalized**

Collision Energy (%): **28**

Orbitrap Resolution: **30000**

Scan Range Mode: **Define First Mass**

First Mass (m/z): **110**

RF Lens (%): **70**

AGC Target: **Custom**

Normalized AGC Target (%): **100**

Maximum Injection Time Mode: **Custom**

Maximum Injection Time (ms): **60**

Microscans: **1**

Data Type: **Centroid**

Polarity: **Positive**

Source Fragmentation: **Disabled**

Loop Control: **All**

Scan Description:

DIA m/z window

DIA m/z window
Calculated m/z Window
800.6138-804.615619
804.615619-808.617438
808.617438-812.619257
812.619257-816.621076
816.621076-820.622895
820.622895-824.624714
824.624714-828.626533
828.626533-832.628352
832.628352-836.630171
836.630171-840.63199

APPENDICES

840.63199-844.633809
844.633809-848.635628
848.635628-852.637447
852.637447-856.639266
856.639266-860.641085
860.641085-864.642904
864.642904-868.644723
868.644723-872.646542
872.646542-876.648361
876.648361-880.65018
880.65018-884.651999
884.651999-888.653818
888.653818-892.655637
892.655637-896.657456
896.657456-900.659275
900.659275-904.661094

150min_300nL-GPS_DIA_898-1004mz

Method Summary

Method Settings

Application Mode: **Peptide**

Method Duration (min): **150**

Global Parameters

Ion Source

Use Ion Source Settings from Tune: **True**

FAIMS Mode: **Not Installed**

MS Global Settings

Infusion Mode: **Liquid Chromatography**

Expected LC Peak Width (s): **30**

Advanced Peak Determination: **True**

Default Charge State: **3**

Internal Mass Calibration: **Off**

Experiment#1 [MS Full]

Start Time (min): **5**

End Time (min): **150**

Master Scan:

Full Scan

Orbitrap Resolution: **60000**

Scan Range (m/z): **350-1200**

RF Lens (%): **50**

AGC Target: **Custom**

Normalized AGC Target (%): **300**

Maximum Injection Time Mode: **Custom**

Maximum Injection Time (ms): **100**

Microscans: **1**

APPENDICES

Data Type: **Profile**

Polarity: **Positive**

Source Fragmentation: **Disabled**

Scan Description:

Experiment#2 [MS 890-1010 mz]

Start Time (min): **5**

End Time (min): **150**

Master Scan:

Full Scan

Orbitrap Resolution: **60000**

Scan Range (m/z): **890-1010**

RF Lens (%): **40**

AGC Target: **Custom**

Normalized AGC Target (%): **300**

Maximum Injection Time Mode: **Custom**

Maximum Injection Time (ms): **100**

Microscans: **1**

Data Type: **Profile**

Polarity: **Positive**

Source Fragmentation: **Disabled**

Scan Description:

Experiment#3 [DIA 4mz windows - 898-1002 mz]

Start Time (min): **5**

End Time (min): **150**

Master Scan:

DIA

Precursor Mass Range: **898-1002**

Multiplex Ions: **False**

Isolation Window (m/z): **4**

Window Overlap (m/z): **0**

Window Placement Optimization: **On**

Mass Defect: **1.0005**

Number Of Scan Events: **25**

Collision Energy Mode: **Fixed**

Collision Energy Type: **Normalized**

Collision Energy (%): **28**

Orbitrap Resolution: **30000**

Scan Range Mode: **Define First Mass**

First Mass (m/z): **110**

RF Lens (%): **70**

AGC Target: **Custom**

Normalized AGC Target (%): **100**

Maximum Injection Time Mode: **Custom**

Maximum Injection Time (ms): **60**

Microscans: **1**

APPENDICES

Data Type: **Centroid**
 Polarity: **Positive**
 Source Fragmentation: **Disabled**
 Loop Control: **All**
 Scan Description:

DIA m/z window

DIA m/z window
Calculated m/z Window
898.6583655-902.6601845
902.6601845-906.6620035
906.6620035-910.6638225
910.6638225-914.6656415
914.6656415-918.6674605
918.6674605-922.6692795
922.6692795-926.6710985
926.6710985-930.6729175
930.6729175-934.6747365
934.6747365-938.6765555
938.6765555-942.6783745
942.6783745-946.6801935
946.6801935-950.6820125
950.6820125-954.6838315
954.6838315-958.6856505
958.6856505-962.6874695
962.6874695-966.6892885
966.6892885-970.6911075
970.6911075-974.6929265
974.6929265-978.6947455
978.6947455-982.6965645
982.6965645-986.6983835
986.6983835-990.7002025
990.7002025-994.7020215
994.7020215-998.7038405
998.7038405-1002.7056595

Experiment#4 [MS Full]

Start Time (min): **5**
 End Time (min): **150**

Master Scan:

Full Scan

Orbitrap Resolution: **60000**
 Scan Range (m/z): **350-1200**
 RF Lens (%): **50**
 AGC Target: **Custom**
 Normalized AGC Target (%): **300**
 Maximum Injection Time Mode: **Custom**

APPENDICES

Maximum Injection Time (ms): **100**

Microscans: **1**

Data Type: **Profile**

Polarity: **Positive**

Source Fragmentation: **Disabled**

Scan Description:

Experiment#5 [MS 890-1010 mz]

Start Time (min): **5**

End Time (min): **150**

Master Scan:

Full Scan

Orbitrap Resolution: **60000**

Scan Range (m/z): **890-1010**

RF Lens (%): **40**

AGC Target: **Custom**

Normalized AGC Target (%): **300**

Maximum Injection Time Mode: **Custom**

Maximum Injection Time (ms): **100**

Microscans: **1**

Data Type: **Profile**

Polarity: **Positive**

Source Fragmentation: **Disabled**

Scan Description:

Experiment#6 [DIA 4mz windows - 900-1004 mz]

Start Time (min): **5**

End Time (min): **150**

Master Scan:

DIA

Precursor Mass Range: **900-1004**

Multiplex Ions: **False**

Isolation Window (m/z): **4**

Window Overlap (m/z): **0**

Window Placement Optimization: **On**

Mass Defect: **1.0005**

Number Of Scan Events: **25**

Collision Energy Mode: **Fixed**

Collision Energy Type: **Normalized**

Collision Energy (%): **28**

Orbitrap Resolution: **30000**

Scan Range Mode: **Define First Mass**

First Mass (m/z): **110**

RF Lens (%): **70**

AGC Target: **Custom**

Normalized AGC Target (%): **100**

Maximum Injection Time Mode: **Custom**

APPENDICES

Maximum Injection Time (ms): **60**

Microscans: **1**

Data Type: **Centroid**

Polarity: **Positive**

Source Fragmentation: **Disabled**

Loop Control: **All**

Scan Description:

DIA m/z window

DIA m/z window
Calculated m/z Window
900.659275-904.661094
904.661094-908.662913
908.662913-912.664732
912.664732-916.666551
916.666551-920.66837
920.66837-924.670189
924.670189-928.672008
928.672008-932.673827
932.673827-936.675646
936.675646-940.677465
940.677465-944.679284
944.679284-948.681103
948.681103-952.682922
952.682922-956.684741
956.684741-960.68656
960.68656-964.688379
964.688379-968.690198
968.690198-972.692017
972.692017-976.693836
976.693836-980.695655
980.695655-984.697474
984.697474-988.699293
988.699293-992.701112
992.701112-996.702931
996.702931-1000.70475
1000.70475-1004.706569

150min_300nL-GPS_DIA_998-1104mz

Method Summary

Method Settings

Application Mode: **Peptide**

Method Duration (min): **150**

Global Parameters

Ion Source

APPENDICES

Use Ion Source Settings from Tune: **True**

FAIMS Mode: **Not Installed**

MS Global Settings

Infusion Mode: **Liquid Chromatography**

Expected LC Peak Width (s): **30**

Advanced Peak Determination: **True**

Default Charge State: **3**

Internal Mass Calibration: **Off**

Experiment#1 [MS Full]

Start Time (min): **5**

End Time (min): **150**

Master Scan:

Full Scan

Orbitrap Resolution: **60000**

Scan Range (m/z): **350-1200**

RF Lens (%): **50**

AGC Target: **Custom**

Normalized AGC Target (%): **300**

Maximum Injection Time Mode: **Custom**

Maximum Injection Time (ms): **100**

Microscans: **1**

Data Type: **Profile**

Polarity: **Positive**

Source Fragmentation: **Disabled**

Scan Description:

Experiment#2 [MS 990-1110 mz]

Start Time (min): **5**

End Time (min): **150**

Master Scan:

Full Scan

Orbitrap Resolution: **60000**

Scan Range (m/z): **990-1110**

RF Lens (%): **40**

AGC Target: **Custom**

Normalized AGC Target (%): **300**

Maximum Injection Time Mode: **Custom**

Maximum Injection Time (ms): **100**

Microscans: **1**

Data Type: **Profile**

Polarity: **Positive**

Source Fragmentation: **Disabled**

Scan Description:

Experiment#3 [DIA 4mz windows - 998-1102 mz]

Start Time (min): **5**

End Time (min): **150**

APPENDICES

Master Scan:

DIA

Precursor Mass Range: **998-1102**
 Multiplex Ions: **False**
 Isolation Window (m/z): **4**
 Window Overlap (m/z): **0**
 Window Placement Optimization: **On**
 Mass Defect: **1.0005**
 Number Of Scan Events: **25**
 Collision Energy Mode: **Fixed**
 Collision Energy Type: **Normalized**
 Collision Energy (%): **28**
 Orbitrap Resolution: **30000**
 Scan Range Mode: **Define First Mass**
 First Mass (m/z): **110**
 RF Lens (%): **70**
 AGC Target: **Custom**
 Normalized AGC Target (%): **100**
 Maximum Injection Time Mode: **Custom**
 Maximum Injection Time (ms): **60**
 Microscans: **1**
 Data Type: **Centroid**
 Polarity: **Positive**
 Source Fragmentation: **Disabled**
 Loop Control: **All**
 Scan Description:

DIA m/z window

DIA m/z window
Calculated m/z Window
998.7038405-1002.7056595
1002.7056595-1006.7074785
1006.7074785-1010.7092975
1010.7092975-1014.7111165
1014.7111165-1018.7129355
1018.7129355-1022.7147545
1022.7147545-1026.7165735
1026.7165735-1030.7183925
1030.7183925-1034.7202115
1034.7202115-1038.7220305
1038.7220305-1042.7238495
1042.7238495-1046.7256685
1046.7256685-1050.7274875
1050.7274875-1054.7293065
1054.7293065-1058.7311255
1058.7311255-1062.7329445

APPENDICES

1062.7329445-1066.7347635
1066.7347635-1070.7365825
1070.7365825-1074.7384015
1074.7384015-1078.7402205
1078.7402205-1082.7420395
1082.7420395-1086.7438585
1086.7438585-1090.7456775
1090.7456775-1094.7474965
1094.7474965-1098.7493155
1098.7493155-1102.7511345

Experiment#4 [MS Full]

Start Time (min): **5**

End Time (min): **150**

Master Scan:

Full Scan

Orbitrap Resolution: **60000**

Scan Range (m/z): **350-1200**

RF Lens (%): **50**

AGC Target: **Custom**

Normalized AGC Target (%): **300**

Maximum Injection Time Mode: **Custom**

Maximum Injection Time (ms): **100**

Microscans: **1**

Data Type: **Profile**

Polarity: **Positive**

Source Fragmentation: **Disabled**

Scan Description:

Experiment#5 [MS 990-1110 m/z]

Start Time (min): **5**

End Time (min): **150**

Master Scan:

Full Scan

Orbitrap Resolution: **60000**

Scan Range (m/z): **990-1110**

RF Lens (%): **40**

AGC Target: **Custom**

Normalized AGC Target (%): **300**

Maximum Injection Time Mode: **Custom**

Maximum Injection Time (ms): **100**

Microscans: **1**

Data Type: **Profile**

Polarity: **Positive**

Source Fragmentation: **Disabled**

Scan Description:

Experiment#6 [DIA 4mz windows - 1000-1104 m/z]

APPENDICES

Start Time (min): **5**
 End Time (min): **150**

Master Scan:

DIA

Precursor Mass Range: **1000-1104**
 Multiplex Ions: **False**
 Isolation Window (m/z): **4**
 Window Overlap (m/z): **0**
 Window Placement Optimization: **On**
 Mass Defect: **1.0005**
 Number Of Scan Events: **25**
 Collision Energy Mode: **Fixed**
 Collision Energy Type: **Normalized**
 Collision Energy (%): **28**
 Orbitrap Resolution: **30000**
 Scan Range Mode: **Define First Mass**
 First Mass (m/z): **110**
 RF Lens (%): **70**
 AGC Target: **Custom**
 Normalized AGC Target (%): **100**
 Maximum Injection Time Mode: **Custom**
 Maximum Injection Time (ms): **60**
 Microscans: **1**
 Data Type: **Centroid**
 Polarity: **Positive**
 Source Fragmentation: **Disabled**
 Loop Control: **All**
 Scan Description:

DIA m/z window

DIA m/z window
Calculated m/z Window
1000.70475-1004.706569
1004.706569-1008.708388
1008.708388-1012.710207
1012.710207-1016.712026
1016.712026-1020.713845
1020.713845-1024.715664
1024.715664-1028.717483
1028.717483-1032.719302
1032.719302-1036.721121
1036.721121-1040.72294
1040.72294-1044.724759
1044.724759-1048.726578
1048.726578-1052.728397
1052.728397-1056.730216

APPENDICES

1056.730216-1060.732035
1060.732035-1064.733854
1064.733854-1068.735673
1068.735673-1072.737492
1072.737492-1076.739311
1076.739311-1080.74113
1080.74113-1084.742949
1084.742949-1088.744768
1088.744768-1092.746587
1092.746587-1096.748406
1096.748406-1100.750225
1100.750225-1104.752044

Appendix 15. Exploris 480 DIA Method Summary.**Method Settings**

Application Mode: **Peptide**
Method Duration (min): **140**

Global Parameters

Ion Source

Use Ion Source Settings from Tune: **True**
FAIMS Mode: **Not Installed**

MS Global Settings

Infusion Mode: **Liquid Chromatography**
Expected LC Peak Width (s): **25**
Advanced Peak Determination: **True**
Default Charge State: **2**
Internal Mass Calibration: **Off**

Experiment#1 [MS]

Start Time (min): **10**
End Time (min): **140**

Master Scan:

Full Scan

Orbitrap Resolution: **60000**
Scan Range (m/z): **380-985**
RF Lens (%): **40**
AGC Target: **Custom**
Normalized AGC Target (%): **100**
Maximum Injection Time Mode: **Custom**
Maximum Injection Time (ms): **100**
Microscans: **1**
Data Type: **Profile**
Polarity: **Positive**
Source Fragmentation: **Disabled**
Scan Description:

Experiment#2 [DIA]

Start Time (min): **10**
End Time (min): **140**

Master Scan:

DIA

Precursor Mass Range: **380-980**
Multiplex Ions: **False**
Isolation Window (m/z): **10**
Window Overlap (m/z): **1**
Window Placement Optimization: **On**

APPENDICES

Mass Defect: **1.0005**
 Number Of Scan Events: **59**
 Collision Energy Mode: **Fixed**
 Collision Energy Type: **Normalized**
 Collision Energy (%): **28**
 Orbitrap Resolution: **15000**
 Scan Range Mode: **Define m/z range**
 Scan Range (m/z): **145-1450**
 RF Lens (%): **70**
 AGC Target: **Custom**
 Normalized AGC Target (%): **200**
 Maximum Injection Time Mode: **Custom**
 Maximum Injection Time (ms): **40**
 Microscans: **1**
 Data Type: **Centroid**
 Polarity: **Positive**
 Source Fragmentation: **Disabled**
 Loop Control: **N**
 N (Number of Spectra): **30**
 Scan Description:

DIA m/z window

Calculated m/z Window
379.922805-390.9273525
389.9273525-400.9319
399.9319-410.9364475
409.9364475-420.940995
419.940995-430.9455425
429.9455425-440.95009
439.95009-450.9546375
449.9546375-460.959185
459.959185-470.9637325
469.9637325-480.96828
479.96828-490.9728275
489.9728275-500.977375
499.977375-510.9819225
509.9819225-520.98647
519.98647-530.9910175
529.9910175-540.995565
539.995565-551.0001125
550.0001125-561.00466
560.00466-571.0092075
570.0092075-581.013755
580.013755-591.0183025
590.0183025-601.02285

APPENDICES

600.02285-611.0273975
610.0273975-621.031945
620.031945-631.0364925
630.0364925-641.04104
640.04104-651.0455875
650.0455875-661.050135
660.050135-671.0546825
670.0546825-681.05923
680.05923-691.0637775
690.0637775-701.068325
700.068325-711.0728725
710.0728725-721.07742
720.07742-731.0819675
730.0819675-741.086515
740.086515-751.0910625
750.0910625-761.09561
760.09561-771.1001575
770.1001575-781.104705
780.104705-791.1092525
790.1092525-801.1138
800.1138-811.1183475
810.1183475-821.122895
820.122895-831.1274425
830.1274425-841.13199
840.13199-851.1365375
850.1365375-861.141085
860.141085-871.1456325
870.1456325-881.15018
880.15018-891.1547275
890.1547275-901.159275
900.159275-911.1638225
910.1638225-921.16837
920.16837-931.1729175
930.1729175-941.177465
940.177465-951.1820125
950.1820125-961.18656
960.18656-971.1911075
970.1911075-981.195655